

VOLUME 80

JULY 29, 1976

NUMBER 16

JPCA x

THE JOURNAL OF
PHYSICAL
CHEMISTRY



PUBLISHED BIWEEKLY BY THE AMERICAN CHEMICAL SOCIETY

THE JOURNAL OF PHYSICAL CHEMISTRY

BRYCE CRAWFORD, Jr., Editor
STEPHEN PRAGER, *Associate Editor*
ROBERT W. CARR, Jr., FREDERIC A. VAN-CATLEDGE, *Assistant Editors*

EDITORIAL BOARD: C. A. ANGELL (1973-1977), F. C. ANSON (1974-1978), V. A. BLOOMFIELD (1974-1978), J. R. BOLTON (1976-1980), L. M. DORFMAN (1974-1978), H. L. FRIEDMAN (1975-1979), H. L. FRISCH (1976-1980), W. A. GODDARD (1976-1980), E. J. HART (1975-1979), W. J. KAUFMANN (1974-1978), R. L. KAY (1972-1976), D. W. McCLURE (1974-1978), R. M. NOYES (1973-1977), W. B. PERSON (1976-1980), J. C. POLANYI (1976-1980), S. A. RICE (1976-1980), F. S. ROWLAND (1973-1977), R. L. SCOTT (1973-1977), W. A. STEELE (1976-1980), J. B. STOTHERS (1974-1978), W. A. ZISMAN (1972-1976)

Published by the
**AMERICAN CHEMICAL SOCIETY
BOOKS AND JOURNALS DIVISION**
D. H. Michael Bowen, Director

Editorial Department: Charles R. Bertsch,
Head; Marianne C. Brogan, Associate
Head; Celia B. McFarland, Joseph E.
Yurvati, Assistant Editors

Graphics and Production Department:
Bacil Guiley, Head

Research and Development Department:
Seldon W. Terrant, Head

Advertising Office: Centcom, Ltd., 50 W.
State St., Westport, Conn. 06880.

© Copyright, 1976, by the American
Chemical Society. No part of this publica-
tion may be reproduced in any form with-
out permission in writing from the Ameri-
can Chemical Society.

Published biweekly by the American
Chemical Society at 20th and Northamp-
ton Sts., Easton, Pennsylvania 18042. Sec-
ond class postage paid at Washington, D.C.
and at additional mailing offices.

Editorial Information

Instructions for authors are printed in
the first issue of each volume. Please con-
form to these instructions when submitting
manuscripts.

Manuscripts for publication should be
submitted to *The Journal of Physical
Chemistry*, Department of Chemistry, Uni-
versity of Minnesota, Minneapolis, Minn.
55455. Correspondence regarding **accepted
papers and proofs** should be directed to
the Editorial Department at the ACS Eas-
ton address.

Page charges of \$60.00 per page are as-
sessed for papers published in this journal.
Ability to pay does not affect acceptance or
scheduling of papers.

Bulk reprints or photocopies of indi-
vidual articles are available. For informa-
tion write to Business Operations, Books
and Journals Division at the ACS Wash-
ington address.

Requests for **permission to reprint**
should be directed to Permissions, Books
and Journals Division at the ACS Wash-
ington address. The American Chemical
Society and its Editors assume no responsi-
bility for the statements and opinions ad-
vanced by contributors.

Subscription and Business Information

1976 Subscription rates—including sur-
face postage

	U.S.	PUAS	Canada, Foreign
Member	\$24.00	\$29.75	\$30.25
Nonmember	96.00	101.75	102.25
Supplementary material	15.00	19.00	20.00

Air mail and air freight rates are avail-
able from Membership & Subscription Ser-
vices, at the ACS Columbus address.

New and renewal subscriptions
should be sent with payment to the Office
of the Controller at the ACS Washington
address. **Changes of address** must include
both old and new addresses with ZIP code
and a recent mailing label. Send all address
changes to the ACS Columbus address.
Please allow six weeks for change to be-
come effective. **Claims** for missing num-
bers will not be allowed if loss was due to
failure of notice of change of address to be
received in the time specified; if claim is

dated: (a) North America—more than 90
days beyond issue date, (b) all other for-
eign—more than 1 year beyond issue date;
or if the reason given is "missing from
files". Hard copy claims are handled at the
ACS Columbus address.

Microfiche subscriptions are available
at the same rates but are mailed first class
to U.S. subscribers, air mail to the rest of
the world. Direct all inquiries to Business
Operations, Books and Journals Division,
at the ACS Washington address or call
(202) 872-4444. **Single issues** in hard copy
and/or microfiche are available from Spe-
cial Issues Sales at the ACS Washington
address. Current year \$4.75. Back issue
rates available from Special Issues Sales.
Back volumes are available in hard copy
and/or microform. Write to Special Issues
Sales at the ACS Washington address for
further information. **Microfilm** editions of
ACS periodical publications are available
from volume 1 to the present. For further
information, contact Special Issues Sales at
the ACS Washington address. **Supplemen-
tary material** must be ordered directly
from Business Operations, Books and Jour-
nals Division, at the ACS Washington ad-
dress.

	U.S.	PUAS, Canada	Other Foreign
Microfiche			
Photocopy	\$2.50	\$3.00	\$3.50
1-7 pages	4.00	5.50	7.00
8-20 pages	5.00	6.50	8.00

Orders over 20 pages are available only on
microfiche, 4 × 6 in., 24X, negative, silver
halide. Orders must state photocopy or mi-
crofiche if both are available. Full biblio-
graphic citation including names of all au-
thors and prepayment are required. Prices
are subject to change.

American Chemical Society
1155 16th Street, N.W.
Washington, D.C. 20036
(202) 872-4600

Member & Subscription Services
American Chemical Society
P.O. Box 3337
Columbus, Ohio 43210
(614) 421-7230

Editorial Department
American Chemical Society
20th and Northampton Sts.
Easton, Pennsylvania 18042
(215) 258-9111

THE JOURNAL OF PHYSICAL CHEMISTRY

Volume 80, Number 16 July 29, 1976

JPCA_x 80(16) 1739-1832 (1976)

ISSN 0022-3654

Some Fast Fluoride Ion Transfer Reactions of CO_3^{+} with Perfluoroalkanes and Sulfur Hexafluoride. Limits on the Heat of Formation of FCO	Michael T. Bowers* and Marian Chau	1739
On the Oxidizing Radical Formed by Reaction of e_{aq}^- and SF_6	Krishan M. Bansal and Richard W. Fessenden*	1743
Motion in Nonionic Surfactant Micelles and Mixed Micelles with Phospholipids. A Carbon-13 Spin-Lattice Relaxation Study on <i>p</i> -tert-Octylphenylpolyoxyethylene Ethers	Anthony A. Ribeiro and Edward A. Dennis*	1746
The Polymorphism of Lithium Palmitate	Marjorie J. Vold,* Hideo Funakoshi, and Robert D. Vold	1753
Electrosorption of 2-Butanol at the Mercury-Solution Interface. 1. Thermodynamic Treatment	Hisamitsu Nakadomari, David M. Mohilner,* and Patricia R. Mohilner	1761
Oxidation of Silicon by Water and Oxygen and Diffusion in Fused Silica	R. H. Doremus	1773
Location of the Cations in Hydrated NaCuY Zeolite	J. Marti, J. Soria,* and F. H. Cano	1776
Synthesis and Characterization of a Complex of Rubenic Acid and Copper(II) Montmorillonite	S. Son, S. Ueda, F. Kanamaru, and M. Koizumi*	1780
Nuclear Spin Relaxation in Methyl Groups Governed by Three- and Sixfold Barriers	Kenneth H. Ladner, Don K. Dalling, and David M. Grant*	1783
Electron Spin Resonance Spectra of the Thiadiazolothiadiazole Radical Anion and Related Sulfur-Nitrogen Heterocycles	C. L. Kwan, M. Carmack, and J. K. Kochi*	1786
Electron Spin Resonance Studies of Spin-Labeled Polymers. 11. Segmental and End-Group Mobility of Some Acrylic Ester Polymers	A. T. Bullock,* G. G. Cameron, and V. Krajewski	1792
Optical Activity of d-d Transitions in Copper(II) Complexes of Dipeptides and Dipeptide Amides. Molecular Orbital Model	Gary Hilmes, Chin-yah Yeh, and F. S. Richardson*	1798
Electronic Properties of <i>N</i> -Formylkynurenine and Related Compounds	Marie-Paule Pileni, Paul Walrant, and Rene Santus*	1804
Spectroscopic Studies of Charge-Transfer Complexes of Diazabenzene with Iodine	P. A. Clark,* T. J. Lerner, S. Hayes, and S. G. Fischer	1809
Raman Spectra of Cystine-Related Disulfides. Effect of Rotational Isomerism about Carbon-Sulfur Bonds on Sulfur-Sulfur Stretching Frequencies	H. E. Van Wart and H. A. Scheraga*	1812
Raman Spectra of Strained Disulfides. Effect of Rotation about Sulfur-Sulfur Bonds on Sulfur-Sulfur Stretching Frequencies	H. E. Van Wart and H. A. Scheraga*	1823

สำนักงานคณะกรรมการ
การวิจัยวิทยาศาสตร์

-ธ.ค.ค. 2519

COMMUNICATIONS TO THE EDITOR

Agreement Concerning the Nature of the Variation of Disulfide Stretching
Frequencies with Disulfide Dihedral Angles

. . . H. E. Van Wart, H. A. Scheraga,* and R. Bruce Martin 1832

■ Supplementary material for this paper is available separately (consult the masthead page for ordering information); it will also appear following the paper in the microfilm edition of this journal.

* In papers with more than one author, the asterisk indicates the name of the author to whom inquiries about the paper should be addressed.

AUTHOR INDEX

Bansal, K. M., 1743	Fischer, S. G., 1809	Ladner, K. H., 1783	Santus, R., 1804
Bowers, M. T., 1739	Funakoshi, H., 1753	Lerner, T. J., 1809	Scheraga, H. A., 1812, 1823, 1832
Bullock, A. T., 1792			Son, S., 1780
Cano, F. H., 1776	Grant, D. M., 1783	Marti, J., 1776	Soria, J., 1776
Carmack, M., 1786		Martin, R. B., 1832	
Cameron, G. G., 1792	Hayes, S., 1809	Mohilner, D. M., 1761	Ueda, S., 1780
Chau, M., 1739	Hilmes, G., 1798	Mohilner, P. R., 1761	
Clark, P. A., 1809		Nakadomari, H., 1761	Van Wart, H. E., 1812, 1823, 1832
Dalling, D. K., 1783	Kanamaru, F., 1780		Vold, M. J., 1753
Dennis, E. A., 1746	Kochi, J. K., 1786	Pilani, M.-P., 1804	Vold, R. D., 1753
Doremus, R. H., 1773	Koizumi, M., 1780	Ribeiro, A. A., 1746	Walrant, P., 1804
Fessenden, R. W., 1743	Krajewski, V., 1792	Richardson, F. S., 1798	Yeh, C., 1798
	Kwan, C. L., 1786		

THE JOURNAL OF PHYSICAL CHEMISTRY

Registered in U. S. Patent Office © Copyright, 1976, by the American Chemical Society

VOLUME 80, NUMBER 16 JULY 29, 1976

Some Fast Fluoride Ion Transfer Reactions of CO^+ with Perfluoroalkanes and Sulfur Hexafluoride. Limits on the Heat of Formation of FCO

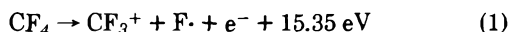
Michael T. Bowers* and Marian Chau

Department of Chemistry, University of California, Santa Barbara, California 93106 (Received December 8, 1975)

The reactions of CO^+ , CO_2^+ , and Kr^+ with CF_4 , C_2F_6 , C_3F_8 , and SF_6 are reported. The CO^+ ion reacts with CF_4 and SF_6 at nearly the collision limit while the nearly isoenergetic ions CO_2^+ and Kr^+ do not exhibit measurable rate constants. It is proposed that CO^+ reacts to form a stable COF^+ product via the reaction $\text{CO}^+ + \text{RF} \rightarrow \text{R}^+ + \text{COF}^+$. By using the RF molecules listed above the thermodynamic limits $D(\text{F}-\text{CO}^+) \geq 29$ kcal/mol and $\Delta H_f^\circ(\text{FCO}^+) \leq -37$ kcal/mol are obtained. Comparison is made with other data yielding the suggested values of $D(\text{F}-\text{CO}^+) = 34 \pm 4$ kcal/mol and $\Delta H_f^\circ(\text{FCO}^+) = -42 \pm 4$ kcal/mol. Each of the ions CO^+ , CO_2^+ , and Kr^+ react with C_2F_6 and C_3F_8 . Both absolute and relative rate constants are measured and discussed in terms of a reaction mechanism.

Introduction

There has been considerable interest in recent years in the mechanism of simple ion-molecule reactions at thermal energies. Charge transfer¹⁻³ and proton transfer⁴ have received considerable attention, and to a lesser extent hydrogen atom transfer,⁵ hydride ion transfer,⁶ and fluoride ion transfer.⁷ In the study of charge transfer reactions in our laboratories it is usual to react a number of atomic and simple molecular ions with a given substrate molecule and use the measured absolute rate constants as diagnostics of reaction mechanism. One such system currently under study is the series of fluorinated methane substrate molecules.⁸ There is considerable evidence that Franck-Condon (FC) factors play an important role in determining the probability of a charge transfer reaction in simple systems,^{1,2} i.e., large FC factors are usually necessary for fast rate constants. For the CF_4 molecule, the lowest energy Franck-Condon accessible ion is CF_3^+ with an onset energy of 15.35 eV⁹



Hence, an ion reacting with CF_4 via dissociative charge transfer must have a recombination energy greater than 15.35 eV if the reaction is to occur at thermal energies. The ions Kr^+ ($^3\text{P}_{3/2}$), CO_2^+ , and CO^+ have nearly identical recombination energies, 13.999, 13.77, and 14.01 eV. None of these ions have enough internal energy to dissociatively ionize CF_4 . When these ions were allowed to react with CF_4 we were thus not surprised that both Kr^+ and CO_2^+ were totally unreactive.

However, we were very surprised when CO^+ reacted with CF_4 at near the collision limit, $k = (7.5 \pm 0.8) \times 10^{-10} \text{ cm}^3/\text{s}$. This paper is the result of pursuing the origins of this surprising observation and reports some very fast F^- transfer reactions and limits on the thermodynamic quantities $D(\text{F}-\text{CO}^+)$ and $\Delta H_f^\circ(\text{FCO}^+)$ derived from these studies.

Experimental Section

All of the experiments reported here were performed on a laboratory built drift cell ICR that has been previously described.^{10,11} Pressures were measured on a Granville-Phillips ion gauge calibrated against a MKS Baratron capacitance monometer. Drift times were measured using trapping plate ejection. Product distributions were measured at constant magnetic field using a Q-spoiler device for calibrating the marginal oscillator.¹² All gases were purchased commercially and used as received. There were no detectable impurities in any of the gases.

Results

The absolute rate constants, heats of reaction, and the theoretical collision rate limits of CO^+ , CO_2^+ , and Kr^+ with CF_4 and SF_6 are given in Tables I and II. The only ionic products observed were CF_3^+ and SF_5^+ , respectively. In Tables III and IV the absolute rate constants, product distribution, heats of reaction, and theoretical collision rate limits are given for CO^+ , Kr^+ , and CO_2^+ reacting with C_2F_6 and C_3F_8 . The low energy portion of the photoelectron spectra of

TABLE I: Absolute Rate Constants, Heats of Reaction, and Collision Limit Rate Constants for $M^+ + CF_4 \rightarrow CF_3^+ +$ Neutral Products

Reactant ion (M^+)	$k \times 10^{10}$ cm ³ /s		ΔH , ^b kcal/mol
	Expt	Theory ^a	
CO ⁺	6.6	8.29	16
CO ₂ ⁺	~0	7.06	22
Kr ⁺	~0	5.83	16

^a G. Gioumoussis and D. P. Stevenson, *J. Chem. Phys.*, **29**, 294 (1958). Assumes $k = 2\rho q(\alpha/\mu)^{1/2}$. ^b Assumed neutral products are F· and M.

TABLE II: Absolute Rate Constants, Heats of Reaction, and Collision Limit Rate Constants for $M^+ + SF_6 \rightarrow SF_5^+ +$ Neutral Products

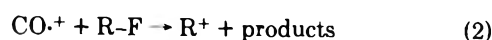
Reactant ion (M^+)	$k \times 10^{10}$ cm ³ /s		ΔH , ^b kcal/mol
	Expt	Theory ^a	
CO ⁺	9.8 ^c	10.0	29
CO ₂ ⁺	~0	8.34	36
Kr ⁺	~0	6.65	30

^a G. Gioumoussis and D. P. Stevenson, *J. Chem. Phys.*, **29**, 294 (1958); Assumes $k = 2\rho q(\alpha/\mu)^{1/2}$. ^b Assumed neutral products are M + F. ^c Fehsenfeld has previously reported a value of 13×10^{10} cm³/s for this rate constant, *J. Chem. Phys.*, **54**, 438 (1971).

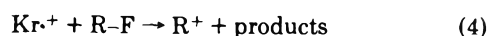
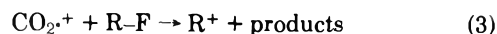
CF₄, SF₆, C₂F₆, and C₃F₈ are given in Figure 1. Also noted in Figure 1 are the recombination energies of CO⁺, CO₂⁺, and Kr⁺. The values of the heats of formation of the ions and neutral molecules used in this work are summarized in Table V.

Discussion

There are a number of observations that can readily be made from the data of Tables I–IV and Figure 1: (i) the reactions

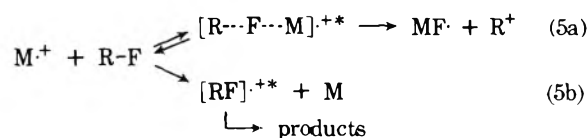


where $R = CF_3^+$, SF₅⁺, C₂F₅⁺, and C₃F₇⁺ are all reasonably fast. If F· and CO are the products for reaction 2, then these reactions are all endothermic ($\Delta H > 15$ kcal/mol) and would not be expected to occur at thermal energies; (ii) the energetically similar reactions



do not have measurable rate constants at thermal energies although they have nearly the same energetics as reaction 2 if the products are F· and CO, CO₂, or Kr; (iii) the photoelectron spectra of CF₄ and SF₆ indicate that neither of these molecules have measurable FC factors at the recombination energy of CO, CO₂, or Kr (see Figure 1); (iv) the experimental rate constants for systems other than those represented by (3) and (4) approach the classical capture collision limits in all cases (except CO₂⁺ reacting with C₂F₆, where about 50% of the classical limit is obtained); (v) multiple reaction channels begin to appear in the C₂F₆ system and much more so in the C₃F₈ system.

These results can be understood using the following reaction mechanism:



where $M = CO, CO_2,$ and Kr. A competition is set up in the collisions between a formal charge transfer reaction (5b) forming an unstable excited intermediate $[RF]^{+*}$ and a formal reaction complex mechanism, (5a), where a $[R \cdots F \cdots M]^{+*}$ intermediate is formed. For all combinations of M and R listed above a complex can theoretically be formed.¹³ Only for M equal to CO, however, is the M–F bond strong enough to make the exit channel (5a) energetically accessible (vide infra). For $M = CO_2$ or Kr the complex merely dissociates to reactants.

The charge transfer channel is energetically accessible only for $R = C_2F_5^+$ and C₃F₇⁺. It is not clear in the cases studied here that charge transfer does not proceed, at least in part, through the complex intermediate of (5a). Recent studies^{1,2} do, however, indicate that favorable FC factors are a requirement for fast charge transfer rate constants in most cases, supporting the dual mechanism model of reaction 5.¹⁴ This is not a rigid requirement, however, particularly when the possible intermediate complex is very stable.¹⁵

Inspection of the data in Table IV, $M^+ + RF$ where $R = C_3F_7^+$ indicates the product distribution cannot be simply predicted on the basis of thermochemical considerations. The CF₄ elimination from $[C_3F_8]^{+*}$ to give C₂F₄⁺ is clearly the most exothermic channel (ca. 50 kcal/mol), but the CF₃⁺ ion dominates the product distribution. The C₃F₈ molecule is formally identical with C₃H₈ except F replaces H. The fragmentation of excited $[C_3H_8]^{+*}$ ions has been the subject of considerable interest, in particular regarding its use as a model for testing quasiequilibrium theory calculations.¹⁶ Interestingly, the C₂H₅⁺ ion formed from loss of ·CH₃ dominates the propane product distribution at 14 eV total energy even though the C₂H₄⁺ + CH₄ products are thermodynamically more stable by about 1 eV. An analysis of the various reasons for this observed fact is given by Vestal,¹⁶ the key reason being the entropy associated with the transition state for both fragmentations. The CH₄ elimination goes through a cyclic transition state (low entropy) and the CH₃ elimination through a simple bond cleavage (high entropy). It is interesting that the perfluoro system so closely imitates the perhydro analogue since often fluorine presents anomalous behavior.

Reaction 5a appears to offer the only feasible explanation of the fast reaction rate of CO⁺ with CF₄ and SF₆ and for the formation of C₂F₅⁺ and C₃F₇⁺ products when CO⁺ reacts with C₂F₆ and C₃F₈, respectively. From the data in Tables I–V it is straightforward to deduce the necessary conditions $D(F-CO) \geq 16, 29, 15, (30)$ kcal/mol using the CF₄, SF₆, C₂F₆, and C₃F₈ data, respectively.¹⁷ Using the relation

$$\Delta H_f^{\circ 298}(FCO) = \Delta H_f^{\circ 298}(F) + \Delta H_f^{\circ 298}(CO) - D^{\circ 298}(F-CO) \quad (6)$$

one obtains $\Delta H_f^{\circ 298}(FCO) \leq -24, -37, -23,$ and (-38) kcal/mol from the CF₄, SF₆, C₂F₆, and C₃F₈ data, respectively. In order to test the upper bound on $D(F-CO)$ and lower bound on $\Delta H_f^{\circ 298}(FCO)$ we attempted to observe the reaction

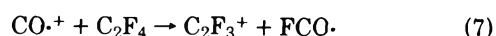


TABLE III: Absolute and Relative Rate Constants, Heats of Reaction, and Theoretical Collision Rate Constants for M⁺ + C₂F₆ → Products

Reactant ion (M ⁺)	$k \times 10^{10}$ cm ³ /s		%	Rel $k \times 10^{10}$	ΔH , ^a kcal/mol	%	rel $k \times 10^{10}$	ΔH , ^b kcal/mol
	Expt	Theory ^c						
CO ⁺	9.3	10.3	66	6.14	-15.3	34	3.16	15.4
CO ₂ ⁺	4.1	8.6	100	4.1	-9	0	0	21.8
Kr ⁺	5.8	6.9	100	5.8	-14.9	0	0	15.8

^a Assumed neutral products are CF₃ + M. ^b Assumed neutral products are F + M. ^c G. Gioumoussis and D. P. Stevenson, *J. Chem. Phys.*, **29**, 294 (1958); assumes $k = 2\pi q(\alpha/\mu)^{1/2}$.

TABLE IV: Absolute and Relative Rate Constants, Heats of Formation, and Theoretical Collision Rate Constants for M⁺ + C₃F₈ → Products

Reactant ion (M ⁺)	$k \times 10^{10}$ cm ³ /s			%	Rel $k \times 10^{10}$	ΔH , ^b kcal/mol	%	Rel $k \times 10^{10}$	ΔH , ^c kcal/mol	%	Rel $k \times 10^{10}$	ΔH , ^d kcal/mol	%	Rel $k \times 10^{10}$	ΔH , ^e kcal/mol
	Expt	Theory	CF ₃ ⁺												
CO ⁺	11.9	12	64.8	7.7	-25.1	17.6	2.1	-55.4	8.7	1.03	-25.5	8.9	1.06	30.3	
CO ₂ ⁺	9.4	10	71.5	6.7	-18.8	24.2	2.3	-49	4.3	0.4	-19.2	0	0	36.7	
Kr ⁺	6.13	7.8	67.4	4.1	-24.7	17	1.04	-55	15.6	0.96	-25.1	0	0	30.7	

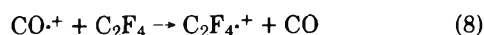
^a G. Gioumoussis and D. P. Stevenson, *J. Chem. Phys.*, **29**, 294 (1958); assume $k = 2\pi q(\alpha/\mu)^{1/2}$. ^b Assumed neutral products are M + C₂F₅. ^c Assumed neutral products are M + CF₄. ^d Assumed neutral products are M + CF₃. ^e Assumed neutral products are M + F.

TABLE V: Heats of Formation of All Species Used in This Work

Species	Neutral ΔH_f° , kcal/mol	Ion ΔH_f° , kcal/mol
CO	-26.4 ^a	297 ^b
CO ₂	-94.05 ^a	223 ^b
Kr	0	² P _{3/2} 323 ^b ³ P _{1/2} 338 ^b
F·	18.7 ^c	
CF ₃ ·	-112.2 ^d	99.3 ^e
CF ₄	-223 ^a	
C ₂ F ₄	-155 ^f	78 ^b
C ₂ F ₅ ·	-212 ^g	≤ -0.9 ⁱ
C ₂ F ₆	-321 ^a	
C ₃ F ₇ ·		-76 ^{f,i}
C ₃ F ₈	-411 ^g	
SF ₅ ·		42 ^h
SF ₆	-292 ^a	

^a Reference 21. ^b J. L. Franklin, J. G. Dillard, H. M. Rosenstock, J. T. Heron, K. Draxl, and F. H. Field, *Natl. Stand. Ref. Data Ser., Natl. Bur. Stand.*, No. 26 (1969). ^c W. A. Chupka and J. Berkowitz, *J. Chem. Phys.*, **54**, 5126 (1971). ^d J. A. Kerr and D. M. Timlin, *Int. J. Chem. Kinet.*, **III**, 427 (1971). ^e T. A. Walker, C. Lifshitz, W. A. Chupka, and J. Berkowitz, *J. Chem. Phys.*, **51**, 3531 (1969). ^f J. Heicklein, *Advan. Photochem.*, **7**, 57 (1969). ^g W. M. D. Bryant, *J. Polym. Sci.*, **56**, 277 (1962). ^h Derived from the heat of formation of SF₆ and the appearance potential of SF₅⁺; V. H. Diebler and J. A. Walker, *J. Chem. Phys.*, **44**, 4405 (1966). ⁱ See ref 17.

Reaction 7 was not observed although the exothermic charge transfer reaction 8 was observed to be fast



The failure to observe a reaction does not prove that the reaction is not exothermic, but for simple ion-molecule reactions it is suggestive that such may be the case. A tentative upper limit on $D(\text{F-CO}\cdot)$ can thus be set, $D(\text{F-CO}\cdot) \leq 53$ kcal/mol

and ΔH_f° (FCO·) ≥ -61 kcal/mol. In summary then $29 \leq D(\text{F-CO}\cdot) \leq 53$ and $-61 \leq \Delta H_f^\circ$ (FCO·) ≤ -37 where all units are in kcal/mol.

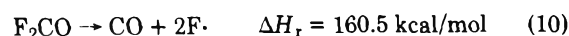
Macneil and Thynne¹⁸ have measured a lower limit on $D(\text{F-CO}\cdot)$ by observing the dissociative electron capture reaction



which has a threshold of 2.1 ± 0.1 eV. Using 3.40 eV¹⁹ for the electron affinity of F· and standard heats of formation of F· and CO, Macneil and Thynne deduce $D(\text{F-CO}\cdot) \geq 32$ kcal/mol, giving ΔH_f° (FCO·) ≤ -40 kcal/mol in good agreement with our results.

Henrici, Lin, and Bauer²⁰ have also estimated $D(\text{F-CO}\cdot)$ and ΔH_f° (FCO·). They have studied the thermal decomposition of F₂CO in a shock tube and have suggested a complex reaction mechanism to fit their experimental data. The radical FCO· is not observed directly by Henrici et al., but is assumed to be a key intermediate in their reaction scheme. They were able to deduce that $D(\text{F-CO}\cdot) \geq 24.2$ kcal/mol corresponding to ΔH_f° (FCO·) ≤ -32 kcal/mol. The best fit to their overall reaction scheme was given by ΔH_f° (FCO·) ≈ -34 kcal/mol with limits of $-37 \leq \Delta H_f^\circ$ (FCO·) ≤ -29 kcal/mol if their data were to fit within acceptable error limits the reaction scheme proposed. Comparison with our much more direct observations, as well as the data of Macneil and Thynne,¹⁸ indicate the estimates of Henrici et al. may be in error by approximately 5–10 kcal/mol and suggest that perhaps their mechanism for interpreting their shock tube data should be reevaluated.

The heat of formation of FCO· has been estimated in the Janaf Tables²¹ from the heat of reaction



and by assuming $D(\text{Cl-ClCO})/D(\text{Cl-CO}\cdot) = D(\text{F-FCO})/$

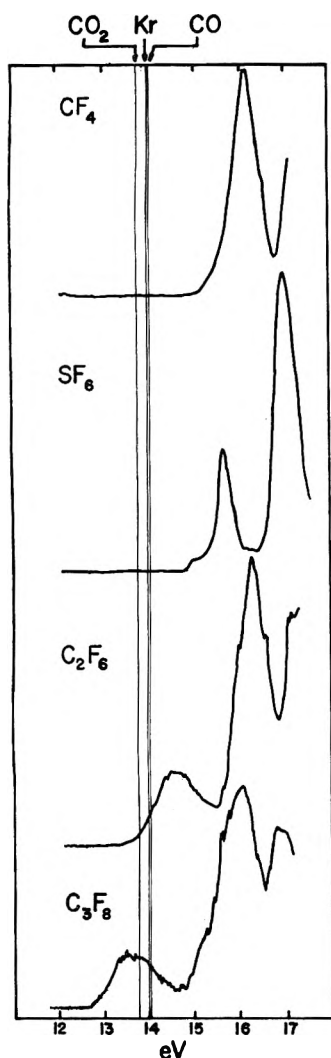


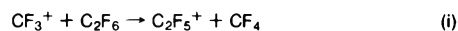
Figure 1. He(I) photoelectron spectra of $\cdot\text{CF}_4$, SF_6 , C_2F_6 , and C_3F_8 between 12 and 17 eV. The recombination energies of ground state Kr^+ , CO^+ , and CO_2^+ are shown as the vertical lines.

$D(\text{F}-\text{CO}\cdot) = 4$. This type of argumentation leads to $\Delta H_f^\circ_{298} = -41 \pm 15$ kcal/mol. This value is in reasonable agreement with the upper limit we present in this work of $\Delta H_f^\circ_{298} \leq -37$ kcal/mol. When all the data are taken into consideration, it is likely that $\Delta H_f^\circ_{298}(\text{FCO}\cdot)$ is near our upper limit and does not approach our lower limit of -61 kcal/mol. Based on our data, the data of Macneil and Thynne,¹⁷ and the arguments of Henrici *et al.*²⁰ and Stull and Prophet²¹ we estimate $\Delta H_f^\circ_{298}(\text{FCO}) \approx -42 \pm 4$ kcal/mol and $D(\text{F}-\text{CO}\cdot) \approx 34 \pm 4$ kcal/mol.

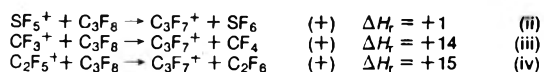
Acknowledgment. The support of the National Science Foundation under Grant MSP74-18397 is gratefully acknowledged. We are also grateful to a referee for pointing out an important reference to us.

References and Notes

- (1) M. T. Bowers and D. D. Elleman, *Chem. Phys. Lett.*, **16**, 486 (1972).
- (2) J. B. Laudenslager, W. T. Huntress, and M. T. Bowers, *J. Chem. Phys.*, **61**, 4600 (1974), and references therein.
- (3) J. Durup, "Interactions between Ions and Molecules", P. Ausloos, Ed., Plenum Press, New York, N.Y., 1975.
- (4) D. K. Bohme, in ref. 3.
- (5) J. K. Kim, L. P. Theard, and W. T. Huntress, *J. Chem. Phys.*, **62**, 45 (1975), and references therein.
- (6) L. W. Sieck and S. K. Searles, *J. Am. Chem. Soc.*, **92**, 2937 (1970); S. G. Lias, in ref. 3, and references therein; M. Moet-Ne' and F. H. Field, *J. Am. Chem. Soc.*, **97**, 2014 (1975).
- (7) J. H. J. Dawson, W. G. Henderson, R. M. O'Malley, and K. R. Jennings, *Int. J. Mass Spectrom. Ion Phys.*, **11**, 61 (1973); R. J. Blint, T. B. McMahon, and J. L. Beauchamp, *J. Am. Chem. Soc.*, **96**, 1269 (1974).
- (8) M. Chau and M. T. Bowers, *Int. J. Mass Spectrom. Ion Phys.*, to be submitted for publication.
- (9) C. R. Brundle, M. B. Robin, and H. Basch, *J. Chem. Phys.*, **53**, 2196 (1970).
- (10) R. M. O'Malley, K. R. Jennings, M. T. Bowers, and V. G. Anicich, *Int. J. Mass Spectrom. Ion Phys.*, **11**, 99 (1973); V. G. Anicich and M. T. Bowers, *ibid.*, **11**, 555 (1973).
- (11) V. G. Anicich, Ph.D. Thesis, University of California at Santa Barbara, 1973.
- (12) P. Kemper and M. T. Bowers, *Rev. Sci. Instrum.*, to be submitted for publication.
- (13) It should be noted that the "complex" suggested here could be very short-lived. The only implication is that the particles sustain an intimate collision allowing for bond breakage and formation.
- (14) For example, it has been suggested that low energy charge transfer reactions proceed via two mechanisms, one with momentum transfer and one without momentum transfer [A. J. Masson, K. Berkenshaw, and M. Henchman, *J. Chem. Phys.*, **50**, 4112 (1969)]. See also, M. T. Bowers and T. Su, *Adv. Electron. Electron Phys.*, **34**, 223 (1973).
- (15) E. E. Ferguson, paper presented at the 22nd Annual Conference of the American Society of Mass Spectrometry and Allied Topics, Philadelphia, Pa., 1974; M. T. Bowers, paper presented at the 22nd Annual Conference of the American Society of Mass Spectrometry and Allied Topics, Philadelphia, Pa., 1974.
- (16) See, for example, M. Vestal in "Fundamental Processes in Radiation Chemistry", P. Ausloos, Ed., Wiley-Interscience, New York, N.Y., 19568.
- (17) A reaction that bears on the thermochemistry considered here is the F^- transfer reaction



Sieck *et al.* [L. W. Sieck, R. Gordon, Jr., and P. Ausloos, *J. Res. Natl. Bur. Stand. (U.S.)*, *Sect. A*, **78**, 151 (1974)] have shown this reaction to be exothermic at thermal energies. Since the heats of formation of CF_3^+ , C_2F_6 , and CF_4 are well known, the value $\Delta H_f^\circ_{298}(\text{C}_2\text{F}_5^+) \leq -0.9$ kcal/mol is obtained as noted in Table V. Reaction i was looked at in the ICR and double resonance experiments performed. When CF_3^+ was ejected from the cell, the C_2F_5^+ signal decreased. When C_2F_5^+ was ejected from the cell, there was no change in the CF_3^+ signal. These results confirm the data of Sieck *et al.* and indicate that (i) is exothermic. Similar experiments were attempted to test the heat of formation of C_3F_7^+ quoted in Table V. The following reactions were investigated using double resonance techniques in the ICR:



The symbol (+) indicates that a positive double resonance signal is obtained when C_3F_7^+ is observed and the reactant ion is irradiated at lower power. When the power is raised to a point where the reactant ion is ejected, the C_3F_7^+ intensity returns to the value it has when no irradiation is taking place. Hence, the conclusion is all three reactions appear to be endothermic. The values of the heat of reactions, in kcal/mol, ΔH_r , are obtained using the value $\Delta H_f^\circ_{298}(\text{C}_3\text{F}_7^+) = -76$ kcal/mol reported in Table V. From reaction ii we conclude $\Delta H_f^\circ_{298}(\text{C}_3\text{F}_7^+) \geq -76$ kcal/mol. The true absolute value of $\Delta H_f^\circ_{298}(\text{C}_3\text{F}_7^+)$ is still uncertain, however, so the number is bracketed in Table V and is not used in the thermochemical determinations of $D(\text{F}-\text{CO}\cdot)$ or $\Delta H_f^\circ_{298}(\text{FCO}\cdot)$.

- (18) K. A. G. Macneil and J. C. J. Thynne, *Int. J. Mass Spectrom. Ion Phys.*, **3**, 35 (1969).
- (19) H. P. Popp, *Z. Naturforsch. A*, **22**, 254 (1967).
- (20) H. Henrici, M. C. Lin, and S. H. Bauer, *J. Chem. Phys.*, **52**, 5834 (1970).
- (21) D. R. Stull and H. Prophet, *Natl. Stand. Ref. Data Ser., Natl. Bur. Stand.*, **No. 37** (1971).

On the Oxidizing Radical Formed by Reaction of e_{aq}^- and SF_6 ¹

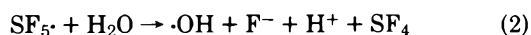
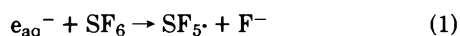
Krishan M. Bansal and Richard W. Fessenden*

Radiation Research Laboratories and Department of Chemistry, Mellon Institute of Science, Carnegie-Mellon University, Pittsburgh, Pennsylvania 15213 (Received January 30, 1976)

Publication costs assisted by the U. S. Energy Research and Development Administration

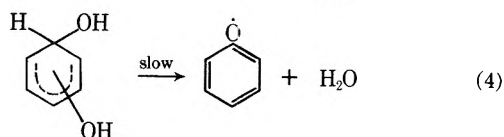
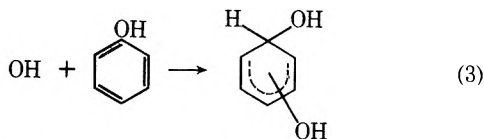
Evidence from optical absorption pulse radiolysis experiments is presented for the existence of an oxidizing radical other than OH produced by the reaction of SF_6 and e_{aq}^- . This radical is capable of oxidizing phenol and hydroquinone directly to phenoxyl and *p*-semiquinone ion radicals, respectively, even at neutral pH. From an analysis of the yield and kinetics of formation of the *p*-semiquinone ion it was found that the intermediate reacts with water with a rate constant of $\sim 1.1 \times 10^5 \text{ s}^{-1}$. The reaction with hydroquinone has a rate constant of $1.7 \times 10^9 \text{ M}^{-1} \text{ s}^{-1}$. Conductometric pulse radiolysis experiments are in agreement with the optical results. The radical $\cdot SF_5$ is the simplest and most probable candidate for the oxidizing species. Sulfur hexafluoride can conveniently be used to introduce a strongly oxidizing radical into various systems where e_{aq}^- can be scavenged. This approach is demonstrated for methanol solution by the production of Br_2^- from 10^{-2} M KBr .

Sulfur hexafluoride has been widely used in radiation chemistry as an electron scavenger but little is known about the subsequent reactions of any intermediates produced. In aqueous solution the reaction $e_{aq}^- + SF_6$ leads ultimately to production of six fluoride ions.²⁻⁵ Both $SF_5\cdot$ and SF_4 have been suggested^{2,4} as successive intermediates.



On the basis of conductometric pulse radiolysis experiments it was concluded previously⁴ that $\cdot SF_5$ has a half-life $< 2 \mu\text{s}$. This value implies that oxidation of water by $SF_5\cdot$ is considerably faster than by other strongly oxidizing radicals such as $SO_4^{\cdot-}$ and Cl which react with water with pseudo-first-order rate constants of 10^3 – 10^4 ^{6,7} and $7 \times 10^4 \text{ s}^{-1}$,^{8,9} respectively. The present paper will describe experiments designed to reveal more details of the reactions of the oxidizing intermediate in SF_6 saturated aqueous solutions.

Initial attempts to demonstrate the presence of an oxidizing radical different than OH involved the use of substituted phenols in optical pulse radiolysis experiments.¹⁰ In neutral solution OH adds to a phenol to form a radical of the hydroxycyclohexadienyl type¹¹ which loses water only slowly, to form a phenoxyl radical.

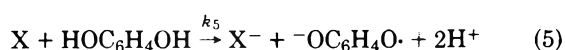


In contrast to this behavior, radicals with more tendency toward electron transfer oxidation, such as $SO_4^{\cdot-}$, produce phenoxyl radicals directly even in neutral solution.¹² Thus, the immediate appearance of the phenoxyl radical in any system demonstrates an oxidizing radical which acts differently than does OH. The absorption spectrum of a phenoxyl

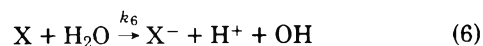
radical is very distinctive with two narrow bands near 400 nm and is sufficiently different than that of the corresponding hydroxycyclohexadienyl radical that the two can easily be distinguished.

An experiment with 1.4 mM *p*-cresol, buffered at pH 6.8 with 1 mM phosphate and saturated with SF_6 , gave the same spectrum for the phenoxyl radical as is produced by $SO_4^{\cdot-}$. (With $SO_4^{\cdot-}$ a spectrum taken 2 μs after the radiolysis pulse showed peaks at 389 and 408 nm with ϵ_{max} of 2300 and $3500 \text{ M}^{-1} \text{ cm}^{-1}$, respectively.) Subsequently, it was found that addition of relatively large amounts of *tert*-butyl alcohol ($\sim 100 \text{ mM}$) to the SF_6 solutions had no effect on the intensity of the phenoxyl radical absorption but did remove the absorption at $\sim 330 \text{ nm}$ caused by the OH adduct. Observation of the phenoxyl radical in this experiment shows that an oxidizing radical other than OH is present and that this radical can be scavenged with relatively low concentrations of reactant.

A similar experiment was carried out with an SF_6 saturated solution of 1 mM hydroquinone at pH 7.2 with 1 mM phosphate buffer. In this case 0.2 M *tert*-butyl alcohol was used to scavenge OH and to prevent production of the semiquinone radical ion from this source.¹³ The absorption rose to a plateau level in less than 1 μs and a spectrum taken at 1–2 μs after the pulse matched that of the *p*-semiquinone ion^{14,15} with an ϵ_{max} of 6100 at 430 nm (based on $G(e_{aq}^-) = 2.7$). With concentrations of hydroquinone in the range 3×10^{-5} to $1 \times 10^{-4} \text{ M}$ the absorption at 430 nm rose more slowly but reached a plateau level and remained completely constant for at least 100 μs . At $3 \times 10^{-5} \text{ M}$ the plateau level was about half that at $1 \times 10^{-3} \text{ M}$ and the formation had a half-life of about 4 μs . This behavior is interpreted as a competition between the reaction of an oxidizing species, X, with hydroquinone



and its reaction with water



which converts it to a form no longer capable of rapidly oxi-

dizing hydroquinone. In this scheme the pseudo-first-order rate constant for reaction of X and for formation of semiquinone is $k_{\text{obsd}} = k_6 + k_5[\text{C}_6\text{H}_4(\text{OH})_2]$. A plot of k_{obsd} for the formation of the semiquinone ion was made for concentrations of hydroquinone in the range 3×10^{-5} to 1×10^{-4} M (see Figure 1). The rate constant for reaction of the oxidizing species with water was found from the intercept to be $1.1 \times 10^5 \text{ s}^{-1}$ and the slope corresponded to a value of $1.7 \times 10^9 \text{ M}^{-1} \text{ s}^{-1}$ for reaction with hydroquinone. Neither an increase in the concentration of phosphate nor a reduction of the *tert*-butyl alcohol concentration to 50 mM significantly affected the competition.

If the reaction of the oxidizing species with water is a direct oxidation, as in reaction 2, then H^+ must be produced and should be detectable in a pulse conductometric experiment. However, the half-life of $7 \mu\text{s}$ implied by the rate constant given above is considerably longer than the value of $<2 \mu\text{s}$ given earlier.⁴ A reexamination of the conductometric behavior seemed in order. Experiments were carried out with an a.c. conductivity apparatus¹⁶ which allows observation of the conductometric signal as soon as $3 \mu\text{s}$ after the pulse. Typical oscilloscope traces for SF_6 saturated solutions (pH ~ 6) are shown in Figure 2 at 5 and $50 \mu\text{s}/\text{cm}$. The first valid point on the faster time scale (Figure 1a) is at $3.5 \mu\text{s}$ after the pulse and corresponds to 1.2 equiv of acid ($\text{H}^+ + \text{F}^-$) per equivalent of e_{aq}^- produced. It is not until about $20 \mu\text{s}$ that the total yield amounts to 2 equiv of acid. On the longer time scale (Figure 1b), the yield approaches the limiting yield^{17,18} of 7–8 equiv of acid as reported by Asmus et al.⁴ Similar curves were obtained in the presence of 0.1 M methanol. Although analysis of these curves for the lifetime of the oxidizing radical is not possible because of the subsequent hydrolysis of SF_4 on a similar time scale, these results are clearly consistent with a lifetime of as long as $7 \mu\text{s}$ as determined from the optical experiments.

The conductometric results reported here differ somewhat from those of Asmus et al.⁴ who indicated that 2 equiv of acid were produced simultaneously with the disappearance of the optical absorption of e_{aq}^- . We note that the quantitative determination of this value is given for 2×10^{-5} M SF_6 solution with certain assumptions regarding the incomplete scavenging of e_{aq}^- at such a low concentration. The present interpretation should not seriously affect the measurements on the hydrolysis of SF_4 .⁴

At this point it is appropriate to consider the nature of the oxidizing intermediate. Spin trapping ESR experiments with the *aci* anion of nitromethane ($\text{CH}_2=\text{NO}_2^-$)¹⁹ were carried out at low concentration of nitromethane in the hope that an intermediate could be detected. No ESR lines attributable to a new adduct were found but strong lines of $^-\text{O}_3\text{SCH}_2\text{NO}_2^-$ did occur. This result shows that SO_3^- is produced at least as a secondary product and that SO_3^{2-} is produced in the hydrolysis of SF_4 as suggested by Asmus et al.⁴ Experiments with 54 mM Cl^- (pH 6.6) or 0.5 M SO_4^{2-} solutions saturated with SF_6 showed approximately 30% conversion to Cl_2^- in the first case ($G \times \epsilon$ at $340 \text{ nm} = 7200$) but no evidence for formation of SO_4^- in the second. Thus the species in SF_6 solution is less strongly oxidizing than is SO_4^- .²⁰ The more rapid reaction with water (as compared with SO_4^-) is thus suggested to have in part the nature of hydrolysis although a net oxidation is probable.⁹ Neither SO_4^- ($k = 8 \times 10^5$)²¹ nor $\cdot\text{SF}_5$ ($k < 2 \times 10^5$)²² reacts rapidly with *tert*-butyl alcohol. An attempt was also made to demonstrate the formation of OH when $\cdot\text{SF}_5$ reacts with water. A low concentration of phenol was used with the hope that the adduct formed from the OH in this latter

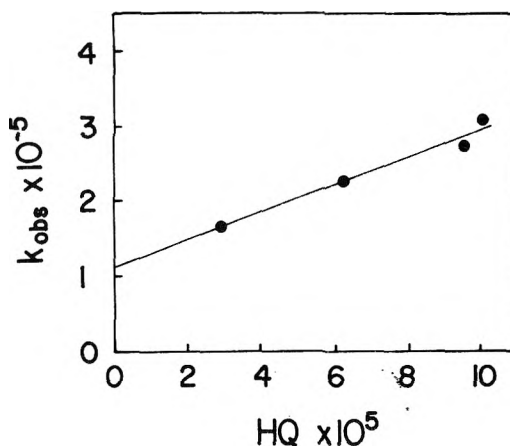


Figure 1. A plot of the pseudo-first-order rate constant for formation of the benzosemiquinone ion as a function of the concentration of hydroquinone in SF_6 saturated solution at pH 6.8. The solution also contained 0.2 M *tert*-butyl alcohol to suppress formation of the semiquinone ion from OH.

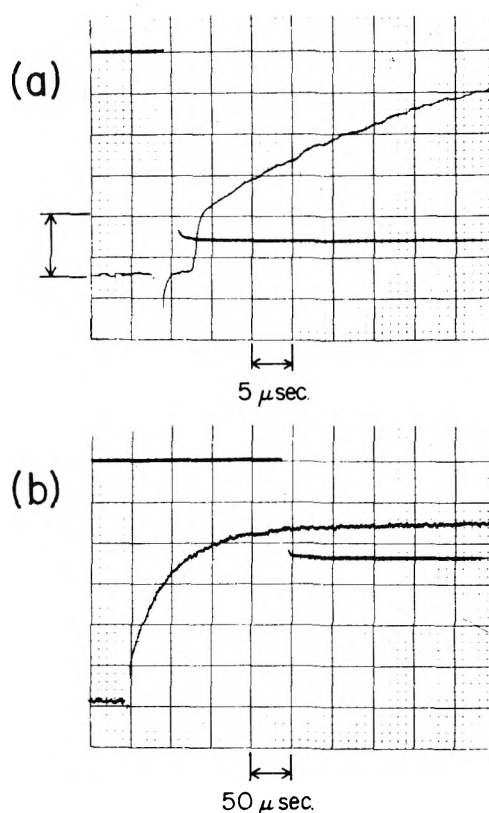


Figure 2. Oscilloscope traces showing the conductivity change (positive going signal) in SF_6 saturated aqueous solution at pH ~ 6.5 . The output from the secondary-emission monitor is represented by the negative-going step. Time bases of 5 (a) and 50 (b) $\mu\text{s}/\text{cm}$ are shown. In (a) the conductivity and dose traces are on the same time base so that the position of the radiolysis pulse ($\sim 1 \mu\text{s}$ long) is as shown. The conductivity detector was gated off for times corresponding to 1.6 to 2.8 cm so that portion of the trace must be ignored. The initial height on trace (a) represented by the arrow corresponds to 1.2 equiv of strong acid per equiv of e_{aq}^- produced. The highest level reached in trace (b) represents 4.8 equiv.¹⁷

reaction could be distinguished from that formed from the primary OH. No conclusions could be drawn, however, because of the overlap of the time scales involved in the two processes. On the basis of the above results, $\cdot\text{SF}_5$ remains the

simplest and most likely candidate for the oxidizing species produced from SF_6 .

The use of SF_6 allows one to produce an oxidizing species without introduction of a reactive compound which could undergo thermal reaction before radiolysis (as $S_2O_8^{2-}$ may do). Because of the low solubility of SF_6 in water, however, its use with various solutes is restricted to conditions where little competition for e_{aq}^- occurs. Use of SF_6 to provide an oxidizing species in other than aqueous solution is more favorable because of higher solubility. For instance, the solubility of SF_6 in methanol and ethanol has been measured to be²³ 22 and 66 mM, respectively. A solution of KBr (10 mM) in methanol was used to demonstrate production of Br_2^- in this solvent. Radiolysis of such a solution of KBr which has been deoxygenated by bubbling with N_2 showed no significant absorption attributable to Br_2^- . When the same solution was saturated with SF_6 at room temperature an absorption peaking at 360 nm was found with a shape similar to that of Br_2^- in water. The absorption at the peak corresponded to a $G \times \epsilon = 21\,000$ after correction for the difference in electron density of water and methanol. If the yield of electron scavenging by SF_6 at this concentration (20 mM) is 1.8 as found by Rząd and Fendler²³ then the value of ϵ for Br_2^- in methanol is calculated to be $11\,700\ M^{-1}\ cm^{-1}$. The value in water has been reported²⁴ to be $12\,000\ M^{-1}\ cm^{-1}$ suggesting that little change occurs upon change of solvent and that efficient production of Br_2^- by SF_6 occurs. This result demonstrates very well the formation of Br_2^- in other than aqueous solution. Studies of the reactivity of Br_2^- with various solutes in methanol could readily be carried out by this method and other applications of the use of SF_6 can readily be imagined.

References and Notes

- (1) Supported in part by the U.S. Energy Research and Development Administration.
- (2) K.-D. Asmus and J. H. Fendler, *J. Phys. Chem.*, **72**, 4285 (1968).
- (3) K.-D. Asmus and J. H. Fendler, *J. Phys. Chem.*, **73**, 1583 (1969).
- (4) K.-D. Asmus, W. Grünbein, and J. H. Fendler, *J. Am. Chem. Soc.*, **92**, 2625 (1970).
- (5) K. N. Jha, T. G. Ryan, and G. R. Freeman, *J. Phys. Chem.*, **79**, 868 (1975).
- (6) E. Hayon, A. Treinin, and J. Willf, *J. Am. Chem. Soc.*, **94**, 47 (1972).
- (7) D. E. Pennington and A. Haim, *J. Am. Chem. Soc.*, **90**, 3700 (1968).
- (8) G. G. Jayson, B. J. Parsons, and A. J. Swallow, *J. Chem. Soc., Faraday Trans. 1*, **9**, 1597 (1973).
- (9) The reaction $Cl + H_2O \rightarrow ClOH^- + H^+$ has more the nature of a hydrolysis. However, the subsequent possible dissociation⁸ of $ClOH^-$ to $Cl^- + OH$ makes the overall reaction an oxidation.
- (10) The computer-controlled radiolysis apparatus described by L. K. Patterson and J. Lilie [*Int. J. Radiat. Phys. Chem.*, **6**, 129 (1974)] was used. Extinction coefficients were measured by comparison with the absorption for $(SCN)_2^-$ in N_2O saturated solution. A total radical yield of 6.0 was used together with $\epsilon_{480} = 7600\ M^{-1}\ cm^{-1}$.
- (11) E. J. Land and M. Ebert, *Trans. Faraday Soc.*, **63**, 1181 (1967).
- (12) K. M. Bansal and R. W. Fessenden, *Radiat. Res.*, in press. In these experiments no intermediate with a lifetime longer than $0.1\ \mu s$ was found. Although fast addition and elimination is always possible, it is most likely, considering the time scale, that direct electron-transfer oxidation occurs.
- (13) The same solution but saturated with N_2O gave an extinction coefficient of only ~ 150 at 430 nm.
- (14) G. E. Adams and B. D. Michael, *Trans. Faraday Soc.*, **63**, 1171 (1967).
- (15) K. B. Patel and R. L. Willson, *J. Chem. Soc., Faraday Trans. 1*, **69**, 814 (1973).
- (16) The basic apparatus described by J. Lilie and R. W. Fessenden [*J. Phys. Chem.*, **77**, 674 (1973)] was used but with added gating circuits to reduce overload by the beam pulse. The response time is $< 1\ \mu s$ but valid data can be taken only to within $3\ \mu s$ of the pulse. Calibration was with CH_2Cl solution [T. I. Balkas, J. H. Fendler, and R. H. Schuler, *J. Phys. Chem.*, **74**, 4497 (1970)] and recording was by means of photographs of the oscilloscope trace (pending rewriting of the computer program for data collection).
- (17) Most of the dose levels used produce sufficient acid that some decrease in yield is observed due to the production of HF rather than the dissociated ions.
- (18) Since H_2SO_3 is produced in addition to six HF the yield of H^+ will be greater than six and will depend on pH.
- (19) D. Behar and R. W. Fessenden, *J. Phys. Chem.*, **76**, 1710 (1972).
- (20) The reaction of SO_4^{4-} with Cl^- has a rate constant of $2.6 \times 10^8\ M^{-1}\ s^{-1}$ (O. P. Chawla, Ph.D. Dissertation, Carnegie-Mellon University, 1973; O. P. Chawla and R. W. Fessenden, *J. Phys. Chem.*, **79**, 2693 (1975)) while the value estimated very roughly for the intermediate in SF_6 solution is about $9 \times 10^5\ M^{-1}\ s^{-1}$.
- (21) J. L. Redpath and R. L. Willson, *Int. J. Radiat. Biol.*, **27**, 389 (1975).
- (22) The value for the rate constant of $\cdot SF_5 + \textit{tert}$ -butyl alcohol is based on the lack of any significant difference in data for $\cdot SF_5 + \textit{tert}$ -butyl alcohol in the presence of 50 or 200 mM *tert*-butyl alcohol.
- (23) S. J. Rząd and J. H. Fendler, *J. Chem. Phys.*, **52**, 5395 (1970).
- (24) D. Zehavi and J. Rabani, *J. Phys. Chem.*, **76**, 319 (1972).

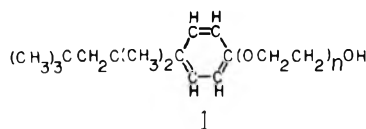
Motion in Nonionic Surfactant Micelles and Mixed Micelles with Phospholipids. A Carbon-13 Spin-Lattice Relaxation Study on *p*-*tert*-Octylphenylpolyoxyethylene Ethers

Anthony A. Ribeiro and Edward A. Dennis*

Department of Chemistry, University of California at San Diego, La Jolla, California 92093 (Received January 22, 1976)

Natural abundance ^{13}C nuclear magnetic resonance spectra of *p*-*tert*-octylphenol and *p*-*tert*-octylphenylpolyoxyethylene ethers (OPE) are presented and the spectral assignments determined from chemical shifts, relative intensities, and nonproton decoupled spectra. One bond coupling constants are also reported. Spin-lattice relaxation times (T_1) were employed to assess the motion of the OPE's (especially Triton X-100) in organic solution and as micelles in aqueous media. These results suggest that free tumbling occurs in organic solution with segmental motion in the polyoxyethylene chain. In aqueous media, these nonionic surfactants form micelles with the alkyl chains in the hydrophobic core and the polyoxyethylene chains in the polar palisade layer. Motion appears maximally restricted at the hydrophobic/hydrophilic interface, and internal and segmental motions of the alkyl and oxyethylene chains appear to be more dominant. ^{13}C chemical shifts, relaxation times, and line widths suggest that the presence of phospholipid in mixed micelles with Triton X-100 does not affect the microenvironment or motional behavior of the micelle.

p-*tert*-Octylphenylpolyoxyethylene ethers (OPE, 1) constitute a major class of nonionic surfactants which are widely



employed as detergents, solubilizers, and emulsifiers. Many of these ethers, in particular Triton X-100 (TX-100) where the average value of n is 9–10, form micelles in aqueous solution^{1,2} and find wide application in biochemical studies involving membranes and protein purification,^{3,4} and lipolytic enzymes.⁵ Our laboratory has been particularly interested in TX-100 since we have shown that it converts phospholipids into mixed micellar structures^{6,7} which serve as an advantageous substrate for studying enzymes of phospholipid metabolism.^{8–10}

^1H nuclear magnetic resonance (NMR) spectra of OPE's with relatively high polyoxyethylene content have been assigned,^{11–13} and chemical shift and relaxation time measurements have been used to investigate the properties of those ethers in solution.^{12–15} The natural abundance ^{13}C NMR spectra of these ethers are assigned here and spin-lattice relaxation times (T_1) are reported. In the ^1H NMR spectrum in organic solvents, the bulk of the polyoxyethylene protons give rise to a single large peak, but in aqueous solution these protons exhibit many overlapping, chemically shifted lines.^{7,12,13} By contrast, ^{13}C NMR allows resolution of several individual carbons in the polyoxyethylene chain of these ethers and an assessment of the mobility along the chain both in organic solvents and in aqueous solution.

^1H NMR has also been used to investigate the interaction of these surfactants with phospholipids, but many phospholipid proton signals overlap signals due to the surfactant protons.^{7,11,13,15} The effect of dimyristoyl phosphatidylcholine on the ^{13}C NMR spectrum of TX-100 is also reported because ^{13}C NMR allows the resolution of groups whose resonance signals overlap in ^1H NMR.

Experimental Section

p-*tert*-Octylphenol (OP, Eastman) was thrice recrystallized from *n*-heptane to give large white needles (mp 85–86 °C).

OPE's included TX-15, TX-35, TX-45, TX-114, and TX-100 manufactured by Rohm and Haas. These commercial preparations are polydisperse¹⁶ with respect to the polyoxyethylene chain and may also have some heterogeneity in the hydrophobic alkylphenol group due to the manufacturing process.¹⁷ Dimyristoyl phosphatidylcholine was obtained from Calbiochem. Deuterated solvents were obtained from Mallinckrodt. Samples in organic solvents were 1.5 M, except for TX-100 samples which were always recorded at concentrations of 0.4 M due to large viscosity changes at higher concentrations in D_2O .¹³

^{13}C NMR spectra were obtained at 25.1 MHz in the Fourier transform mode on a JEOL PFT-100 Fourier transform system equipped with a Nicolet 1085 computer and disk and operating at a field strength of 23 kG. Samples were locked onto the internal deuterium of the solvent. Proton decoupling was employed except where indicated. The probe temperature was 40 ± 1 °C as monitored with a small thermometer or thermocouple inserted into an NMR sample tube containing water. The Fourier transform spectra were usually obtained with a spectral window of 5000 Hz and with pulse recycling times of at least 3 times the longest T_1 value of the sample. Relaxation times were measured by the $180^\circ - \tau - 90^\circ$ sequence of Vold et al.¹⁸ Peak heights (I_τ) were hand measured on expanded spectra of the appropriate resonance lines and the T_1 values obtained from least-squares plots of $\log(I_\infty - I_\tau)$ vs. τ . All plots were found to be linear, except where noted. Where indicated, separate sets of data were obtained for protonated and nonprotonated carbons. The T_1 runs were generally made with 4096 channels, yielding 2048 real points after Fourier transformation.

Measurements on samples in D_2O were made in 10-mm NMR sample tubes (Wilmad) which were outfitted with a coaxial insert containing CCl_4 when chemical shift determinations were made. These samples were not degassed. NMR measurements on samples in organic solvents were made in 10-mm custom-made thick-walled NMR sample tubes containing a capillary constriction. The constriction prevents vortexing upon spinning of the sample and minimizes diffusion between gas and liquid phases.¹⁹ TMS was employed as an internal standard. For relaxation time measurements, these samples were thoroughly degassed by five–six freeze–pump–thaw cycles.

TABLE I: Observed Chemical Shifts and Proposed Assignment for ^{13}C NMR Spectra of OP and OPE a , b

Compd	n	Solvent	Alkyl region						Oxyethylene region ^c						Phenol region								
			a	b	c	d	e	f	g	h	i	j	k	l	m	n	o	p					
OP		CDCl ₃	31.7	31.8	32.3	38.0	57.1	61.0	67.2	69.6	70.2	70.4	70.6	70.6	70.6	70.6	70.6	71.8	71.8	114.9	127.2	142.5	152.6
TX-15 ^d	1	CDCl ₃	31.6	31.7	32.2	37.8	56.9	61.3	67.1	69.6	70.2	70.4	70.6	70.6	70.6	70.6	70.6	71.8	71.8	113.7	126.9	142.3	156.2
TX-35	3	CDCl ₃			32.2	37.8	56.9	61.3	67.1	69.6	70.2	70.4	70.6	70.6	70.6	70.6	70.6	71.8	71.8	113.7	126.8	142.1	156.2
TX-45	5	CDCl ₃			31.7	37.7	56.9	61.2	67.2	69.6	70.2	70.4	70.6	70.6	70.6	70.6	70.6	71.8	71.8	113.7	126.7	141.8	156.3
TX-114	7-8	CDCl ₃			31.7	37.7	56.9	61.2	67.2	69.6	70.2	70.4	70.6	70.6	70.6	70.6	70.6	71.8	71.8	113.7	126.7	141.8	156.3
TX-110	9-10	CDCl ₃			31.7	37.9	57.0	61.6	67.2	69.7	70.3	70.5	71.0	71.0	71.0	71.0	71.0	72.6	72.6	113.8	126.9	142.2	156.3
		CD ₃ OD			31.7	37.9	57.4	61.4	67.9	70.2	70.6	70.8	70.8	70.8	70.8	70.8	70.8	72.9	72.9	114.3	127.4	142.5	157.2
		D ₂ O			31.7	37.7	56.8	60.4	67.1	69.7	70.6	70.6	70.6	70.6	70.6	70.6	70.6	71.8	71.8	113.8	126.6	141.5	156.3

^a In CDCl₃ and in CD₃OD shifts are referenced to internal TMS₁ in D₂O, shifts are referenced to external CCl₄ in a coaxial NMR tube and converted by $\delta\text{TMS} = \delta\text{CCl}_4 + 96.0$ ppm. See p 49 of Strothers.²⁰ ^b Parentheses have been placed around peaks a and b and brackets around peaks c and d as the assignments within each of these pairs of peaks may be the reverse. Reasons for preferring the assignments shown here are given in the Discussion. ^c Peak j is the major oxyethylene carbon signal; peaks i and k are shoulders on this peak and these shoulders are not always resolvable. ^d The oxyethylene signals for TX-15 (OPE with n = 1) are listed as peaks f and l. Note that the OPE's used are polydisperse so that other observed small, resonance lines in the phenol and oxyethylene regions of TX-15 (Figure 1) contain contributions from OP and OPE's with more than one oxyethylene group.

TABLE II: Observed Relative Intensities for ^{13}C Spectra of OP and OPE and Their Oxyethylene Content^a

Compd	Pulse recycling time, s	Alkyl region						Oxyethylene region						Phenol region					
		a/b	c	d	e	f	g	h	i/j/k	l	m	n	o	p	N(expt) ^c	N(theory) ^d			
OP	60	4.7	1.2	0.97	0.88	0.88	0.82	1.0	2.4	0.94	1.9	2	1.00	1.1	0.91	1			
TX-15	30	4.3	1.2	0.79	0.77	0.88	0.82	1.0	2.4	0.81	1.9	2	0.73	0.77	0.91	1			
TX-35	30	4.5	1.1	0.84	0.78	1.0	0.88	1.0	2.4	0.81	1.9	2	0.83	0.84	3.0	3			
TX-35	35	4.9	1.2	0.91	0.84	1.1	0.88	1.0	6.5	1.02	1.9	2	0.85	0.90	5.2	5			
TX-114 ^b	4	4.4	1.1	0.64	0.75	1.0	0.85	0.99	12.0	1.06	2.0	2	0.45	0.45	8.0	7-8			
TX-100	95	4.7	1.0	0.94	0.66	0.71	0.56	0.84	18.0	0.83	1.9	2	0.84	0.91	10.0	9-10			

^a Peak heights (I_j) relative to peak n which was assumed to be representative of two carbons. ^b Low intensities for nonprotonated carbons are presumably due to the short delay time employed vs. long T₁ relaxation times. ^c Average oxyethylene content calculated from ^{13}C relative intensities. ^d Average oxyethylene content specified by Rohm and Haas Co. product literature.

TABLE III: One Bond ^{13}C - ^1H Coupling Constants^a

Compd	Alkyl region						Oxyethylene region						Phenol region					
	a/b	c	d	e	f	j	l	m	n	o	p	N(expt) ^c	N(theory) ^d					
OP	124.5(Q)	(S)	(S)	120.9(T)	142.5(T)	141.0(T)	143.1(T)	158.3(D)	155.9(D)	(S)	(S)							
TX-15	125.1(Q)	(S)	(S)	125.3(T)	142.5(T)	141.0(T)	143.1(T)	159.0(D)	155.9(D)	(S)	(S)							
TX-100	125.7(Q)	(S)	(S)					158.7(D)	155.6(D)	(S)	(S)							

^a $J(^{13}\text{C}-^1\text{H})$ given in Hertz for nondecoupled spectra in CDCl₃. Splitting patterns are Q = quartet, T = triplet, D = doublet, and S = singlet.

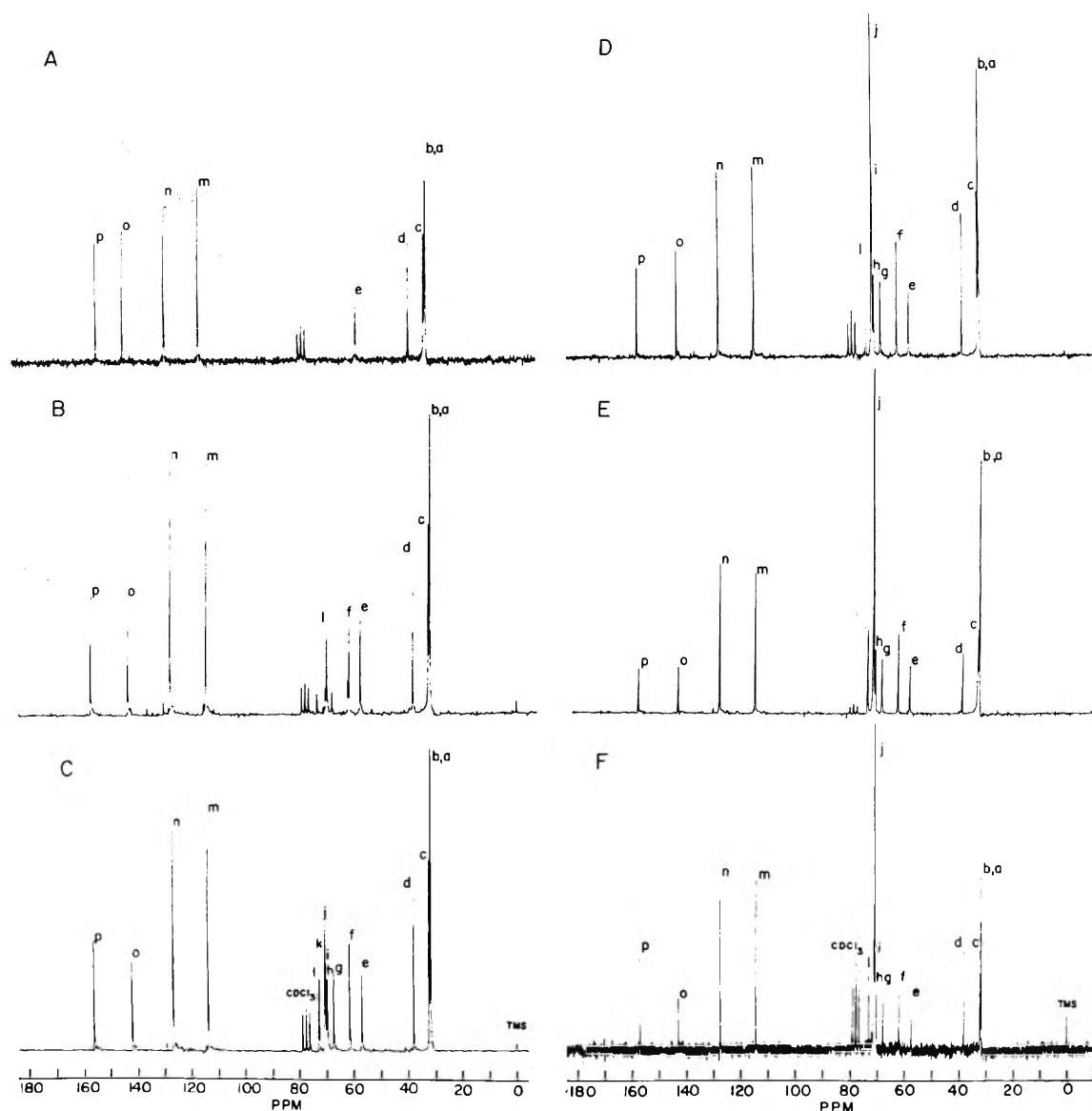


Figure 1. Natural abundance ^{13}C NMR spectra in CDCl_3 -1% TMS are shown and the assignments are listed in Table I. The spectra were obtained under the following conditions:

Spectrum	Compound	Scans	Pulse recycle time, s	Exponential broadening, Hz	Approx rel signal amplitude
A	OP	128	30	0.39	0.7
B	TX-15	128	30	0.39	1
C	TX-35	128	30	0.78	1
D	TX-45	132	35	0.39	1
E	TX-114	128	4	0.39	0.75
F	TX-100	160	35	None	0.5

Results

^{13}C NMR spectra of OP and various OPE's in CDCl_3 are shown in Figure 1 and of TX-100 in CD_3OD and D_2O in Figure 2. Chemical shift data are listed in Table I along with the proposed spectral assignment. It is clear that OP does not show any NMR lines in the region of 60–73 ppm; thus resonance lines in this region for the ethers can be attributed to polyoxyethylene carbons. For the five kinds of alkyl carbons, there appear to be only four obvious resonance lines. This is because the alkyl region at about 31.7 ppm actually consists

of two overlapping lines, peaks a and b, which can be resolved as shown for OP and TX-15 in Figure 3. These peaks were not generally resolvable for the higher homologues. Finally, in the phenyl region, the ^{13}C NMR chemical shifts for peaks m and p appear about 1.2-ppm upfield and 3.7-ppm downfield, respectively, upon substitution of the phenol hydroxyl with oxyethylene units.

The ^{13}C chemical shifts do not appear to change significantly among the OPE's consistent with observations of ^1H chemical shifts.¹² For TX-100, large changes are not observed

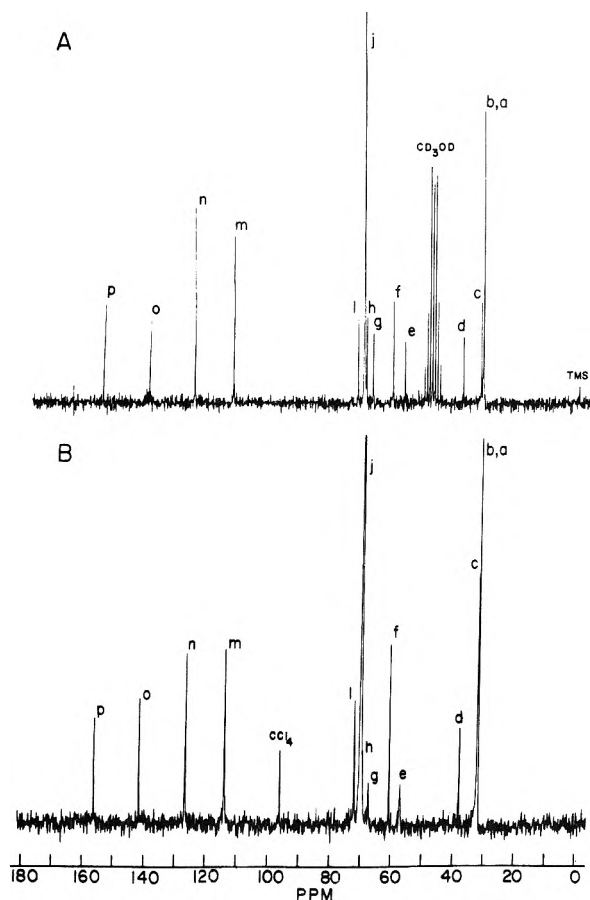


Figure 2. Natural abundance ¹³C NMR spectra acquired with 30-s pulse recycle time, broadened exponentially by 0.1 Hz, and displayed with identical signal amplitudes for 0.4 M TX-100 in (A) CD₃OD containing TMS, 150 scans (B) D₂O, 256 scans. Assignments are listed in Table I.

between the ¹³C NMR spectra in CDCl₃ and CD₃OD. If the differences between internal and external reference standards are not large, it appears that the alkyl and phenol regions of TX-100 have very similar chemical shifts both in organic solvents and in micellar form in D₂O. This finding is consistent with a similar local microenvironment for these hydrophobic groups in micelles and in organic solution. By contrast, except for peak g assigned to the oxymethylene group adjacent to the phenyl ring, all of the hydrophilic oxyethylene carbons of micellar TX-100 in D₂O appear to shift upfield by about 1 ppm from their positions in CDCl₃.

Relative carbon intensities are listed in Table II and are approximately proportional to the number of nuclei, although this need not be the case for ¹³C spectra due to differing NOE on each carbon and insufficient pulse recycling times relative to the T₁ values. The polyoxyethylene content calculated from these carbon intensities are reasonably consistent with the manufacturer's specifications (Table II). Nondecoupled spectra were acquired by the alternate pulse method of Gansow and Schittenhelm²¹ as shown for OP in Figure 4. Peaks c, d, o, and p are retained as singlets while peak e is split into a triplet and peaks a/b into two overlapping quartets. True one-bond coupling constants J_{13C-1H} derived from these experiments are listed in Table III and observed values of J_{13C-1H} correspond to expected values for the various carbon groups.²⁰

Spin-lattice relaxation times (T₁) in various samples are listed in Table IV and plots of NT₁ values for the protonated carbons against the molecular axis are shown in Figure 5. The

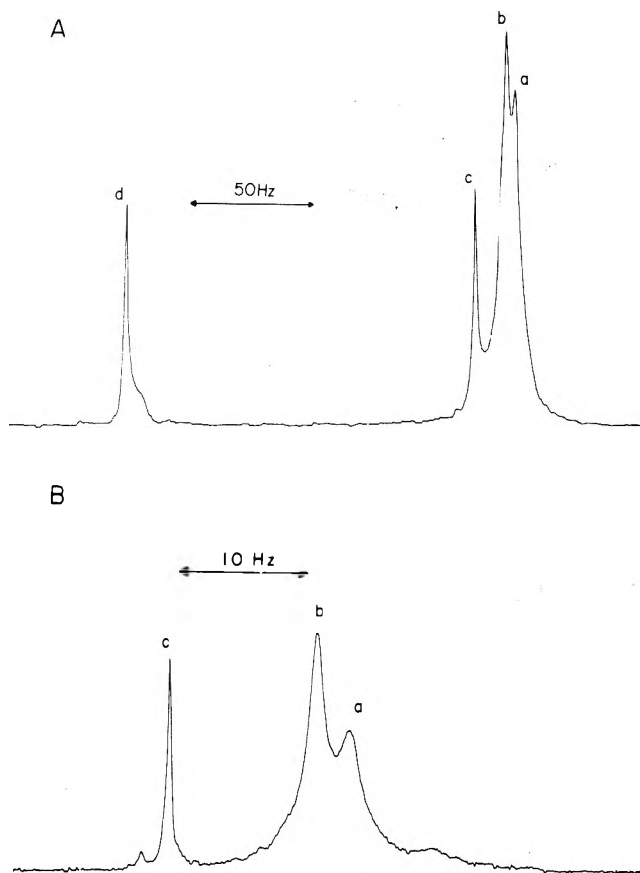


Figure 3. Natural abundance ¹³C NMR spectra in CDCl₃-1% TMS for the approximate chemical shift ranges of (A) OP, about 30-40 ppm and (B) TX-15, about 29-33 ppm. No exponential broadening was employed.

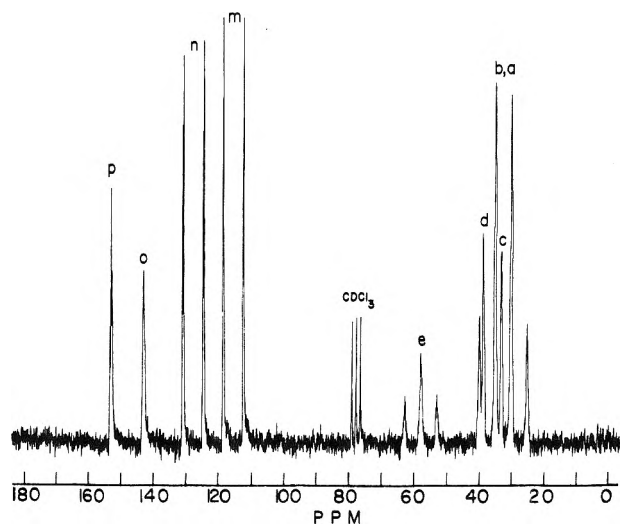


Figure 4. Natural abundance ¹³C nondecoupled NMR spectrum in CDCl₃-1% TMS of OP acquired by the alternate pulse NMR method²¹ with 128 scans and 60-s recycle times.

longest times are associated with peaks c, d, o, and p and are consistent with the assignment of the resonance lines as nonprotonated carbons from the nondecoupled spectra. In organic solvents, the relaxation times appear similar for OP, TX-15, and TX-35. They are somewhat longer for TX-100 but this is probably due to a decrease in concentration by a factor of about 4. Only small differences are observed for the T₁

TABLE IV: ^{13}C Spin-Lattice Relaxation Times (T_1)^a

Compd	Solvent	Alkyl region										Oxyethylene region						Phenol region					
		Pulse recycling										f	g	h	i	j	k	l	m	n	o	p	
		ab	bb	c	d	e																	
OP	CDCl_3	15	0.52	1.1	(9.2)	(6.7)	0.49										0.98	0.96	(11)	(7.1)			
TX-15	CDCl_3	12	0.95	0.95	(7.6)	(6.8)	0.49	0.90									0.56	1.1	(11)	(13)			
TX-35	CDCl_3	24	0.75	0.75	7.1	4.8	0.83	0.97	0.46	0.51	0.78	0.67	0.67	0.67	0.67	0.67	1.2	0.71	0.69	8.1			
TX-100	CDCl_3	35	1.0	1.0	10	8.7	0.66 ^c	3.1	0.93 ^c	1.0 ^c	1.5	1.4	1.4	1.4	1.4	1.4	2.8	1.5 ^c	1.4 ^c	(14)			
	CD_3OD	4	0.42	1.3	(14) ^d	8.0 ^d	0.70	3.4 ^d	0.97	0.93	0.93	1.6	1.6	1.6	1.6	1.6	3.3 ^d	1.7	1.5	(11) ^d			
	D_2O	4	0.09	0.41	2.0 ^e	2.1 ^e	0.10	1.2 ^e	0.10	0.10	0.10	0.45	0.45	0.45	0.45	0.45	0.96	0.15	0.15	1.8 ^e			

^a T_1 values reported in seconds. On the assumption that relaxation processes follow a strict exponential decay, the ideal T_1 measurement requires $5T_1$ recycling times. Many of the T_1 values presented satisfy this requirement. At $3T_1$ transient magnetizations equilibrate to about 95% of equilibrium value. Delay times below $3T_1$ are not sufficient for return to equilibrium magnetizations, and apparent T_1 values obtained from a semilog plot are low. Parentheses are placed around those apparent T_1 values and these serve as lower limits on the correct values. ^b Peaks a and b overlap as shown in Figure 3. For T_1 determinations, it was necessary to measure intensities as though there was only one peak. Plots of $\log(I_\infty - I_r)$ vs. τ showed a small deviation from linearity at low τ values suggesting the existence of a long and a shorter component. Where possible, curve stripping²² was employed to obtain two T_1 values. The dominant component, which yielded the longer T_1 value, is listed under peak b on the basis of the differences of the ^1H T_1 values for the dimethyl and *tert*-butyl groups, although this does not constitute definitive evidence for this assignment. ^c 4-s pulse recycling time. ^d 35-s pulse recycling time. ^e 15-s pulse recycling time.

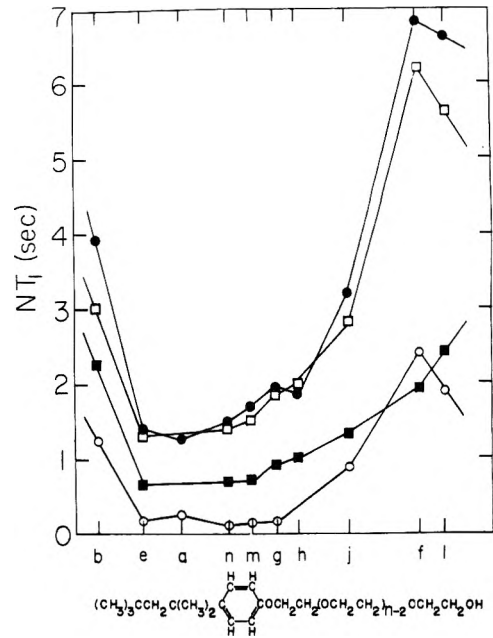


Figure 5. A plot of NT_1 values of protonated carbons of OPE against the long molecular axis of the OPE molecule: TX-35 in CDCl_3 (■) and TX-100 in CDCl_3 (□), CD_3OD (●), and D_2O (○).

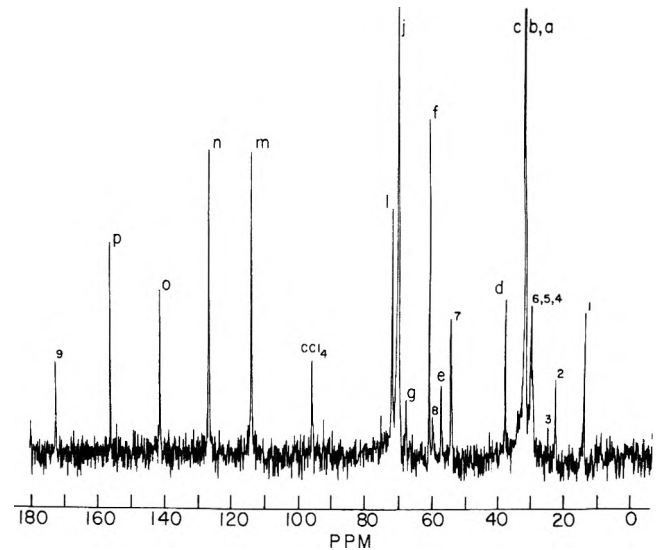
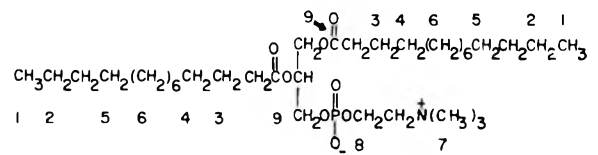


Figure 6. Natural abundance ^{13}C NMR spectrum of 0.4 M TX-100 and 0.133 M dimyristoyl phosphatidylcholine in D_2O . TX-100 resonance lines are assigned in Table I; resolvable phospholipid peaks are indicated as follows:



values of TX-100 in the two organic solvents, but in aqueous media where micelles are present, the relaxation times are decreased consistent with ^1H T_1 results.¹³ The NT_1 plots suggest a mobility gradient exists in the long chain OPE's from the phenyl ring to the terminal oxyethylene unit (see Discussion).

The ^{13}C NMR spectrum of mixed micelles of dimyristoyl phosphatidylcholine and Triton X-100 is shown in Figure 6.

TABLE V: Effect of Dimyristoyl Phosphatidylcholine (PC) on ^{13}C Parameters of TX-100 Micelles^a

Carbon peak	Chemical shifts, ppm		T_1 relaxation times, s		Observed line widths, Hz	
		+ PC		+ PC		+ PC
a			0.09	0.08		
b	31.7	31.6	0.40	0.34	(3.3)	(3.5)
c	32.0	32.0	2.0 ^b	1.8 ^b	1.1	0.95
d	37.8	37.6	2.1 ^b	2.0 ^b	1.0	1.1
e	56.8	56.9	0.10	0.07	14	14
f	60.4	60.4	1.2	1.3	2.0	2.6
g	67.1	67.2	0.10			
j	69.7	69.7	0.45	0.45	(7.5)	(7.4)
l	71.8	71.8	0.96	1.05	3.2	3.8
m	113.8	113.9	0.15	0.17	5.3	5.8
n	126.6	126.6	0.15	0.17	5.5	5.3
o	141.5	141.5	1.8 ^b	1.7 ^b	1.7	2.3
p	156.3	156.4	2.0 ^b	1.8 ^b	1.1	1.7

^a Chemical shifts listed downfield from TMS and calculated from CCl_4 as in Table I. T_1 values were generally obtained with a pulse recycling time of 4 s. Line widths were obtained from spectra at a digital resolution of about 0.25 Hz. Parentheses have been placed around apparent line width values for resonance lines with overlapping resonances. ^b 15-s pulse recycling time.

Data for micelles of TX-100 in D_2O are compared with similar data for mixed micelles in Table V. Chemical shifts, T_1 relaxation times, and line widths of the surfactant resonance lines are not significantly different in mixed micelles and pure Triton micelles.

Discussion

¹³C NMR Assignment of OPE. Evidence is presented in this paper for the ¹³C spectral assignment of various OPE's. ¹³C chemical shifts due to substituents are largely additive, and predictions of ¹³C chemical shifts on the basis of empirical correlations with model compounds are usually successful.²³⁻²⁵ The assignment of the p-tert-octyl region is made by comparison with reported ¹³C shifts of model compounds such as 2,2,4-trimethylpentane and 2,2-dimethylhexane,²⁴ N-methyl-1,1,3,3-tetramethylbutylamine and 1,1,3,3-tetramethylbutylamine,²⁶ 3-tert-butyl-2,2,5,5,7,7-hexamethyloctane and 2,2,4,4,7,7,9,9-octamethyldecane,²⁷ and calculations of expected shifts from the parameters of Lindemann and Adams²⁴ for alkanes. Specifically, peaks (a,b), (c,d), and e can be assigned on the basis of the expected shifts, spectral intensities, T_1 values, nondecoupled spectra, and previous assignments in the model compounds. However, definitive differentiation of the carbon signals in the peak pairs (a,b) and (c,d) cannot be made from the data available. However, the expanded spectra (Figure 3) might suggest that the peak which appears somewhat larger and narrower (peak b) corresponds to the tert-butyl group, and the other peak (peak a) to the dimethyl group.

Also, the peak pair (c,d) cannot be assigned unequivocally between the two alkyl quaternary carbon groups. Perhaps, the preferred assignment would be that which is analogous to 1,1,3,3-tetramethylbutylamine²⁶ assuming that the phenyl group shifts the dimethyl quaternary carbon downfield as does the amino group. Recently, Ernst²⁸ has suggested that alkane shift parameters can be used to predict shifts of branched alkyl chains in alkylbenzenes. Using this assumption, calculations with the Lindemann and Adams²⁴ terms for alkanes indicate expected shifts of 32.1 and 37.4 ppm for the tert-butyl and dimethyl quaternary carbons, respectively. However, it should be noted that in the branched alkanes 3-tert-2,2,5,5,7,7-hexamethyloctane and 2,2,4,4,7,7,9,9-octamethyldecane, the assignments of Mendenhall et al.²⁷ for the interior dimethyl quaternary carbons and the tert-butyl qua-

ternary carbons are the reverse of that predicted by the Lindemann and Adams²⁴ parameters.

In the phenol region, peaks (m,n) and peaks (o,p) can be assigned from the data given in the Results section and each pair can be differentiated by the changes in chemical shift in going from OP to OPE and by the known substituent effects of groups on phenyl rings as documented by Levy and Nelson²⁵ and Stothers²⁰ and by considering shifts observed in phenol, anisole, and cumene.

The main oxyethylene band absorbs at about 70.5 ppm and this observation agrees with reported shifts of about 71 ppm for interior oxymethylene groups in n-propyl ether,²⁰ glyme and ethylene glycol monobutyl ether,²⁹ and crown ethers.³⁰ Peaks f and l are tentatively assigned to the terminal oxyethylene unit by analogy to the oxyethylene unit in ethylene glycol monobutyl and monoethyl ethers²⁹ and the observation that these two peaks have the longest T_1 values of the oxyethylene carbons. Peaks g and h are tentatively assigned to the first oxyethylene unit adjacent to the phenyl ring. This assignment is suggested as these two peaks have the shortest T_1 values of the oxyethylene carbons. Also, the methyl carbon in an aliphatic methyl ether absorbs at 58.4–58.6 ppm while the methyl carbon in anisole absorbs at 54.7 ppm²⁹ suggesting that the phenyl group causes a small upfield shift of about 3.7–3.9 ppm. This shift is close to the 3.2-ppm upfield shift of peak g from the main oxyethylene band, peak j.

Segmental Motion of OPE. Protonated carbon nuclei are generally dominated by dipole-dipole interactions between the carbons and their directly attached protons. If we assume that this is the case for the OPE's,³¹ and that the molecular motion is sufficiently fast so that the "extreme narrowing limit" applies, then the effective correlation time (τ_{eff}) for motion can be related to the observed T_1 values by³²⁻³⁴

$$\frac{1}{NT_1} = \frac{\hbar^2 \gamma_H^2 \gamma_C^2}{r_{C-H}^6} \tau_{\text{eff}} \quad (1)$$

where N is the number of directly attached protons, γ_H and γ_C are the gyromagnetic ratios of the proton and carbon nuclei, \hbar is Planck's constant, and r_{C-H} is the carbon-hydrogen bond length. When a molecule is rigid and undergoing isotropic motion, τ_{eff} is then the correlation time for molecular reorientation. If internal rotation occurs or the molecular reorientation is anisotropic, then τ_{eff} would correspond to an average correlation time for the several motions.^{32,34}

Plots of NT_1 vs. the molecular axis of OPE in Figure 5 suggest that the slowest motions occur in the alkyl methylene, dimethyl, and protonated phenyl carbons, since larger NT_1 values occur for the other groups. This result agrees with previous ^1H NMR relaxation time values.^{12,13,15} In organic solvents, the NT_1 values of the alkyl methylene and phenyl ring carbons are approximately identical and presumably reflect molecular tumbling. Equation 1 then indicates a correlation time of about 3×10^{-11} s for the tumbling of TX-100 in organic solvents.

The *tert*-butyl methyl carbons and the carbons of the polyoxyethylene group exhibit higher NT_1 values than the protonated ring carbons and presumably include contributions from internal motions. The NT_1 values for the dimethyl carbons also suggest some internal motions of those methyl groups, but this should not be viewed as definitive since curve stripping was employed to obtain those values. The observed trends in the NT_1 values appear quite reasonable as Corey-Pauling-Koltung models suggest that the alkyl methylene and the dimethyl groups are hindered between the *tert*-butyl group and the phenyl ring. On the other hand, the *tert*-butyl methyl carbons at one end of the molecule and the carbons of the long oxyethylene chain appear quite free to undergo internal motions.

For the polyoxyethylene chain, "zig-zag" and "meander" configurations have been previously suggested.³⁵ Presumably the NT_1 values monitor *trans*-*gauche* rotations³⁶ of the individual polyoxyethylene groups. In addition, however, the NT_1 values indicate a gradient in segmental motion in the flexible polyoxyethylene chain occurs, analogous to that which occurs in the alkyl chain of liquid decanol.³⁷ The degree of segmental motion may increase as the polyoxyethylene chain length increases, but our data are not definitive on this point.

Influence of Micelle Formation on Molecular Motion. The exact state of aggregation of OPE's in CD_3OD and CDCl_3 is not known. The nonylphenylpolyoxyethylene ethers may be monomeric in CH_3OH ,³⁸ while two reports suggest that in ethanol-water mixtures, no micelle formation by polyoxyethylene lauryl alcohol and a number of other nonionic surfactants occurs.^{39,40} In other organic solvents such as decane, these nonionic surfactants may form inverse micelles.^{16,38}

In water, TX-100 is known to form micelles^{1,2} of molecular weight about 90 000.⁴¹ Upon micelle formation, these amphipathic nonionic surfactant molecules are thought to pack with their hydrophobic alkyl and all or part of the phenyl groups forming an apolar region in the interior of the micelle and with the polar polyoxyethylene chains forming an exterior "sheath" or "palisade layer" containing a significant amount of water. Extensive ^1H NMR studies^{12,13} have supported these ideas. A significant decrease in all NT_1 values of the protonated carbons and the T_1 values of the nonprotonated carbons is observed for TX-100 in micelles in D_2O as compared to the organic solutions. This result appears quite reasonable since in the micelle each molecule would be somewhat restricted from free tumbling, although the same pattern in relative mobility should be retained.

In micelles, the site of maximal restriction occurs in the phenyl group and the phenyl-adjacent oxymethylene carbon, as they exhibit the largest reductions in NT_1 . These groups would constitute the hydrophobic/hydrophilic interface in these nonionic micelles. The hydrophobic alkyl groups and the hydrophilic oxyethylene groups, however, may still exhibit internal motions as much smaller reductions in NT_1 are observed. In fact, the NT_1 value of the *tert*-butyl methyl carbons is 8.1 times the NT_1 of the protonated ring carbons, suggesting

that methyl rotation is relatively more dominant than the molecular tumbling. This situation approaches the theoretical value of 9 for the fast internal motion of methyl rotors on the reorienting axis of a molecule.^{33,34} Similarly, upon micelle formation the local segmental motions of the flexible oxyethylene chain become relatively more dominant. The segmental motion appears most restricted in groups near the phenyl ring at the hydrophobic/hydrophilic interface. Less restrictions occur in the terminal groups at the periphery of the nonionic micelle. Previous ^1H T_1 measurements^{12,13} suggested that such a gradient in mobility existed in the polyoxyethylene layer of these micelles; however, overlapping lines prevented a definitive conclusion.

Hence, the ^{13}C NMR studies suggest that in nonionic micelles of the alkylphenylpolyoxyethylene ethers, segmental motions in both the oxyethylene and the alkyl chains might occur, from the interface outward along the polar chain and inward along the hydrophobic chain. This is quite different from that which occurs in micelles formed from ionic surfactants which contain small charged polar head groups and exhibit segmental motion only in the long alkyl chains.⁴²⁻⁴⁴

Heterogeneity and Polydispersity of Surfactant. The ^{13}C NMR spectrum of TX-15 shows several small peaks in addition to the main resonance lines. These peaks are presumably due to the heterogeneity of residual OP, OPE₁, and multimeric oxyethylated adducts in the commercial preparation of TX-15 used. The presence of these compounds has been confirmed by thin-layer chromatography.⁴⁵

When the average OPE chain length is increased, the small peaks are no longer detectable. This is expected as commercial preparations of longer OPE's should be polydisperse¹⁶ in the polyoxyethylene chain and not heterogeneous. The NMR experiments here then observe only the average ^{13}C NMR signals for the oxyethylene resonance lines of all the various polyoxyethylene adducts in any one sample. It should be clear that the polydispersity of the oxyethylene chain should not affect the ^{13}C NMR assignment or the trends of motion of these ethers, and data obtained (particularly on long chain ethers) should be indicative of the same parameters for monodisperse surfactants.

Effect of Phospholipids on Triton X-100 Micelles. In our previous work, we found that excess TX-100 converts phospholipid bilayers into mixed micellar structures based on ^1H NMR^{7,11} and gel chromatographic studies.⁶ The ^{13}C data (Table V) suggest that the presence of phospholipid in mixed micelles with TX-100 does not greatly affect the microenvironment of the surfactant micelles, nor the motional behavior of individual groups in the micelle. This finding extends the previous ^1H NMR relaxation data^{13,15} to other nonoverlapping resonance signals. An evaluation of the phospholipid peaks by ^{13}C NMR and the finding that the phospholipid in mixed micellar structures is in a less restricted physical state than in sonicated vesicles or unsonicated multibilayers is discussed elsewhere.⁴⁶

Acknowledgment. We are grateful to Dr. David Dalrymple, Department of Chemistry, University of Delaware, for the use of his ^{13}C retrieval and assignment of chemical environments and shifts (RACES) search program⁴⁷ which was employed in our literature search of model compounds. We also thank Mr. Stacey Zones for his help in recrystallizing OP and Dr. John Wright for aid in the operation of the PFT-100 NMR system. This work was supported by National Science Foundation Grant No. BMS-75-03560. The UCSD NMR/MS Research Resource Center was operated by National Institutes of

Health Grant No. RR-00,708. A.A.R. was supported as a Public Health Service Predoctoral Trainee of the National Institute of General Medical Sciences (GM-1045).

References and Notes

- (1) E. H. Crook, D. B. Fordyce, and G. F. Trebbi, *J. Phys. Chem.*, **67**, 1987 (1963).
- (2) A. Ray and G. Némethy, *J. Am. Chem. Soc.*, **93**, 6787 (1971).
- (3) A. Helenius and K. Simons, *Biochim. Biophys. Acta*, **415**, 29 (1975).
- (4) S. Razin, *Biochim. Biophys. Acta*, **285**, 241 (1972).
- (5) E. A. Dennis, *J. Supramol. Struct.*, **2**, 682 (1974).
- (6) E. A. Dennis, *Arch. Biochem. Biophys.*, **165**, 764 (1974).
- (7) A. A. Ribeiro and E. A. Dennis, *Biochim. Biophys. Acta*, **332**, 26 (1974).
- (8) R. A. Deems, B. R. Eaton, and E. A. Dennis, *J. Biol. Chem.*, **250**, 9013 (1975).
- (9) T. G. Warner and E. A. Dennis, *J. Biol. Chem.*, **250**, 8003 (1975).
- (10) E. A. Dennis, *Arch. Biochem. Biophys.*, **158**, 485 (1973).
- (11) E. A. Dennis and J. M. Owens, *J. Supramol. Struct.*, **1**, 165 (1973).
- (12) F. Podo, A. Ray, and G. Némethy, *J. Am. Chem. Soc.*, **95**, 6164 (1973).
- (13) A. A. Ribeiro and E. A. Dennis, *Biochemistry*, **14**, 3746 (1975).
- (14) A. A. Ribeiro and E. A. Dennis, *Chem. Phys. Lipids*, **12**, 31 (1974).
- (15) A. A. Ribeiro and E. A. Dennis, *Chem. Phys. Lipids*, **14**, 193 (1975).
- (16) P. Becher in "Nonionic Surfactants, Surfactant Science Series", Vol. 1, M. J. Schick, Ed., Marcel Dekker, New York, N.Y., 1967, pp 478-515.
- (17) C. R. Enyeart in ref 16, pp 44-85.
- (18) R. L. Vold, J. S. Waugh, M. P. Klein, and D. E. Phelps, *J. Chem. Phys.*, **48**, 3831 (1968).
- (19) T. C. Farrar and E. D. Becker, "Pulse and Fourier Transform NMR", Academic Press, New York, N.Y., 1971, p 43.
- (20) J. B. Stothers, "Carbon-13 NMR Spectroscopy", Academic Press, New York, N.Y., 1972.
- (21) O. A. Gansow and W. Schittenhelm, *J. Am. Chem. Soc.*, **93**, 4294 (1971).
- (22) J. H. Noggle and R. E. Schirmer, "The Nuclear Overhauser Effect: Chemical Applications", Academic Press, New York, N.Y., 1971, pp 233-235.
- (23) D. M. Grant and E. G. Paul, *J. Am. Chem. Soc.*, **86**, 2984 (1964).
- (24) L. P. Lindemann and J. Q. Adams, *Anal. Chem.*, **43**, 1245 (1971).
- (25) G. C. Levy and G. L. Nelson, "Carbon-13 Nuclear Magnetic Resonance for Organic Chemists", Wiley-Interscience, New York, N.Y., 1972.
- (26) H. Eggert and C. Djerassi, *J. Am. Chem. Soc.*, **95**, 3710 (1973).
- (27) G. D. Mendenhall, D. Griller, D. Lindsay, T. T. Tidwell, and K. U. Ingold, *J. Am. Chem. Soc.*, **96**, 2441 (1974).
- (28) L. Ernst, *Tetrahedron Lett.*, **35**, 3079 (1974).
- (29) L. F. Johnson and W. C. Jankowski, "Carbon-13 NMR Spectra", Wiley-Interscience, New York, N.Y., 1972.
- (30) M. Fedarko, *J. Magn. Resonance*, **12**, 30 (1973).
- (31) For the nonprotonated carbons, we observe line widths of about 0.45 Hz in the alkyl chain and 0.5-0.6 Hz in the phenyl ring (at a digital resolution of 0.25 Hz), suggesting no obvious chemical shift anisotropy in these molecules. Also, the intensities suggest full NOE for all carbons in OPE. These observations imply that the T_1 values of the nonprotonated carbons are also interpretable in terms of dipole-dipole interactions.
- (32) K. F. Kuhlmann, D. M. Grant, and R. K. Harris, *J. Chem. Phys.*, **52**, 3439 (1970).
- (33) A. Allerhand, D. Doddrell, and R. Komoroski, *J. Chem. Phys.*, **55**, 189 (1971).
- (34) D. Doddrell, V. Glushko, and A. Allerhand, *J. Chem. Phys.*, **56**, 3683 (1972).
- (35) M. Rosch in ref 16, pp 753-792.
- (36) Y. Takahashi and H. Tadokoro, *Macromolecules*, **6**, 672 (1973).
- (37) D. Doddrell and A. Allerhand, *J. Am. Chem. Soc.*, **93**, 1558 (1971).
- (38) A. Ray, *Nature (London)*, **231**, 313 (1971).
- (39) P. Becher, *J. Colloid Sci.*, **20**, 728 (1965).
- (40) H. Sasaki and N. Sata, *Koll. Z.*, **199**, 49 (1964).
- (41) L. M. Kushner and W. D. Hubbard, *J. Phys. Chem.*, **58**, 1163 (1954).
- (42) E. Williams, B. Sears, A. Allerhand, and E. H. Cordes, *J. Am. Chem. Soc.*, **95**, 4871 (1973).
- (43) R. T. Roberts and C. Chachaty, *Chem. Phys. Lett.*, **22**, 348 (1973).
- (44) G. C. Levy, R. A. Komoroski, and J. A. Halstead, *J. Am. Chem. Soc.*, **96**, 5456 (1974).
- (45) R. Robson and E. A. Dennis, unpublished experiments.
- (46) A. A. Ribeiro and E. A. Dennis, *J. Colloid Interface Sci.*, **55**, 94 (1976).
- (47) B. A. Jezl and D. L. Dalrymple, *Anal. Chem.*, **47**, 203 (1975).

The Polymorphism of Lithium Palmitate

Marjorie J. Vold,*¹ Hideo Funakoshi,² and Robert D. Vold¹

Department of Chemistry, University of Southern California, University Park, Los Angeles, California 90007 (Received September 10, 1975; Revised Manuscript Received April 9, 1976)

Four polymorphic forms of lithium palmitate in addition to isotropic liquid were identified, and some structural information deduced for each, by correlation of results obtained by visual and microscopic observation, differential scanning calorimetry, and x-ray diffraction as a function of temperature. Transition temperatures and heats of transition were determined. LiP I (obtained by crystallization from aqueous ethanol) is a lamellar crystal of hexagonal platelike habit, with a long spacing of 37.4 Å at 25 °C and an angle of inclination of the chains to the planes of the polar head groups of 58.4°. LiP II (obtained by heating LiP I) is also crystalline, with a long spacing of 40.5 Å independent of temperature, and an angle of tilt 67.7°. In LiP II the arrangement of the chains may resemble hexagonal close packing. LiP III (obtained by heating LiP II) is a viscous, doubly refracting, fluid mesophase in which the chains are hexagonally close-packed. LiP IV (present at room temperature after cooling from the melt) is crystalline with a long spacing of 38.5 Å. The transition from LiP I to LiP II occurs at 106 °C with $\Delta H = 5.09$ kcal/mol, and is reversible. The transition from LiP II to LiP III occurs on heating at 208 °C but is irreversible. LiP III melts to liquid at 222 °C with $\Delta H = 5.60$ kcal/mol. The liquid undercools, so LiP III is partly but not completely recovered even after holding for 2 h 3 °C below the melting point. Heat is evolved over three temperature ranges during cooling to room temperature, but these are not believed to signify phase changes. On reheating, LiP IV exhibits no transitions except for melting to liquid at 221 °C. Variable values of apparent heat of fusion of 5.0 to 6.3 kcal/mol were obtained, reflecting varying degrees of incomplete crystallization in the different samples. Comparisons and contrasts with previous work are discussed.

Introduction

The alkali metal salts of normal fatty acids with an even number of carbon atoms from C₈ to C₂₆ (soaps) are characterized by the existence of a plurality of polymorphic forms.

Some different forms may be present at room temperature as the result of crystallization from different solvents or different thermal history of the sample, while others are formed only above transition temperatures occurring between room tem-

perature and the final melting point to isotropic liquid. Many of the latter are mesomorphic (liquid crystalline). Large discrepancies exist in the literature as to the temperatures and, in some cases, even the number of transitions. For example, Vold, Macomber, and Vold³ encountered discrepancies of up to 100 °C in the reported melting points of a series of sodium soaps, and of as much as 65 °C in the temperature of formation of liquid crystal. Although the cited literature is old (1899–1938), the situation is still far from being completely clarified. In 1971 Ripmeester and Dunnel⁴ published a table of transition temperatures of the alkali metal stearates on samples of varying thermal history studied by a variety of methods showing examples of varying numbers of transitions, and discrepancies of up to 18 °C in transition temperatures.

In the case of lithium palmitate, Vold⁵ had reported transitions at 102, 187, and 224–225 °C, with two crystalline and one waxy intermediate phase in addition to the isotropic liquid. Gallot and Skoulios⁶ recently reported four transitions (at 102, 190, 211, and 223 °C), postulating the existence of two crystalline phases, two “ribbonlike” intermediate phases, and the isotropic liquid. Careful study of the literature on soap phases suggests that most of the major discrepancies are not due to impurities or experimental imprecision, but arise from failure to maintain equilibrium, or confusion of one phase with another (especially when more than one mesomorphic phase exists), or the ability of one technique to detect a given transition which cannot be indicated by another (as in a case where the heat of transition is very small but the change in volume quite appreciable).

To clarify the situation for lithium palmitate, a correlation was made of the results of three different techniques, visual and microscopic observation, differential scanning calorimetry, and x-ray diffraction, over the temperature range from 25 to above 250 °C on both heating and cooling at different rates, and with varied thermal history of the sample. Calorimetry is most suitable for accurate determination of transition temperatures, with visual and microscopic observations, heats of transition, and x-ray diffraction patterns most revealing as to the nature of the structural changes occurring at the transitions.

Experimental Section

Materials. Eastman Kodak highest quality palmitic acid was further purified by three recrystallizations from absolute ethanol. It had a melting point of 62.8 °C. Lithium palmitate (LiP) was prepared by neutralizing the acid in hot 50 vol % aqueous ethanol to pH 8 with an aqueous solution of lithium hydroxide (Matheson Coleman and Bell, reagent grade). The precipitated LiP was washed with cold absolute ethanol, was twice recrystallized from 50 vol % ethanol–water, again washed with cold absolute ethanol, and finally air dried at room temperature. That the LiP was completely solvent-free and did not form a hydrate is shown by the fact that the calorimetrically observed transition at 106 °C is found at the same temperature and with the same heat of transition after repeated heating and cooling to temperatures as high as 200 °C. Likewise, the x-ray diffraction pattern of a sample held 1 h at 203 °C and cooled to room temperature is identical in every respect with that of the freshly crystallized and dried material at the same temperature. The sample lost no weight on air drying 24 h at 95 °C.

Calorimetry. A Perkin-Elmer differential scanning calorimeter Model DSC-1B was used to determine transition temperatures and heats of transition. The temperature scale was calibrated using palmitic and benzoic acids, purified in

this laboratory, and indium, tin, and lead supplied by the Perkin-Elmer Corp. Transitions are taken as the points at which the curve of calories/second of input vs. temperature first departs from the smooth, nearly horizontal base line, or, in cases of severe premelting, as the point of intersection of the extrapolated steep portion of the curve with the baseline. The heat of transition is proportional to the area under the peak. The constant of proportionality was determined from the area under the fusion peak of tin and its known heat of fusion. The accuracy of transition temperatures obtained with the DSC for sharp transitions was ± 0.5 °C. The uncertainty in the heat of transition, compounded of the uncertainties in measuring peak areas with a planimeter and in weighing the sample (typically 1 mg weighed on a Sartorius semimicro balance to 0.02 mg) is about $\pm 3\%$. These estimates of the accuracy of transition temperatures and heats of transition agree well with the findings of Chu⁷ using the same model calorimeter. Since the pan covers of the sample holders are not air tight, a slow stream of nitrogen was passed through the chamber containing sample and reference in order to prevent oxidative decomposition at the higher temperatures.

X-Ray Diffraction. Two instruments were used. With the General Electric diffractometer (Model XRD-6) diffraction patterns can be obtained only at room temperature. Values of d/n corresponding to twice the Bragg angle are detectable to within 1° of the primary beam. The average value of the differences in 2θ on duplicate runs at different sensitivities was 0.08°, although the positions of individual peaks can be determined within 0.02°. The intensity of the different lines is directly proportional to the size of the peak on the recorder output of counting rate vs. diffraction angle. Most measurements were made at a current of 22.5 mA at an applied voltage of 45 kV, a scan rate of 2°/min, and a sensitivity such that 200 counts/s resulted in full-scale deflection. Intensities tabulated on this scale are designated as I_{200} . More intense peaks resulting in off scale counting rates were measured at sensitivities of 1000 cps for full-scale deflection (I_{1000}), or 10 000 cps ($I_{10\,000}$), and the results converted to I_{200} for comparative purposes. This technique was used to obtain the patterns at room temperature after the sample had been subjected to various thermal treatments.

The second instrument used was a Seeman Laboratory Debye–Scherer-type heating camera of 12 cm diameter. The camera was calibrated using sodium chloride as a reference material. The sample was finely ground and loaded into a thin-walled glass capillary. Heating is accomplished by a small electric furnace surrounding the sample. Temperatures were held constant by control of the voltage to the furnace. A voltage–temperature calibration curve was determined using a chromel–alumel thermocouple in the place of the sample. Blackening of the film due to the primary beam prevented determination of diffraction patterns at values of 2θ less than 10.6°. The average difference in position of diffraction lines measured by two different investigators was ± 0.093 mm corresponding to differences in d/n of 0.03 to 0.002 Å at the extremes of the angle range investigated. This camera was used to obtain diffraction patterns at room temperature and at various elevated temperatures, approached from both higher and lower values.

Cu $K\alpha$ radiation was used in both instruments.

Results

Visual and Microscopic Observations. Visual observations were made of ca. 0.5-g samples sealed under vacuum in a ca. 7-mm i.d. glass tube heated and cooled in a transparent white

TABLE I: Calorimetric Behavior of LiP Crystallized from Aqueous Ethanol

Heating rate, °C/min	LiP I → LiP II		LiP II → LiP III ^a T, °C	LiP III → liquid	
	T, °C	ΔH, kcal/mol		T, °C	ΔH, kcal/mol
0.625	105.9	5.10	202.6	223.5	
2.5	105.4	5.09	206.6	221.8	5.52
5.0 ^b	106.0	5.09	209.1	221.6	5.63
10.0	107.0	5.09	210.8	222.8	5.54
Av ^c	106.0	5.09	208.1	222.1	5.60
Av dev	0.2		2.0	0.6	0.04

^a Slumping of the sample from a crystalline powder to a coherent liquid crystal prevents determination of ΔH in this case. ^b Average of four runs. ^c All seven runs are weighted evenly in the average.

mineral oil bath at a rate of ca. 3 °C/min. The freshly crystallized material is a lustrous white crystalline powder. No change in appearance was detected until at ca. 210 °C the powder began to sinter and flow together, becoming a highly viscous, very slightly turbid, straw-colored fluid which is doubly refracting (bright when viewed between crossed polaroid sheets). A marked decrease in viscosity, loss of double refraction, and complete transparency accompanied fairly sharp melting near 225 °C. On cooling, the sample became progressively more turbid, but remained somewhat translucent to temperatures well below the temperature of sintering observed on heating. The cooled material at room temperature is a slightly off-white, glassy-looking, brittle solid. Reheating produced a gradual increase in translucency until final melting occurred, again at 225 °C. In one cooling, a cracking noise, accompanied by a sudden small contraction occurred, at 95 °C.

Microscopic observations were made at 100× using a Nikon polarizing microscope equipped with a heating stage. They show that the initial crystals are thin plates, many nearly perfect hexagons. No changes were observed on heating that had not been observed macroscopically. On cooling, the material is initially present in isotropic, drop-shaped blobs, within which irregular darker and brighter patches gradually appear (first noted at ca. 110 °C), indicative of partial crystallization.

The conclusions drawn from these observations are that (a) the initial crystals are thin plates of hexagonal shape; (b) lithium palmitate exhibits a liquid crystalline phase on first heating; (c) both the liquid and the liquid crystalline phases undercool extensively, at least when cooled at a rate of 3 °C/min.

Calorimetric Results on Samples Crystallized from Aqueous Ethanol. This crystalline material is designated LiP I. In the differential scanning calorimeter (DSC), it first undergoes a sharp, first-order phase transition at 106.0 °C with a heat of transition of 5.09 kcal/mol. After it was discovered that this transition did not recur in a second run (the first run had been carried to 250 °C, above the visually observed melting point), the following sequence of runs was carried out. A sample was heated in the DSC at 5 °C/min to 120 °C, held there 20 min, and then cooled in the DSC at the same rate. This procedure was repeated many times with progressively higher holding temperatures. Up to 200 °C the peak at 106 °C on heating was followed by a dip on cooling beginning at the same temperature and having the same area (i.e., heat absorbed on heating was the same as that evolved on cooling). However, after holding 20 min at 207 °C, the cooling dip and subsequent reheating peak had much smaller areas, though still occurring at 106 °C. After holding at 210 °C, the transition at 106 °C was entirely absent on both

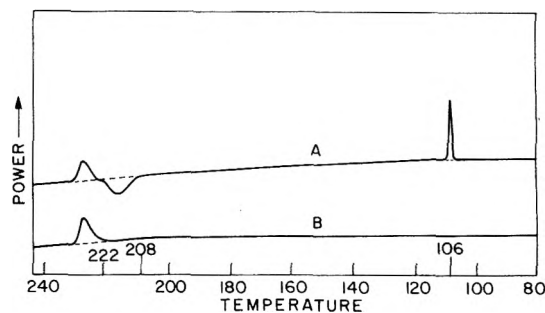


Figure 1. Heating curves for lithium palmitate obtained with the differential scanning calorimeter: (A) sample recrystallized from aqueous ethanol; (B) sample cooled from the melt.

heating and cooling. The material first formed on heating above 106 °C is fully crystalline, as indicated by the microscopic observations and confirmed by x-ray diffraction, and is designated LiP II. The transition between LiP I and LiP II is completely reversible. It was later established that the limiting temperature above which neither LiP I nor LiP II re-form on cooling corresponds to the formation of the mesophase (liquid crystal) at 208 °C, designated LiP III.

The results of heating LiP I from room temperature to 250 °C at varying heating rates are shown in Table I and a typical thermogram is shown as curve A of Figure 1. The transition from LiP I to LiP II has already been discussed. At a mean temperature of 208 °C, noticeably dependent on the rate of heating, a pronounced dip extending over ca. 10 °C occurs in the baseline as is clearly evident from curve A of Figure 1. It would be an error to interpret this dip as a slow evolution of heat. At this temperature the crystalline powder, LiP II, flows together into the viscous fluid liquid crystalline LiP III, making better thermal contact with the bottom of the sample pan which therefore requires less power input to keep it at the same temperature as the reference pan, just as if the sample were evolving heat. This artifact masks whatever heat is absorbed at the transition which therefore cannot be even estimated, although it is probably small. Moreover, the area between the actual curve and an extrapolated horizontal baseline corresponds to an apparent evolution of heat varying over seven runs from 6.9 to 14.5 kcal/mol with no relation to the rate of heating, contrasted with the 3% accuracy established for normal transitions.

A further peak occurs at a mean temperature of 222.1 °C with a heat of transition of 5.60 kcal/mol where LiP III melts to isotropic liquid. There is no systematic dependence of this transition temperature on the rate of heating.

Calorimetric Results on Samples Cooled from the Melt. It has already been shown that undercooling occurs, and that the material cooled from any temperature above 208 °C (i.e.,

TABLE II: Calorimetric Behavior of LiP Cooled from the Melt^a

Rate of heating or cooling, ^b °C/min	Peak on heating		Dips on cooling					
	T, °C	ΔH, kcal/mol	T, °C	ΔH, kcal/mol	T, °C	ΔH, kcal/mol	T, °C	ΔH, kcal/mol
0.625 ^c	223	5.36	219	-0.89	215	-2.81	135	-1.53
2.5 ^d	222	6.23	216	-0.99	210	-2.20	130	-2.02
5.0 ^e	221	5.95	218	-1.56	207	-2.66	135	-2.28
10.0 ^f	223	6.07	218	-1.97	203	-2.41	134	-2.50

^a Since these samples have crystallized to varying degrees because of undercooling, average values of ΔH are meaningless. ^b On heating there are seven runs at 5 °C/min and one at each of the other rates. On cooling there are: ^c Two runs. ^d Two runs. ^e Eight runs. ^f Three runs.

from LiP III) is not LiP I. X-ray diffraction studies show that it is at least partly crystalline and different from both LiP I and LiP II. It is therefore designated LiP IV. The calorimetric results of heating LiP IV and of cooling the melt are shown in Table II, and a typical heating thermogram is shown as curve B of Figure 1. Only one peak occurs on heating at 221 °C. This is close to the previously observed melting point (222 °C), but the heat of transition fluctuates by amounts far outside experimental error (from 5.03 to 6.52 kcal/mol averaging 6.0 in ten runs on seven independent samples, with no dependence on the rate of heating). The lack of reproducibility is ascribed to variable extents of undercooling. That some values are less than the heat of transition of LiP III to liquid suggests that even at room temperature the sample may have contained some undercooled liquid crystal, or even liquid. That some are higher shows, in agreement with the visual and x-ray diffraction results, that some crystal formation has occurred on cooling the melt to room temperature.

Cooling runs in the DSC (see Table II) show three shallow dips (heat evolution) beginning at the temperatures tabulated and extending over several degrees. Though conspicuous on the recorder chart, these curves are not shown in Figure 1, since the dips are too shallow to show well on a journal-size reduction. The temperatures are fairly reproducible although the variations are larger than the precision of the method, but the apparent "heats of transition" fluctuate widely. The total of the three is sometimes greater and sometimes less than the heat absorbed on heating the same sample. There is no relation to the rate of heating or cooling. There is no obvious explanation for the rough concordance of the temperatures of heat evolution on cooling, but the variability of the heats of transition can be attributed to varying degrees of undercooling.

X-Ray Studies on Samples Crystallized from Aqueous Ethanol. Despite the fact that only a few soaps have been obtained as single crystals suitable for x-ray work, their powder diffraction patterns have much in common^{6,8,9} and are relatively simple, so that considerable structural information can be obtained from them. The paraffin chains lie side by side arranged "head to head" with the heads lying in parallel planes (00*l*). These lead to a series of lines beginning at low angles ($2\theta < 20^\circ$) and continuing out to $2\theta = \text{ca. } 50^\circ$. These are submultiples of a long spacing (the *c* crystallographic axis) which is generally somewhat shorter than twice the extended length of the soap molecule. Low orders are intense with odd orders more intense than even. Both the alternation and the total intensity diminish rapidly with increasing order. The remaining lines in the patterns are associated principally with the interchain packing, a value of $d/n = \text{ca. } 4.2\text{--}4.4 \text{ \AA}$ corresponding to the distance between chains being very common.

First a pattern of LiP I was obtained at 25 °C. Then the

sample was heated and held at 203 °C for 1 h, and another pattern obtained, characteristic of LiP II. A further pattern was obtained after cooling to 25 °C, which is identical with the original in every respect. This result, in accord with the calorimetric results, confirms the absence of effects due to retained solvent, and the reversibility of the LiP I-LiP II transition. Diffraction patterns were then obtained with the Seeman camera at two temperatures within the range of existence of LiP I (as indicated calorimetrically), four within the range of existence of LiP II, two within the range of LiP III (liquid crystalline), and two in the isotropic liquid. A characteristic pattern of each phase is shown in Table III. The important points to be considered for all ten patterns obtained are: (1) classification of the lines as side spacings or orders of the long spacing, (2) determination of what changes in pattern occur for the various phases identified calorimetrically, and (3) determination of what changes in pattern occur as a function of temperature for each phase.

The subdivision into side spacings and orders of the long spacing is accomplished by seeking submultiples of a common value. This identification of the lines is shown in Table III. At 25 °C there are seven of the lines, classed as side spacings, all weak or very weak, which yield a value of $36.2 \pm 0.5 \text{ \AA}$ if interpreted as the 8th, 11th, 12th, 14th, 15th, 17th, and 18th orders of a long spacing. This fact is believed to be a coincidence rather than evidence of yet another crystalline form of LiP since (a) the lower orders, which should be more intense, do not occur; (b) those of the same lines which are still present in LiP I at 87 °C where the whole pattern is weaker, have increased with the increased temperature in such a way that they no longer correspond to any single second long spacing; and (c) the simultaneous deposition of two different crystal forms on several recrystallizations from the same solvent is highly improbable. The pertinent lines are marked with an asterisk in Table III.

The patterns of the material designated LiP I and LiP II on the basis of calorimetric data differ in several respects. LiP I at 25 °C has a long spacing of $37.40 \pm 0.19 \text{ \AA}$ which increases with temperature (38.05 \AA at 87 °C). LiP II has a long spacing of $40.47 \pm 0.16 \text{ \AA}$ (average of values at four temperatures) independent of temperature over the range 113–203 °C. Inspection of Table III shows that the side spacings of the two forms are also different. This observation is particularly conclusive of the fact that LiP I and LiP II are different crystal forms by comparison of the lines of strong and medium intensity at the two temperatures. In such cases there is no question that the absence of a line at 113 °C which is present at 25 °C might be due to the general weakening of the diffraction pattern with rising temperature rather than to the presence of a different crystal form. For example, the very strong line at 3.941 \AA at 25 °C is missing at 113 °C. Many other differences can be found by studying Table III. Most side

TABLE III: Characteristic X-Ray Diffraction Patterns on Progressive Heating of Lithium Palmitate Crystallized from Aqueous Ethanol (Seeman Camera)^a

Temp Order	LiP I at 25 °C			LiP II at 113 °C			LiP III at 215 °C	
	<i>d/n</i> , Å	<i>I</i>	<i>d</i> , Å	<i>d/n</i>	<i>I</i>	<i>d</i>	<i>d/n</i>	<i>I</i>
	Long Spacings (00 <i>l</i>)							
5 ^b	(7.615)	w	37.25	(8.338)	m	40.54		
	(7.284)	vw		(7.879)	m			
7 ^b	(5.398)	vw	37.26	(5.914)	w	40.52	none	
	(5.246)	vw		(5.662)	w			
12	3.125	vw	37.50	3.288	w(b)	39.45		
13	2.858	vw	37.15	3.110	vw	40.44		
16	2.335	w	37.36					
17	2.232	m	37.94	2.364	vw	40.18		
18	2.083	w	37.49					
19	1.960	w	37.23					
Av			37.40			40.42		
	Other Spacings (<i>hkl</i>)							
	4.513	vw*						
	4.303	vw						
	(4.224) ^c	s		(4.312) ^c	vs		4.424	m(vb)
	(4.095) ^c	s		(4.197) ^c	vs			
	3.941	vs						
	3.745 ^d	m		3.844	m			
	3.520	s(b)		3.672 ^e	m(b)			
	3.346	vw*		3.469	m(b)			
	2.978	vw*		2.932	vw			
	2.554	vw*						
	2.453	w*		2.485	m		2.530	vw(b)
	2.146	w*		2.291	vw			
	2.011	vw*						

^a Selected from films at 25, 87, 113, 164, 178, 203, 215, 219, 246, 282, and 312 °C. s, strong; m, medium; w, weak; vs, very strong; etc; b, broad. ^b The appearance of these 00*l* orders as a doublet is an artifact for which the authors have no explanation. Only a single sharp line is obtained in the diffractometer patterns. ^c The average value of this pair of lines gives a not unreasonable value for the long spacing if calculated as its ninth order, but the high intensity suggests it is due primarily to a side spacing. ^d This line gives a not unreasonable value for the long spacing if calculated as its tenth order but the high intensity suggests it is due primarily to a side spacing. ^e This line gives a not unreasonable value for the long spacing if calculated as its eleventh order, but the high intensity suggests it is due primarily to a side spacing. An asterisk indicates lines which give an apparent second long spacing of 36.2 ± 0.5 Å (8th, 11th, 12th, 14th, 15th, 17th, and 18th orders) but only coincidentally. See text. An opening parenthesis signifies that the bracketed lines appear as a doublet on the film.

spacings within the phase field of both LiP I and LiP II increase with increasing temperature but there is little difficulty in identifying corresponding lines, showing that there are no additional phase changes, undiscovered calorimetrically or visually, between 25 and 203 °C. With LiP II there is a single change in pattern occurring somewhere between 164 and 178 °C in which a very strong doublet occurring at 4.322 and 4.250 Å at 164 °C, believed to be related to an interchain spacing, is replaced by a very strong singlet at 4.353 Å at 178 °C, although no other changes occur except for small changes in side spacings due to thermal expansion. This observation is not indicative of a phase change, but can be accounted for in terms of a relaxation of a restraint on the interchain packing on the basis of a model proposed by Stosick,¹⁰ as is explained in the Discussion.

LiP III at 215 °C shows no long spacing in the x-ray camera, although one might be present but too weak to register, in view of the fact that at room temperature weak long spacings are detected in crystalline LiP IV by the more sensitive x-ray diffractometer as discussed later, whereas none are found in the pattern obtained with the Seeman camera. There are only two side spacings, a medium broad halo centered at 4.424 Å and a weak one centered at 2.530 Å. These two spacings are nearly related by $\sqrt{3}$ ($2.530\sqrt{3} = 4.382$). This is the pattern

TABLE IV: Representative X-Ray Diffraction Patterns of Lithium Palmitate at Various Temperatures after Stepwise Cooling from the Melt^a

Temp, °C	Values of <i>d/n</i> (Å) and intensities ^d
219	4.424 w (vb,d)
206	4.424 m (vb,d), 2.524 vw (b)
168	4.332 s, 2.510 w (t), 2.26 vw (vd), 2.01 vw (vd)
93	4.214 s, 3.990 m (b), 3.629 m (d), 3.23 vw (vd), 2.91 vw (vd)
	2.457 w, 2.26 w (vd), 2.03 w (vd)
25 ^b	4.168 vs, 3.948 m (b), 3.580 m (b,d), 3.178 vw (vd), 2.887 vw (vd), 2.457 w, 2.26 w (vd), 2.03 w (vd)
145 ^c	4.303 vs (b), 2.494 w, 2.25 w (vb,d), 1.69 w (vb,d)

^a The results shown were selected from 15 runs at various temperatures. The 00*l* spacings are not found on the films although x-ray diffractometer results (Table V) show that they are actually present at 25 °C, although very weak, in samples cooled from the melt. ^b Pattern of the best crystallized of three samples at 25 °C. The same pattern was also found for a sample cooled continuously from the melt to 25 °C in 10 min. Note also that these values are unchanged from those found at 93 °C except for the shortening due to thermal contraction. ^c Sample reheated to 145 °C after cooling from the melt to 25 °C. ^d w, weak; vb,d, very broad, diffuse; m, medium; vs, very strong.

TABLE V: X-Ray Diffractometer Patterns of Lithium Palmitate at 25 °C

Order	Crystallized from aqueous ethanol (LiP I)			Cooled from the melt in vacuo in 2 h (LiP IV)			Cooled from the melt under argon in 20 min (LiP IV)		
	$d/n, \text{Å}$	I_{200}^a	$d, \text{Å}$	$d/n, \text{Å}$	I_{200}	$d, \text{Å}$	$d/n, \text{Å}$	I_{200}	$d, \text{Å}$
	Long Spacings (00l)								
1	36.371	3097 ^b	36.37	38.918	29.8	38.92	39.795	2.70	39.80
2	18.722	64.6	37.44	19.215	1.52	38.43			
3	12.433	518 ^b	37.30	12.810	5.90	38.43	12.980	2.00	38.94
4	9.340	6.09	37.36	9.804	0.95	39.22	9.540	1.40	38.16
5	7.456	105.1	37.28	7.642	1.75	38.21	7.782	1.75	38.91
6		Missing		6.449	0.65	39.69	6.478	1.60	38.87
7	5.338	22.0	37.37	5.502	1.00	38.51			
8	4.671	0.90	37.37	4.804	1.10	38.43			
9	4.157 ^d	2.39	37.41	4.234 ^e	9.78	38.10	4.248 ^e	4.43	38.23
10		Missing		3.821	2.78	38.21			
11	3.406	0.61	37.47	3.470	1.70	38.17	3.546	1.45	39.01
12	3.120	0.90	37.44	3.201	0.90	38.41	3.177	0.75	38.12
13	2.888	1.13	37.54	2.965	0.70	38.55	2.973	0.70	38.65
14	2.680	0.95	37.52	2.559	0.50	38.39			
15	2.497	1.31	37.46	2.422	0.50	38.75			
16	2.344	0.90	37.50				2.259	0.55	38.40
17	2.205	2.18	37.49	2.130	0.60	38.34	2.147	0.55	38.65
18	2.080	20.9	37.44	2.009	0.70	38.17	2.028	0.40	38.53
19	1.970	9.68	37.43						
20	1.870	0.60	37.58						
21	1.783	0.75	37.44						
Av			37.44 ^c			38.47			38.59 ^c
	Other Spacings (hkl)								
	8.230	2.92		4.541	1.65		4.513	2.03	
	4.536	0.40					4.396	2.20	
	4.372	0.35		4.183 ^f	9.78		4.248 ^f	4.43	
	4.157 ^d	2.39		4.019	5.58		4.040	3.05	
	3.969	0.45		3.737	2.60				
	3.810	0.50		3.696	2.80		3.699	2.15	
	3.032	0.35		3.620	2.88		3.627	1.80	
	2.304	0.90		2.806	0.55		2.793	0.70	
	1.920	0.35		2.487	0.88		2.464	0.70	

^a Peak height at a sensitivity such that 200 cps gives full scale deflection on the recorder chart. ^b Calculated to I_{200} (where the peak is off scale) from a run at I_{10000} . ^c Excluding the first order. ^d This reflection is possibly a superposition of an hkl spacing on $00l$. ^e The abnormally high intensity may be due to superposition of an unresolved side spacing. ^f The high intensity here may be due to superposition of a partially resolved long spacing.

to be expected of a liquid crystalline mesophase with hexagonally close-packed chains.

Liquid LiP at 314 °C shows no observable diffraction pattern with the available camera.

X-Ray Studies of LiP during Cooling from the Melt. Four samples of LiP I were heated well above the melting point (to 314 °C) and diffraction patterns obtained on cooling to successively lower temperatures. The total cooling time was 8 h (2 h for temperature equilibration and x-ray exposure time per photograph at each temperature) in three cases. In the fourth, the melt was cooled directly to 25 °C (about 10 min). Typical results are shown in Table IV. Traces of the LiP III pattern are evident at 219 °C, just below the melting point, although the calorimetric data show that its formation is not complete there. The liquid crystalline lines persist as the temperature is lowered below the transition point (208 °C) found on heating for LiP II → LiP III. In two cases, the first trace of additional lines, indicating crystallization, occurred at 145 °C, and in one case at 168 °C. There was a considerable increase in the number of side spacings when cooling reached 93 °C, but no additional lines were found on reaching room temperature. The long spacing lines were not observed on samples cooled to room temperature, but the more sensitive

x-ray diffractometer shows that they are present there, though weak. It is evident that the few lines which are present at room temperature after cooling from the melt cannot be attributed to either LiP II or LiP I. The new form is designated LiP IV. In summary, the x-ray data confirm the calorimetric observation that both liquid and liquid crystalline LiP undercool, and that the solid form resulting at room temperature is a new form, LiP IV.

Comparison of LiP I and LiP IV at 25 °C Based on X-Ray Diffractometer Studies. Table V shows the x-ray diffractometer patterns at 25 °C of lithium palmitate crystallized from aqueous ethanol (LiP I) and of two samples cooled from the melt at different rates (LiP IV).

Comparison of the patterns for LiP I found with the Seeman camera (Table III) and the diffractometer (Table V) reveals both similarities and differences. The long spacing has virtually identical values by the two methods ($37.40 \pm 0.19 \text{ Å}$ vs. $37.44 \pm 0.06 \text{ Å}$). However, in the diffractometer the orders of the long spacing are much more intense than the side spacings, while the reverse is generally true in the camera. Moreover, out of 13 side spacings in the camera pattern and eight in the diffractometer, only three are at all similar! This effect is due to sample orientation in the diffractometer. Sets

of crystal planes must have their normals lying in the same plane as the incident and "reflected" x-ray beam, and therefore the planes must be parallel to the sample surface in the diffractometer, in order to give diffraction, as well as satisfying the familiar Bragg relation, $n\lambda = 2d \sin \theta$. The crystallites of LiP I are thin plates which are preferentially oriented parallel to the surface when packed into the diffractometer sample holder and the surface smoothed. If the 00*l* planes lie parallel to the plate face, they will diffract strongly. The intense side spacings (*hkl* with zero or low *l*) will correspondingly make large angles with the sample surface, few will satisfy the conditions for diffraction, and hence the corresponding lines will be weak or absent. Some *hkl* planes with low *h* and *k* and high *l* which are expected to diffract weakly will, nevertheless, be in a position to diffract since they are nearly parallel to the 00*l* planes, and the orientation of the platelike crystallites is not perfect. The effect of this orientation has been demonstrated experimentally¹¹ by use of a special holder permitting variation of the angle of incidence of the x-ray beam. The same diffraction conditions apply to the Seeman camera but here the sample, ground to a fine powder and packed in a narrow glass capillary, is much more apt to have randomly oriented crystallites, and, in addition the sample is rotated during exposure.

The orientation effect does not preclude comparison of the patterns of LiP I and LiP IV taken with the diffractometer under the same conditions. There is some difficulty, especially in the faster-cooled sample, in distinguishing very weak lines from electronic noise. In general "peaks" with $I_{200} < 1.0$ were ascribed to noise unless (a) they gave consistent values when interpreted as orders of the long spacing or (b), in the case of LiP IV, were present in both samples. The principal conclusion from these data is at once apparent. LiP I and LiP IV are different crystal forms. The long spacings differ, 37.44 vs. 38.5 Å, a difference of 1.1 Å where the maximum uncertainty is 0.2 Å. The side spacings of the two polymorphs are also very different.

In the diffractometer patterns the relative intensity of the long spacings with respect to the side spacings is enormously greater with LiP I than with LiP IV, and considerably greater for a sample of LiP IV prepared by slow cooling than by fast cooling. Also, different side spacings of LiP IV are present in the camera pattern (Table III) than in the diffractometer pattern (Table V). Both these effects are due to the presence of orientable crystallites which, however, are smaller and less orientable in LiP IV than in LiP I, and in the fast-cooled than in the slow-cooled LiP IV. All the lines of the faster-cooled LiP IV sample are weaker than those of the slower-cooled one, suggesting either less complete or less perfect crystallization. The calorimetric finding of variable heats evolved on cooling the melt and reheating the cooled material, and the microscopic observation of incomplete recrystallization on cooling, suggests that both factors are operative.

Discussion

Comparison with Previous Work. There are some striking similarities and some glaring discrepancies between the results presented here and those reported previously by Gallot and Skoulios.⁶ Reconciliation of the differences is impossible, however, since very little of the data on which their conclusions are based is given in the published paper. Also, in the present work it was not possible to obtain x-ray diffraction patterns at elevated temperatures at values of 2θ less than about 11° , which is precisely the region of greatest concern in their work.

The present paper reports two lamellar crystal forms of lithium palmitate, designated LiP I and LiP II, with a transition temperature of 106°C . Gallot and Skoulios also find two lamellar crystal forms, designated LC₁ and LC₂, with a transition temperature of 102°C . For LC₁ they report a long spacing of 37.5 Å where the present film data give 37.40 Å and the diffractometer data 37.44 Å at 25°C . For LC₂ they report the long spacing as 40.3 Å where the present work gives 40.5 Å if the results at 113, 164, 178, and 203°C are averaged. The melting point to isotropic liquid was found to be 222°C in the present investigation, and 223°C by the earlier investigators.

However, Gallot and Skoulios postulate the existence of two different phases, ribbon phases BR₁ and BR₂, between the high temperature crystalline form and the melt, the first forming at 190°C and the second at 211°C . These are said to be characterized by 10 to 20 sharp lines at small diffraction angles and a halo about 4.5 Å. Figure 4 of their paper³ shows only seven or eight of these, the shortest of which corresponds to a spacing of about 12 Å, already longer than the longest spacing determinable in our heating camera.

Calorimetrically, there is no indication of evolution or absorption of heat at 190 or 211°C . Instead, there is but a single thermal transition at 208°C , which may well correspond to their value of 211°C . Moreover, the x-ray patterns at 178 and 203°C were the same with respect to both the presence and value of long spacing, and the position of the half dozen side spacing lines. In the temperature range above 208°C , where the phase present is here described as a liquid crystal, there is only a very broad line at 4.42 Å, corresponding to the 110 index of a hexagonally close packed net, with a weak line at 2.53 Å corresponding to the 110 index. The present data therefore indicate that there is no transition at 190°C , and that liquid crystal is formed from LiP II at 208°C which in turn melts to isotropic liquid at 222°C . A very different structure is inferred here for the phase existing just below the melting point than that postulated by the earlier investigators.

Another major discrepancy concerns the reversibility of the transitions. Gallot and Skoulios report that all transitions are completely reversible. The present work shows that the transition between the two crystalline forms LiP I and LiP II at 106°C is reversible, but that the transition from LiP II to LiP III at 208°C is irreversible, and that on cooling LiP III crystallizes in a new form (LiP IV). Once the sample has been cooled from the melt, on subsequent heating no calorimetrically detectable transitions were found between room temperature and melting at 222°C .

The transition temperatures reported earlier on the basis of visual observation with no investigation of either reversibility or nature of the intermediate phases³ are 102, 187, and 225°C (melting to liquid). The reported value of 187°C is of passing interest in view of Gallot and Skoulios' reported observation at 190°C , but (as already described) it is not confirmed by any technique in the present work (including comparable visual studies).

Structure of the Phases. It has already been pointed out that the x-ray pattern of LiP III is in accord with the hypothesis of a liquid crystalline mesophase containing hexagonally closed-packed paraffin chains. This structure differs from that proposed by Gallot and Skoulios⁶ for either of their forms, BR₁ and BR₂ in roughly the same temperature range, which involve irregularly kinked chains with a two-dimensional ordered packing of polar heads and "pieces" of this sort of structure 36 Å in length arranged in a rectangular superlattice $87.6 \text{ \AA} \times 37 \text{ \AA}$ for BR₁ of LiP (BR₂ is stated to be similar

but with different dimensions). Although the authors regard such a structure as unlikely, this interpretation cannot be checked since Gallot and Skolious did not publish their actual data, and low angle diffraction equipment usable at elevated temperatures was not available in our laboratory.

Usually very little information about crystal structure can be obtained from powder data but special circumstances make some conclusions possible about LiP I and LiP II. Gallot and Skolious⁶ show that these two structures (which they call LC₁ and LC₂) are common to the Li soaps from C₁₀ through C₁₈, and that a plot of the long spacing vs. the number of carbon atoms in the chain yields a pair of straight lines (one for each form) from which the angles (α) between the axis of the chain and the plane of the polar "head" groups may be calculated (see Figure 8 of ref 6). Curiously, Gallot and Skolious did not publish calculated values of α . From their tabulated long spacings (which agree with ours for C₁₆ within 0.1 Å for LiP I and 0.2 Å for LiP II) we calculate $\alpha = 58.4^\circ$ for LiP I at 25 °C, and $\alpha = 67.7^\circ$ for LiP II at 150 °C. It was suggested by Bau¹² that the anomalously high intensity of the 0-0-18 line of LiP I at 25 °C (see Table V) may be due to all the methylene groups happening to scatter "in phase". If so, $\alpha = \arcsin 2.08/2.54 = 55.0^\circ$, in fair agreement with the value calculated from the data of Gallot and Skolious. A similar enhancement of a high order of the long spacing has been observed for other paraffin-chain compounds (calcium stearate¹³ and cetyl palmitate¹⁴).

Knowledge of the values of α makes possible calculation of the linear distance, L , occupied by the LiP molecule in the crystal for comparison with its length calculated from standard bond angles, covalent radii, and ionic crystal radii.¹⁵ Since $L = d/2 \sin \alpha$, for LiP I at 25 °C, $L = 22.0$ Å (at 87 °C it is 22.3 Å), making the assumption that α is a constant of the crystal structure and therefore independent of temperature. The calculated length of the LiP molecule is 21.7 Å, making the reasonable assumption that the lithium ion is nestled as closely as possible between the two oxygens of the carboxyl group. The gap in the packing along the axis of the chain is thus only 0.3 Å at 25 °C but increases with increasing temperature to 0.6 Å at 87 °C. For LiP II, $L = 21.9$ Å independent of temperature, so the gap is only 0.2 Å. Perhaps this tight packing in LiP II accounts for the constancy of the long spacing with temperature.

An attempt was made to apply an hypothesis of Stosick,¹⁰ designed for soaps in general and successfully applied to some sodium soaps by him and by Vold and Smith¹³ to calcium stearate, in order to gain further insight into the structure of the crystalline phases of LiP. It fails for LiP I and LiP IV but has possible application to LiP II.

According to Stosick, not all soap solid phases are perfectly crystallized; many consist instead of sheets of double molecules hexagonally close-packed and stacked together in disorderly fashion, with no correlation between the polar head groups of successive sheets. On this model, the occurrence of the succession of sharp $00l$ lines (the long spacing) remains unaffected by the stacking disorder but the side spacings are broadened and only three can occur (the ones of indices $100 = 010 = 1\bar{1}0$ near $2\theta = 20^\circ$ using Cu K radiation, indices $110 = 2\bar{1}0 = 1\bar{2}0$ near $2\theta = 35^\circ$, and the one with indices $200 = 020 = 2\bar{2}0$ near $2\theta = 40^\circ$). This happens because the reciprocal lattice becomes equivalent to a two-dimensional net with equal reciprocal axes between which the angle is 60° . The values of d/n corresponding to 20, 35, and 40° are respectively 4.4 Å, $4.4/\sqrt{3} = 2.5$ Å, and $4.4/2 = 2.2$ Å.

It is apparent from Tables III and V that this hypothesis

cannot apply directly to any of the crystalline forms of LiP. There are many more than three clearly resolved side spacings. Moreover, for LiP I and LiP IV there are side spacings greater than 4.4 Å, for which there are no possible indices on the original scheme.

However, a slight modification of the scheme may be applicable to LiP II. The chains are not, in fact, perfect cylinders, so that if they do not show a random orientation about the chain axis the packing could be closely but not exactly hexagonal. In this event the two reciprocal axes of the $hk0$ net could be slightly unequal, in which case there would be three lines near $2\theta = 20^\circ$ instead of one; or the angle between still equal reciprocal axes could differ slightly from 60° , in which case there would be two lines instead of one. In addition, the postulated stacking disorder might not be complete, in which case a few hkl lines with $l \neq 0$ would be expected to be resolved.

LiP II at 113 °C has a strong doublet at 4.312 and 4.197 Å so that the scheme with equal reciprocal axes is indicated. If the first of these is taken as $1\bar{1}0$ and the second as $100 = 010$, the calculated angle between the reciprocal axes is 58.2° , not far from the 60° of truly hexagonal packing. Other $hk0$ lines may be readily calculated but only one of them is found, 210 , 2.467 calcd vs. 2.485 obsd. Others, if present, must be too weak to show under the experimental conditions used. Five lines, at $20^\circ < 2\theta < 35^\circ$, remain to be interpreted as hkl lines with $l \neq 0$. This scheme provides a reasonable explanation for the observation, referred to in the results section, that the strong doublet, which has increased spacings at 164 °C due to thermal expansion (4.332 and 4.250 Å), is replaced by a very strong singlet at 178 °C, 4.353 Å. This would imply that the angle between the reciprocal axes shifts to 60° with rising temperature. There is no first-order phase change since no trace of a heat of transition is found during either heating or cooling, and the rest of the pattern at 178 °C is the same as that 164 °C (constant long spacing as characteristic of LiP II and the same side spacings, at both 164 and 178 °C). The validity of the interpretation of the shift from doublet to singlet as due to an angle change is further confirmed by the presence of a line at 178 °C, very weak and absent at both 113 and 164 °C, at 2.520 Å, which is interpretable as 110 (calcd 2.513 Å). It is possible that a second-order phase change has occurred between 164 and 178 °C involving onset of free rotation of the chains, but such a change would not be detected by any of the techniques employed.

In conclusion, it is shown possible but not proven that in LiP II the chains are nearly hexagonally close packed when the phase is first formed from LiP I, and become fully so at some higher temperature, between 164 and 178 °C.

One further curious observation: lithium stearate, which has two successive crystalline forms exactly similar to LiP I and LiP II, has a lathlike crystal habit^{6,16} in contrast to the hexagonal plates of LiP and, unlike the behavior of LiP, the initial room temperature crystal form is regained on cooling from the melt.

Explanation of the various discrepancies will require much further investigation of calorimetric and x-ray behavior as a function of thermal history (maximum temperature to which samples have been heated, rate of cooling, time allowed for establishment of thermal equilibrium in the vicinity of transition temperatures, etc.), and of x-ray diffraction patterns at very small angles at high temperatures. The present data, however, are sufficient to show the general nature of the results to be expected.

Acknowledgment. The authors wish to thank Professors

J. C. Warf and R. Wang for their assistance in the operation respectively of the heating camera and the x-ray diffractometer, and Professor R. Bau for helping to establish the precision of the x-ray film data.

References and Notes

- (1) 17465 Plaza Animado #144, San Diego, Calif. 92128. Reprint requests should be addressed to the University of Southern California.
- (2) Department of Chemistry, Fukuoka University of Education, 729, Akama, Munakata-cho, Munakata-gun, Fukuoka, Japan.
- (3) M. J. Vold, M. Macomber, and R. D. Vold, *J. Am. Chem. Soc.*, **63**, 168 (1941).
- (4) J. A. Ripmeester and B. A. Dunell, *Can. J. Chem.*, **49**, 2906 (1971).
- (5) M. J. Vold, *J. Am. Chem. Soc.*, **65**, 465 (1943).
- (6) B. Gallot and A. Skoulios, *Kolloid-Z. Z. Polym.*, **209**, 164 (1966).
- (7) J. Y. C. Chu, *J. Phys. Chem.*, **79**, 119 (1975).
- (8) R. D. Vold and G. S. Hattlangdi, *Ind. Eng. Chem.*, **41**, 2311 (1949).
- (9) R. D. Vold, J. D. Grandine, II, and H. Schott, *J. Phys. Chem.*, **56**, 128 (1952).
- (10) A. J. Stosick, *J. Chem. Phys.*, **18**, 1035 (1950).
- (11) M. J. Vold, *J. Phys. Chem.*, **57**, 26 (1953).
- (12) R. Bau, personal communication.
- (13) R. D. Vold and T. D. Smith, *J. Am. Chem. Soc.*, **73**, 2006 (1951).
- (14) R. Kohlhaas, *Z. Kristallogr.*, **98**, 418 (1938).
- (15) L. Pauling, "The Nature of the Chemical Bond", Cornell University Press, Ithaca, N.Y., 1960.
- (16) M. J. Vold, Y. Uzu, and R. F. Bills, *NLGI Spokesman*, **32**, 362 (1969).

Electrosorption of 2-Butanol at the Mercury-Solution Interface. 1. Thermodynamic Treatment¹

Hisamitsu Nakadomari,² David M. Mohilner,^{*3} and Patricia R. Mohilner

Departments of Chemistry and Computer Science, Colorado State University, Fort Collins, Colorado 80523 (Received January 28, 1976)

Publication costs assisted by the Air Force Office of Scientific Research

The electrosorption of 2-butanol on mercury from aqueous sodium sulfate solutions has been measured with a computer-controlled capillary electrometer. In these experiments, two requirements of the thermodynamic theory of electrocapillarity, which have generally been ignored in the past, have been obeyed. First, the measurements have been made in a series of solutions in which the concentration of the organic compound was varied but in which the activity of the electrolyte, instead of its concentration, was held constant. Second, the activity of the organic compound in each electrolyte solution was determined and the thermodynamic analysis of the electrocapillary data was carried out using the organic activity instead of the organic concentration. Because the thermodynamic analysis was carried out in this way it was possible to detect a reorientation of the 2-butanol molecules on the electrode surface. Analysis with concentrations instead of activities failed to reveal this molecular reorientation. The electrosorption is shown to be congruent neither with respect to electrode potential nor with respect to excess surface charge density. The accuracy of the determined relative surface excesses has been estimated with the aid of a statistical treatment of the propagation of errors for derived quantities.

I. Introduction

The electrosorption of neutral organic molecules on metal electrodes from aqueous electrolyte solutions is a phenomenon which primarily involves the inner (compact) part of the electrical double layer with little or no complication from the diffuse layer. The study of this phenomenon can therefore provide significant information on the structure and intermolecular interactions of the inner layer. In addition to information on the behavior of the organic sorbates themselves, which has been the thrust of most prior studies,⁴ such investigations should also help illuminate the role of the water molecules in the inner layer. Of particular interest is any information on the structure of water in the inner layer, how this structure changes as a function of the electrical state of the system, and what relation the structure of the surface water bears to that of bulk water. This study of the electrosorption of 2-butanol on mercury from aqueous sodium sulfate solutions was undertaken partly with this view in mind. In this paper the experimental measurements and the thermodynamic analysis of the data are presented. In part 2,⁵ the results will be further interpreted in terms of a theory of noncon-

gruent organic electrosorption based on a model of the surface layer as a two-component nonelectrolyte solution.

To our knowledge, this is the first experimental study of organic electrosorption in which proper account⁶ has been taken of two important requirements of the thermodynamic theory of electrocapillarity⁷ which have generally been ignored^{8,9} in the past. These thermodynamic requirements are: (i) that the activity (chemical potential) rather than the concentration of the electrolyte should be held constant as the concentration of the organic compound is varied, and (ii) that the thermodynamic analysis of the electrosorption data should be carried out using the activity rather than the concentration of the organic compound in the electrolyte solutions. In addition, in these experiments the electrode potential was measured with respect to a proper indicator electrode (see section II, D) instead of with respect to an ordinary reference electrode such as a calomel electrode.

II. Experimental Section

A. General. It was necessary to perform three different kinds of experiments for this research. The main experiments

were electrocapillary measurements. However, before the electrocapillary measurements could be done, a series of emf measurements on reversible galvanic cells without a liquid junction was needed to establish the recipe for the preparation of the series of solutions required for the electrocapillary measurements, and before the electrocapillary data could be thermodynamically analyzed it was necessary to determine the activity of the 2-butanol in each of these electrolyte solutions. The latter two kinds of experiments have never been included, and indeed, have generally been thought to be unnecessary in previous studies of organic electrosorption.^{4,8-10} The reasons why these two types of experiments are necessary can best be explained by a comparison of the exact, thermodynamic equation for the relative surface excess of the organic compound with the approximate equation which has been employed in earlier work.

The thermodynamic electrocapillary equation⁷ for a pure mercury electrode in contact with a three-component aqueous solution containing one electrolyte and one neutral organic compound at constant temperature and pressure is

$$d\gamma = -\sigma^M dE^\pm - RT\Gamma_{AW} d \ln a_A - RT(\Gamma_{\pm W}/\nu_{\pm}) d \ln a_e \quad (1)$$

In eq 1 γ is the interfacial tension of the electrode, and σ^M is the excess charge density on the metal surface. E^\pm is the potential of the ideal polarized electrode with respect to an electrode dipping into the same solution which is reversible either to the cation (E^+) or to the anion (E^-) of the electrolyte. This special kind of reference electrode required by the thermodynamic theory of electrocapillarity will hereafter be referred to as the *indicator electrode*.¹¹ Γ_{AW} is the relative surface excess of the organic compound (A) with water (W) taken as the reference component, and a_A is the activity of the organic compound in the bulk solution.¹³ $\Gamma_{\pm W}$ denotes the relative surface excess of the ion of the electrolyte to which the indicator electrode is not reversible, and ν_{\pm} is the number of moles of this ion in 1 mol of the electrolyte. a_e is the activity of the electrolyte in the bulk solution.¹⁴ R is the gas constant, and T is the absolute temperature.

It follows from eq 1 that at constant temperature and pressure the true relative surface excess of the organic compound is given by

$$\Gamma_{AW} = -(1/RT)(\partial\gamma/\partial \ln a_A)_{T,p,E^\pm,a_e} \quad (2)$$

(The subscript p in eq 2 implies that the measurements are made at constant pressure.) In contrast, the approximate equation is

$$\Gamma_{AW,app} = -(1/RT)(\partial\gamma/\partial \ln c_A)_{T,p,E_{ref},c_e} \quad (3)$$

The additional subscript, *app*, on the symbol for the relative surface excess in eq 3 is added to emphasize the fact that this quantity is only an apparent one. c_A in eq 3 is the bulk concentration of the organic compound in the solution. E_{ref} is the potential of the ideal polarized mercury electrode with respect to a constant potential reference electrode and includes a liquid junction potential. c_e is the bulk concentration of the electrolyte in the solution. Use of eq 3 in place of eq 2 is justifiable only if all three of the following implicit assumptions are true. (i) The addition of the organic compound to a solution with fixed electrolyte concentration, c_e , does not change the electrolyte activity, a_e . (ii) Holding the potential of the ideal polarized electrode constant with respect to a constant potential reference electrode as the organic concentration in the solution is changed is equivalent to holding the potential constant with respect to a proper indicator electrode. (iii) The

activity coefficient of the organic compound in the bulk solution remains constant over the concentration range studied, i.e., the organic compound obeys Henry's law throughout this concentration range.

It is evident from a survey of the literature^{4,16} that assumption (i) has never been seriously questioned before.¹⁷ However, it was recently shown in this laboratory,^{6,18} on the basis of emf measurements, that at least in the cases of 2-butanol and 2-methyl-2-propanol in aqueous solutions of sodium sulfate this assumption is untenable. In fact, addition of the organic compound to an electrolyte solution can significantly raise the chemical potential of the electrolyte. Therefore, in order to keep the chemical potential of the electrolyte constant as the concentration of the organic compound is increased, it is necessary to lower the analytical concentration of the electrolyte in the solution. Thus, it is necessary to perform preliminary experiments to determine the recipe for preparation of the series of solutions of varying organic activity but constant electrolyte activity. The effect of the organic compound on the activity of the electrolyte is probably due^{6,18} to the promotion of water structure in the form of clathrate-like cages of water¹⁹⁻²¹ around the organic molecules, i.e., to the "iceberg" effect.²² Such structured water in the form of cages around the organic molecules is evidently, on the average, unavailable to the ions of the electrolyte. Thus, the addition of the organic compound to the solution raises the effective concentration of the electrolyte in the remaining water, and hence, the electrolyte activity is raised.⁶ For the experiments described in this paper, the chemical potential of the Na_2SO_4 was held the same in each solution as it is in a 0.1 M (0.10045 m) solution of sodium sulfate in pure water at 25 °C in which the mean ionic activity,^{23,24} $a_{\pm} = 0.07087$. In order to keep a_{\pm} at the same value in the presence of 2-butanol it was necessary to lower the concentration of the Na_2SO_4 considerably as the organic concentration was raised. (Cf. Table I.) There appears to be no reason to believe that the two butyl alcohols we studied have any special structure-making ability over that of many other organic compounds.²¹ Therefore, we believe this effect of the organic compound on the chemical potential of the electrolyte should always be taken into account in electrosorption studies; failure to do so may result in serious errors.

Assumption (ii) will necessarily be wrong whenever assumption (i) is wrong because the change in the electrolyte activity produced by the organic compound will produce a corresponding change in the potential of an indicator electrode with respect to a constant potential reference electrode. If the activity of the electrolyte is maintained constant in the series of solutions of varying organic concentration as indicated above, only a small error would probably result from the use of a constant potential reference electrode because the change of liquid junction potential would be small. If, on the other hand, the concentration of the electrolyte instead of its activity is held constant, the errors in the measurement will be compounded by use of a constant potential reference electrode. The recent advent of a large number of reliable ion selective electrodes makes it much easier to employ indicator electrodes today. In this work we used a Corning NAS 11-18 sodium ion electrode.

Assumption (iii) may or may not be true depending on the concentration range of the organic compound studied.⁶ If the concentrations are sufficiently low, the organic compound will obey Henry's law and the assumption is true. It is usually desirable, however, in organic electrosorption studies to include rather high concentrations which do not lie in the

TABLE I: Solution Composition

Molarity of alcohol	Mole fraction of alcohol	Activity of alcohol	Mole fraction of water	Activity of water	Molarity of salt	Molality of salt
0.0000	0.000 000	0.0000	0.9982	0.9957	0.100 00	0.100 45
0.0130	0.000 235	0.0056	0.9980	0.9955	0.099 35	0.099 79
0.0160	0.000 289	0.0068	0.9979	0.9954	0.099 20	0.099 65
0.0200	0.000 362	0.0086	0.9978	0.9953	0.099 00	0.099 45
0.0250	0.000 452	0.0107	0.9978	0.9953	0.098 75	0.099 21
0.0310	0.000 561	0.0133	0.9977	0.9951	0.098 45	0.098 91
0.0370	0.000 670	0.0158	0.9976	0.9950	0.098 14	0.098 62
0.0460	0.000 834	0.0197	0.9974	0.9949	0.097 69	0.098 17
0.0580	0.001 052	0.0249	0.9972	0.9947	0.097 09	0.097 58
0.0700	0.001 270	0.0300	0.9970	0.9944	0.096 49	0.096 99
0.0860	0.001 563	0.0369	0.9967	0.9941	0.095 69	0.096 20
0.1050	0.001 910	0.0451	0.9964	0.9938	0.094 73	0.095 26
0.1250	0.002 277	0.0538	0.9960	0.9934	0.093 73	0.094 28
0.1470	0.002 682	0.0634	0.9956	0.9930	0.092 63	0.093 19
0.1750	0.003 199	0.0756	0.9951	0.9925	0.091 22	0.091 80
0.2100	0.003 848	0.0909	0.9945	0.9919	0.089 47	0.090 05
0.2550	0.004 687	0.1107	0.9937	0.9910	0.087 21	0.087 83
0.3000	0.005 533	0.1307	0.9929	0.9902	0.084 95	0.085 62
0.4200	0.007 810	0.1845	0.9907	0.9879	0.078 93	0.079 64
0.5000	0.009 356	0.2210	0.9892	0.9864	0.074 92	0.075 71
0.6000	0.011 299	0.2669	0.9874	0.9844	0.069 90	0.070 67
0.7000	0.013 271	0.3135	0.9855	0.9825	0.064 88	0.065 64
0.8400	0.016 083	0.3710	0.9828	0.9800	0.057 86	0.058 62
1.0000	0.019 368	0.4411	0.9797	0.9770	0.049 83	0.050 57
1.2000	0.023 575	0.5118	0.9756	0.9738	0.039 80	0.040 46
1.4000	0.027 916	0.5652	0.9715	0.9713	0.029 77	0.030 33

Henry's law region in order to define adequately the electro-sorption isotherm. In the case of this study it was found that 2-butanol did obey Henry's law up to 0.7 M, but for all solutions of higher concentration there were significant negative deviations from Henry's law.

B. *Emf Measurements to Determine the Recipe for Preparation of the Solutions for the Electrocapillary Measurements.* Since the activity of a single electrolyte in solution can be determined^{15,23} from measurements of the emf of a galvanic cell without liquid junction in which one of the electrodes is reversible to the cation while the other is reversible to the anion, the recipe for solution preparation was determined by measuring the emf of such cells. Solutions containing different concentrations of the organic compound which yield the same emf will have equal electrolyte chemical potentials. In the past, such emf measurements for alkali metal salts have been inconvenient because the only satisfactory alkali metal electrodes were dilute amalgams. Nevertheless, very satisfactory measurements of the activity of sodium sulfate in aqueous solutions were accomplished in 1954 by Harned and Hecker²⁵ who used a cell consisting of a sodium amalgam electrode and a two-phase lead amalgam–lead sulfate electrode. The advent of commercially available glass electrodes which respond to Na⁺ or K⁺ ions has now made such emf measurements much easier, and successful determinations of the activity of NaCl and KCl in water and various water–organic mixtures have been reported.^{26,27} Therefore, the emf of galvanic cells consisting of a Corning NAS 11-18 sodium ion electrode and a two-phase lead amalgam–lead sulfate electrode²⁸ in the three component mixtures of sodium sulfate, water, and 2-butanol¹⁸ was measured.

The two-phase lead amalgam was prepared by cathodic deposition of lead from a lead nitrate solution into pure mercury (triple vacuum distilled). The lead sulfate was prepared from reagent grade chemicals by the method of Harned and Hecker²⁵ and stored under distilled water until used. A

three-compartment, jacketed, borosilicate glass cell was employed. One compartment contained the glass electrode. The other two compartments contained identical lead amalgam–lead sulfate electrodes. Temperature was controlled at 25 ± 0.05 °C by pumping water from a thermostat through the jacket. Each compartment was provided with a sintered glass bubbler for deaeration of the solution with prepurified nitrogen prior to measurement and with an inlet and outlet for nitrogen above the solution surface to maintain a nitrogen atmosphere during measurements. Platinum wires were sealed through the walls of the amalgam compartments to provide electrical contact. The cell was dewetted with the vapor of dichlorodimethylsilane to prevent the solution from creeping between the cell wall and the amalgam pool, because spurious emf readings can result if solution comes in contact with the platinum wire at the point where it makes contact with the amalgam pool. Two lead amalgam–lead sulfate electrodes were used to ensure that equilibrium had been established. No emf values were accepted until the difference of potential between these two electrodes was less than 50 μV.

The emf between the glass electrode and the lead amalgam–lead sulfate electrode was measured with a Keithley Model 610CR solid state electrometer with input impedance greater than 10⁺¹⁵ ohm. The glass electrode was connected to the electrometer with a Keithley Model 6107 pH electrode adapter. The unity gain output of the electrometer was read on a Fluke Model 8300A digital voltmeter to within 10 μV.

To ensure that this galvanic cell responded correctly to the sodium sulfate activity, a test was made using solutions of the salt in pure water. Seven different solutions of sodium sulfate in pure water in the concentration range, 0.050 29–1.348 8 m, were used.¹ The emf of the cell at 25 °C was measured for each solution. The value of the mean ionic activity, a_{\pm} , for each solution was calculated²⁴ from the tabulated stoichiometric mean molal activity coefficients,²³ and the slope and standard deviation of the slope of the linear regression of the emf on ln

a_{\pm} were calculated.³⁰ The theoretical slope is $1.5RT/F$ where F is the faraday. The found slope was $1.4998RT/F$ with a standard deviation less than $0.0005RT/F$. Therefore, this galvanic cell obeys the thermodynamic relationship almost perfectly in the case of solutions of sodium sulfate in pure water.

To prove that the cell also behaved correctly in the case of solutions containing 2-butanol, an additional check was made. The emf of the cell was measured for solutions saturated with solid sodium sulfate in the absence and presence of 2-butanol. The observed values of the emf were 0.615 39 and 0.615 38 V, respectively, which proves that the cell still behaves correctly in the presence of the organic compound. Therefore, its emf can be taken as a direct measure of the chemical potential of the sodium sulfate in the presence of 2-butanol. The procedure used to determine the recipe for preparation of the solution has been described.⁶ (Cf. Table I.)

C. *Solution Preparation.* The 25 solutions (Table I) containing 2-butanol in the concentration range 0.0103–1.400 M, each with the appropriate concentration of Na_2SO_4 , were prepared by weighing 2-butanol and sodium sulfate into a volumetric flask, which was then filled to the mark with water after temperature equilibration at 25 °C. The density of each solution at 25 °C was measured using a calibrated 10-cm³ pycnometer. From the density and the composition data, the mole fractions of 2-butanol and of water and the molality of the Na_2SO_4 (in moles of electrolyte/kilogram of water, *not* /kilogram of water organic mixture) were calculated for each solution. In order to eliminate traces of adsorbable organic impurities, the water used in the solutions was distilled from alkaline permanganate using a still equipped with a splash trap and a heated column of glass helices, and then it was redistilled to eliminate the possibility of any carry-over of traces of permanganate. The 2-butanol (Eastman reagent grade) was twice distilled; each time only the middle 50% fraction boiling at 93.4 ± 0.2 °C at local atmospheric pressure was collected. Gas chromatography revealed only a single peak. Fisher reagent grade sodium sulfate was used without further purification because a prior experiment revealed no differences in the electrocapillary curves of 0.1 M Na_2SO_4 prepared from the reagent after recrystallization and from the reagent as received.

D. *Electrocapillary Measurements.* The electrocapillary curves for the 0.1 M solution of Na_2SO_4 in pure water and for each of the 25 solutions (Table I) containing 2-butanol were measured using the computer-controlled capillary electrometer described earlier.³¹ The precision of this instrument was, however, improved over that indicated in our earlier publication as a result of two modifications, one hardware, the other software. The hardware modification was to replace all of the older model operational amplifiers (Philbrick P series) with encapsulated solid state amplifiers (Philbrick 101A, 1023 and 1700) having much lower noise levels. The software modification was to add a data rejection and remeasurement program (overlay RJCT) to the set of disk overlay programs. After all points on an electrocapillary curve have been measured in triplicate, overlay RJCT calculates the average value of the interfacial tension, γ , at each electrode potential and its standard deviation. If the standard deviation exceeds 0.033% of the average value of γ , a routine based on Dixon's statistical analysis of extreme values³² is entered to determine whether rejection of one of the three individual measurements at the potential in question is justified.³³ If data rejection is statistically justified, the outlying value is discarded and the measurement is repeated automatically.

The maximum bubble pressure (MBP) electrode³¹ was calibrated using 0.05 M Na_2SO_4 at 25 °C for which Smolders and Duyvis³⁵ reported that the value of the interfacial tension at the electrocapillary maximum is 426.2 ± 0.2 dyn cm⁻¹ on the basis of sessile drop measurements.

The electrocapillary curves for 0.1 M Na_2SO_4 in pure water and for each of the 25 solutions containing 2-butanol (Table I) were measured in triplicate at 61 different electrode potentials. The potential of the MBP electrode was controlled vs. the Corning NAS 11-18 sodium ion electrode in the same solution. The Corning NAS 11-18 electrode thus served as a true indicator electrode, and potentials were on the E^{\ddagger} scale. The high impedance glass indicator electrode was connected to the voltage follower of the potentiostat by means of the Keithley Model 610CR electrometer which served as an impedance matching preamplifier. The potential range covered was -1.300 to +0.200 V. The potential interval between points was 25 mV. Each point was measured with a relative standard deviation of less than 0.033%. Figure 1 shows the complete set of electrocapillary curves. A complete table of the electrocapillary data is available as supplementary material (see paragraph at end of text regarding supplementary material).

E. *Determination of the Activity of the 2-Butanol and of the Water in the Electrolyte Solutions.* The activity of the 2-butanol in the electrolyte solutions was measured by the gas chromatographic method³⁶ which we described recently. Direct measurements of the alcohol activity were made only for the seven highest concentrations (Table I). The results are shown in Figure 2. The relative standard deviations for the activity measurements were about 0.5%. It was found that when the activity of the 2-butanol was plotted (Figure 2) against the mole fraction, x_A , of the alcohol in the bulk solution the points for the three lowest concentrations (0.50, 0.60, and 0.70 M) for which measurements were made lay accurately on a straight line passing through the origin. Therefore, these three solutions obey Henry's law and so, necessarily, must all more dilute solutions. The activities of the 2-butanol in all the more dilute solutions were therefore obtained by interpolation on the Henry's law line. It can be seen from Figure 2 that for the four highest concentrations (0.84, 1.00, 1.20, and 1.40 M) there are increasing negative deviations from Henry's law.

The upper curve in Figure 2 is for the water activity, a_W , in the bulk electrolyte solutions.³⁷ It was calculated from the activity data for the 2-butanol by integration of the Gibbs–Duhem equation. Since the chemical potential of the electrolyte was held constant as the activity of the 2-butanol in these solutions was varied, the Gibbs–Duhem equation for this three-component system reduces to

$$d \ln a_W = -(x_A/x_W) d \ln a_A \quad (4)$$

x_W in eq 4 is the mole fraction of water in the bulk solution and the other symbols are as defined previously. Equation 4 was integrated from $x_A = 0$ to the values of x_A for each of the 25 solutions to obtain the water activity (Table I). The value of the water activity at the lower limit of integration was obtained for the 0.100 45 *m* solution of Na_2SO_4 in pure water by cubic interpolation from the table of practical osmotic coefficients given in the extensive compilation of Voznesenskaya.³⁸

F. *Data Analysis.* The electrocapillary data were analyzed by digital computer (CDC 6400) using extensions to previously published^{39,40} techniques. In this section three major parts of the data analysis will be outlined: (1) calculation of excess charge density and relative surface excess as functions of electrode potential and solution composition, (2) transfor-

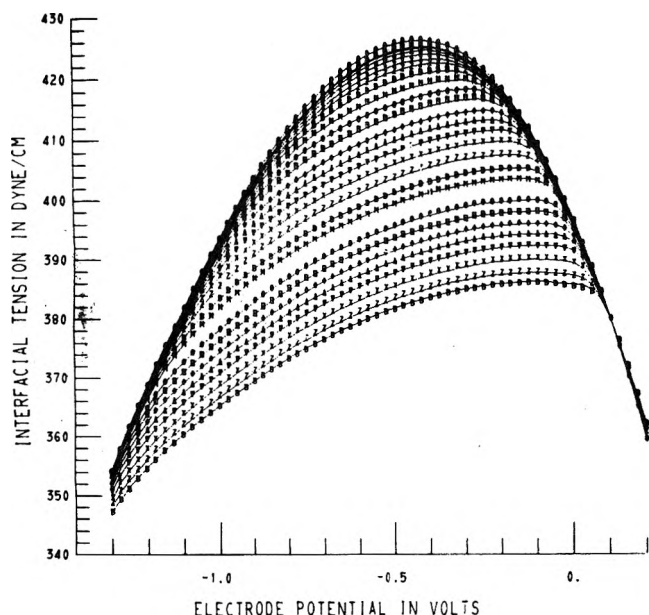


Figure 1. Complete set of electrocapillary curves. In the center section, top curve is base electrolyte curve. Succeeding 25 curves from top to bottom are for increasing concentrations of 2-butanol as listed in Table I.

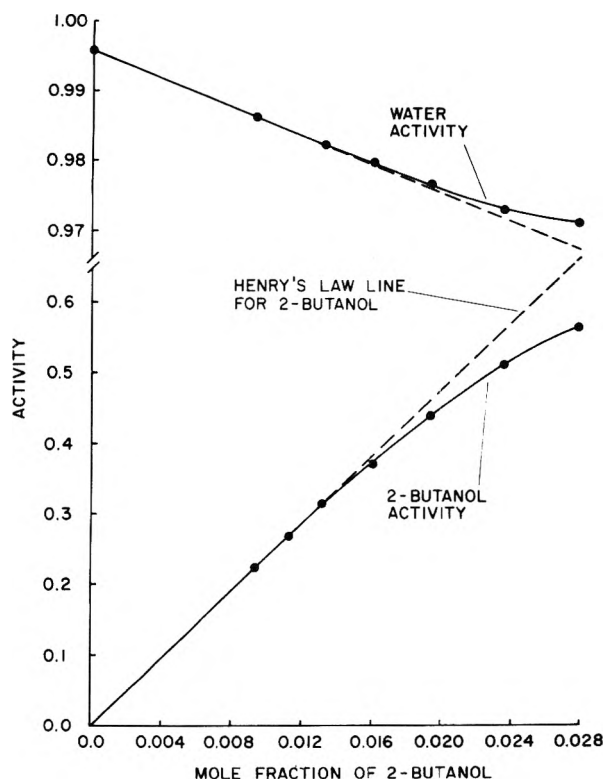


Figure 2. Activity of 2-butanol and of water in solutions in which $a_{\pm} = 0.07087$ as function of mole fraction of 2-butanol.

mation of relative surface excess from the basis of electrode potential to the basis of excess charge density as the independent electrical variable, and (3) determination of confidence limits for the relative surface excess.

1. The excess charge density, σ^M , the relative surface excess, Γ_{AW} , and the smoothed values of the interfacial tension, γ , were calculated by means of a moving least-squares patch on

the electrocapillary surface, $\gamma = \gamma(E^+, \ln a_A)$. The individual patches on this surface were fit by a least-squares polynomial in two independent variables which included terms up to the fourth degree in E^+ and second degree in $\ln a_A$. In those parts of the data where the relative surface excess is small (and the experimental error of $\pm 0.1 \text{ dyn cm}^{-1}$ [see below] is comparable to the changes in γ from one solution to the next) special precautions were taken to ensure that the random errors did not overwhelm the analysis. These precautions took the form of two stages of pretreatment of the data. In the first stage, the base electrolyte solution electrocapillary curve was smoothed by a moving least-squares polynomial in one independent variable (E^+) of degree three, and the excess charge density and smooth values of the interfacial tension were calculated. In the second stage, the interfacial tensions for the nine lowest solution activities, a_A , and the smoothed base electrocapillary curve were subjected to treatment by a moving least-squares patch on the surface $\gamma = \gamma(E^+, a_A)$ subject to the constraints that the smooth interfacial tension for the base curve would be exactly that already determined in the two-dimensional least-squares smoothing of that curve, and that the relative surface excess for the base curve would be exactly zero. For the five solutions of lowest organic concentration, the resulting smooth values of interfacial tension were substituted for the raw data. The complete analysis was then performed on this revised data by a moving least-squares patch on the surface $\gamma = \gamma(E^+, \ln a_A)$ excluding the base electrolyte electrocapillary curve for which $\ln a_A$ is not defined. During this processing, precautions were taken to avoid distortion of the data by requiring each fitted patch on the electrocapillary surface to meet the conditions that the excess charge density at constant organic activity is an increasing function of electrode potential and that the relative surface excess at any electrode potential is either always positive or always negative. Whenever a fitted least-squares patch failed to meet either of these conditions additional points were added to the patch, and it was refit until the conditions were met. The relative surface excesses and the excess charge densities were smoothed and their partial derivatives calculated by similar moving least-squares patch procedures on the surfaces $\sigma^M = \sigma^M(E^+, \ln a_A)$ and $\Gamma_{AW} = \Gamma_{AW}(E^+, \ln a_A)$.

2. The relative surface excess data were transformed from a constant electrode potential basis to a constant excess charge density basis by (a) fitting the electrode potential to the smoothed excess charge density by a moving fourth degree polynomial and interpolating the electrode potential to a defined master set of excess charge densities, and (b) similarly fitting the smoothed relative surface excesses to electrode potential and interpolating the relative surface excess to the electrode potential corresponding to the desired excess charge density. These calculations were carried out for each solution separately.

3. To determine the confidence limits for the data, especially the relative surface excesses, three independent determinations of the electrocapillary curve for 0.1 M Na_2SO_4 were made using the data rejection method described above. For each curve a freshly prepared solution was used, and the pressure transducer and the MBP capillary of the computer-controlled capillary electrometer were independently recalibrated. At each electrode potential the interfacial tension for the three solutions was averaged and the variance was calculated. A chi-square test for the homogeneity of variance³⁰ indicated no significant differences among the variances of the interfacial tension at the different electrode potentials. Therefore, it was justifiable to pool the variances⁴¹ to establish

a single variance of $0.0090 \text{ dyn}^2 \text{ cm}^{-2}$ (standard deviation = $0.095 \text{ dyn cm}^{-1}$) for the interfacial tension. Thus, using the *t*-table, the 95% confidence interval for any interfacial tension measured in triplicate on the computer-controlled capillary electrometer is $\pm 0.1 \text{ dyn cm}^{-1}$.

The variance and standard deviation for the relative surface excess were then calculated from $(\partial\Gamma_{AW}/\partial\gamma)_{E^+}$ and the variance of γ using the single random variate form for the propagation of errors of derived quantities. This partial derivative was calculated at each data point by a moving polynomial at constant electrode potential. The variance of the relative surface excess was then given by⁴²

$$\text{var } \Gamma_{AW} = [(\partial\Gamma_{AW}/\partial\gamma)_{E^+}]^2 \text{var } \gamma \quad (5)$$

where "var" means "the variance of". The standard deviation of Γ_{AW} is shown as a function of Γ_{AW} in Figure 3. In this figure the points are the square roots of the pooled variances⁴¹ for all values of Γ_{AW} lying $\pm 0.1(10)^{-10} \text{ mol cm}^{-2}$ from the plotted abscissae. Only those points are shown for which pooling of the variance was valid according to the chi-square test for the homogeneity of variance.³⁰ A sample electroadsorption isotherm is shown in Figure 4 with the error bars representing 95% confidence limits calculated by multiplying the standard deviations given on the smooth curve in Figure 3 by 1.96.

III. Results and Discussion

A. Excess Charge Density-Potential Curves. At each point on the experimental electrocapillary surface, $\gamma = \gamma(E^+, \ln a_A)$, the partial derivatives of interfacial tension with respect to both E^+ and $\ln a_A$ were obtained simultaneously from the parameters of the moving least-squares fit (section II.F). The excess charge density on the metal surface, σ^M , was then calculated at each experimental point by means of the Lippmann equation⁷ using the determined value of $(\partial\gamma/\partial E^+)_{T,p,a_A,a_e}$ at that point, i.e.

$$\sigma^M = -(\partial\gamma/\partial E^+)_{T,p,a_A,a_e} \quad (6)$$

The results are shown in Figure 5 which shows the σ^M vs. E^+ curves for the base electrolyte (0.1 M Na_2SO_4 in pure water) and for each of the 25 different activities of 2-butanol (Table I) in Na_2SO_4 at the same mean ionic activity ($a_{\pm} = 0.07087$) as the base electrolyte. The points on these curves are the values of σ^M determined directly from the electrocapillary surface, and the smooth curves are the result of the moving least-squares smoothing of the excess charge density surface, $\sigma^M = \sigma^M(E^+, \ln a_A)$ as described in section II.F.1. (A complete table of the smoothed excess charge densities is available as supplementary material.) Superficially, these σ^M - E^+ curves have the shape typical of most published results for organic compounds,^{4,16} i.e., they appear to all cross at a single point, and they appear to be merging back with the base electrolyte curve at extreme potentials where there is complete desorption of the organic compound.

If all of these σ^M - E^+ curves really did cross at a single point, then the coordinates of the point of intersection would give the unique potential of maximum adsorption, E^+_{max} , and the corresponding unique charge density of maximum adsorption, σ^M_{max} , because it follows from the thermodynamic theory of electrocapillarity⁷ that

$$(\partial\sigma^M/\partial \ln a_A)_{T,p,E^+,a_e} = RT(\partial\Gamma_{AW}/\partial E^+)_{T,p,a_A,a_e} \quad (7)$$

and

$$(\partial E^+/\partial \ln a_A)_{T,p,\sigma^M,a_e} = -RT(\partial\Gamma_{AW}/\partial\sigma^M)_{T,p,a_A,a_e} \quad (8)$$

However, when the σ^M - E^+ data are plotted on an expanded

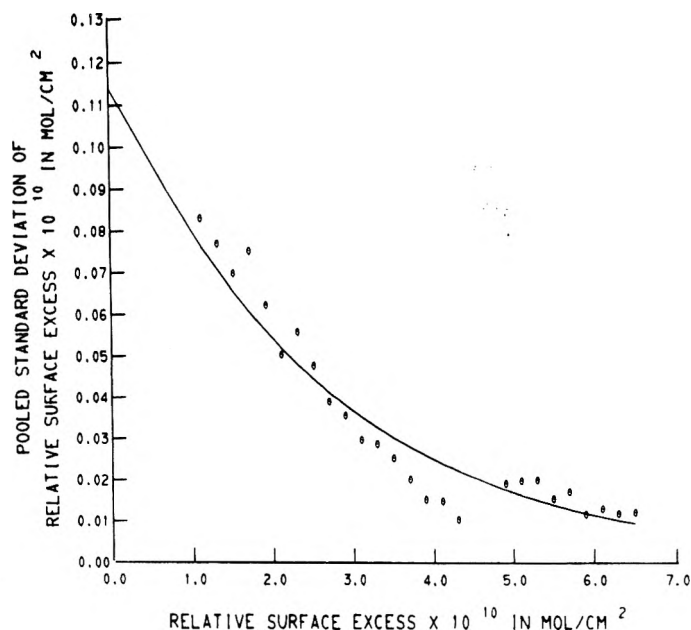


Figure 3. Standard deviation of relative surface excess, Γ_{AW} , as function of the value of Γ_{AW} .

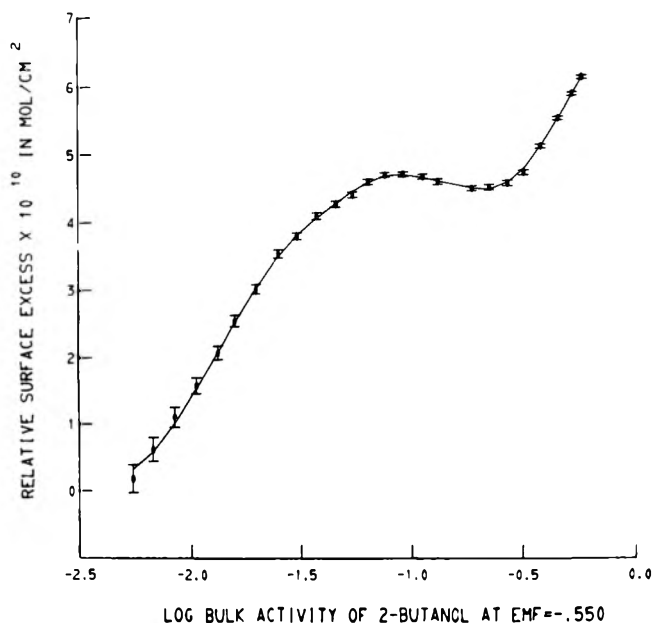


Figure 4. Electroadsorption isotherm for 2-butanol at $E^+ = -0.55 \text{ V}$. Error bars are 95% confidence limits of Γ_{AW} .

scale in the vicinity of the apparent crossing point in Figure 5 it is found that although the curves for the base electrolyte and for the 15 lowest concentrations of 2-butanol do cross quite accurately at a single point ($E^+_{\text{max}} = -0.550 \text{ V}$, $\sigma^M_{\text{max}} = -2.40 \mu\text{C cm}^{-2}$) the curves for the higher concentrations do not. This means that a single potential and a single excess charge density of maximum adsorption should be observed for the lower concentrations, but for the higher concentrations the potential and charge of maximum adsorption should shift away from this value. (See Figures 8 and 10.)

At the extreme positive electrode potentials there is indeed complete desorption of the 2-butanol as is shown in section III.B. Therefore, it would ordinarily have been expected that the σ^M - E^+ curves for all concentrations of 2-butanol would

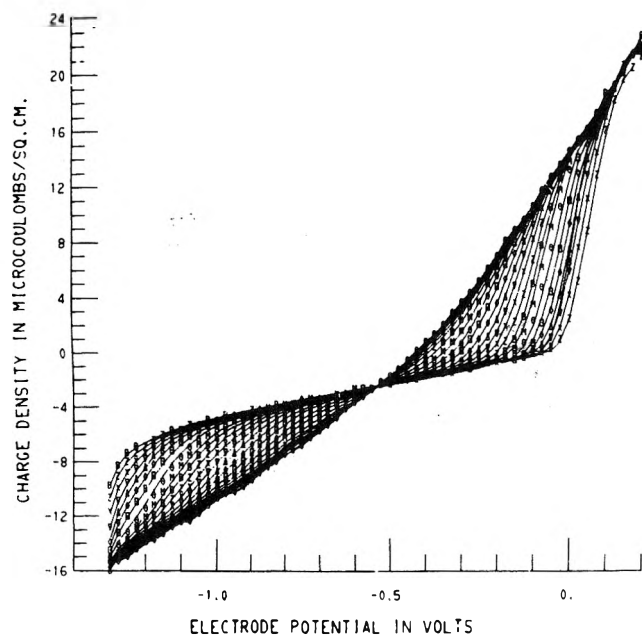


Figure 5. Excess charge density, σ^M , as function of electrode potential. For portion of figure to right of crossing point, top curve is for base electrolyte solution. Succeeding 25 curves from top to bottom are for increasing concentrations of 2-butanol as listed in Table I.

merge with that of the base electrolyte in this potential region. This is because it has been thought⁴³ that in the region of complete desorption the electrocapillary curves in the presence of organic compound merge with that of the base electrolyte. However, we have found in this study the electrocapillary curves for the high concentrations of 2-butanol do not merge with that of the base electrolyte, but, in fact, cross over the base electrolyte curve and lie above it. Therefore, the σ^M - E^+ curves for the high concentrations do not merge with the base electrolyte either. It can be seen from Figure 5 that in the extreme positive E^+ region the excess charge densities for the high concentrations are actually smaller than the σ^M value at the same potential for the base electrolyte. This result is completely consistent with the electrocapillary data (cf. Figure 7) and, as we shall show, is actually to be expected on theoretical grounds (cf. section III.B).

B. Electrosorption Isotherms at Constant Electrode Potential. At each point on the experimental electrocapillary surface the partial derivative, $(\partial\gamma/\partial \ln a_A)_{T,p,E^+,a_e}$ was determined from the parameters of the moving least-squares fit, and the value of the relative surface excess, Γ_{AW} , was calculated from eq 2. Figure 6 shows a set of isotherms at several representative constant electrode potentials. The points on these curves are the values of Γ_{AW} determined directly from the moving least-squares smoothing of the electrocapillary surface, and the smooth curves are the result of the moving least-squares smoothing of the relative surface excess surface, $\Gamma_{AW} = \Gamma_{AW}(E^+, \ln a_A)$, as described in section II.F.1. (A complete table of the smoothed relative surface excesses is available as supplementary material.) The isotherm for $E^+ = -0.55$ V in Figure 6 is the one for the potential of maximum adsorption for the lower 15 concentrations of 2-butanol. This is the same isotherm shown in Figure 4 with the error bars indicating the 95% confidence limits of Γ_{AW} . The main conclusion reached from the error analysis (section II.F.3) was that the error in Γ_{AW} depends on the magnitude of Γ_{AW} , becoming smaller as Γ_{AW} becomes larger, but it is essentially independent of electrode potential. Therefore, if error bars

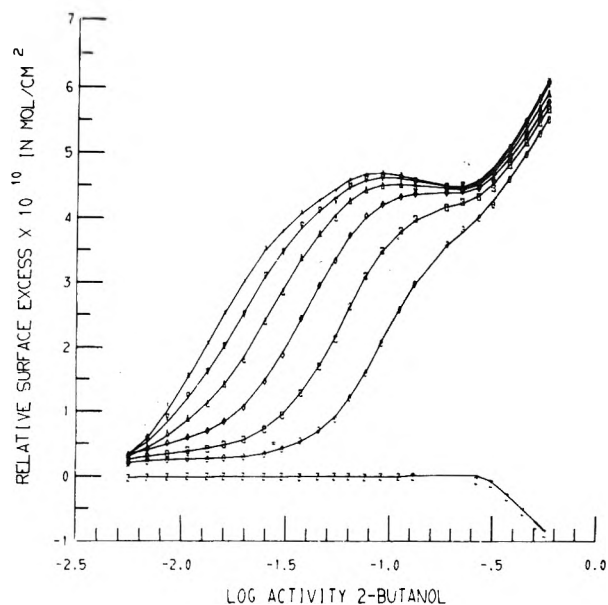


Figure 6. Electrosorption isotherms at constant electrode potential as function of $\ln a_A$. E^+ values: X, -0.55 V; ▽, -0.70 V; △, -0.80 V; ◇, -0.90 V; □, -1.00 V; ○, -1.10 V; Z, $+0.15$ V.

had been shown in Figure 6, they would have the same size as the ones shown in Figure 4 for the same values of Γ_{AW} . For clarity, error bars are not shown in Figure 6 because they would overlap between isotherms which are close together. The constant potential electrosorption isotherms shown in Figure 6 have three features which are different from previously published ones of which we are aware.

First, it is usually expected that an electrosorption isotherm for an organic compound will be S-shaped, rising to a plateau corresponding to monolayer coverage. Depending on the value of the electrode potential the isotherms in Figure 6 do rise with an S-shape to a plateau, but as the activity of the 2-butanol in the bulk solution is increased there is a second rise. We believe this second rise is due to a reorientation of the adsorbed organic molecules from a horizontal to a vertical position. This reorientation will be discussed in detail in section III.F.

Second, the plateau which does appear in these isotherms is not perfectly flat but has a dip in it which is beyond the experimental error (cf. Figure 4). That this dip is real and not an experimental artifact was proved by preparing new samples of all of the solutions in the dip region and remeasuring the electrocapillary curves for these solutions. The agreement between the original and the remeasured electrocapillary curves was within the error of the computer-controlled capillary electrometer.

Third, negative adsorption appears at the highest concentrations for the extreme positive potentials. From eq 2 it follows that the only way Γ_{AW} can be negative is for the interfacial tension to rise at constant electrode potential as the activity, a_A , is increased. Close inspection of Figure 1 reveals that the interfacial tension for the highest concentrations does rise at very positive potentials above the electrocapillary curve for the base electrolyte solution. This rise can be seen more clearly in Figure 7 which is an expanded view of the electrocapillary data in the potential region $+0.1 \leq E^+ \leq +0.2$. It is usually stated⁴³ that the electrocapillary curve for an uncharged substance at the extreme potential ends of the potential range coincides with the curve for the base electrolyte solution because at extreme potentials the neutral substance is com-

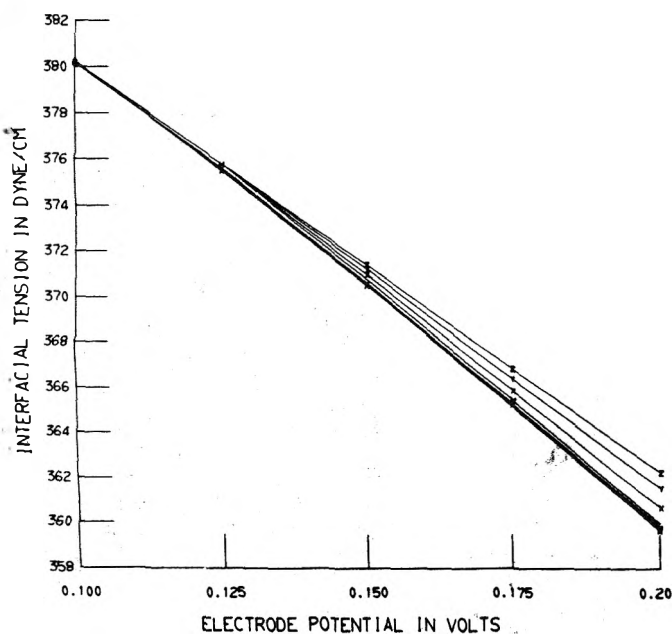


Figure 7. Expanded view of electrocapillary curves (Figure 1) in the region of desorption of 2-butanol. Top curve is for highest concentration of 2-butanol. Succeeding curves, top to bottom, are in order of decreasing concentrations as listed in Table I. Bottom curve is for base electrolyte.

pletely desorbed from the electrode surface. In fact, if the organic molecules are completely desorbed one should expect the relative surface excess Γ_{AW} to become negative because, by definition?

$$\Gamma_{AW} = \Gamma_A - (x_A/x_W)\Gamma_W \quad (9)$$

where Γ_A is the Gibbsian surface excess⁴⁴ (or true surface concentration) of the organic compound, and Γ_W is the Gibbsian surface excess of the adsorbed water. As Γ_A approaches zero it is clear from eq 9 that Γ_{AW} should become negative, and this is the result observed.

Figure 8 shows how Γ_{AW} changes with electrode potential for a representative selection of constant bulk concentrations of 2-butanol. For the lower concentrations, it can be seen that there is a well-defined, constant potential of maximum adsorption, $E^+_{max} = -0.55$ V, corresponding to the crossing point on the σ^M-E^+ curves in Figure 5. However, in the high concentration region corresponding to the second rise on the isotherms in Figure 6, it can be seen that E^+_{max} shifts in the positive direction. We believe such a shift in E^+_{max} is consistent with a reorientation of the 2-butanol molecules from a horizontal to a vertical position because the molecular dipole-electric field interaction in the two orientations should be different. This figure also shows clearly that the relative surface excess becomes negative at extreme positive potentials for the higher concentrations.

C. Electrosorption Isotherms at Constant Excess Charge Density. The relative surface excesses were transformed from a constant electrode potential to a constant charge density basis as indicated in section II.F.2. Figure 9 shows such isotherms for a representative selection of constant values of σ^M . These isotherms also illustrate the first plateau with a dip followed by a second rise at high bulk concentrations. Figure 10 shows the behavior of Γ_{AW} vs. excess charge density at constant bulk concentration. As in the case of the constant potential isotherms, there is a well-defined constant excess charge density of maximum adsorption, $\sigma^M = -2.40 \mu\text{C cm}^{-2}$,

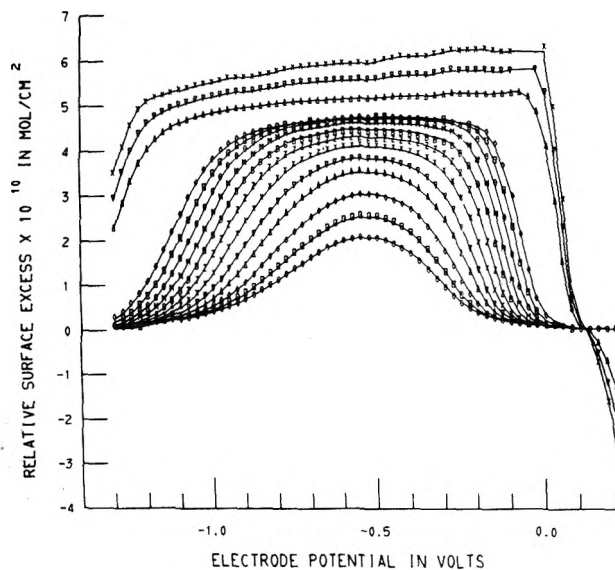


Figure 8. Relative surface excess of 2-butanol at selected concentrations as function of electrode potential. Concentrations of 2-butanol, left section, bottom to top (cf. Table I): 0.0310–0.2550 M and 0.8400–1.200 M.

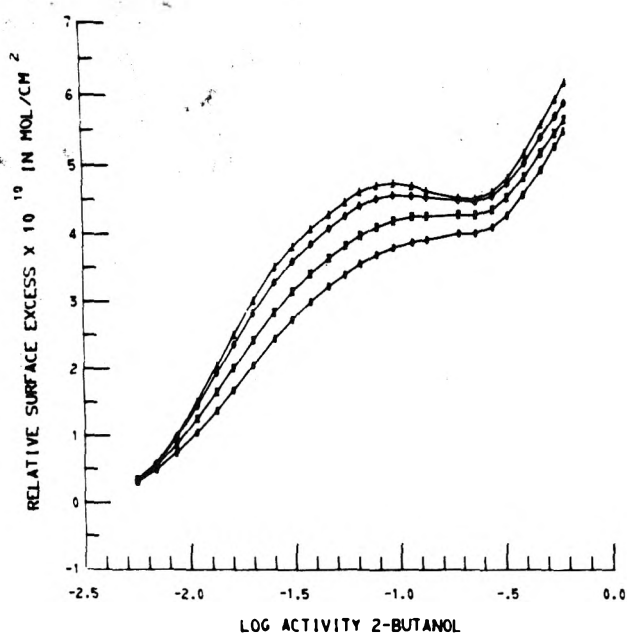


Figure 9. Electrosorption isotherms at constant excess charge density as a function of $\ln a_A$. σ^M values in $\mu\text{C cm}^{-2}$: \odot , -6.00 ; \square , -5.00 ; \diamond , -3.75 ; Δ , -2.20 .

corresponding to the crossing point on the σ^M-E^+ curves in Figure 5 for the lower concentrations, but for higher concentrations in the region of molecular reorientation σ^M_{max} shifts in the positive direction.

D. Congruence of the Electrosorption Isotherms. The concept of the congruence of the electrosorption isotherm with respect to one of the electrical variables (E^\pm or σ^M) arose out of the hope^{45,46} that, if only the proper electrical variable were held constant, the interaction parameters derived from the isotherm would be a true reflection of the particle-particle interactions in the adsorbed layer and would be independent of the electrical state of the system. Thus, the concept of congruence has implicit in it the idea that one of the two experimentally accessible electrical variables, electrode potential

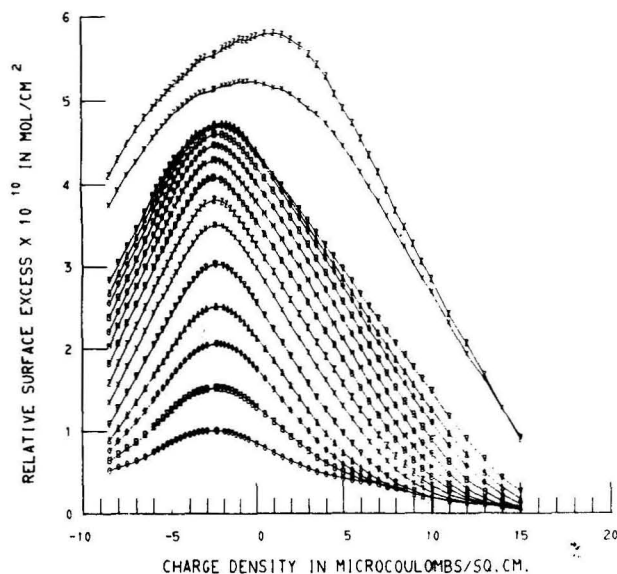
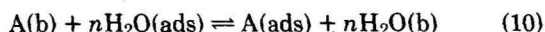


Figure 10. Relative surface excess of 2-butanol at selected concentrations as function of excess charge density. Concentration of 2-butanol center section, bottom to top (cf. Table I): 0.0200–0.2550 M and 0.8400–1.0000 M.

or excess charge density, is somehow more "fundamental" than the other, even though from a purely thermodynamic point of view⁷ it is clear that they are of equivalent importance. In our opinion the concept of congruence, although elegant in its simplicity, is fundamentally unsound, and in part 2⁵ we shall discuss our reasoning on a molecular basis. Nevertheless, because of the emphasis which has been placed on congruence in the past, and especially because of the controversy over whether the electrode potential^{4,47} or the excess charge density^{10,45,46,48,49} is the more fundamental variable, we tested whether the electrosorption of 2-butanol is congruent with respect to either E^+ or σ^M .

The adsorption equilibrium for an organic compound can be expressed by the following chemical equation



where n is the number of water molecules displaced from the electrode surface by one adsorbing organic molecule, (b) indicates the molecule in the bulk of the solution, and (ads) means the molecule is adsorbed. From eq 10 one derives

$$[\exp(-\overline{\Delta G^\circ}/RT)](a_A/a_W^n) = a_A^{ads}/(a_W^{ads})^n \quad (11)$$

where $\overline{\Delta G^\circ}$ is the standard electrochemical free energy of adsorption and a_A^{ads} and a_W^{ads} denote the activities of the adsorbed organic and water molecules in the inner layer, respectively. At constant temperature and pressure $\overline{\Delta G^\circ}$ is a function only of the electrical state of the system, i.e., it is a function either of E^+ or σ^M . If the isotherm is congruent, then the ratio of activities of the adsorbed species, $a_A^{ads}/(a_W^{ads})^n$, will be a function only of the relative surface excess, Γ_{AW} . Therefore, if the isotherm is congruent eq 11 takes the form

$$[\exp(-\overline{\Delta G^\circ}/RT)](a_A/a_W^n) = F(\Gamma_{AW}) \quad (12)$$

(Note that in previous treatments it has always been assumed that $a_W = 1$.)

On the basis of eq 12 we can devise a sensitive test for congruence which is a modification of one proposed by Damaskin.⁵⁰ Consider the electrical state to be fixed by holding either E^+ or σ^M constant, depending on whether the isotherm is

congruent with respect to electrode potential or excess charge density. Then $\overline{\Delta G^\circ}$ is fixed. Now for this electrical state consider the particular value of the ratio of bulk activities, $(a_A/a_W^n)'$, which causes Γ_{AW} to have some arbitrarily chosen value, Γ_{AW}' . Then

$$[\exp(-\overline{\Delta G^\circ}/RT)](a_A/a_W^n)' = F(\Gamma_{AW}') \quad (13)$$

Division of eq 12 by eq 13 at this chosen value of the electrical state causes $\overline{\Delta G^\circ}$ to cancel yielding a normalized adsorption isotherm

$$(a_A/a_W^n)/(a_A/a_W^n)' = F(\Gamma_{AW})/F(\Gamma_{AW}') = G(\Gamma_{AW}) \quad (14)$$

since $F(\Gamma_{AW}')$ is just a constant. From eq 14 it follows that for a congruent isotherm if the proper electrical variable is held constant, the relative surface excess will be the same function of the ratio, $[(a_A/a_W^n)/(a_A/a_W^n)']$, for all values of the electrical variable. For convenience in notation let us denote this ratio of ratios of activities by $(R/R_{ref})'$ where R_{ref} is the particular ratio of bulk activities which causes Γ_{AW} to equal Γ_{AW}' . The normalized form of the congruent isotherm can then be rewritten:

$$\Gamma_{AW} = H(R/R_{ref}) \quad (15)$$

When $R = R_{ref}$, $\Gamma_{AW} = \Gamma_{AW}'$.

We tested our electrosorption data for 2-butanol by choosing $\Gamma_{AW}' = 4.0(10)^{-10}$ mol cm⁻², and to make the test more sensitive we plotted Γ_{AW} vs. $\ln(R/R_{ref})$ instead of (R/R_{ref}) . (For this test we chose $n = 5$ on the basis of molecular models, but the test for congruence is rather insensitive to the value of n , and similar results were obtained for other reasonable choices.) If the isotherm is congruent with respect to the electrical variable, then all plots of Γ_{AW} at different constant values of the electrical variable vs. $\ln(R/R_{ref})$ will superimpose. On the other hand, if the electrosorption is non-congruent, such plots of Γ_{AW} vs. $\ln(R/R_{ref})$ will intersect at the arbitrarily chosen value of Γ_{AW}' but will otherwise diverge. Figure 11 is the test for congruence with respect to E^+ , and Figure 12 is the test for congruence with respect to σ^M . It is clear from Figures 11 and 12 that the electrosorption of 2-butanol on mercury from aqueous sodium sulfate solutions is congruent neither with respect to electrode potential nor with respect to excess charge density.

It might be argued that one would not expect congruence on the basis of either of the theories of congruent electrosorption when molecular reorientation occurs. However, it is evident from Figures 11 and 12 that there is definite non-congruence with respect to either E^+ or σ^M in the portion of the isotherms corresponding to horizontal orientation, because the deviation of the normalized isotherms from each other in that region exceeds the 95% confidence limits of Γ_{AW} (cf. Figure 4). It must be admitted, however, that for the horizontal orientation congruence with respect to electrode potential is a better approximation than congruence with respect to excess charge density.

E. Importance of the Bulk Activity Measurements for 2-Butanol. The activity vs. mole fraction plot in Figure 2 shows that if the usual assumption^{4,10} had been made that the organic compound obeys Henry's law over the entire composition range, the values of the relative surface excess obtained in the high concentration region would have been too low. In the region of negative deviations from Henry's law the slope of a plot of the interfacial tension, γ , vs. $\ln a_{AH}$, where a_{AH} is the activity on the Henry's law line, would be less steep than a plot of γ vs. $\ln a_A$ which should be used according to eq 2. Figure 13 shows the effect of assuming that Henry's law is

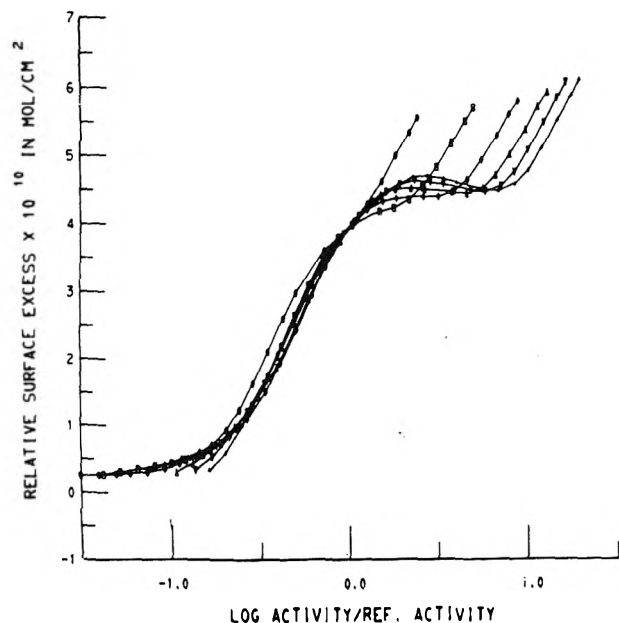


Figure 11. Test for congruence of electrosorption with respect to electrode potential. E^+ values: \odot , -1.10 V; \square , -1.00 V; \diamond , -0.90 V; \triangle , -0.80 V; ∇ , -0.70 V; \times , -0.55 V.

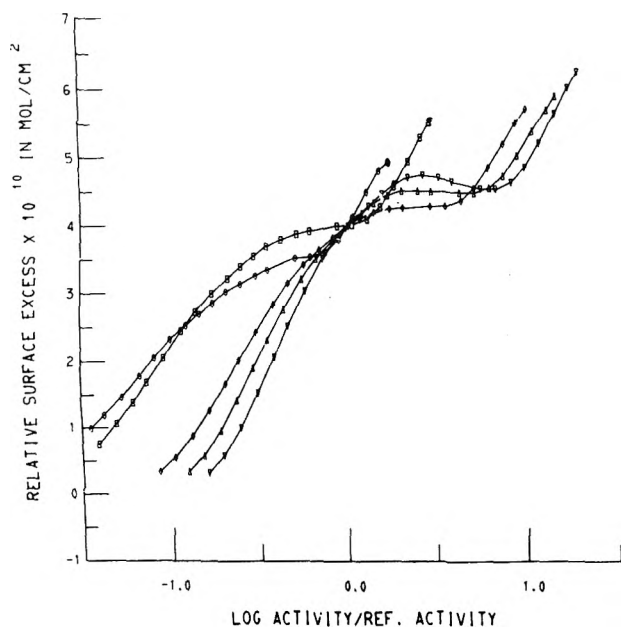


Figure 12. Test for congruence of electrosorption with respect to excess charge density. σ^M values in $\mu\text{C cm}^{-2}$: \odot , -7.5 ; \square , -3.0 ; \diamond , -5.0 ; \triangle , -4.0 ; ∇ , -2.2 .

valid over the entire concentration range. The isotherms in Figure 13 are for the same constant electrode potentials used in Figure 6, but the values of the relative surface excess were calculated by differentiating the interfacial tension with respect to $\ln a_{\text{AH}}$ instead of $\ln a_{\text{A}}$. In the region of low concentrations there are no differences between the two sets of isotherms in Figures 6 and 13, but in the region of high concentrations the differences are striking, namely: there is no indication in Figure 13 of the second rise in the isotherms which indicates molecular reorientation. Thus, if the activity of the 2-butanol had not been measured, the incorrect conclusion would have been reached that the compound merely adsorbs

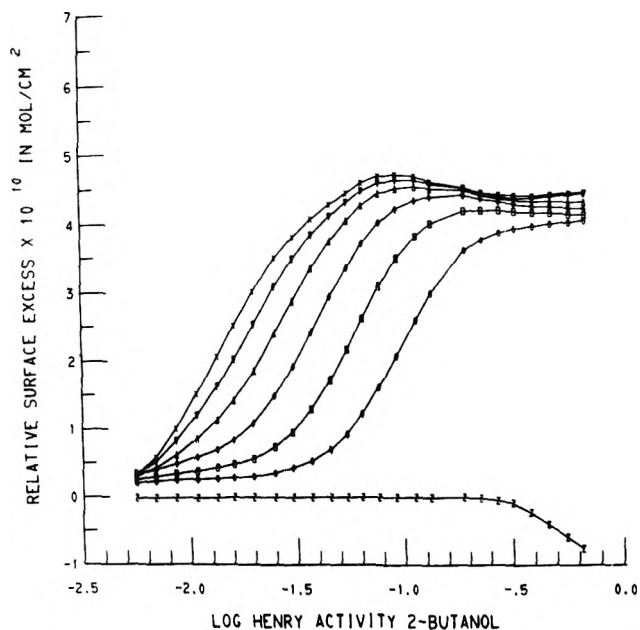


Figure 13. Apparent electrosorption isotherms at constant electrode potential obtained by differentiating interfacial tension with respect to $\ln a_{\text{AH}}$ (cf. Figure 2). E^+ values: \times , -0.55 V; ∇ , -0.70 V; \triangle , -0.80 V; \diamond , -0.90 V; \square , -1.00 V; \odot , -1.10 V; Z , $+0.15$ V.

to form at most a monolayer of horizontally oriented molecules. This result demonstrates that the measurement of the bulk activity of the organic compound in the electrolyte solution can be much more important than has been hitherto suspected.⁵¹ We believe it is likely that in other cases of straight chain aliphatic compounds a molecular reorientation similar to that found in this work for 2-butanol actually occurs in the high concentration region, but this reorientation has been missed as a consequence of the electrochemist's having assumed Henry's law is valid throughout the entire concentration range.

F. Molecular Reorientation of 2-Butanol on the Electrode Surface. The second rise in the electrosorption isotherms (Figures 6 and 9) which occurs with increasing bulk activity of the 2-butanol can be explained on the basis of a molecular reorientation⁵⁴ of the adsorbed organic molecules on the electrode surface. At first the 2-butanol molecules will tend to adsorb in a horizontal orientation in such a way as to allow as much as possible of the hydrocarbon chain to escape from the aqueous phase, i.e., to come in contact with the metal surface. As the bulk activity is increased, the adsorbed molecules will tend to reorient to a vertical position when the surface concentration reaches some critical value which depends on the electrical state of the system.

The experimental electrosorption isotherms, which will hereafter be referred to as the *relative isotherms*, can be derelativized for either the horizontal or vertical orientation by simultaneous solution of eq 9 and the following equation which expresses the fact that the whole surface of the electrode is covered either by the organic compound or by water (there being negligible specific adsorption of sulfate ions in the case considered⁵³):

$$10^{-16}L S_{\text{A}} \Gamma_{\text{A}} + 10^{-16}L (S_{\text{W}}/L_{\text{W}}) \Gamma_{\text{W}} = 1 \quad (16)$$

In eq 16 L is Avagadro's number, S_{A} is the area (in \AA^2) occupied by one organic molecule in its given orientation, S_{W} is the area occupied (in \AA^2) by one adsorbed water molecule, and L_{W} is the number of layers of water molecules lying between the

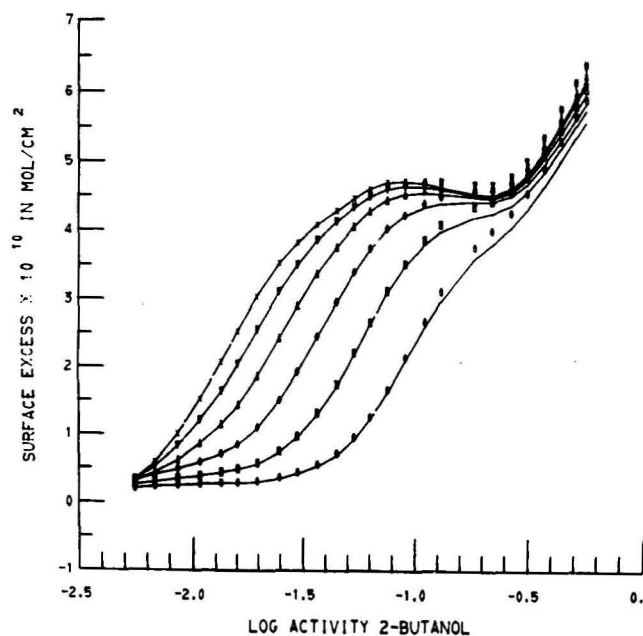


Figure 14. Derelativization of surface excess at constant electrode potential. Points are derelativized surface excesses and corresponding smooth curves are relative surface excesses. E^+ values: \circ , -1.10 V; \square , -1.00 V; \diamond , -0.90 V; \blacktriangle , -0.80 V; \blacktriangledown , -0.70 V; \times , -0.55 V.

dividing surface⁴⁴ and the metal surface. Thus, the model is not a monolayer model for the water because molecular models (Fisher-Taylor-Hershfelder) show that for either orientation of 2-butanol more than one layer of water is required to occupy a layer equal in thickness to a monolayer of 2-butanol. From geometrical considerations it follows that

$$(S_W/L_W) = (S_A/n) \quad (17)$$

where n is the number of adsorbed water molecules displaced by one adsorbing organic molecule (cf. eq 10). When eq 17 is substituted into eq 16 and the resulting equation is solved simultaneously with eq 9, one obtains the following equation for the absolute surface concentration, i.e., the Gibbsian surface excess⁴⁴ of the organic compound in terms of the relative surface excess, the bulk solution mole fractions of the organic compound and of water, and the model parameters for the surface layer.

$$\Gamma_A = \frac{10^{16}L^{-1}n(x_A/x_W) + S_A\Gamma_{AW}}{S_A[n(x_A/x_W) + 1]} \quad (18)$$

The relative isotherms were derelativized by application of eq 18 using $S_A = 34.3 \text{ \AA}^2$ for the horizontal orientation, $S_A = 20.3 \text{ \AA}^2$ for the vertical orientation, and $n = 5$ in both cases. The results for a representative set of constant electrode potential isotherms are shown in Figure 14. The points in this figure are the derelativized surface excesses, and the smooth curves are the relative surface excesses. It can be noted that the dips in the plateau regions of the relative isotherms (Figure 6) at electrode potentials in the neighborhood of the potential of maximum adsorption for the horizontal orientation ($E^+ = -0.55$ V) disappear in the derelativized isotherms. The origin of the dip in the relative isotherms is the increase in Γ_W which occurs when the molecules reorient (cf. eq 9). The reason dips do not appear in the relative isotherms for more extreme electrode potentials where reorientation begins at lower values of Γ_{AW} is evidently because the relative increase of Γ_W on reorientation for these potentials is considerably less than at the potential of maximum adsorption.

It would be expected that as the activity of the organic compound is increased, a second plateau would eventually appear on the electrosorption isotherm corresponding to the formation of a close-packed monolayer of vertically oriented molecules. In the case of this study, this second plateau could not be reached because it was not possible to increase the activity of the 2-butanol in the bulk solution sufficiently due to the limited solubility of 2-butanol in the electrolyte solution.

IV. Conclusions

The electrosorption of 2-butanol on mercury from aqueous sodium sulfate solutions has been measured with a computer-controlled capillary electrometer. Constant chemical potential of sodium sulfate was maintained in the series of solutions studied, and the activity of the 2-butanol in each solution was determined. Because the thermodynamic analysis was carried out taking account of activities it was possible to detect a reorientation of the 2-butanol molecules on the electrode surface. It was shown that if the analysis of the data had been performed using concentrations instead of activities the molecular reorientation would have escaped detection. The electrosorption was shown to be congruent neither with respect to electrode potential nor with respect to excess charge density.

Acknowledgments. This work was supported by the United States Air Force Office of Scientific Research under Grant No. AF-AFOSR-70-1887. We thank Professor M. M. Siddiqui, Department of Statistics, Colorado State University, for valuable discussion of the propagation of errors in derived quantities.

Supplementary Material Available: Tables of the original electrocapillary data, the excess charge density (smoothed) as a function of electrode potential and 2-butanol activity, and relative surface excess (smoothed) as a function of electrode potential and 2-butanol activity for all solutions (Table I) (21 pages). Ordering information is available on any current masthead page.

References and Notes

- (1) Taken in part from the Dissertation of Hisamitsu Nakadomari, submitted to the Department of Chemistry and the Faculty of the Graduate School of Colorado State University in partial fulfillment of the requirements for the degree of Doctor of Philosophy, 1974.
- (2) Present address: Department of Applied Science, Brookhaven National Laboratory, Upton, L.I., N.Y. 11973.
- (3) To whom correspondence and requests for reprints should be addressed at the Department of Chemistry.
- (4) B. B. Damaskin, O. A. Petrii, and V. V. Batrakov, "Adsorption of Organic Compounds on Electrodes", Plenum Press, New York, N.Y., 1971.
- (5) D. M. Mohilner, H. Nakadomari, and P. R. Mohilner, *J. Phys. Chem.*, to be submitted for publication.
- (6) D. M. Mohilner and H. Nakadomari, *J. Electroanal. Chem.*, **65**, 843 (1975).
- (7) For a review, cf. D. M. Mohilner in "Electroanalytical Chemistry", Vol. 1, A. J. Bard, Ed., Marcel Dekker, New York, N.Y., 1966, pp 241-409.
- (8) A. de Battisti and S. Trasatti, *J. Electroanal. Chem.*, **54**, 1 (1974).
- (9) A. Abd-el-Naby, A. De Battisti, and S. Trasatti, *J. Electroanal. Chem.*, **56**, 101 (1974).
- (10) E. Dutkiewicz, J. D. Garnish, and R. Parsons, *J. Electroanal. Chem.*, **16**, 505 (1968).
- (11) The special kind of reference electrode required by the thermodynamic theory of electrocapillarity⁷ behaves exactly like an indicator electrode in a potentiometric titration, i.e., its potential with respect to a standard hydrogen electrode is a direct measure of the activity in the solution of the ion to which it is reversible. In order to avoid confusion between this special kind of electrode and an ordinary, constant potential reference electrode such as the standard hydrogen electrode or the saturated calomel electrode, it has been recommended^{8,7,12} that it be denoted the "indicator electrode" rather than the "reference electrode" in discussions of electrocapillarity.
- (12) D. M. Mohilner and N. Hackerman, *Electrochim. Acta.*, **11**, 1669 (1966).
- (13) a_A is based on the pure organic compound at 25 °C as the standard state.
- (14) a_A is based on the hypothetical standard state¹⁵ derived from the properties

- of the infinitely dilute solution of the electrolyte in pure water, *not* on the infinitely dilute solution of the electrolyte in each water-organic mixture. Thus, constancy of the bulk activity, a_{∞} , of the electrolyte in a series of water-organic mixtures based on this standard state implies constancy of the electrolyte chemical potential in the same series of mixtures.
- (15) I. M. Klotz, "Chemical Thermodynamics", Revised edition, W. A. Benjamin, New York, N.Y., 1966.
- (16) For recent reviews, cf. R. Payne, *J. Electroanal. Chem.*, **41**, 277 (1973); S. Trasatti, *ibid.*, **53**, 355 (1974).
- (17) There are a few isolated instances in the literature in which the chemical potential of the electrolyte was held constant because the organic electro-sorption was studied in solutions saturated with a solid salt. For example: (a) J. P. Tverdovskii and A. N. Frumkin, *Zh. Fiz. Khim.*, **21**, 819 (1947); (b) R. S. Maislish, I. P. Tverdovskii, and A. N. Frumkin, *ibid.*, **28**, 87 (1954); (c) K. Doblhofer and D. M. Mohilner, *J. Phys. Chem.*, **75**, 1658 (1971).
- (18) D. M. Mohilner and H. Nakadomari, *J. Phys. Chem.*, **77**, 1594 (1973).
- (19) I. M. Klotz in "Membranes and Ion Transport", E. E. Bittar, Ed., Wiley-Interscience, New York, N.Y., 1970; I. M. Klotz, *Science*, **128**, 815 (1958).
- (20) G. A. Jeffrey in "Proceedings of the Conference on Desalination Research", Publ. No. 942, NAS-NRC, Washington, D.C., 1963, pp 156-172.
- (21) F. Franks in "Water, A Comprehensive Treatise", Vol. 2, F. Franks, Ed., Plenum Press, New York, N.Y., 1973, Chapters 1 and 5.
- (22) H. S. Frank and M. W. Evans, *J. Chem. Phys.*, **13**, 507 (1945).
- (23) H. S. Harned and B. B. Owen, "The Physical Chemistry of Electrolytic Solutions", 3rd ed, Reinhold, New York, N.Y., 1958.
- (24) This mean ionic activity was obtained from the table²³ of the stoichiometric mean molal activity coefficients of aqueous solutions of Na₂SO₄ at 25 °C by cubic interpolation.
- (25) H. S. Harned and J. C. Hecker, *J. Am. Chem. Soc.*, **56**, 650 (1934).
- (26) R. D. Lanier, *J. Phys. Chem.*, **69**, 2697, 3992 (1965).
- (27) M. H. Lietzke and R. W. Stoughton, *J. Tenn. Acad. Sci.*, **42**, 26 (1967).
- (28) The two-phase lead amalgam-lead sulfate electrode was used because it is impossible to obtain satisfactory emf measurements with the more common mercury-mercurous sulfate electrode in neutral sodium sulfate solutions. In neutral solutions yellow basic substances are formed which produce a drifting emf as was first noted by Åkerlöf²⁹ in 1926.
- (29) G. Åkerlöf, *J. Am. Chem. Soc.*, **48**, 1160 (1926).
- (30) W. J. Youden, "Statistical Methods for Chemists", Wiley New York, N.Y., 1951.
- (31) J. Lawrence and D. M. Mohilner, *J. Electrochem. Soc.*, **118**, 1596 (1971).
- (32) W. J. Dixon, *Ann. Math. Stat.*, **21**, 488 (1950); **22**, 68 (1951).
- (33) The criterion for data rejection was made much less conservative than is usual because automatic repetition of a measurement with the computer controlled capillary electrometer is so fast. Therefore rejection was based on the 40% confidence level instead of the well-known Q-test³² criterion of 90%.
- (34) R. B. Dean and W. J. Dixon, *Anal. Chem.*, **23**, 636 (1951).
- (35) C. A. Smolders and E. M. Duyvis, *Recl. Trav. Chem. Pays-Bas*, **80**, 635 (1961).
- (36) D. M. Mohilner, L. M. Bowman, S. J. Freeland, and H. Nakadomari, *J. Electrochem. Soc.*, **120**, 1658 (1973); **121**, 1194 (1974).
- (37) The standard state upon which the water activity is based is pure water at 25 °C.
- (38) I. E. Voznesenskaya in "Voprosy Fizicheskoi Khimii Rastvorov Elektrolitov", G. I. Mikulina, Ed., Izdatel'stvo "Khimiya", Leningradskoe Otdelenie, 1968, pp 172-201. (Available from the Library of Congress. Call no. QD561/V64.)
- (39) D. M. Mohilner and P. R. Mohilner, *J. Electrochem. Soc.*, **115**, 261 (1968).
- (40) P. R. Mohilner and D. M. Mohilner in "Computers in Chemistry and Instrumentation", Vol. 2, J. S. Mattson, H. B. Mark, Jr., and H. C. MacDonald, Jr., Ed., Marcel Dekker, New York, N.Y., 1972, pp 3-44.
- (41) W. J. Dixon and F. J. Massey, Jr., "Introduction to Statistical Analysis", McGraw-Hill, New York, N.Y., 1957, p 109.
- (42) H. D. Young, "Statistical Treatment of Experimental Data", McGraw-Hill, New York, N.Y., 1962, pp 96-98.
- (43) Cf. for example, R. Parsons, *J. Electroanal. Chem.*, **5**, 397 (1963).
- (44) The Gibbsian surface excesses⁷ referred to in eq 9 are reckoned on the basis of a dividing surface placed just on the solution side of the layer of adsorbed organic molecules on the metal surface. This choice of the location of the dividing surface ensures that Γ_A is equal to the actual surface concentration of adsorbed organic molecules.
- (45) R. Parsons, *Trans. Faraday Soc.*, **51**, 1518 (1955); **55**, 999 (1959).
- (46) R. Parsons, *J. Electroanal. Chem.*, **7**, 136 (1964).
- (47) A. N. Frumkin, B. B. Damaskin, and A. A. Survila, *J. Electroanal. Chem.*, **16**, 493 (1968).
- (48) J. O'M. Bockris, M. A. V. Devanathan, and K. Muller, *Proc. R. Soc. London, Ser. A*, **274**, 55 (1963).
- (49) A. de Battisti and S. Trasatti, *J. Electroanal. Chem.*, **48**, 213 (1973).
- (50) B. B. Damaskin, *J. Electroanal. Chem.*, **7**, 155 (1964).
- (51) It can be especially misleading in attempting to estimate the importance of using organic activities instead of concentrations merely to consider the value of the logarithm of the rational activity coefficient,¹⁵ γ_{Ar} , which is based on the hypothetical standard state of unit mole fraction obeying Henry's law. For example, from the data of Butler⁵² it could be estimated that for a 0.5 M solution of 1-butanol the logarithm (base 10) of the rational activity coefficient was only -0.03. Therefore, it was concluded¹⁰ that because of this small value of $\log \gamma_{Ar}$ only a negligible error in the relative surface excess would result from analysis of the electrocapillary data for this compound in 0.0995 M NH₄F solutions using concentrations in place of activities. However, for the four highest concentrations of 2-butanol used in our study (0.84, 1.0, 1.2, and 1.4 M) the logarithm (base 10) of the rational activity coefficients are, respectively, only -0.0103, -0.0159, -0.0367, and -0.0669. Nevertheless, these small deviations of $\log \gamma_{Ar}$ from 0.000 are entirely responsible for the differences between the correct isotherms in Figure 6 and the incorrect isotherms in Figure 13.
- (52) J. A. V. Butler, D. W. Thomson, and W. H. Maclellan, *J. Chem. Soc.*, 674 (1933).
- (53) R. Payne, *J. Electroanal. Chem.*, **60**, 183 (1975).
- (54) To our knowledge, molecular reorientation has not been proposed previously for straight chain aliphatic molecules adsorbed at the mercury-solution interface. However, molecular reorientation of adsorbed aromatic compounds (pyridine and aniline) was proposed more than a decade ago by Damaskin and coworkers.⁵⁵⁻⁵⁷ Reorientation of the adsorbed aromatic anion, benzene-*m*-disulfonate, was proposed in 1966 by Parry and Parsons.⁵⁸
- (55) L. D. Klukina and B. B. Damaskin, *Izv. Akad. Nauk SSSR, Otd. Khim. Nauk*, No. 6, 1022 (1963).
- (56) B. B. Damaskin, I. P. Mishutushkina, V. M. Gerovich, and R. I. Kaganovich, *Zh. Fiz. Khim.*, **38**, 2495 (1964).
- (57) B. B. Damaskin, *Electrochim. Acta*, **9**, 231 (1964).
- (58) J. M. Parry and R. Parsons, *J. Electrochem. Soc.*, **113**, 992 (1966).

Oxidation of Silicon by Water and Oxygen and Diffusion in Fused Silica

R. H. Doremus

Rensselaer Polytechnic Institute, Materials Engineering Department, Troy, New York 12181 (Received January 29, 1976)

Publication costs assisted by Rensselaer Polytechnic Institute

A model for the oxidation of silicon by diffusion of molecular oxygen or water through the silicon oxide layer is compared to experimentally measured oxidation rates, using diffusion coefficients and solubilities measured for fused silica. Good agreement between calculated and measured rates results in three respects: the absolute rate, and its pressure and temperature dependence. The model of molecular diffusion therefore provides the most satisfactory explanation for diffusion-controlled oxidation of silicon.

Introduction

Diffusion of components through a coherent film of oxide often controls the rate of oxidation of metals and semiconductors; then the square of the oxide thickness is proportional to time (parabolic rate). Diffusion of metallic or oxygen ions is usually considered to control the oxidation rate; however, diffusion of the oxidizing species themselves (water or oxygen molecules) through the oxide can control the rate of oxidation if such molecular diffusion is rapid enough.

In this paper evidence is presented that the diffusion-controlled oxidation of silicon by water or oxygen results from molecular diffusion of these gases through the silicon dioxide layer. First experimental results on the oxidation of silicon are briefly reviewed, and then molecular diffusion of gases in fused silica is discussed. X-ray diffraction experiments have shown that the oxide layer on silicon is amorphous and similar to fused silica;¹ the density of the layer is also about that of fused silica, so the film is probably quite similar to fused silica. Models for the oxidation of silicon by molecular diffusion are presented and compared to oxidation rates and diffusion coefficients of water and oxygen in fused silica. Good agreement between the models, oxidation experiments, and these diffusion coefficients is found in three respects: the pressure dependence, the absolute value of the oxidation rate, and the temperature dependence. Thus molecular diffusion of water and oxygen in the oxide layer provide the most satisfactory explanation for diffusion-controlled oxidation of silicon.

Oxidation of Silicon by Dry Oxygen

Early results were reviewed by Deal and Grove,² and they reported results of their own. More recent reports are in ref 3-5. These authors all agree that there are two different time dependencies during the oxidation of silicon by dry oxygen: initially there is a linear region; then the rate becomes parabolic. The layer thickness X as a function of oxidation time t is given by the equation

$$X^2 + AX = B(t + \tau) \quad (1)$$

where A and B are coefficients independent of time and τ provides for a thin layer present before experimental oxidation begins. At long times and large thicknesses

$$2X \, dX/dt = B \quad (2)$$

B is the parabolic rate constant related to diffusion-controlled oxidation. Deal and Grove found that $B = 3.2(10)^{-14} \text{ cm}^2/\text{s}$ at 1000 °C and 1 atm of oxygen with a temperature dependence

$$B = B_0 \exp(-Q/RT) \quad (3)$$

and the activation energy Q was 28 kcal/mol. B was directly proportional to oxygen pressure. Similar results were found by most other investigators. Growth occurred at the silicon-oxide interface, so one can conclude that an oxidizing species must diffuse through the oxide film to this interface.

Oxidation of Silicon by Water

Deal and Grove discussed their own and earlier work;² later reports are in ref 3, 5, and 6. Again there was an initial linear dependence of layer thickness on time and subsequently parabolic dependence; eq 1 reasonably represented the results. B was proportional to pressure, and oxidation occurred at the silicon-oxide interface, so an oxidizing species was diffusing through the oxide layer.

Deal and Grove found $B = 9.45(10)^{-13} \text{ cm}^2/\text{s}$ at 1000 °C and 1 atm of water, and Ota and Butler agreed closely with this result. The temperature dependence followed eq 3 with $Q = 16 \text{ kcal/mol}$.

Diffusion in Fused Silica

Fused silica contains silicon-oxygen tetrahedra linked together strongly in a three-dimensional network. The resulting amorphous structure shows considerable short-range order but no long-range order beyond a few tetrahedral distances. The structure is quite open, and can be thought of as containing interstices or holes a few angstrom units in diameter and 5 to 10 Å apart.

Gas molecules dissolve and diffuse easily in fused silica.⁷ The solubilities of helium, neon, and hydrogen in fused silica are about the same, are almost independent of temperature, and are proportional to gas pressure. The solubility of oxygen is somewhat lower, but the concentration dissolved is still about 1% of the surrounding concentration of oxygen gas.⁸

The activation energies Q for molecular diffusion in fused silica are related to molecular sizes, and are given by the equation⁷

$$Q^{1/2} = a + br \quad (4)$$

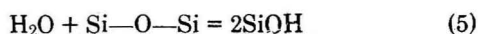
where a and b are constants and r is the molecular radius. This equation holds well for gases with molecular radii from helium ($r = 1.0 \text{ Å}$) to xenon ($r = 2.5 \text{ Å}$). Activation energies for molecular diffusion of oxygen⁸ and water^{9,10} are consistent with their molecular sizes. Thus these gases can diffuse readily through fused silica, and analogously through the silica layer on oxidized silicon.

The high silicon-oxygen bond energy of 106 kcal/mol leads

one to predict a low concentration of oxygen vacancies and a low diffusion coefficient of lattice oxygen in silica. The activation energy for diffusion of lattice oxygen in fused silica has not been reliably measured, but in soda-lime glass, in which Q should be lower than in fused silica, the activation energy for diffusion of lattice oxygen was measured to be about 66 kcal/mol.¹¹ Therefore it is highly unlikely that diffusion of lattice oxygen contributes appreciably to the oxidation of silicon, with its relatively high rate and low activation energy. Furthermore direct proportionality of oxidation rate to gas pressure would not be expected for diffusion of lattice oxygen.

One might also imagine that oxygen ions could be introduced into the silica from the gas phase. However, to introduce a concentration of oxygen ions sufficient to give the experimental rates of oxidation would require the formation of an impossibly large space charge in the oxide. Thus compensating positive ions would have to be introduced along with the negative oxygen ions. There are no likely candidates for these positive ions, or evidence for their existence.

The diffusion of water in fused silica is complicated by the reaction of water with silicon-oxygen bonds:



The apparent solubility of water in fused silica is much higher than the molecular solubilities of other gases because of this reaction, and the solubility is proportional to the square root of the water vapor pressure, as expected from eq 5. Reaction 5 also influences the diffusion of water in fused silica, leading to a concentration-dependent diffusion coefficient.⁹

These complications are taken into account in a model of molecular diffusion plus reaction to immobile SiOH groups.¹⁰ The concentration of reacted water S at any point in the glass is much greater than the concentration of molecularly dissolved water C , and these concentrations are related by $S = KC^{1/2}$, as derived from reaction 5, where K is a concentration-independent coefficient. Under these conditions diffusion is controlled by an effective diffusion coefficient D_e :

$$D_e = 2DS/K^2 = 2DC/S \quad (6)$$

where D is the diffusion coefficient of molecularly dissolved water. The profile of S vs. penetration distance derived from eq 6 is in good agreement with experimental data for water in fused silica.¹⁰ Thus it is possible to derive values of the diffusion coefficient of molecular water from profiles of the reacted water S vs. distance. There are several printing errors in ref 7 and 10. The diffusion coefficient of molecular water at 1000 °C in Table II, p 133, ref 7, and Table I, p 670, ref 10, should be $3.6(10)^{-7}$ cm²/s, as derived in the Appendix.

Models for Diffusion-Controlled Oxidation of Silicon

The diffusion of oxygen in silica is not complicated by its reaction with the silica lattice. The equation for the diffusion-controlled moving boundary problem for formation of an oxide layer of thickness X is¹²

$$X \frac{dX}{dt} = \frac{c_i D}{\rho} \quad (7)$$

where D is the diffusion coefficient of the oxidizing species in the layer, c_i is its concentration at the outer oxide surface, and ρ is the concentration of oxygen in the film. For eq 7 to be valid $c_i \ll \rho$, and the concentration of oxidant at the silicon-oxide surface is negligible. From eq 7 and 2, the parabolic rate constant B is

$$B = 2c_i D / \rho \quad (8)$$

The diffusion coefficient of molecular oxygen in fused silica at 1000 °C is $6.6(10)^{-9}$ cm²/s with an activation energy of 27 kcal/mol.⁸ The value of c_i is about 0.01 of the oxygen gas concentration,⁸ or $9.6(10)^{-8}$ mol of O₂/cm³ for 1 atm pressure. The concentration ρ of oxygen (O) in the oxide is $7.3(10)^{-2}$ mol of O/cm³. The value of B calculated from eq 8 is therefore $3.4(10)^{-14}$ cm²/s, in good agreement with Deal and Grove's value of $3.2(10)^{-14}$ cm²/s for the oxidation of silicon in 1 atm of dry oxygen. The concentration or solubility c_i for fused silica is directly proportional to pressure, as is the value of B for oxidation of silicon in dry oxygen. Deal and Grove found an activation energy for B of about 28 kcal/mol, in good agreement with the value of 27 kcal/mol for fused silica, since c_i is little dependent on temperature for molecular solubility in silica.⁷

The good agreement between calculated and measured values of B , between pressure dependencies of B , and between activation energies of B give strong support to the present model based on diffusion of uncharged oxygen molecules through a silica layer for explaining the oxidation rate of silicon in dry oxygen. Major¹³ also concluded that diffusion of molecular oxygen was controlling the rate of oxidation of silicon in oxygen from a proton activation study.

The molecular diffusion of water in silica is complicated by its reaction with the silica lattice (eq 5). However, if the molecular diffusion coefficient D from eq 6 is substituted into eq 8, the following relation for B is found:

$$B = D_e S_i / \rho \quad (9)$$

where D_e is the effective (measured) diffusion coefficient of water in silica and S_i is the concentration of reacted water in equilibrium with gaseous water vapor. The validity of this substitution is considered in the Appendix. At 1000 °C and a water vapor pressure of 1 atm Moulson and Roberts found⁹ $D_e = 6.3(10)^{-10}$ cm²/s and $S_i = 1.1(10)^{-4}$ mol of H₂O/cm³ for fused silica, so from eq 9, $B = 9.5(10)^{-13}$ cm²/s, in fortuitously good agreement with Deal and Grove's value² of $9.5(10)^{-13}$ cm²/s for oxidation of silicon at 1000 °C in 1 atm of water vapor.

The activation energy for oxidation of silicon by water is about 16 kcal/mol,² in good agreement with a value of 18 kcal/mol for diffusion of water in fused silica.⁹ The solubility S_i of water in fused silica was not much changed with temperature above about 900 °C.

From eq 6, $D_e S_i = 2Dc_i$. Since D should be independent of pressure and the molecular solubility c_i proportional to it, B is predicted to be proportional to pressure from eq 9, as found experimentally.

Again the good agreement between calculated and measured values of B for the oxidation of silicon in water, and between predicted and measured temperature and pressure dependencies of B , strongly support the model that diffusion of uncharged water molecules controls the rate of oxidation of silicon in water vapor.

The profile of hydrogen in the silica layer on silicon oxidized in water is also consistent with a model of molecular diffusion of water, as shown in a subsequent paper.¹⁴

Appendix. Molecular Diffusion and Chemical Reaction of Water in Fused Silica

The concentration S of reacted water, or SiOH groups (eq 5), at a particular point in the silica is given by

$$S = kc^{1/2} \quad (A1)$$

where c is the concentration of dissolved water. If $S \gg c$, the equation of continuity (Fick's second law) is (ref 12, p 122)

$$\frac{\partial S}{\partial t} = \frac{\partial}{\partial x} \left[\frac{2DS}{K^2} \frac{\partial S}{\partial x} \right] \quad (\text{A2})$$

Since the molecular diffusion coefficient D is independent of the concentration of molecularly dissolved water, which is small, eq A2 has the same solution for a diffusion coefficient directly proportional to concentration S (eq 6). A solution to eq A2 for semiinfinite geometry with constant surface concentration agreed well¹⁰ with data⁹ on the profile of SiOH groups in fused silica after contact with water vapor at about 1000 °C.

The condition $S \gg c$ allows one to neglect $\partial c/\partial t$ compared to $\partial S/\partial t$, with eq A2 as the result. For fused silica at 1000 °C the equilibrium solubility $S_i = 1.1(10)^{-4}$ mol of $\text{H}_2\text{O}/\text{cm}^3$ and the concentration of molecularly dissolved water should be about 0.01 the concentration in the gas phase, or about $9.6(10)^{-8}$ mol of $\text{H}_2\text{O}/\text{cm}^3$ for 1 atm pressure, so the inequality is valid. These values give a molecular diffusion coefficient D for water of about $3.6(10)^{-7}$ cm^2/s at 1000 °C from eq 6.

In the present case a solution of eq A2 for a film of increasing dimension is desired. For diffusion without reaction (i.e., oxygen in silica) the condition $c \ll \rho$ results in a linear dependence of the diffusant concentration as a function of distance in the film, and consequently in the validity of eq 7. Physically the condition $c \ll \rho$ may be regarded as follows. The flux of diffusant that must pass through the film to grow it a certain amount is large, because ρ is large; thus the time to grow to a layer of thickness X is so large that the average diffusion distance of the diffusing molecules is much greater than X . Consequently these molecules behave as if they had reached a steady state, and the solution of moving-boundary problem is the same as the steady-state solution for diffusion through a flat layer or membrane with surface concentrations held constant.

Therefore if the condition $S_i \ll \rho$ holds, the steady-state solution to eq A2 should be valid. Since $\rho = 7.3(10)^{-2}$ mol of O/cm^3 , this condition is effective, and one can assume $\partial S/\partial t = 0$. Then from eq A2

$$\frac{2DS}{K^2} \frac{\partial S}{\partial x} = P_1 \quad (\text{A3})$$

where P_1 is a constant to be determined from the boundary conditions: when

$$\begin{aligned} x = 0, S &= S_1 \\ x = X, S &= 0 \end{aligned} \quad (\text{A4})$$

Integration of eq A3 gives

$$S^2 = \frac{P_1 K^2 x}{D} + P_2 \quad (\text{A5})$$

and from the boundary conditions

$$S^2/S_1^2 = 1 - (x/X) \quad (\text{A6})$$

From eq A1

$$c/c_i = 1 - (x/X) \quad (\text{A7})$$

Therefore the concentration c of molecularly dissolved water has a linear dependence of distance x in the oxide film, whereas the amount of reacted water is proportional to the square root of the distance $(x - X)$ in the film.

Under these conditions eq 7 is valid for the dependence of layer thickness on the diffusion of molecular water in the film, and with the substitution of eq 6, eq 9 results.

References and Notes

- (1) M. B. Brodsky and D. Cubicciotti, *J. Am. Chem. Soc.*, **73**, 3497 (1951).
- (2) B. E. Deal and A. S. Grove, *J. Appl. Phys.*, **36**, 3770 (1965).
- (3) A. G. Revesz and R. J. Evans, *J. Chem. Phys. Solids*, **30**, 551 (1969).
- (4) G. A. Haas and H. F. Grey, *J. Appl. Phys.*, **46**, 3885 (1975).
- (5) M. A. Hopper, R. A. Clarke, and L. Young, *J. Electrochem. Soc.*, **122**, 1216 (1975).
- (6) Y. Ota and S. R. Butler, *J. Electrochem. Soc.*, **121**, 1107 (1974).
- (7) R. H. Doremus, "Glass Science", Wiley, New York, N.Y., 1973, p 121 ff.
- (8) F. J. Norton, *Nature (London)*, **191**, 701 (1961).
- (9) A. J. Moulson and J. P. Roberts, *Trans. Faraday Soc.*, **57**, 1208 (1961).
- (10) R. H. Doremus in "Reactivity of Solids", Mitchell, DeVries, Roberts, and Cannon, Ed., Wiley, New York, N.Y., 1969, p 667.
- (11) W. D. Kingery and J. A. Lecron, *Phys. Chem. Glasses*, **1**, 87 (1960).
- (12) J. Crank, "The Mathematics of Diffusion", Oxford University Press, London, 1956, p 117.
- (13) S. D. Major, Master's Thesis, Case Western Reserve University, 1975.
- (14) D. J. Breed and R. H. Doremus, to be submitted for publication.

Location of the Cations in Hydrated NaCuY Zeolite

J. Marti, J. Soria,*

Instituto de Catálisis y Petroleoquímica, C.S.I.C. Serrano, 119. Madrid (6), Spain

and F. H. Cano

Departamento de Rayos X, Instituto Rocasolano, C.S.I.C., Serrano, 119. Madrid (6), Spain (Received December 29, 1975)

Publication costs assisted by Instituto de Catálisis

Three samples of NaY zeolites cation exchanged with Cu^{2+} ions have been studied in hydrated form by x-ray diffraction. The variation of the electron density maxima with the copper concentration indicates that the copper ions are placed out mainly in the supercage, particularly in sites S(II) and S(III). At high copper concentrations part of the Cu^{2+} ions remain unlocalized, possibly moving freely in the supercage.

Introduction

The copper exchanged zeolites have been the subject of many publications, particularly from the point of view of electron spin resonance.¹⁻⁴ This technique gives quick and precise information about the characteristics of the copper ions inside the zeolite. However, in many cases, the ESR spectra can be interpreted in different ways and it is necessary to obtain information by other techniques to clarify the results.

One of these cases is the use of the ESR to determine the location of the copper ions. Several types of signals can be obtained with different pretreatment of the samples; some are interpreted as Cu^{2+} in a crystal field with axial symmetry, while others as hydrated Cu^{2+} moving freely or due to copper clusters. Most of these assignments are well established but the problem starts when the copper cations are assigned to particular sites, since there are several sites with axial symmetry. The interacting copper ions can be placed in the sodalite cage or in the supercage, and it is difficult to decide about the locations of hydrated ions.

If it is possible with a different technique to locate the cations, then the ESR information will be unambiguous and we will have the advantage of a faster experimental technique. The technique normally used to determine cation positions is x-ray diffraction. In this work we have studied the location of the copper ions in partially exchanged hydrated zeolites. This must be the starting point in order to study the effect of the dehydration temperature, so well studied by ESR.

Experimental Section

A specimen of a commercially available molecular sieve (Type SK-40 from Union Carbide Corp.) was used as starting material for this work. The samples were prepared by introducing the NaY zeolites in CuCl_2 water solutions, at different concentrations. The chemical analysis of the sodium ions present in the solution, after the copper exchange, and the analysis of the sodium and copper cations in the samples, with atomic absorption spectroscopy, have permitted a determination of the number of sodium cations remaining, and copper ions and protons substituting for the sodium in the zeolite. In Table I, the chemical composition of the three samples is presented; the number of water molecules has not been measured and it has been taken from the literature.²⁰ The samples, dried at 100 °C after ion exchange, were exposed to room air.

The x-ray diffraction profiles were obtained on a Philips PW 1051 diffractometer, with a proportional counter. Slits of different size were used for diverse ranges of 2θ , particularly to enhance the diffraction maxima at high Bragg angles.

The overlapping peaks have been resolved using the program of Phytha and Jones⁵ adapted for diffractogram curves. All diffraction lines were compatible with the space group $Fd\bar{3}m$. The cell constants have been calculated from values of 2θ corrected with silicon as an internal standard, using the Guinier⁶ and Lsuec⁷ programs. The values obtained for the cell parameter, *a*, were 24.70, 24.70(2), and 24.68(2) Å for CuY 1, 2, and 3, respectively.

As Y-zeolite has cubic symmetry, therefore peaks can correspond to several reflections (*hkl*) for which the sum $N = h^2 + k^2 + l^2$ is satisfied. The intensities $I_1, I_2, I_3, \dots, I_n$ were determined considering $I_1/I_2 \approx m_1 F_{c1}^2 / m_2 F_{c2}^2$, where m_1 and m_2 are the planes multiplicities,⁸ and F_{c1} and F_{c2} are the corresponding structure factors calculated for the silica-alumina framework.

The coordinates determined by Eulenberger et al.⁹ for the NaY zeolites were assigned to the initial model of the silica-alumina lattice, using our measured cell parameter, *a*, for each sample.

The Lorentz-polarization and multiplicity corrections have been applied to all intensities. The structures have been solved considering peak 88 with $N \leq 276$ corresponding to 147 independent structure factors. The intensities for the unobserved reflections have been taken as half the intensity of the smallest observed one. The atomic scattering factors $f(\text{O}^-)$, $f(\text{Na}^+)$, and $f(\text{Cu}^{2+})$ corresponding to oxygen, sodium, and copper ions, and $f(\text{Si}^{3+})$ corresponding to silicon and aluminum ions, have been taken from standard tables.¹⁰

The extraframework ions were located from sections of electron density maps. The x-ray system¹¹ has been used for the calculations.

Results

The values for distances and angles between the atoms in the framework have been taken from Eulenberger.⁹ In Table II, the calculated values for distances and angles between the species and the framework oxygens are also presented. The names of the sites and oxygens have been taken from Smith;¹² the sequence along the ternary axis is shown in Figure 1a. It is observed that O(3) is the closest oxygen to sites S(I) and S(I'), remaining between both sites the planes formed by three O(2) and three O(3).

TABLE I: Chemical Composition of the Original Samples

Sample	Unit cell formula	a_0 , Å
CuY 1	$\text{Si}_{136}\text{O}_{384}\text{Al}_{56}\text{Cu}_7\text{Na}_{29}\text{H}_{13}\cdot 250\text{H}_2\text{O}$	24.70
CuY 2	$\text{Si}_{136}\text{O}_{384}\text{Al}_{56}\text{Cu}_{12}\text{Na}_{21}\text{H}_{11}\cdot 250\text{H}_2\text{O}$	24.70(2)
CuY 3	$\text{Si}_{136}\text{O}_{384}\text{Al}_{56}\text{Cu}_{15}\text{Na}_{16}\text{H}_{10}\cdot 250\text{H}_2\text{O}$	24.68(2)

TABLE II: Interatomic Distances (Å) and Bond Angles (deg)^a

Distances	CuY 1	CuY 2	CuY 3
S(I)-O(1)	3.61(4)	3.61(5)	3.61(2)
S(I)-O(2)	3.50(9)	3.51(1)	3.50(8)
S(I)-O(3)	2.61(3)	2.61(1)	2.60(9)
S(I')-O(2)	3.37(3)	3.31(5)	3.33(5)
S(I')-O(3)	2.85(8)	2.77(3)	2.80(4)
S(II)-O(2)	3.11(4)	3.17(7)	3.10(1)
S(II)-O(4)	3.79(6)	3.85(7)	3.78(7)
S(II)-O(2)	2.32(1)	2.32(5)	2.32(3)
S(II)-O(4)	2.91(9)	2.93(3)	2.91(3)
S(II*)-O(2)	3.71(2)	3.63(8)	3.59(9)
S(I)-S(I')	3.37(7)	3.23(9)	3.28(7)
S(I')-S(II')	3.90(4)	3.94(9)	3.99(7)
S(II')-S(II)	2.01(4)	2.02(8)	2.03(1)
S(II)-S(II*)	0.2863	2.95(5)	
S(II)-S(II*)	0.2840	2.93(5)	
S(II)-S(II*)	0.2829		2.77(9)
S(III)-O(1)	3.49(3)	3.49(4)	3.49(1)
S(III)-O(2)	3.06(3)	3.06(4)	3.06(2)
S(III)-O(4)	3.70(8)	3.70(9)	3.70(6)
S(III)-S(II)	3.76(5)	3.83(5)	3.73(8)
S(III)-S(II*)	0.2863	2.13(3)	
S(III)-S(II*)	0.2840	2.13(3)	
S(III)-S(II*)	0.2829		2.13(8)

Angles	CuY 1	CuY 2	CuY 3
O(3)-S(I)-O(3)	89.14	89.14	89.14
O(3)-S(I')-O(3)	81.18	84.25	83.05
O(2)-S(II)-O(2)	119.94	119.67	119.99
O(2)-S(II*)-O(2)	65.54	67.10	67.86
O(4)-S(III)-O(1)	88.26	88.24	87.28

^a In the table, site S(II*) is followed by the position $x = y = z$ on the threefold axis in fractional coordinate.

Outside the ternary axis, in the supercage and close to the 12-membered ring, though inclined toward a O(2), a maximum of electron density was found. This site is in the region of the not well-defined site S(III), mentioned by several authors.^{13,14}

In Tables III and IV, the atomic parameters and the isotropic temperature factor (B) of the zeolite are presented. In the third column the occupancy of extraframework sites in terms of O^- ions has been considered, just to compare the different electron densities of the sites. The electron density maxima along the ternary axis are presented in Figures 1(b), 2, and 3.

Discussion

The increasing copper concentration in the three samples does not significantly affect the electron density at the cationic sites. In general, the occupancy decrease for sites S(I) and S(III), and increases for sites S(II) while remaining essentially constant for other maxima. To make the assignment of particular cations to the sites, we must consider the distribution of sodium, copper, and water molecules.

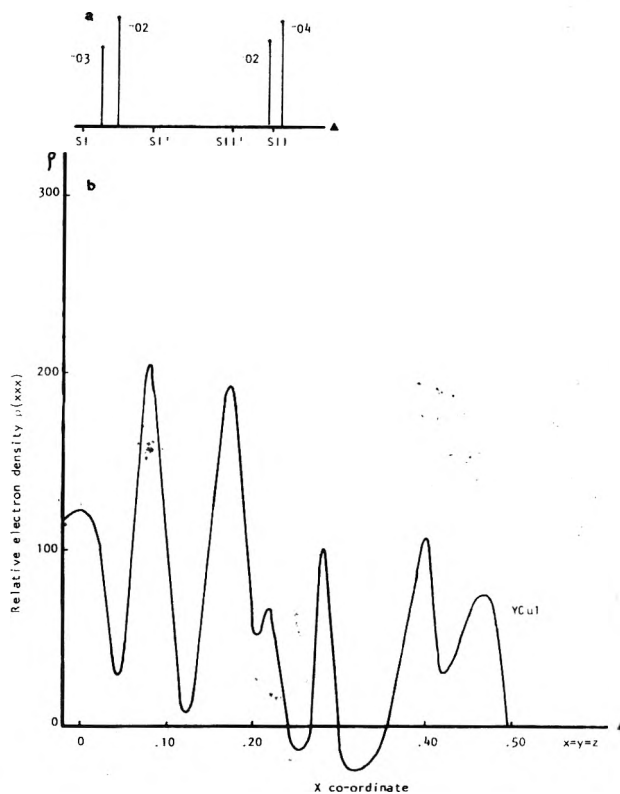


Figure 1. (a) Position of the oxygens relative to the sites in the ternary axis for CuY 1. (b) Electron density for nonframework sites for CuY 1.

Site S(I) is placed in the center of the hexagonal prism, at a distance of 2.61 Å from O(3), the closest oxygen. This distance is higher than 2.32 Å found for NaY zeolite,¹⁵ due mainly to the displacement from (0,0,0) in the latter sample, and remains constant for the three samples in which a considerable part of Na^+ has been exchanged by Cu^{2+} and protons. The distance S(I)-O(3) is too short to consider S(I) occupied by water molecules, and it is larger than the sum of ionic radii of sodium-oxygen or copper-oxygen.

The fact that increasing copper concentration decreases the electron density at S(I), to almost a base level, suggests that this position is occupied by sodium cations, and the increase of the S(I)-O(3) distance from the value of 2.32 Å found for the NaY is due to a rearrangement of the electrostatic field by the presence of Cu^{2+} , decreasing the tendency shown by Na^+ to be closer to three O(3) than to the others.¹⁵ The maxima of electron density are equivalent to 4.5, 3.6, and 0.8 sodium ions for the samples 1, 2, and 3, respectively.

The maximum at site S(I') is rather constant for all the samples, and therefore appears to be independent of copper concentration. The distance S(I')-O(3) is also similar for the three samples with a mean value of 2.80 Å, slightly higher than 2.73 Å found for NaY.¹⁵ The difference, though close to the experimental error, can be attributed to changes of the electrostatic fields affecting the lattice. Olson et al.¹⁷ have shown for decationated zeolites that the presence of protons increases the bond length Si-O by 0.08 Å, which is about the same amount found in our case. The fact that the S(I')-O(3) distance does not decrease also suggests that copper ions do not occupy S(I'). This position was assigned as Na^+ in the case of NaY;¹⁵ the cationic population is close to 16 ions in S(I) and S(I') as indicated by Sherry¹⁶ for NaY. In the present cases there are enough sodium ions to fill both sites. With these

TABLE III: Atomic Parameters (Origin at $\bar{3}m$)

Site	$x = y = z$			Position	Oxygen population			$B, \text{\AA}^2$		
	CuY 1	CuY 2	CuY 3		CuY 1	CuY 2	CuY 3	CuY 1	CuY 2	CuY 3
S(I)	0.0000	0.0000	0.0000	16(c)	5.0	3.9	0.9			
S(I')	0.0788	0.0757	0.0769	32(e)	14.9	13.5	15.5	3.95	4.15	3.81
S(II')	0.1701	0.1680	0.1704	32(e)	15.5	15.6	14.9	3.96	3.01	3.87
S(II)	0.2172	0.2154	0.2179	32(e)	5.7	4.3	8.9	2.95	3.10	2.84
S(II*)	0.2863	0.2840	0.2829	32(e)	9.1	5.8	11.0	4.25	5.02	4.87

TABLE IV: Atomic Parameters (Origin at $\bar{3}m$)

	CuY 1	CuY 2	CuY 3
Site	S(III)	S(III)	S(III)
$x = y$	0.1826	0.1818	0.1817
z	0.2193	0.2141	0.2180
Position	96(g)	96(g)	96(g)
Oxygen population	27.1	28.6	19.4
$B, \text{\AA}^2$	5.91	4.88	5.88

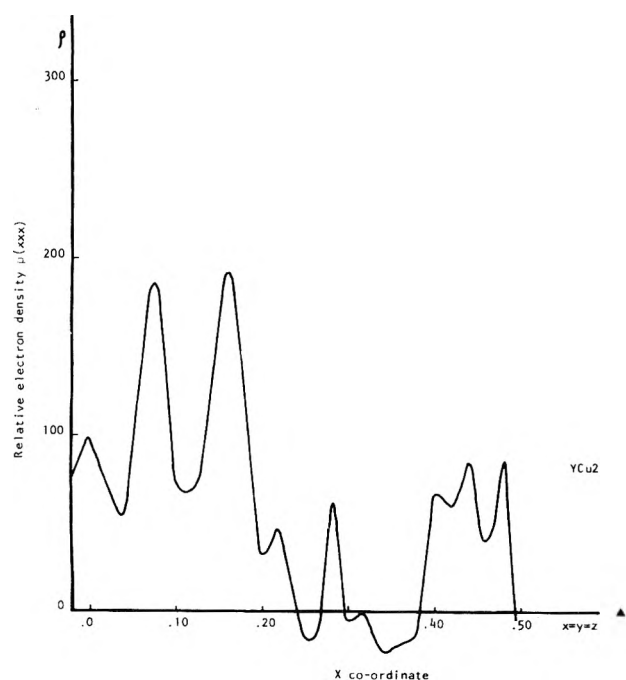


Figure 2. Electron density for nonframework sites for CuY 2.

considerations we assign also Na^+ , with a partial occupancy of 14.9, 13.5, and 15.5 sodium cations for the samples 1, 2, and 3, respectively.

The next maximum along the ternary axis is site S(II'), because S(U) practically has disappeared, S(II') is placed at 3.1 Å from the closest oxygens, O(2). This distance is too large to be assigned to a cation-oxygen bond, and the shape of the maximum is rather broad, suggesting that this position is occupied by water molecules. The electron density of S(II') for the samples 1, 2, and 3 represent 15.5, 15.6, and 14.9 water molecules, respectively.

In many cases, for hydrated Y zeolites, the cations in S(I') are bonded to water molecules in S(U). In the present case, S(U) is overshadowed by S(II') and the maximum is at 3.9 Å from S(I'). This distance is somewhat large, but the broadness of the maximum is such that its closest part to S(I') possibly represents the water molecules bonded to Na^+ in S(I') and the

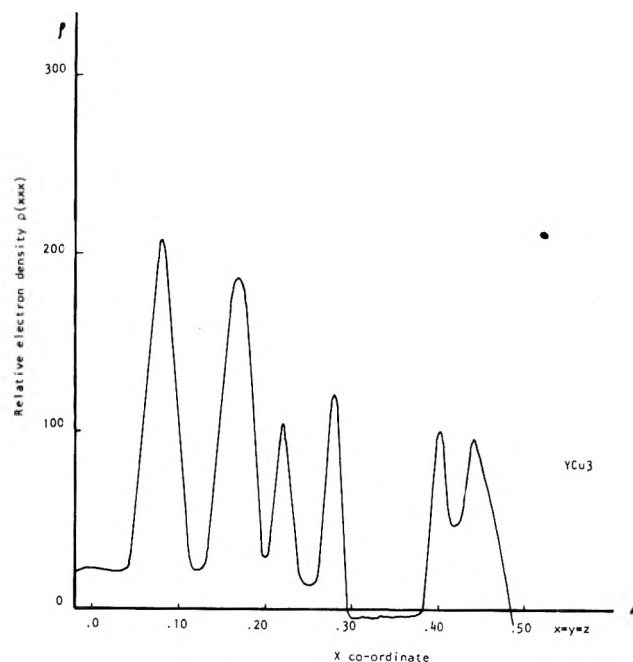


Figure 3. Electron density for nonframework sites for CuY 3.

opposite part of the maximum are from water molecules bonded with cations in site S(II). The distance S(II')-S(II) is 2.03 Å. The distance S(I')-S(II) is larger than S(II')-S(II) which suggests that the water molecules are more attracted by cations in S(II) than in S(I').

The distance S(II)-O(2) = 2.32 Å is a little larger than the sum of ionic radius, $r_{\text{Cu}^{2+}} + r_{\text{O}^{2-}} = 2.09 \text{ \AA}$, but in Table II, it is shown that the distance O(2)-ternary axis is 2.30 Å, then no shortest distance can be expected if the cation remains in the ternary axis. The maximum at S(II) increases from the value of 1.3 equivalent O^- for NaY to about 5 O^- for samples 1 and 2 and to 8.9 for sample 3, which also indicates that its electron density is due to the copper occupancy of this site. The electron density in S(II) represents 1.9, 1.5, and 3.0 Cu^{2+} for the samples 1, 2, and 3, respectively.

The distance S(II')-S(II) is acceptable for the water- Cu^{2+} bond, stronger than the water- Na^+ bond, S(I')-S(II'), whose length increases with increasing copper concentration in S(II).

Site S(II*) is at 2.95 Å from S(II), with a distance to the closest lattice oxygen a little larger. This maximum, and several smaller ones placed along the ternary axis, are too far from the lattice and, generally, have been assigned to water molecules¹⁸ or a mixture of cations and water molecules.¹⁹

In the study of NaY zeolite a maximum of electron density was found at the S(III) position which was determined considering its distances to the lattice oxygens, S(III)-O(2) = 3.05 Å, S(III)-O(1) = 3.49 Å, and S(III)-O(4) = 3.71 Å. These

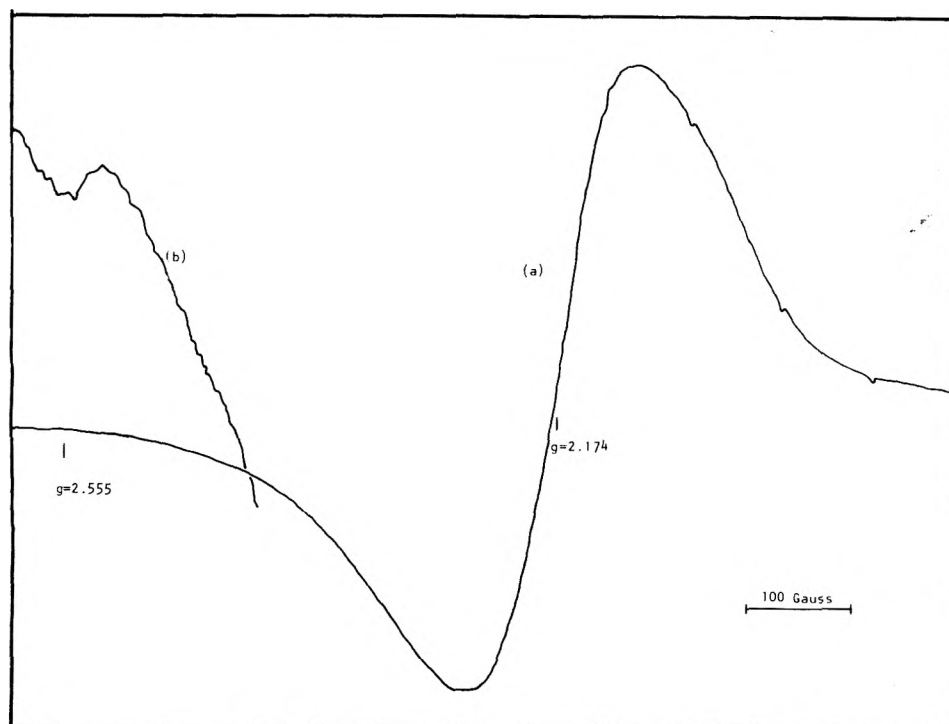


Figure 4. (a) ESR signal of Cu^{2+} in the CuY 3 sample. The small peaks are due to the manganese standard. (b) Second derivative curve.

distances are large in relation with the sum of ionic radius of cations and oxygen, but they are reasonable considering hydrated cations. In the series of copper zeolites the position of S(III) remains constant, at the same distance of the lattice oxygen as in NaY,¹⁵ but in relation with the latter the electron density of this maximum decreases when copper ions are first introduced.

The pattern of sodium substitution by copper can be interpreted in the following way: As indicated by the chemical analysis, during the exchange proceedings there is a direct exchange of sodium by protons, almost independent of the amount of copper exchanged. The contribution of the protons is higher for low degree of exchange.

Thus, the first lost of the sodium electron density is not entirely compensated by copper ions, and we observe mainly the substitution of Na^+ by Cu^{2+} in S(II) and the diminution of sodium cations in S(III), and probably the lost of the sodium moving freely in the supercage. Later there is a decrement of Na^+ from S(I) and S(III), with Cu^{2+} occupying S(II) and S(III). In this scheme, we consider S(III) occupied by sodium and copper cations in the following amounts: 9.7Na^+ and 5.4Cu^{2+} for CuY 1, 2.4Na^+ and 8.7Cu^{2+} for CuY 2, and 6.5Cu^{2+} for CuY 3. With those assignments all cations, Na^+ and Cu^{2+} , are located for CuY 1 but some cations, mainly copper because of its higher tendency toward hydration, will remain unlocalized in the supercage for CuY 2 (2Cu^{2+}) and CuY 3 (5.6Cu^{2+}).

This interpretation is consistent with the results obtained by ESR. This technique shows that most of the copper ions in the hydrated zeolites move rather freely surrounded by water molecules.¹ Figure 4 shows mainly a symmetrical line with a small contribution of hyperfine structure at the low field side. This structure is assigned to the component g_{\parallel} of the signal produced by Cu^{2+} in a field of axial symmetry. A field of this type can be produced at S(II), but it is doubtful

at S(III), with hydrated Cu^{2+} weakly attached to the lattice.

In a recent work on copper exchanged faujasite single crystals by Maxwell and de Boer¹³, they localize copper mainly in site S(I'), but as they do not know the Cu^{2+} and K^+ concentration in the sample, this site could be occupied by K^+ instead of Cu^{2+} . Furthermore, as they have only one sample they cannot differentiate between water and copper in other positions.

The values of the cation population for the CuY sample are slightly out of place in relation with the other two samples, but considering NaY (% Cu^{2+}) it keeps the same tendency as CuY 2 and 3. The pretreatment was the same for the three samples, but perhaps there was some difference in the water content.

Acknowledgments. It is a pleasure to acknowledge Professor S. Garcia-Blanco for his suggestions and comments and Drs. M. Martínez Ripoll and J. Fayos Alcañiz for invaluable discussions and help on the realization of this work.

References and Notes

- (1) J. Turkevich, Y. Ono, and J. Soria, *J. Catal.*, **25**, 44 (1972).
- (2) C. Naccache and Y. Ben Taarit, *Chem. Phys. Lett.*, **11**, 11 (1971).
- (3) H. Bremer, W. Morgne, R. Schodel, and F. Vogt, *Adv. Chem. Ser.*, No. **121**, 249 (1973).
- (4) C. Chao and J. H. Lusford, *J. Chem. Phys.*, **57**, 2890 (1972).
- (5) J. Phytha and R. N. Jones, National Research Council of Canada, Ottawa, 1968.
- (6) Guinier, Freiburg University, 1973.
- (7) Lsuvre, Freiburg University, 1973.
- (8) P. Gallezot and B. Imelik, *Chim. Phys.*, **68**, 1 (1971).
- (9) G. R. Eulenberger, D. P. Shoemaker, and J. G. Keil, *J. Phys. Chem.*, **71**, 1812 (1967).
- (10) "International Tables for X-Ray Crystallography", The Kynoch Press, Birmingham, England, 1959.
- (11) "X-Ray System of Crystallographic Programs", University of Maryland, College Park, Md.
- (12) J. V. Smith, *Adv. Chem. Ser.*, No. **101**, 171-200 (1971).

- (13) I. E. Maxwell and J. J. de Boer, *J. Phys. Chem.*, **79**, 1874 (1975).
 (14) W. J. Mortier and H. J. Bosmans, *J. Phys. Chem.*, **75**, 3327 (1971).
 (15) J. Marti, J. Soria, and F. H. Cano, in press.
 (16) H. S. Sherry, *J. Phys. Chem.*, **74**, 2758 (1970).
 (17) D. H. Olson and E. Dempsey, *J. Catal.*, **13**, 221-231 (1969).
 (18) W. H. Baur, *Am. Mineral.*, **49**, 697 (1964).
 (19) J. M. Bennett and J. V. Smith, *Mater. Res. Bull.*, **3**, 933 (1968).
 (20) D. W. Breck, "Zeolite Molecular Sieves", Wiley, New York, N.Y., 1974.

Synthesis and Characterization of a Complex of Rubeanic Acid and Copper(II) Montmorillonite

S. Son, S. Ueda, F. Kanamaru, and M. Koizumi*

The Institute of Scientific and Industrial Research, Osaka University, Suita, Osaka 565, Japan (Received February 2, 1976)

The Cu(II)-rubeanic acid complex was stably formed between the silicate layers of montmorillonite by soaking Cu(II)-saturated montmorillonite in a rubeanic acid-acetone solution. The basal spacing of rubeanic acid-Cu(II)-montmorillonite was 12.6 Å. Both chemical analysis and thermogravimetry indicated that the molar ratio of cupric ion to rubeanic acid was 1:2. The infrared spectrum of the complex showed that the intercalated complex is not a polymer but a monomer. The electron spin resonance spectra indicated that the molecular plane of the Cu(II)-rubeanic acid complex was parallel to the interlamellar surfaces of montmorillonite. From these results, the structure of the complex was deduced.

Introduction

Rubeanic acid (RA) used as a guest organic molecule in the present study is a famous analytical reagent with a tetradentate as shown in Figure 1. This reagent reacts with many kinds of transition metals to produce so-called coordination polymers. Among them, a coordination compound of the cupric ion and RA has attracted considerable attention, because the compound exhibits semiconductivity and antiferromagnetism, and studies on its preparation and properties have been extensively performed.^{1,2} The Cu(II)-RA coordination polymer was usually prepared by adding a RA-ethyl alcohol solution to an aqueous solution of CuSO₄. Two kinds of configurations, which are shown in Figure 2, have been estimated for the Cu(II)-RA complex, however, there is a possibility that the reaction product is a mixture of these two types, i.e., a linear configuration and a three-dimensional one. Due to the difficulty in separating both complexes, it is not easy to make a theoretical interpretation of the physicochemical properties of the compound. The first study to control tacticity of the coordination compound was carried out by Kanda et al.³ who synthesized the polymer by the so-called monolayer method, that is, making monomolecular films by spreading a ligand solution on the surface of an aqueous solution containing cupric ions. However, in actuality, it is very difficult to prepare the perfect monomolecular film on the surface of an aqueous solution by using the before-mentioned method. On the other hand, the first attempt to prepare two-dimensional micro-molecules in interspaces between the silicate layers of clay minerals was made by Blumstein.^{4,5} Since then, such polymerizations with controlled tacticity have been carried out on many polar monomers using montmorillonite as a template. These results suggest that the stereospecific synthesis of the coordination polymer of the cupric ion and RA is possible by utilizing the interlayer spaces of clay. In the present investigation, a fundamental attempt to produce such a coordination polymer in the interlayer spaces of clay was made.

Experimental Section

Materials and Preparations. The ligand used is rubeanic acid (dithiooxamide) NH₂C(S)C(S)NH₂ from Mallinckrodt Chemical Works. It was recrystallized from ethanol. Reagent grade cupric chloride was used without further purification. The clay mineral used here was montmorillonite from Tsukinuno mine, Yamagata, Japan. The chemical formula of the mineral is (Ca_{0.09}Na_{0.16}K_{0.03})(Al_{1.48}Fe_{0.13}Mg_{0.40})[Si_{3.99}Al_{0.01}]O₁₀(OH)₂·nH₂O. Powders (under 2-μ particle size) of the montmorillonite were put into a 0.5 N cupric chloride solution at 60 °C for 10 days. After washing the fractions several times with hot water followed by air drying, the pale green montmorillonite saturated with cupric ions was obtained. The product was soaked in an acetone solution saturated with rubeanic acid at 60 °C for 10 days, and was air dried. With this treatment, the color of the sample changed from pale green to black. This product is denoted RA-Cu-mont (mont = montmorillonite) in this paper.

Measurements. To characterize this rather complicated compound, besides elemental analyses, x-ray diffraction, thermogravimetric analyses, infrared spectra, and electron spin resonance spectra were utilized. The x-ray diffraction powder patterns of Cu-mont and its RA complex were measured on a Rigaku-Denki diffractometer Model 4001 A₂ by using Cu Kα radiation. Thermogravimetric analysis and differential thermal analysis on both samples of Cu-mont and its RA complex were conducted for the interpretation of the elemental analysis data. The temperature was raised at a constant rate of 10 °C/min.

The infrared spectra of the powdered specimens of Cu-mont, its rubeanic acid complex, and Cu-RA were taken with a Hitachi-Perkin-Elmer spectrophotometer fitted with a sodium chloride prism. All compounds were dispersed in potassium bromide disks. The ESR spectra of the thin self-supporting film of RA-Cu-mont were recorded on a KESME-X spectrometer with 100-kHz field modulation at -196

TABLE I: X-Ray Diffraction Data

Cu-mont			RA-Cu-mont		
<i>h k l</i>	<i>I</i>	<i>d</i> , Å	<i>h k l</i>	<i>I</i>	<i>d</i> , Å
0 0 1	vs	15.7	0 0 1	vs	12.6
0 0 3	w	5.24	0 0 2	w	6.32
0 0 5	w	3.15	0 0 4	w	3.12

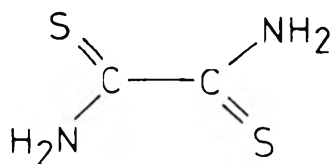


Figure 1. A molecular structure of rubeanic acid.

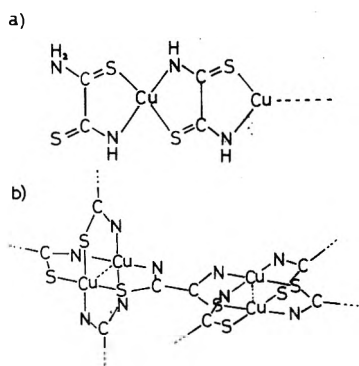


Figure 2. Two kinds of models of Cu(II)-RA complex, where (a) indicates a linear model and (b) a three-dimensional one.

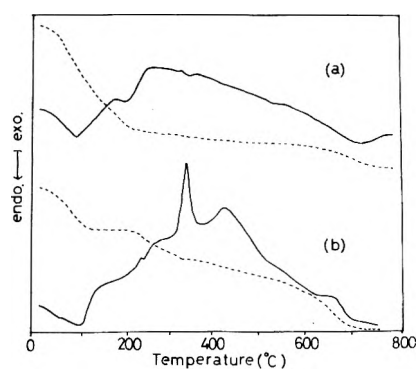


Figure 3. Thermal analysis data of (a) Cu-mont and (b) RA-Cu-mont. Solid and broken lines indicates TG and DTA curves, respectively.

°C, and the spectra of oriented film were measured at various orientations of the film plane with respect to the magnetic field.

Results and Discussion

The x-ray diffraction data of Cu-mont and its RA complex were tabulated in Table I. The interlayer spacing of Cu-mont was found to be 15.7 Å. This value indicates that cupric ions are octahedrally coordinated with six water molecules forming double water layers in the interlayer region. While the interlayer spacing of RA-Cu-mont was 12.6 Å, this value, together

TABLE II: Vibrational Frequencies (in cm^{-1}) of RA, Cu-RA, and RA-Cu-mont

RA	Cu-RA	RA-Cu-mont	Assignment ^a
3275 m		3250 sh	$\nu(\text{NH})$
3190 m	3197 vw		
3115 m			
	1610 mb		
1585 vsb	1505 w	1500 wb	$\delta(\text{NH}_2)$
1429 sb		1430 mb	$\nu(\text{CN})$
1200 m	1282 s	1280 sh	$\delta(\text{NH}_2)$
	1046 m	1120 sh	
	857 s		$\nu(\text{CS})$
835 s	774 m		
695 w			

^a Assignment for RA and Cu-RA were taken from ref 3.

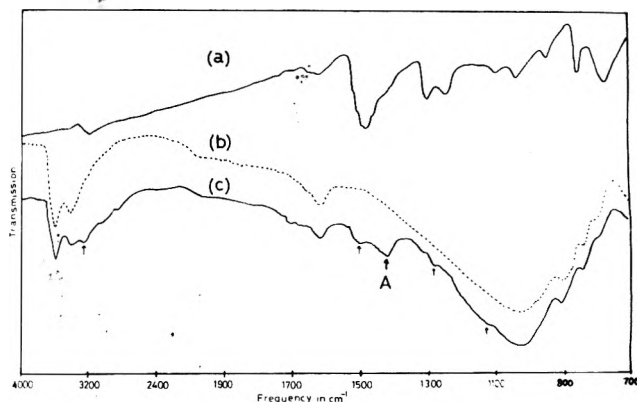


Figure 4. Infrared spectra of (a) Cu-RA, (b) Cu-mont, and (c) RA-Cu-mont.

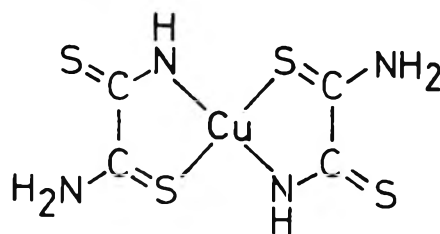


Figure 5. An estimated molecular structure of the Cu-RA complex prepared in the interlayer space.

with black color of the complex, suggests that the intercalated RA molecules coordinate to cupric ions in such a way that the molecular plane of the RA molecule is parallel to the silicate layers.

The results of thermal analysis are shown in Figure 3. Solid lines indicate DTA curves and broken lines TG curves. In the case of Cu-mont, interlayer water was desorbed by 13.1% in a temperature range from 30 to 200 °C. Above 700 °C Cu-mont decomposed to an oxides mixture with a weight loss of 5.0%. On the other hand, in the case of RA-Cu-mont, water molecules were desorbed in the temperature region from 30 to 100 °C with a weight loss of 6.55%. The dehydration temperature of the complex is considerably lower than that of Cu-mont, indicating that the water molecules in the complex are not coordinated to cupric ions such as in Cu-mont, but stay among Cu-RA complex even though the water molecules are intercalated. Decomposition of the intercalated RA takes place in the temperature range from 200 to 600 °C with a

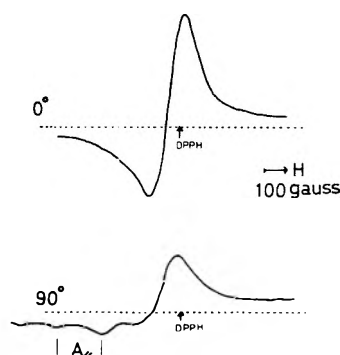


Figure 6. ESR spectra of a thin self-supporting film of RA-Cu-mont at -196°C . Angles between the film plane and magnetic field are (a) 0° and (b) 90° .

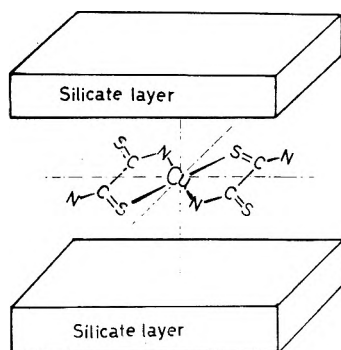


Figure 7. Proposed orientation of the Cu-RA complex in the interlayer region of montmorillonite.

weight loss of 10.6%. The silicate layer began to decompose at 700°C as was the case for Cu-mont. From the results of these thermal analyses and CHN chemical analysis of the complex, the amount of intercalated RA was found to be 94 mmol/100 g of clay, while the amount of interlayer cupric ion was determined as 47.5 mmol/100 g of clay by atomic absorption analysis. These facts indicate that the molar ratio of RA to cupric ion is 2:1.

The results of the infrared spectra are shown in Figure 4 and Table II. The broken line indicates the spectrum of Cu-mont and the solid line at the bottom is that of RA-Cu-mont. The solid line at the top is the spectrum of the Cu-RA complex (coordination polymer). The spectrum of the RA-Cu-mont has several extra absorption bands denoted with arrows in comparison with that of Cu-mont. The position of extra bands was the same as that of spectra of the Cu-RA complex except for the absorption line denoted A. The band at 3250 cm^{-1} is assigned to the N-H stretching vibration and the band at 1500 cm^{-1} to the C-N stretching vibration.³ Though the absorption band at 1430 cm^{-1} was not found in the spectra of the Cu-RA complex, the band was observed at the same position in the

ir spectrum of the free ligand RA, which is also assigned to the C-N stretching vibration.³ From these results, together with the molecular ratio of RA to cupric ion, the Cu-RA complex ion formed in the interlayer region is considered to have the structure shown in Figure 5, where one of the two NH_2 groups coordinates to the cupric ion, but the other is free. This means that the Cu-RA complex obtained in the present study is not a polymer such as a complex prepared by the usual precipitation method, but a monomer.

ESR spectra of the thin self-supporting film of RA-Cu-mont are shown in Figure 6. The top spectrum was obtained when the plane of the film was parallel to the magnetic field. This spectrum is derived from only the perpendicular components g_{\perp} . Rotation of the film about an in-plane axis toward 90° with respect to the magnetic field caused a decrease of the intensity of the perpendicular components, together with an increase of the intensity of the parallel components, g_{\parallel} and A_{\parallel} . The ESR parameters were $g_{\perp} = 2.07$, $g_{\parallel} = 2.33$, and $A_{\parallel} = 160\text{ G}$. These values are close to those for the chelate complex of the cupric ion with a square-planar configuration. The observed angular variation and ESR parameters indicate that adsorption of RA on Cu-mont results in the formation of a complex having a planar or axially elongated tetragonal structure on the interlamellar surfaces of montmorillonite. The symmetry axis of the complex is oriented perpendicular to the silicate layer of montmorillonite.

Summary

The present results are summarized below. In this study, Cu-RA complex ions were prepared in the interlayer region of montmorillonite by the reaction of Cu-saturated montmorillonite and RA in an acetone solution. From the results of DTA, TG, ir, ESR, and CHN chemical analysis, it was deduced that each cupric ion is coordinated with two molecules of RA in such a way that the molecular plane of the ligand is parallel to the silicate layer, and that the symmetry axis of the complex ions is perpendicular to the silicate layers of the montmorillonite. This structure is illustrated in Figure 7. Efforts to find a suitable condition for producing a coordination polymer in the interlayer spaces of clay will be continued in the future.

Acknowledgment. The authors wish to thank Professor S. Kanda of Tokushima University for helpful discussions, Mr. H. Miyamoto for ESR measurements, and Dr. T. Fujimoto for CHN chemical analyses.

References and Notes

- (1) S. Kanda, *J. Chem. Soc. Jpn., Pure Chem. Sect. (Nippon Kagaku Zasshi)*, **83**, 560 (1972).
- (2) S. Kanda, K. Ito, and T. Nogaito, *J. Polym. Sci., Part C*, (17), 151 (1967).
- (3) S. Kanda, A. Suzuki, and K. Ohkawa, *Ind. Eng. Chem., Prod. Res. Dev.*, **12**, 88 (1973).
- (4) A. Blumstein, J. Herz, V. Sinn, and C. Sadron, *C. R. Acad. Sci.*, **246**, 1856 (1958).
- (5) A. Blumstein, *Bull. Soc. Chim. Fr.*, 899 (1961).

Nuclear Spin Relaxation in Methyl Groups Governed by Three- and Sixfold Barriers

Kenneth H. Ladner, Don K. Dalling, and David M. Grant*

Department of Chemistry, University of Utah, Salt Lake City, Utah 84112 (Received February 26, 1976)

Publication costs assisted by the National Institutes of Health

The carbon-13 spin-lattice times, T_1 , and ^{13}C - ^1H nuclear Overhauser enhancements were measured at 36 °C in a series of methyl-substituted aromatic compounds. The C-H dipolar relaxation time, T_{1D} , was separated from the overall relaxation time, and then used to estimate the magnitude of the methyl rotational barriers. The results can be described by hindered rotation of the methyl group with the jumping rates and activation energies dependent upon the group arrangement.

Introduction

Internal motion of methyl groups attached to an aromatic ring system has been investigated by a number of workers using a variety of techniques. While the majority of investigations relating relaxation times to systems dynamics have been carried out via proton magnetic resonance, several recent studies of methyl group rotation have focused on the determination of carbon-13 spin-lattice times (T_1).¹⁻⁴ The theoretical treatment of the behavior of methyl groups undergoing hindered rotation with respect to molecules in a liquid has drawn keen interest in past investigations since the group forms an isolated three spin ($^{-12}\text{CH}_3$) or four spin system ($^{-13}\text{CH}_3$) which is quite amenable to interpretation.⁵⁻⁹

Theory

The principle mode of spin-lattice relaxation in most molecular systems is by spin-spin dipolar interactions. Simple theory predicts that the intrinsic dipolar relaxation rate, $R_{1D}(I,S)$, for two spins I and S is given by¹⁰

$$R_{1D}(I,S) \equiv 1/T_{1D} = \alpha \left(\frac{\gamma_I \gamma_S \hbar}{r_{IS}^3} \right)^2 \tau_{\text{eff}} \quad (1)$$

where $\alpha = 3/2$ for like spins and $\alpha = 1$ for unlike spins¹¹ and, of course, extreme narrowing is assumed. γ_I and γ_S are the gyromagnetic ratios of nuclei I and S, respectively, r_{IS} is the I-S distance, and τ_{eff} is the effective correlation time. The total dipolar relaxation of spin I due to coupling with all other spins, S, is given by

$$R_{1D}(I) = \sum_{S \neq I}^N R_{1D}(I,S) \quad (2)$$

Where $R_{1D}(I,S)$ is given by eq 1 and N is the number of spins. In this work it is assumed that all pair wise interactions are additive and that cross correlation effects may be neglected.¹²

In the case of a ^{13}C nucleus relaxed by a ^1H , eq 1 reduces to

$$R_{1D}(C,H) \equiv 1/T_{1D} = (2.25 \times 10^{10} \text{ s}^{-2}) \tau_{\text{eff}} \quad (3)$$

where a C-H distance of 1.08 Å is assumed. If the internal rotation of a methyl group takes place by rotational diffusion about the symmetry axis of the methyl group, the effective correlation time is related to the rotational diffusion constant for internal rotation by¹³⁻¹⁵

$$\tau_{\text{eff}} = \frac{1}{4} \left(\frac{A}{6D} + \frac{B}{6D + D_{\text{int}}} + \frac{C}{6D + 4D_{\text{int}}} \right) \quad (4)$$

If the bonding at the methyl carbon is assumed to be tetrahedral then

$$A = (3 \cos^2 \theta - 1)^2 = 36/81$$

$$B = 12 \sin^2 \theta \cos^2 \theta = 96/81$$

$$C = 3 \sin^4 \theta = 192/81$$

where θ is the angle between the methyl group reorientation axis and the methyl C-H vector. Equation 4 assumes that the methyl group is fixed to a hydrodynamic sphere whose motion is characterized by an overall diffusion constant D . The internal reorientation axis for D_{int} lies along the symmetry axis. In the model described by eq 4 it is also assumed that internal motion and overall motion are stochastically independent.

In general τ_{eff} is a quite complicated function of the molecular geometry and intrinsic molecular dynamics. In this study, the dynamic implications of the dipolar relaxation in methyl groups will be probed assuming the overall diffusion to be isotropic.

From Figure 1 it is easily seen that information about the internal motion obtained from the spin-spin dipolar mechanism can only be obtained in the region $\sigma = 1$ to approximately $\sigma = 20$ where $\sigma = (D + D_{\text{int}})/D$. Within this region the dipolar relaxation rate can be used as a decreasingly sensitive probe to study the effects of steric interactions on the rotation of methyl groups. When the methyl group rotation becomes faster than the overall motion the effect of this motion averages out and no reliable information can be obtained in the value of σ . This is a direct consequence of the fact that, in the extreme narrowing limit, R_{1D} is most sensitive to the slowest motion governing reorientation of the interacting spins, except as the very rapid motion results in a static geometrical attenuation of the interaction.

It should be noted, however, that if σ becomes inordinately large ($\sigma \gtrsim 20$) cross correlation effects can become important and it is then possible to extract "motional" information from multispin multiplet relaxation effects.^{12,16}

An alternate first-order approximation of methyl group motion under hindered conditions starts with the hydrogen nuclei in three orientations, 120° apart.^{5,15} The methyl group is assumed to undergo instantaneous random jumps among these three orientations. The effective correlation time assuming this motional model is given by

$$\tau_{\text{eff}} = \frac{1}{4} \frac{A}{6D} + \frac{B + C}{6D + \frac{n}{2} \nu} \quad (5)$$

where D , θ , A , B , and C are as defined in eq 4, ν is the internal methyl jump rate in s^{-1} , and $n = 3$ for this threefold barrier model. In the case of a methyl group subject to a sixfold barrier

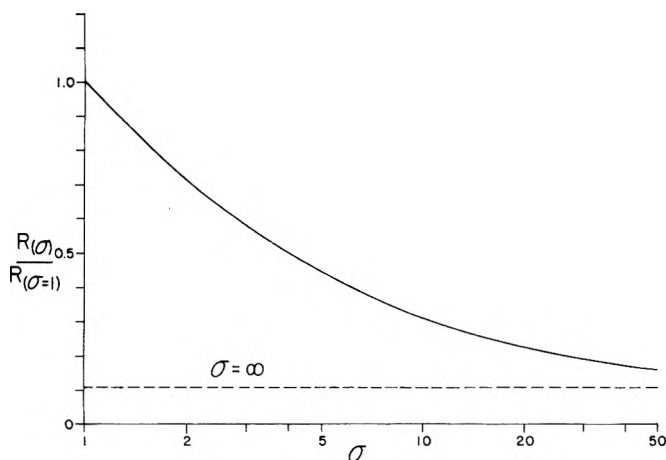


Figure 1. The dipolar rate, $R_{1D}(\sigma)$ for a C-H interaction normalized by the value of $\sigma = 1$ as a function of $\sigma = (D + D_{int})/D$ where $1 \leq \sigma \leq \infty$. When the internal rotation is much greater than the overall motion, $\sigma \gg 1$, and when the methyl group is locked with respect to the overall motion $\sigma = 1$.

the methyl hydrogens assume six orientations, 60° apart and therefore $n = 6$.

It is assumed that the overall rotation of the aromatic ring system is characterized by small step diffusion. Wilbur and Jonas,¹⁷ using the Chi test initially employed by Wallach and Huntress¹⁸ and applied in several cases,¹⁹⁻²³ found that small step diffusion was a reasonable model for toluene- d_8 at low temperature and at higher pressure. Small deviations (factor of 2 or less) from this assumption because of the larger molecular weights of compounds used in this study should be of little consequence in the following section.

The Chi test may also be used to estimate the validity of the 120° jump as a model for internal rotation. If the methyl group reorientation is impeded by a relatively high barrier, the time $1/\nu$ between jumps of 120° should be long compared to the time it takes a free rotor to reorientate through 120° ,¹⁵ and

$$\chi = \frac{1}{\nu} \left/ \left[(2\pi/3)(I/kT)^{1/2} \right] \right. \gg 1 \quad (6)$$

It has been shown that if $\chi > 5$ then the molecule is in the 120° jump regime. Upon substitution of the moment of inertia of a methyl group about its C_3 axis ($I_{CH_3} = 5.35 \times 10^{-40}$ g cm²) into eq 6 one finds that the jump rate must be smaller than 8.6×10^{11} s⁻¹ in order to satisfy the Chi test.

It is further assumed that the effects of multispin dipolar cross correlation on the NOE enhancement factor are negligible. Werbelow and Grant²⁴ and Buchner²⁵ have shown that cross correlation effects are relatively unimportant for methyl relaxation where $D_{int}/D < 20$. It is expected that such conditions are valid in the present studies.

Experimental Section

All data were obtained on a Varian XL-100-15-FT NMR spectrometer at a temperature of $36 \pm 1^\circ$ C. Decoupling was accomplished using a specially constructed decoupler employing a Hewlett-Packard 1505 A frequency synthesizer and an ENI Model 310 power amplifier.

1-Methylnaphthalene, 1,4-dimethylnaphthalene, and 7,12-dimethylbenz[*a*]anthracene were obtained from Aldrich Chemical Co. 1,8-Dimethylnaphthalene was prepared using the method of Vaughan et al.²⁶ Samples were degassed by four freeze-pump-thaw cycles on a vacuum line. Because of the low

solubility of 7,12-dimethylbenz[*a*]anthracene the signal-to-noise, SN, obtained was in the range 12-30:1. The SN obtained for the remaining compounds was in excess of 160:1.

Results and Discussion

The relaxation rates and nuclear Overhauser enhancements (η) of the ring and methyl carbons for this series of compounds are given in Table I. Using these values the T_1 data are separated into T_{1D} dipolar times and an effective time, T_{10} , for all other relaxation processes.²⁷⁻³³ The large η values obtained for the various carbons demonstrates that the relaxation process is dipolar dominated.

Values of D , D_{int} , and ν calculated using eq 1 and 2 are given in Table II. 1-Methylnaphthalene (1-MN) and 1,4-dimethylnaphthalene (1,4-DMN) have similar parameters inasmuch as the methyl groups experience the same steric hindrance to rotation with respect to the peri proton of the ring system resulting in a threefold barrier. When both the C_1 and C_8 positions contain methyl groups (1,8-dimethylnaphthalene), it is reasonable to expect the increase found in the barrier to rotation because of the close proximity of the two methyl groups. Activation energies for internal rotation have been measured for 1-MN³⁴⁻³⁶ and 1,8-DMN³⁴⁻³⁷ by proton spin-lattice relaxation methods and these are also given in Table II confirming the general magnitudes found in this study.

Table II also gives the methyl group jump and diffusion rates, and these are approximately the same for both 1-MN and 1,4-DMN. The methyl interaction with a peri proton prevents rapid rotation of the methyl group resulting in a reasonably large activation energy for 1-MN (2.4 kcal mol⁻¹) as compared to, for example, the methyl group in toluene (0.014 kcal mol⁻¹).³⁸ In the case of 1,8-DMN the steric interactions are further increased resulting in a larger barrier to rotation and a decrease in the jump and diffusion rates.

The jump rate, ν , has been related to an activation energy for methyl group internal rotation using the simple relationship.¹⁻³

$$\nu = \nu_0 \exp(-V_0/RT) \quad (7)$$

where ν_0 is the jump rate for zero barrier. A convenient measure of ν_0 is the rate of rotation of a methyl fragment in the gas phase $(kT/I_{Me})^{1/2}$. Substitution of this calculated ν_0 and the values of ν from Table II allows one to obtain V_0 from eq 7. These calculated activation energies are given in Table II.

For comparative purposes several activation energies for internal rotation obtained from proton spin-lattice relaxation methods are also given. The agreement between the values obtained from proton spin-lattice relaxation and those calculated from C-H dipolar relaxation is quite good when one considers the coarse approximations used in making the calculations and in modeling the system. Thus, a close relationship between activation energies for internal methyl group rotation and ¹³C spin-lattice relaxation rates is exhibited.

Since the intramolecular dipolar relaxation mechanism is a sensitive probe to internal motion in the simple aromatic systems, the motional behavior of the two methyl groups in 7,12-dimethylbenz[*a*]anthracene was also investigated. From Figure 2 it can be seen that the 7-methyl and 12-methyl groups experience quite different proton interactions. The 7-methyl group interacts with two peri protons, while the 12-methyl group interacts with a peri proton and the C_1 ring proton. Because of low signal-to-noise (as discussed in the Experimental Section) and the expected deviation from overall isotropic diffusional motion of this molecule, a 15% error exists

TABLE I: Spin-Lattice Relaxation Rates and Nuclear Overhauser Enhancement Factors

Compound	$T_1^{-1}(\text{ring}),$ s^{-1}	η	$T_{1D}^{-1}(\text{ring}),$ s^{-1}	$T_1^{-1}(\text{Me}),$ s^{-1}	η	$T_{1D}^{-1}(\text{Me}),$ s^{-1}
1-Methylnaphthalene	0.2	2.0	0.2	0.2	2.0	0.2
1,4-Dimethylnaphthalene	0.4	1.9	0.4	0.3	2.0	0.3
1,8-Dimethylnaphthalene	0.2	2.0	0.2	0.3	2.0	0.3
7,12-Dimethylbenz[a]anthracene	0.5	2.0	0.5			
7-methyl				0.15	2.0	0.15
12-methyl				1.4	2.0	1.4

TABLE II: Motional Parameters and Activation Energies for Internal Methyl Rotation

Compound	$D(\times 10^{-10}),$ s^{-1}	$D_{\text{int}}(\times 10^{-10}),$ s^{-1}	$\nu(\times 10^{-10}),$ jumps s^{-1}	$V_0(\text{eq}),$ kcal/mol	$V_0(\text{lit.}),$ kcal/mol
1-Methylnaphthalene	1.5	18.8	27.7	2.1	2.4 ^a
1,4-Dimethylnaphthalene	0.9	16.4	23.5	2.2	
1,8-Dimethylnaphthalene	2.0	5.2	8.8	2.8	3.0 ^b 3.2 ^a
7,12-Dimethylbenz[a]anthracene	~ 0.8				
7-methyl		~ 234	~ 447	< 0.4	
12-methyl		~ 0.40	~ 0.7	> 4.4	

^a References 34–36. ^b Reference 37.

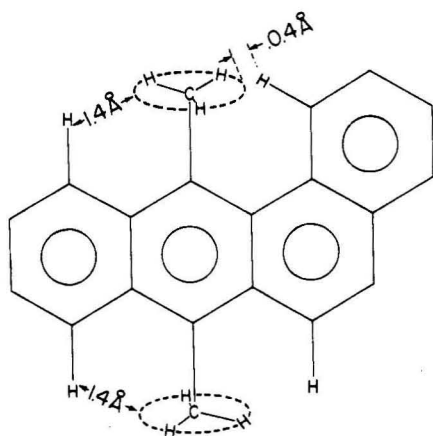


Figure 2. Structure of 7,12-dimethylbenz[a]anthracene showing the distances of closest approach between the methyl protons and the adjacent ring protons. Only the ring protons pertinent to the discussion are shown.

in the relaxation data. Figure 3 illustrates how these relatively large errors allow one to determine only lower and upper limits on the jump rates for the 7-methyl and 12-methyl groups. Using this approximate method one assigns a lower limit of 4.5×10^{12} jumps s^{-1} to the 7-methyl group and an upper limit of 7.0×10^9 jumps s^{-1} to the 12-methyl group, as shown in Figure 3. The jump rate of the 7-methyl group is rather large, because of the sixfold symmetry of the two peri proton interactions. A highly sterically hindered group will reorientate rapidly if the unfavorable interactions are comparable for all rotameric conformers as in this sixfold barrier case. The 7-methyl group spins rapidly because no rotameric conformer has significantly lower energy.³⁹

Although the 12-methyl group also experiences two sterically unfavorable interactions the jump rate at its upper limit is only $7.0 \times 10^9 \text{ s}^{-1}$ because now a strong threefold barrier dominates the sixfold term. Using ideal geometry and standard covalent radii to estimate geometrical parameters one calculates that the closest approach of the 7-methyl protons

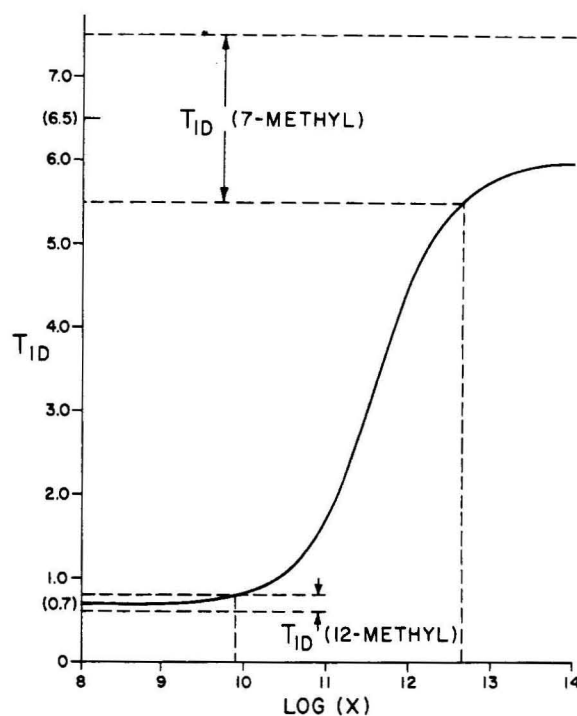


Figure 3. Dipolar relaxation time of methyl carbon as a function of $\log x$, where $x = \frac{3}{2}\nu$ for the 12-methyl group and $x = 3\nu$ for the 7-methyl group. The statistical range of the relaxation times of the 12-methyl carbon ($T_{1D} = 0.7 \text{ s}$) and the 7-methyl carbon ($T_{1D} = 6.5 \text{ s}$) are given by the dashed lines.

to the peri protons is 1.4 \AA . On the other hand, the 12-methyl protons would only be separated from the C_1 proton by 0.4 \AA at the point of closest approach. Of course, these extremely low estimates cannot be correct and considerable deformation from ideal geometry must be expected. Qualitatively, however, it is this methyl- C_1 -proton interaction that essentially locks the rotation of the 12-methyl group as compared to the 7-methyl group. Physically this suggests that internal reorientation of the 12-methyl group occurs in distinct jumps while

the 7-methyl group is approaching the rotation rate of a free rotor. This can be seen from Figure 3 and also from the previous discussion of the Chi text.

Previous studies⁴⁰ of the methyl T_1 's in the several geometrical isomers of retinal revealed results analogous to those above. Sterically hindered *gem*-dimethylretinal exhibited the shortest values, while those involved in sixfold rotation barriers had the longest T_1 's and methyls involved in threefold barriers were found to have intermediate rates of relaxation. Although only a qualitative analysis was made of the retinal methyl relaxation data, the detailed analysis of the compounds in this work, whose geometrical relationships are similar to those of the retinals, suggests the relevance of the findings in this work to an interpretation of the retinal study.

Acknowledgment. This investigation was supported by Grant No. 5-F32-CA-5131-02 awarded by the National Cancer Institute, National Institutes of Health, and also under Grant No. GM08521 and RR057 supported by the National Institutes of Health. Helpful discussions with R. J. Pugmire and L. G. Werbelow are also acknowledged.

References and Notes

- (1) T. D. Alger, D. M. Grant, and R. K. Harris, *J. Phys. Chem.*, **76**, 281 (1972).
- (2) J. R. Lyerla, Jr., and D. M. Grant, *J. Phys. Chem.*, **76**, 3213 (1972).
- (3) K. F. Kuhlmann and D. M. Grant, *J. Chem. Phys.*, **55**, 2998 (1971).
- (4) C. F. Schmidt, Jr., and S. I. Chan, *J. Magn. Reson.*, **5**, 151 (1971).
- (5) P. S. Hubbard, *J. Chem. Phys.*, **52**, 563 (1969).
- (6) A. Allerhand, *J. Am. Chem. Soc.*, **95**, 8228 (1973).
- (7) W. Buchner, *J. Magn. Reson.*, **12**, 79 (1973).
- (8) H. Versmold, *J. Chem. Phys.*, **58**, 5649 (1973).
- (9) L. G. Werbelow, *J. Am. Chem. Soc.*, **95**, 5132 (1973).
- (10) I. Solomon, *Phys. Rev.*, **99**, 559 (1955).
- (11) A. Abragam, "The Principles of Nuclear Magnetism", University Press, Oxford, 1973, p 297.
- (12) L. G. Werbelow and D. M. Grant, *J. Chem. Phys.*, **63**, 544 (1975).
- (13) D. E. Woessner, *J. Chem. Phys.*, **37**, 647 (1962).
- (14) D. E. Woessner, *J. Chem. Phys.*, **36**, 1 (1962).
- (15) D. E. Woessner and B. S. Snowden, Jr., *Adv. Mol. Relaxation Processes*, **3**, 181 (1972).
- (16) L. G. Werbelow, private communication.
- (17) D. J. Wilbur and J. Jonas, *J. Chem. Phys.*, **62**, 2800 (1975).
- (18) D. Wallach and W. Huntress, *J. Chem. Phys.*, **50**, 1219 (1969).
- (19) W. M. M. J. Bovee and J. Smidt, *Mol. Phys.*, **28**, 1617 (1974).
- (20) K. T. Gillen and J. H. Noggle, *J. Chem. Phys.*, **53**, 801 (1970).
- (21) D. E. Woessner and B. S. Snowden, *Adv. Mol. Relaxation Processes*, **3**, 181 (1972).
- (22) R. A. Assink and J. Jonas, *J. Chem. Phys.*, **53**, 1710 (1970).
- (23) W. T. Huntress, *Adv. Magn. Reson.*, **4**, 1 (1970).
- (24) L. G. Werbelow and D. M. Grant, *J. Chem. Phys.*, **63**, 4742 (1975).
- (25) W. Buchner, *J. Magn. Resonance*, **12**, 82 (1973); **17**, 229 (1975).
- (26) W. J. Mitchell, R. D. Topsom, and J. Vaughan, *J. Chem. Soc.*, 2526 (1962).
- (27) K. F. Kuhlman, D. M. Grant, and R. K. Harris, *J. Chem. Phys.*, **52**, 3439 (1970).
- (28) T. D. Alger and D. M. Grant, *J. Phys. Chem.*, **75**, 2538 (1971).
- (29) J. R. Lyerla, Jr., D. M. Grant, and R. K. Harris, *J. Phys. Chem.*, **75**, 585 (1971).
- (30) T. D. Alger, D. M. Grant, and J. R. Lyerla, Jr., *J. Phys. Chem.*, **75**, 2539 (1971).
- (31) C. H. Wang, D. M. Grant, and J. R. Lyerla, Jr., *J. Chem. Phys.*, **55**, 4674 (1971).
- (32) J. R. Lyerla, Jr., D. M. Grant, and C. H. Wang, *J. Chem. Phys.*, **55**, 4676 (1971).
- (33) T. D. Alger, S. W. Collins, and D. M. Grant, *J. Chem. Phys.*, **54**, 2820 (1971).
- (34) J. U. von Schutz, H. C. Wolf, and F. Noack, *Magn. Reson. Relat. Phenom., Proc. Congr. AMPERE 16th, 1970*, 644-647 (1971).
- (35) J. U. von Schutz and H. C. Wolf, *Z. Naturforsch. A*, **27**(1), 42 (1972).
- (36) J. U. von Schutz, W. Guttler, and H. C. Wolf, *Z. Naturforsch. A*, **28**(1), 69 (1973).
- (37) A. Saika, A. Kawamori, and R. Takagi, *J. Magn. Reson.*, **7**, 324 (1972).
- (38) H. D. Rudolph, A. Jaeschke, and P. Wendling, *Ber Bunsenges. Phys. Chem.*, **70**, 1172 A (1968).
- (39) G. C. Levy, *Acc. Chem. Res.*, **6**, 161 (1973).
- (40) R. S. Becker, S. Berger, D. K. Dalling, D. M. Grant, and R. J. Pugmire, *J. Am. Chem. Soc.*, **96**, 7008 (1974).

Electron Spin Resonance Spectra of the Thiadiazolothiadiazole Radical Anion and Related Sulfur-Nitrogen Heterocycles

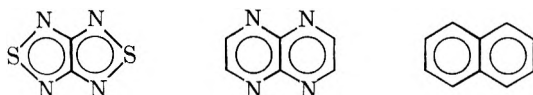
C. L. Kwan, M. Carmack, and J. K. Kochi*

Chemistry Department, Indiana University, Bloomington, Indiana 47401 (Received April 7, 1976)

The anion radical of the unique aromatic sulfur-nitrogen heterocycle, thiadiazolothiadiazole (TT), has been prepared by alkali metal reduction in ethereal solvent. The electron spin resonance parameters are compared with those calculated by McLachlan's perturbation method using two models for the sulfur atom, one including participation of the 3d orbitals and the other neglecting it. The 3d model affords good agreement with experimental results, although a similar distribution is obtained from the p orbital model. The same molecular orbital parameters can be used to predict hyperfine splittings in a series of aromatic anion radicals of related thiadiazolo analogues including benzothiadiazole, thiadiazolopyrazine, and thiadiazoloquinoxaline.

Introduction

The replacement of the peripheral atoms of naphthalene with heteroatom equivalents consisting of sulfur and nitrogen is represented in thiadiazolothiadiazole.

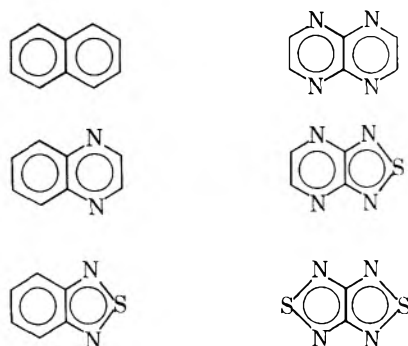


This highly symmetrical heterocycle is a unique extension of naphthalene and tetraazannaphthalene, effected by replacing $[-CH=CH-]$ groups with $[-S-]$ in order to generate a planar aromatic system with no substituents. The close relationship between thiadiazolothiadiazole and naphthalene is shown by their similar physical properties,¹ and it raises the question of comparative molecular bonding in this interesting heteroaromatic system.

Electron spin resonance (ESR) spectroscopy of aromatic anion radicals offers a direct method of assessing the effect of heteroatoms on the odd-electron distribution in the highest occupied molecular orbital.² This technique has been used extensively in a variety of nitrogen-containing aromatic systems.³⁻⁸ Sulfur-containing heterocycles are especially noteworthy, since sulfur not only has unshared 3p electrons, but also vacant 3d orbitals. Sulfur can behave, thus, as an electron donor as well as a potential acceptor. Indeed, Longuet-Higgins⁹ has suggested that the vacant 3d orbitals of the sulfur atom in thiophene are as important in the π bonding as the occupied 3p orbitals. On this basis, thiadiazolothiadiazole would contain at least one tetravalent sulfur as represented pictorially in the uncharged valence bond forms I and II. ESR



studies of the radical ions of dibenzothiophene, [2,1,3]benzothiadiazole and related heterocycles have indicated, however, that a p orbital model alone without d orbital participation was sufficient to describe the unpaired π -spin distribution in sulfur containing aromatic systems.⁹⁻¹⁵ In this paper, we examine this point further by comparing the spin densities in the series of sulfur/nitrogen heterocyclic anion radicals shown below.



Results

ESR Spectrum of Thiadiazolothiadiazole Radical Anion (TT). Reduction of [1,2,5]thiadiazolo[3,4-c][1,2,5]thiadiazole in tetrahydrofuran (THF) with a sodium mirror produced a wine-red solution of the radical anion (TT). The ESR spectrum in Figure 1 consists of nine groups of lines with intensity ratios of 1:3.9:9.1:14.7:17:13.1:7.4:2.7:0.8 which is close to the theoretical ratios of 1:4:10:16:19:16:10:4:1 expected from hyperfine splittings due to four equivalent nitrogens. Each group of lines is further split into four lines of equal intensity by the sodium counterion. Closer examination shows that the high-field components in the spectrum are broader than the low-field ones. Following the analysis by Kaplan, Bolton, and Fraenkel,¹⁷ we conclude that $a_N\rho_N > 0$ in this radical anion. Since ρ_N is usually positive for such azaromatic ring systems, a_N is also positive.

The nitrogen and sodium hyperfine coupling constants of 3.17 and 0.31 G, respectively, did not change appreciably on lowering the temperature of the solution down to -60°C , the sodium splitting remaining in the range of 0.30–0.33 G, and the change in the nitrogen splitting being undetected. However, in methyltetrahydrofuran solution the value of a_{Na} increased perceptibly to 0.40 G and a_N was 3.15 G. No selective

line broadening of the spectrum was detected in this temperature range. Furthermore, no triplet spectrum was observed when the solution was frozen at liquid nitrogen temperatures, suggesting that dimeric ion pairs (ion quartets) are unimportant, in contrast to the situation with ketyl and related anion radicals.¹⁸ These observations with TT anion radical are similar to those obtained with the naphthalene anion radical, which apparently forms a contact ion pair, with the sodium counterion sitting atop the aromatic ring.^{18,19}

The inset in Figure 1 was taken in more concentrated solutions and focuses on the broadened [$m_N = -4$] line in which all of the sodium lines are obliterated. Under these conditions the presence of weak satellite lines in the spectrum can be seen with intensities approximately 0.2% of the main group of lines. We tentatively assign these additional lines to ³³S hyperfine splittings ($I = \frac{3}{2}$, natural abundance = 0.74%) of about 5 G with predicted intensity ratios of 0.38%, which is about that observed. Alternative assignments based on ¹³C splittings are disfavored since the π -electron density by the HMO method has a node at carbon. (Although McLachlan perturbation theory indicates a negative spin density on carbon, the magnitude of the ¹³C splitting would be too small to be resolved.) Furthermore, the satellite lines are not due to ¹⁵N splittings since the spectral width of TT containing a ¹⁵N is expected to be smaller than that of the anion radical containing all normal isotopic nitrogens due to the smaller magnetic moment of ¹⁵N compared to ¹⁴N.

Experimental spin densities in TT are listed in Table I, together with those calculated from HMO and McLachlan perturbation methods (see Experimental Section).

ESR Spectrum of the Anion Radical of Thiadiazolopyrazine (NT). Reduction of [1,2,5]thiadiazolo[3,4-b]pyrazine in dimethoxyethane (DME) gave a blue solution which afforded the ESR spectrum in Figure 2. The hyperfine coupling constants and unpaired spin densities in NT are listed in Table II. The higher values of the nitrogen coupling constants were assigned to positions 1 and 3 on the basis of the molecular orbital calculations in Table II.

ESR Spectrum of Benzothiadiazole Anion Radical (BT). The ESR spectrum of the anion radical of [2,1,3]benzothiadiazole was first examined by Strom and Russell, who prepared it by electron transfer from the anion of propiophenone in dimethyl sulfoxide (80%)/*tert*-butyl alcohol (20%) solution containing an excess of potassium *tert*-butoxide.¹⁰ BT was also prepared in ethereal solutions with potassium mirror at -40°C by Kamiya and Akahori.¹⁴ However, they only observed unresolved singlets at higher temperatures, which they attributed to the existence of more than one radical species. We repeated the reduction of benzothiadiazole in THF with potassium, and found the purple solutions to be stable at room temperatures for periods exceeding 10 months.

The spectrum of BT in Figure 3a obtained at -40°C exhibits well-resolved potassium splittings. The hyperfine splittings in Table III are in general agreement with those previously reported under different experimental conditions.^{10,12,14} At room temperature, the spectrum of this solution broadens selectively as shown in Figure 3b. The alternate line broadening in the spectrum is shown in greater detail in Figure 3c.

The correlation diagram in Figure 4 was constructed according to Freed and Fraenkel,²⁰ and indicates that the alternating line width phenomenon is best accounted for by an in-phase modulation²¹ of the hyperfine splittings due to the two protons at positions 4 and 7. A dynamic process involving the potassium counterion in which the 4, 7 protons remain

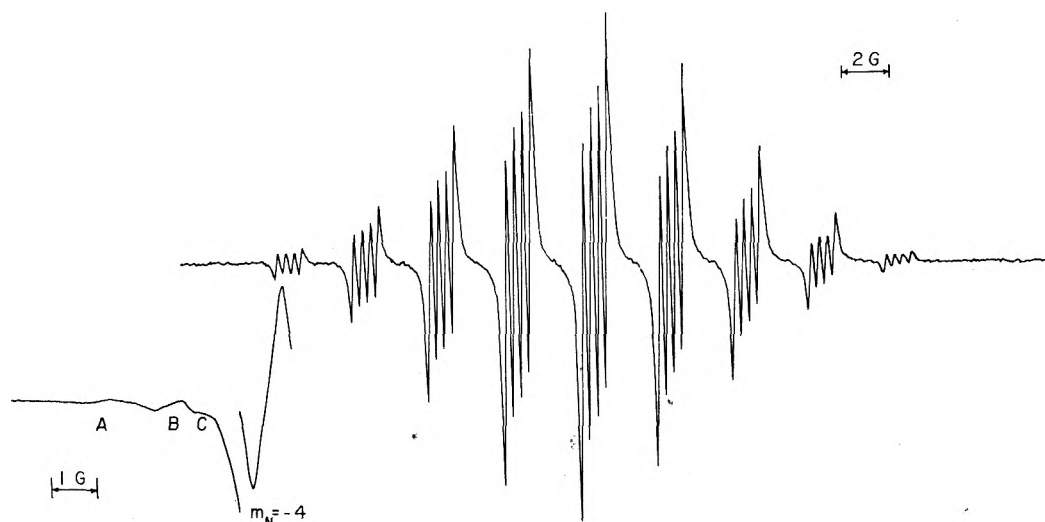


Figure 1. ESR spectrum of sodium [1,2,5]thiadiazolo[3,4-c][1,2,5]thiadiazole anion radical in THF solution at room temperature. The inset below shows $m_N = -4$ line at high gain and in concentrated solution to obliterate the sodium splittings. Assignment of satellite lines given as: (A) $m_N = -4$, $m_S = -\frac{3}{2}$; (B) $m_N = -3$, $m_S = -\frac{3}{2}$; (C) $m_N = -4$, $m_S = -\frac{1}{2}$

TABLE I: ESR Parameters and Unpaired Spin Densities in TT Anion Radical^a

Position	<i>a</i> , G	Unpaired π -electron density ^b	HMO ^c ρ_i	McLachlan ^d S_i	
				p	d
1, 3, 4, 6(N)	3.17	0.144	0.136	0.137	0.148
2, 5(S)	5.0	0.152 ^e	0.227	0.259	0.230
7, 8(C)			0.000	-0.033	-0.024
Na ⁺	0.31				

^a (*g*) = 2.0065. ^b From McConnell's equation, see the Experimental Section. ^c Odd electron density, see text. ^d Total spin density. ^e Based on $Q_S = 33$ G and reliability limited by lack of additional data (see Experimental Section for discussion).

TABLE II: ESR Parameters and Unpaired Spin Densities in NT Anion Radical^a

Position	<i>a</i> , G	Unpaired π -electron density	HMO ρ_i	McLachlan S_i	
				p	d
1, 3(N)	3.25	0.147	0.133	0.137	0.144
2(S)			0.227	0.270	0.228
8, 9(C)			0.000	-0.029	-0.024
4, 7(N)	3.40	0.154	0.140	0.149	0.152
5, 6(H)	3.25	0.121	0.114	0.108	0.114
K ⁺	0.15				

^a (*g*) = 2.0045. See footnotes, Table I, for explanations.

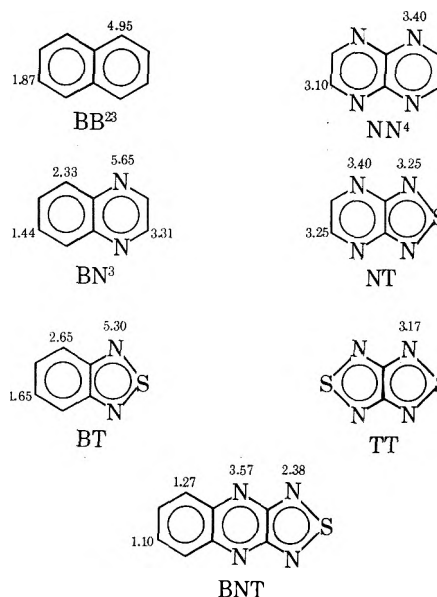
equivalent but undergo exchange pairwise would account for the line broadening behavior.^{19,22}

ESR Spectrum of the Anion Radical of Thiadiazoloquinoxaline (BNT). Reduction of [1,2,5]thiadiazolo[3,4-*b*]-

quinoxaline in dimethoxyethane with a potassium mirror afforded a dark purple solution. The 25 prominent lines comprising the experimental spectrum are shown in Figure 5, together with the computer simulation based on the parameters listed in Table IV. The hyperfine splittings were assigned on the basis of the McLachlan calculations.

Discussion

The experimental proton and nitrogen hyperfine splittings in the anion radical of naphthalene together with its nitrogen and sulfur analogues are collected below for comparison.



Each proton hyperfine splitting in this series of anion radicals is directly related to the spin density on carbon to which it is bonded.² Comparisons of these hfsc values in the anion radical of BN relative to that of BT, and NN relative to NT, indicate that [-S-] can be considered to be almost equivalent to [-CH=CH-]. There is, however, a consistent trend toward a slightly increased electron release due to [-S-] in the thiadiazolo moiety compared to the pyrazino analogue.²⁴ Indeed, molecular orbital calculations presented in Tables I-IV

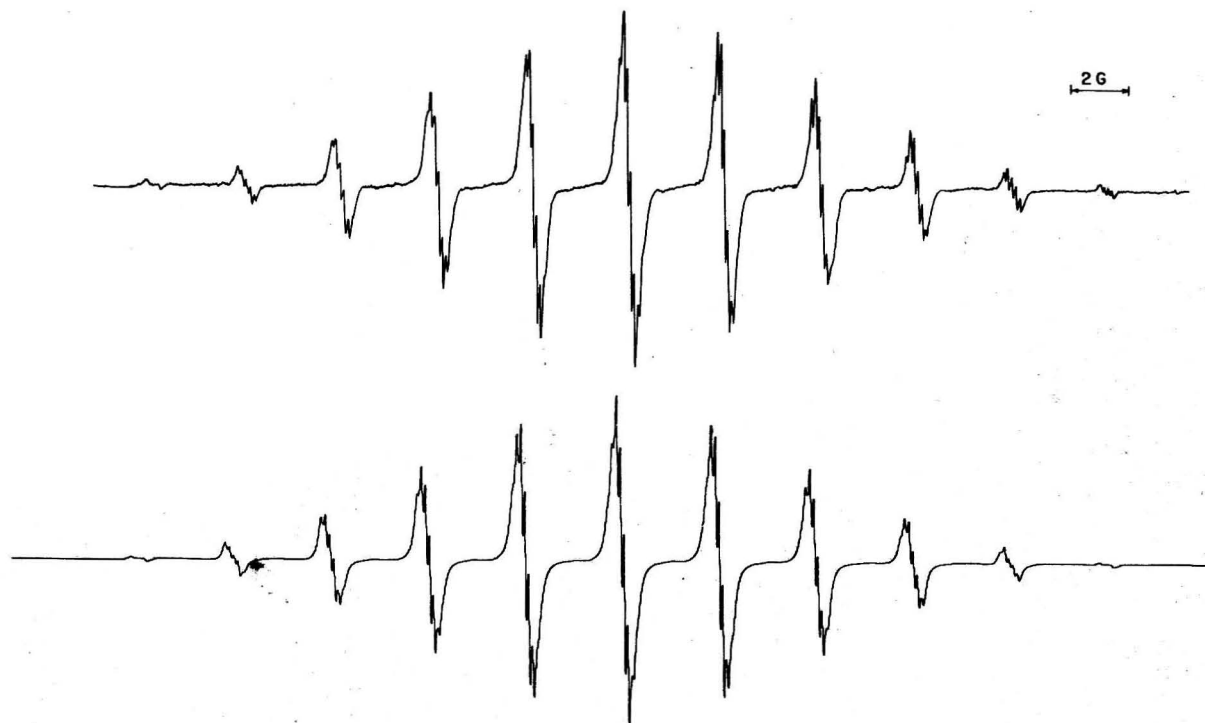


Figure 2. Upper ESR spectrum of potassium [1,2,5]thiadiazolo[3,4-*b*]pyrazine anion radical in dimethoxyethane solution at room temperature. Lower: Computer simulated spectrum using the parameters in Table II.

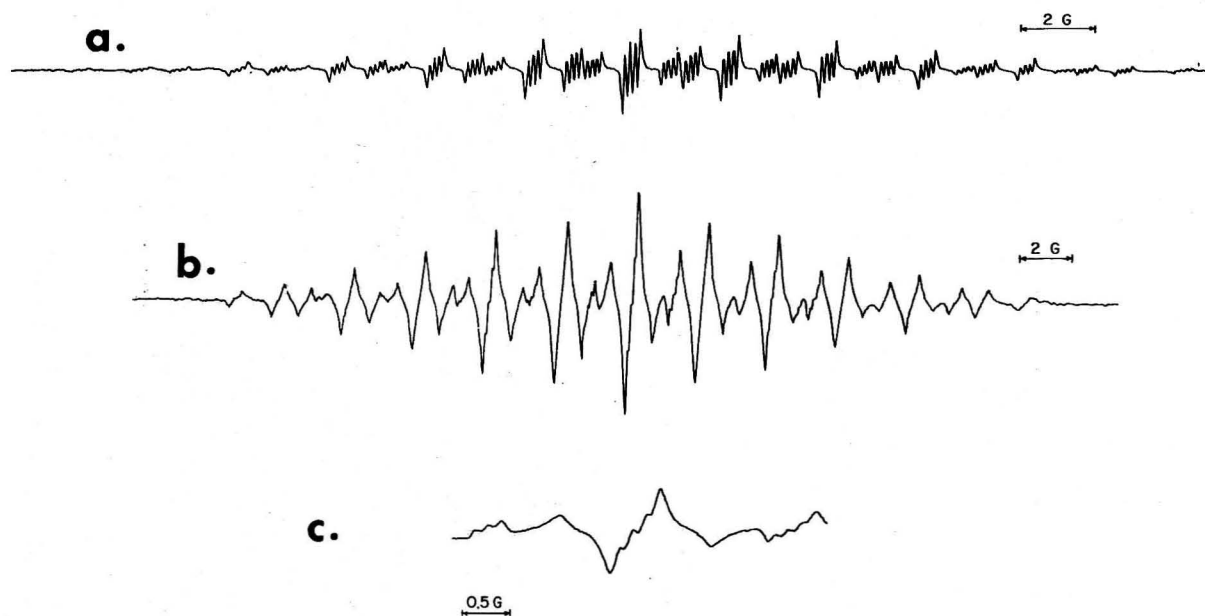
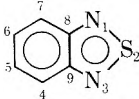


Figure 3. (a) ESR spectrum of potassium [2,1,3]benzothiadiazole anion radical in THF solution at -40°C . (b) same solution at 25°C . (c) Central portion (5 lines) of spectrum b showing alternate line broadening. Note the different magnetic sweep widths in all three spectra.

indicate that better agreement between experimental and theoretical values of the hyperfine splittings (or spin densities) is obtained from a model incorporating contributions from the 3d orbitals of sulfur. The latter corresponds to the Longuet-Higgins treatment,⁹ in which sulfur is more or less considered in the secular equations as a mathematical equivalent to a two-carbon center.

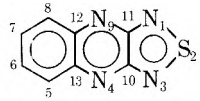
For the molecular orbital calculations, we used BN and NN as test compounds to find the most appropriate values of the nitrogen Coulomb integral and carbon–nitrogen resonance integral. Of the parameters suggested by Danieli, Lunazzi, and

Placucci,⁴ Strom and Russell,¹⁰ as well as Talcott and Myers,⁸ we found the latter to agree best with the experimental data for the two test compounds and for the anion radicals examined in this study. For the thiadiazolo anion radicals, we increased the value of the sulfur–nitrogen resonance integral in the p orbital model from 0.566β suggested by Strom and Russell to 0.778β . This particular number for β_{SN} was chosen according to Lucken²⁵ in order to generate the same symmetric odd-electron orbital as that obtained in the d orbital model [i.e., $\beta_{\text{SN}}(\text{d}) = 2^{1/2}\beta_{\text{SN}}(\text{p})$]. The higher value of β_{SN} can be justified by the observation of a shorter sulfur–nitrogen

TABLE III: ESR Parameters and Unpaired Spin Densities in BT Anion Radical^a


Position	<i>a</i> , G	Unpaired π -electron density	HMO ρ_i	McLachlan S_i	
				<i>p</i>	<i>d</i>
1, 3(N)	5.30	0.241	0.199	0.214	0.222
2(S)			0.259	0.305	0.256
8, 9(C)			0.013	-0.018	-0.009
4, 7(H)	2.65	0.099	0.103	0.113	0.115
5, 6(H)	1.65	0.061	0.055	0.039	0.044
K ⁺	0.13 (25 °C)				
	0.15 (-43 °C)				

^a $\langle g \rangle = 2.0043$. See footnotes in Table I.

TABLE IV: ESR Parameters and Unpaired Spin Densities in BNT Anion Radical^a


Position	<i>a</i> , G	Unpaired π -electron density	HMO ρ_i	McLachlan S_i	
				<i>p</i>	<i>d</i>
1, 3(N)	2.38	0.108	0.092	0.087	0.095
2(S)			0.211	0.262	0.224
10, 11 (C)			0.010	-0.011	-0.010
4, 9(N)	3.57	0.162	0.158	0.181	0.184
12, 13 (C)			0.042	0.027	0.031
5, 8(H)	1.27	0.047	0.047	0.048	0.048
6, 7(H)	1.10	0.041	0.045	0.038	0.040
K ⁺	~0.15				

^a $\langle g \rangle = 2.0051$. See footnotes in Table I.

bond length of 1.62 Å in TT²⁶ compared to the sulfur-carbon bond length of 1.78 Å in dithiin.²⁷ Furthermore, the agreement with the experimental hyperfine splittings are better with this value of β_{SN} .

The HMO method does not differentiate between the *p* orbital model and the *d* orbital model for the thiadiazole anion radicals examined in this study. Due to the presence of a plane of symmetry through the sulfur atom in these systems, the contribution of the 3*d* orbital is absorbed into that of the 3*p* orbital for the totally symmetric odd-electron orbital.²⁵ Since our choice of parameters assumed the same symmetric orbitals for the two models, identical results were indeed obtained by the HMO treatment. However, spin density calculations by McLachlan's perturbation method²⁸ include corrections in which contributions from all the occupied molecular orbitals are taken into account. Thus, the two models would no longer afford identical results. The calculations presented in Tables I-IV do show that McLachlan's method distinguishes the *d* orbital model from the *p* orbital model in the thiadiazole anion radicals. The difference between the two models is not sufficiently large to warrant further discussion at this level.

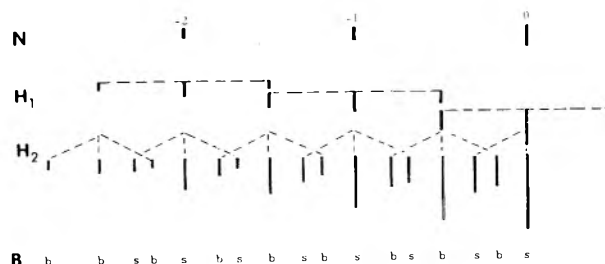


Figure 4. Correlation diagram (one-half) for the ESR spectrum of potassium benzothiadiazole anion radical. L.B. indicates lines in the spectrum in Figure 3b which are broadened (b) or remain sharp (s).

Conclusions

Experimental hyperfine splittings in a series of related aromatic thiadiazole anion radicals are in good agreement with those obtained from McLachlan perturbation calculations employing the 3*d* orbitals for sulfur. This result is in harmony with the valence bond description in which tetravalent sulfur is included in the bonding.²⁹

Experimental Section

Materials. Tetrahydrofuran, 2-methyltetrahydrofuran, or 1,2-dimethoxyethane was refluxed over calcium hydride and distilled into a storage bottle containing Na-K alloy, and thence transferred in vacuo as needed. [1,2,5]Thiadiazolo[3,4-*c*][1,2,5]thiadiazole, [1,2,5]thiadiazolo[3,4-*b*]pyrazine, [2,1,3]benzothiadiazole, and [1,2,5]thiadiazolo[3,4-*b*]quinoxaline were kindly supplied by Dr. A. P. Komin after purification as described elsewhere.^{1,30}

Preparation of Radical Anions. The aromatic heterocycles dissolved in ethereal solvents were reduced by either a sodium or potassium mirror which was prepared separately in a capillary attached as a side arm to an ESR tube. The capillary was constricted in three places and the alkali metal sublimed in vacuo sequentially past each of the constrictions by gently heating upward from the bottom of the side arm. The side arm was then sealed at the last constriction to isolate the sublimed sodium or potassium mirror. Reduction was carried out by bringing the solution the aromatic compound contained in a separate side arm in contact with the metal mirror after sealing the tube in vacuo. The concentration of the radical anion could be adjusted in the sealed tube simply by distilling solvent bulb-to-bulb into or out of the solution with the aid of a cold bath.

Electron Spin Resonance Spectra. The ESR measurements were carried out either on a Varian E4 spectrometer or a modified Varian 4502 spectrometer equipped with a frequency counter and an NMR field marker as described previously.³¹

Calculation of Odd Electron and Spin Density Distributions in the Radical Anions. All computations were carried out on a CDC 6600 computer. The programs for Hückel molecular orbital calculations and the McLachlan perturbation corrections ($\lambda = 0.75$)^{25,28} were tested by comparing them with those previously obtained for naphthalene, 1,4,5,8-tetraazaphthalene, and 1,4-dithiin radical anions.^{4,25,32} Other studies have indicated that spin density calculations for aromatic systems such as these are not improved greatly by the use of more accurate configuration interaction methods³² or SCF-MO calculations using unrestricted Hartree-Fock wave functions.^{3,13}

(1) **Unpaired Spin Density Distributions.** The Hückel molecular orbitals were calculated for the thiadiazole systems

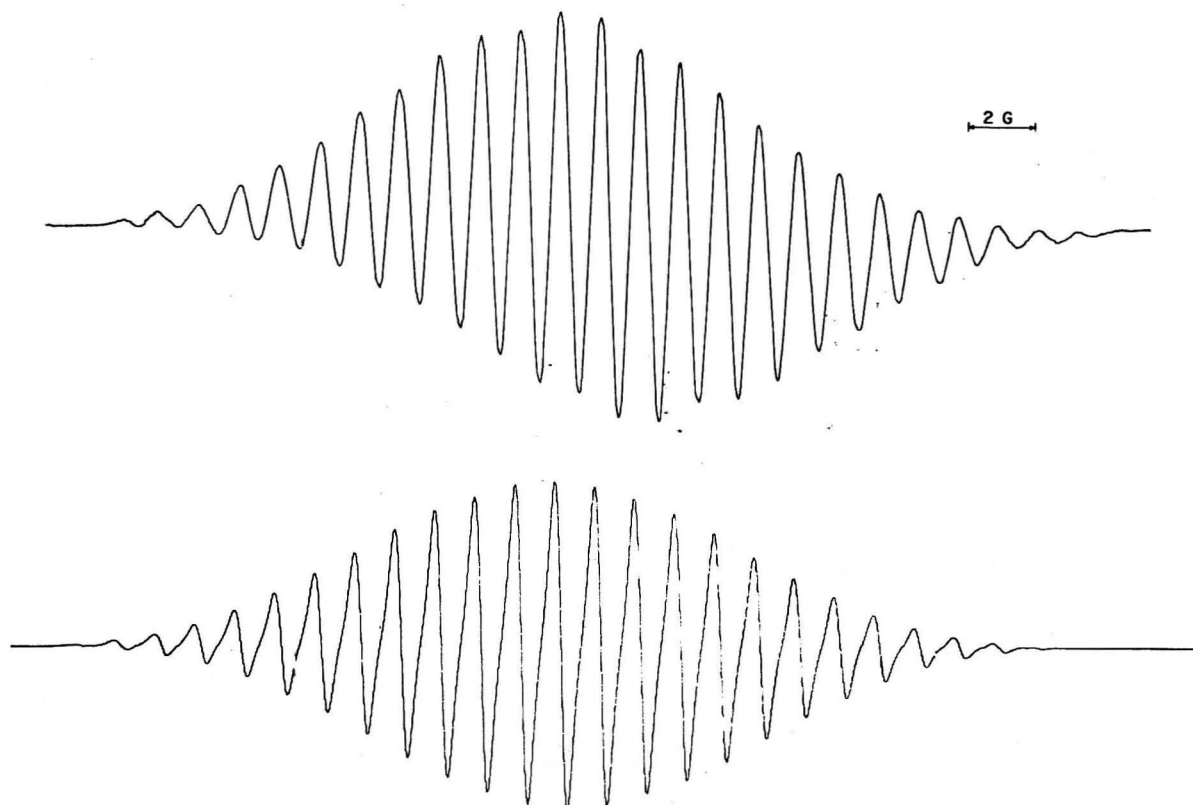


Figure 5. Upper: ESR spectrum of potassium [1,2,5]thiadiazolo[3,4-b]quinoxaline anion radical in dimethoxyethane solution at room temperature. Lower: Computer simulated spectrum using the ESR parameters in Table IV.

TABLE V: Calculated Values of a_N/ρ_N^π for Thiadiazolo Anion Radicals

Anion radical	a^N	ρ_N^π	ρ_S^π	a_N/ρ_N^π	ρ_S^π/ρ_N^π
BT	5.30	0.222	0.256	23.9	1.15
NT	3.25	0.144	0.228	22.6	1.58
TT	3.17	0.148	0.230	21.4	1.55
BNT	2.38	0.095	0.224	25.1	2.36

using the parameters suggested by Talcott and Myers.⁸ Two sets of integrals corresponding to a p orbital model^{10,11} and a d orbital model^{9,25} were employed; i.e., the p orbital model has $\alpha_S = \alpha_C + \beta_{CC}$, $\alpha_N = \alpha_C + 0.8\beta_{CC}$, $\beta_{CN} = 1.076\beta_{CC}$, $\beta_{NS} = 0.778\beta_{CC}$ and the d orbital model has $\alpha_S = \alpha_C$, $\alpha_N = \alpha_C + 0.8\beta_{CC}$, $\beta_{CN} = 1.076\beta_{CC}$, $\beta_{NS} = 1.1\beta_{CC}$, $\beta_{CC} = \beta_{SS}$.

(2) *Hyperfine Coupling Constants.* Proton hyperfine coupling constants were related to the spin density on carbon by the McConnell equation, $a^H = Q_H\rho_C$. The value of Q_H was assigned to be the same (26.9 G) as that for naphthalene anion radical, the spectral width of which resembles most closely the anions examined here.³³

For nitrogen and sulfur hyperfine splittings, the same types of relationships were used, viz., $a^N = Q_N\rho_N$ and $a^S = Q_S\rho_S$, respectively. Q_N was taken to be 22 G (vide infra) and Q_S as 33 G.³⁴ The use of the simplified equation for the calculation of the unpaired π -electron density on nitrogen can be justified in the following manner. In the systems examined in this study, nitrogen bonded to sulfur can be considered analogous to carbon bonded to carbon in aromatic hydrocarbons. Following the treatment developed by Karplus and Fraenkel^{33,35} for ¹³C splittings we obtain

$$a^N = [S_N^N + Q_{NS}^N + Q_{NC}^N]\rho_N^\pi + Q_{SN}^N\rho_S^\pi + Q_{CN}^N\rho_C^\pi$$

In our compounds, the last term can be neglected since Q_{CN} is very small (-1.7 G^8) and $\rho_C \approx 0$. Letting $Q_N = [S_N^N + Q_{NS}^N + Q_{NC}^N]$, then

$$\frac{a^N}{\rho_N^\pi} = Q_N + Q_{SN}^N \frac{\rho_S^\pi}{\rho_N^\pi}$$

Interestingly, values of a^N/ρ_N^π listed in Table V for the anion radicals examined here all cluster between 21.5 and 25 G. From a least-squares treatment, we obtain $Q_N = 22 \text{ G}$ and $Q_{SN}^N = 0.9 \text{ G}$. It appears, thus, that a single McConnell type relationship is appropriate in this system since $Q_{SN}^N \ll Q_N$. The value of 22 G is smaller than that employed by Talcott and Myers⁸ in aza aromatic systems, the difference being $[Q_{NS}^N - Q_{NC}^N]$.

A similar treatment can be applied to sulfur, namely

$$a^S = (S_S^S + 2Q_{SN}^S)\rho_S^\pi + 2Q_{NS}^S\rho_N^\pi$$

The value of $Q_S = 33 \text{ G}$ obtained for sulfur heterocycles³⁴ is not necessarily valid in our system, the difference being $2[Q_{SN}^S - Q_{SC}^S]$. Unfortunately, the lack of data prohibits a better evaluation of Q_S for these systems. However, a simple analysis obtained from TT anion radical suggests a value of 22 G.

Acknowledgment. We wish to thank Dr. A. P. Komin for kindly providing the samples used in this study and the National Science Foundation for financial support to C. L. Kwan.

References and Notes

- (1) A. P. Komin, R. W. Street, and M. Carmack, *J. Org. Chem.*, **40**, 279 (1975).
- (2) J. R. Bolton in "Radical-Ions", E. T. Kaiser and L. Kevan, Ed., Wiley-Interscience, New York, N.Y., 1960, Chapter 1.
- (3) J. A. Pedersen and C. T. Muus, *Mol. Phys.*, **16**, 589 (1969).

- (4) R. Danieli, L. Lunazzi, and G. Placucci, *J. Am. Chem. Soc.*, **93**, 5850 (1971).
- (5) J. Chaudhuri, S. Kume, I. Jagur-Grodzinski, and M. Szwarc, *J. Am. Chem. Soc.*, **90**, 6421 (1968).
- (6) L. Lunazzi, A. Mangini, C. F. Pedulli, and F. Taddei, *J. Chem. Soc. B*, 163 (1970).
- (7) P. Cavalieri d'Oro, R. Darieli, G. Maccagnani, G. F. Pedulli, and P. Palmieri, *Mol. Phys.*, **20**, 365 (1971).
- (8) C. L. Talcott and R. J. Myers, *Mol. Phys.*, **12**, 549 (1967).
- (9) H. C. Longuet-Higgins, *Trans. Faraday Soc.*, **45**, 174 (1949).
- (10) E. T. Strom and G. A. Russell, *J. Am. Chem. Soc.*, **87**, 3326 (1965).
- (11) R. Gerdil and E. A. C. Lucken, *J. Am. Chem. Soc.*, **87**, 213 (1965).
- (12) N. M. Atherton, J. N. Cckwell, and R. Dietz, *J. Chem. Soc. A*, 771 (1967).
- (13) J. Fajer, B. H. J. Bielski, and R. H. Felton, *J. Phys. Chem.*, **72**, 1281 (1968).
- (14) M. Kamiya and Y. Akahori, *Bull. Chem. Soc. Jpn.*, **43**, 268 (1970).
- (15) M. F. Chiu, B. C. Gilbert, and P. Hanson, *J. Chem. Soc. B*, 1700 (1970).
- (16) M. M. Urberg and E. T. Kaiser, ref 2, Chapter 8.
- (17) M. Kaplan, J. R. Bolton, and G. K. Fraenkel, *J. Chem. Phys.*, **42**, 955 (1965).
- (18) (a) N. Hirota, ref 2, Chapter 2; (b) K. S. Chen and N. Hirota, "Techniques in Chemistry", A. Weissberger and G. Hammes, Ed., Vol. 6, part 2, Wiley, New York, N.Y., 1973, Chapter 12; (c) cf. also G. A. Russell and J. L. Gerlock, *J. Am. Chem. Soc.*, **96**, 5838 (1974); T. L. Staples and M. Szwarc, *ibid.*, **92**, 5022 (1970).
- (19) (a) J. H. Sharp and M. C. R. Symons in "Ions and Ion-Pairs in Organic Reactions", M. Szwarc, Ed., Vol. 1, Wiley-Interscience, New York, N.Y., 1972, Chapter 5; (b) L. Lee, R. Adams, J. Jagur-Grodzinski, and M. Szwarc, *J. Am. Chem. Soc.*, **93**, 4149 (1971).
- (20) J. H. Freed and G. K. Fraenkel, *J. Chem. Phys.*, **39**, 326 (1963).
- (21) P. D. Sullivan and J. R. Bolton, *Adv. Mag. Resonance*, **4**, 39 (1970).
- (22) J. L. Sommerdijk and E. deBoer, ref 19, Chapter 8.
- (23) N. M. Atherton and S. I. Weissman, *J. Am. Chem. Soc.*, **83**, 1330 (1961).
- (24) The reverse trend is observed, however, in nitrogen splittings in NT compared to TT.
- (25) E. A. C. Lucken, *Theor. Chim. Acta*, **1**, 397 (1963).
- (26) R. Schaeffer, unpublished results cited in ref 1.
- (27) P. A. Howell, R. M. Curtis, and W. N. Lipscomb, *Acta Crystallogr.*, **7**, 498 (1954).
- (28) A. D. McLachlan, *Mol. Phys.*, **3**, 233 (1960).
- (29) A recent ab initio SCF-MO calculation of the simple thiomethyl anion, $\text{CH}_3\text{SCH}_2^-$, suggests that sulfur stabilizes carbanions by polarization rather than d orbital conjugation. [A. Streitwieser, Jr., and J. E. Williams, Jr., *J. Am. Chem. Soc.*, **97**, 192 (1975).]
- (30) A. P. Komin and M. Carmack, *J. Heterocycl. Chem.*, in press.
- (31) D. J. Edge and J. K. Kochi, *J. Am. Chem. Soc.*, **94**, 6485 (1972).
- (32) W. J. Van der Hart, "Proton Splittings in ESR Spectroscopy", Blonder Offset, Rotterdam, 1968.
- (33) J. E. Wertz and J. R. Bolton, "Electron Spin Resonance", McGraw-Hill, New York, N.Y., 1972.
- (34) P. D. Sullivan, *J. Am. Chem. Soc.*, **90**, 3618 (1968).
- (35) M. Karplus and G. K. Fraenkel, *J. Chem. Phys.*, **35**, 1312 (1961).

Electron Spin Resonance Studies of Spin-Labeled Polymers. 11. Segmental and End-Group Mobility of Some Acrylic Ester Polymers

A. T. Bullock,* G. G. Cameron, and V. Krajewski

Department of Chemistry, University of Aberdeen, Old Aberdeen, Scotland, AB9 2UE (Received March 8, 1976)

Poly(methyl acrylate), poly(*n*-butyl methacrylate), and two samples of poly(methyl methacrylate) have been spin labeled at random ester groups along the chain. The density of labeling was low and a study of the electron spin resonance line widths of dilute solutions of the spin-labeled polymers clearly showed the dominant effect of segmental rotation. Three further samples of poly(methyl methacrylate) were labeled specifically at one end of the chain. Solution studies showed a nonlinear Arrhenius plot of $\log \tau_c$ vs. $1/T$ which reflected the temperature dependence of the termination rate coefficient in the free radical polymerization of methyl methacrylate. For the low molecular weight end-labeled samples ($\bar{M}_n = 25\,000$ and 2300) there was some evidence for anisotropy in the rotational diffusion of the whole polymer molecules.

Introduction

In parts 1-10 of this series it has been shown that electron spin resonance (ESR) studies of spin-labeled synthetic polymers provide a useful and complementary addition to existing methods of studying polymer relaxations in dilute solution¹⁻³ and in the solid state.⁴ Further, the effects of increasing polymer concentration in solution are readily delineated and evidence favoring one particular theory of concentrated solution has been obtained.³ The present work is concerned with segmental relaxation on poly(methyl acrylate) (PMA), poly(methyl methacrylate) (PMMA), and poly(*n*-butyl methacrylate) (PBMA) in dilute solution. In addition the rotational behavior of the chain end has been observed in three samples of end-labeled PMMA in dilute solution. The results are

discussed in terms of the rate-determining step in the radical polymerization of methyl methacrylate and the anisotropic end-over-end rotational diffusion of the macromolecules. The importance of spectral simulation in deriving values of τ_c , the rotational correlation time, from inhomogeneously broadened lines is emphasized throughout.

Experimental Section

Materials. (i) *Side-Chain Labeled Polymers.* These were prepared from acrylic ester-acrylic acid chloride copolymers by reaction in benzene solution of the acid chloride moieties with 4-hydroxy-2,2,6,6-tetramethylpiperidin-1-oxy (I) in the presence of pyridine. The generalized reaction is

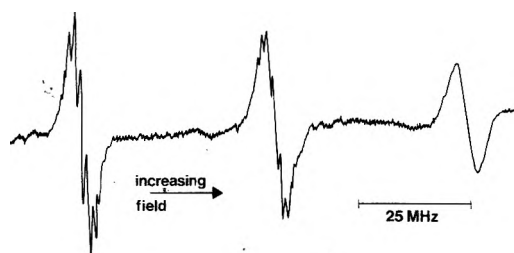


Figure 1. ESR spectrum of side-chain labeled PMMA in toluene at 21 °C.

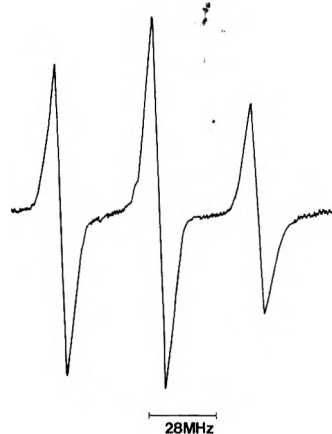


Figure 2. ESR spectrum of end-labeled PMMA.

pendence upon the nuclear spin quantum numbers m_i such that⁸

$$T_2^{-1}(m_1, m_2, \dots, m_n) = A + \sum_{i=1}^n B_i m_i + \sum_{i=1}^n C_i m_i^2 + \sum_{i \neq j=1}^n E_{ij} m_i m_j \quad (1)$$

As in the case of labeled polystyrene² it was possible to select lines for which the resultant ^1H spin quantum number, Σm_H , was zero. Such lines have widths depending only on m_I , the component of the ^{14}N nuclear spin, components of the anisotropic g and hyperfine coupling tensors (g_{ii} and T_{jj} , respectively), the applied magnetic field, and the rotational correlational time τ_c . Again as for earlier labeled polymers, nonsecular contributions to the line widths were negligible and substituting for the various coefficients in eq 1 gives

$$T_2(m_I)^{-1} = \left[\frac{3b^2}{20} + \frac{4}{45} (\Delta\gamma B_0)^2 + \frac{b^2}{8} m_I^2 - \frac{4}{15} b \Delta\gamma B_0 m_I \right] \tau_c + X \quad (2)$$

where

$$b = (4\pi/3)[T_{zz} - \frac{1}{2}(T_{xx} + T_{yy})]$$

$$\Delta\gamma = -\frac{|\beta|}{\hbar} [g_{zz} - \frac{1}{2}(g_{xx} + g_{yy})]$$

B_0 is the applied magnetic field and X represents contributions to the line width which are independent of m_I . For convenience in later discussion eq 2 may be recast into the form of eq 1, thus

$$T_2(m_I)^{-1} = A + B m_I + C m_I^2 \quad (3)$$

where $B = -(4/15)b\Delta\gamma B_0 \tau_c$ and $C = (b^2/8)\tau_c$.

(a) *Side-Chain Labeled Polyacrylates*. From earlier studies in this series² together with the work of Poggi and Johnson⁹ allowance had to be made for unresolved and partially resolved couplings to protons in the piperidinyl ring (a point ignored in earlier studies using this label^{10,11}). Kreilick¹² and Brière et al.¹³ have separately reported NMR contact shift measurements of proton coupling constants in nitroxides structurally similar to those used here as labels. We have noted elsewhere¹⁴ that the values given by Brière et al.¹³ gave satisfactory spectral simulations whereas those of Kreilick¹² did not. This finding has been independently confirmed by Whishnant, Ferguson, and Chestnut.¹⁵ The proton coupling constants (MHz) used were thus $a^{\text{H}}_{(\gamma\text{-CH})} = 0.23$, $a^{\text{H}}_{(\alpha\text{-CH}_3, \text{axial})} = 0.0$, $a^{\text{H}}_{(\alpha\text{-CH}_3, \text{equatorial})} = -1.21$, $a^{\text{H}}_{(\beta\text{-CH}_2, \text{axial})} = -0.87$, and $a^{\text{H}}_{(\beta\text{-CH}_2, \text{equatorial})} = -1.35$. Kreilick¹² found a sharp temperature dependence of several of the proton coupling constants below ca. 5–10 °C. Our measurements were thus restricted to the range 20–80 °C where the variation in the values of a^{H} were negligible for our purposes. The simulations were initially performed for the Tatpo small radical analogue (IV) and then on the various labeled polymers. Typical results are shown in Figures 3 and 4.

The determination of the parameters b and $\Delta\gamma$ involves a knowledge of $a^{\text{N}}_{\text{iso}}$, g_{iso} , T_{zz} , and g_{zz} . The isotropic parameters were readily determined by measurement in toluene solution. However, the usual method of measurement of T_{zz} and g_{zz} ¹⁶ from the extrema positions in the spectrum of the solid powdered polymers was not applicable in the present case since measurements over a range of temperatures revealed that the rigid limit had not been reached at the lowest temperature of measurement, namely, 77 K. However, it was found that a satisfactory extrapolation to 0 K of both high- and low-field extrema positions and their difference could be obtained by a least-squares curve fitting procedure to a polynomial in the temperature. This is illustrated in Figure 5 for $2T_2^*$, the separation of high- and low-field extrema. Since $a^{\text{N}}_{\text{iso}} = \frac{1}{3}(T_{xx} + T_{yy} + T_{zz})$ and $g_{\text{iso}} = \frac{1}{3}(g_{xx} + g_{yy} + g_{zz})$, then $b = 2\pi(T_{zz} - a^{\text{N}}_{\text{iso}})$ and $\Delta\gamma = \frac{3}{2}(|\beta|/\hbar)(g_{zz} - g_{\text{iso}})$. Table II lists the relevant parameters for the both side- and end-labeled polymers.

Unfortunately, the poor resolution of the high-field multiplet ($m_I = -1$) did not allow measurements of $T_2(-1)$. Measurements were therefore confined to the low- and mid-field lines. The general principles of the analysis together with the use of spectral simulation to obtain true line widths have been given elsewhere.²

Both samples of PMMA gave values of τ_c which closely fitted a common Arrhenius plot (Figure 6) characterized by an activation energy, E_a , of 20 ± 1 kJ mol⁻¹. Since the molecular weights of the two samples differ by more than an order of magnitude it is clear that the motion of the label is largely determined by segmental relaxation of the chain and that any contribution from "end-over-end" or whole molecule rotation of the polymer is negligible. The activation energy is comparable to, although slightly lower than, the value obtained by dielectric relaxation measurements in this solvent, namely, ca. 27 kJ mol⁻¹. Ironically, when the rather poorer spectral simulations based on Kreilick's values for the H coupling constants were used, the activation energy for PMMA agreed exactly with the dielectric results. This sensitive dependence of E_a upon the details of the spectral simulation accords with the comments of Poggi and Johnson.⁹

Poly(methyl acrylate) and poly(*n*-butyl methacrylate) gave activation energies of 19 ± 3 and 14.6 ± 0.6 kJ mol⁻¹, respectively. The value for PMA is again slightly lower than that of 23 kJ mol⁻¹ obtained from dielectric measurements.¹⁷

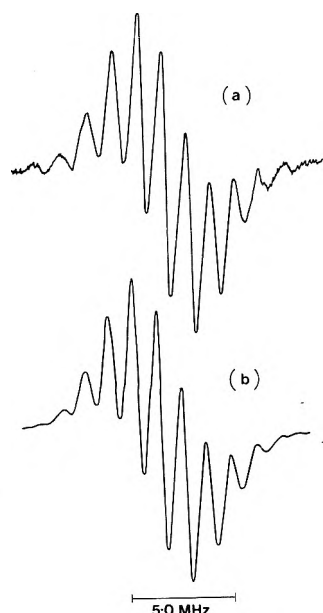


Figure 3. (a) Experimental and (b) simulated low-field $[m\chi(^{14}\text{N}) = +1]$ multiplet of Tatpo in toluene. Simulation based on the data of ref 13 (see text).

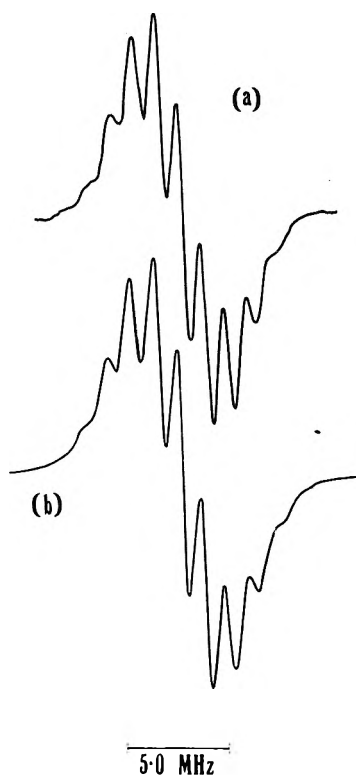


Figure 4. (a) Experimental and (b) simulated low-field multiplet of PBMA in toluene at 45 °C. Coupling constants are from ref 13 (see text).

To conclude this section we note that during the course of this work Kurosaki, Lee, and Okawara used a similar technique to prepare spin-labeled PMMA and polystyrene.¹⁸ However, they obtained poorly resolved spectra and did not observe splittings from the piperidinyI protons. This is almost certainly the result of a high density of spin labels causing exchange and dipolar broadening of the spectral lines.

(b) *End-Labeled Poly(methyl methacrylate)*. The three samples PMMA-1E, PMMA-2E, and PMMA-3E (mol wt =

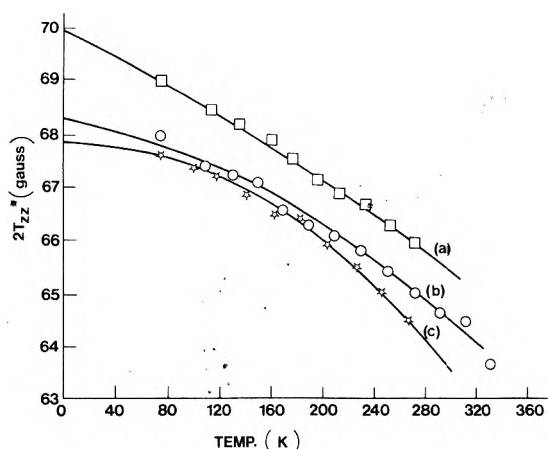


Figure 5. Variation with temperature of the field separation of the low- and high-field extrema in the powder spectra of side-chain labeled PMA (a), PMMA (b), and PBMA (c). The solid lines are least-squares plots of the polynomial $2T_{zz}^* = a + bT + cT^2$ where T is the temperature (K).

81 000, 25 000, and 2300, respectively) were all studied as 5% solutions in ethyl acetate over the temperature range -60 to $+18$ °C. The reason for these choices lies in a study by Hughes and North^{19,20} in which they examined the free-radical polymerization of methyl methacrylate in this solvent at low temperatures. They found a nonlinear Arrhenius dependence of k_t , the termination rate coefficient, upon temperature. This was interpreted in terms of a model in which the rate-determining step in the termination reaction was not considered to be the translational diffusion of two macroradicals together but rather the diffusion, via a segmental reorientation process, of the radical ends to within reaction distance once the propagating macroradicals have come sufficiently close together. The "knee" in the Arrhenius plot of k_t vs. $1/T$ was said to arise from a "phase transition" in solution from a rigid random coil to a flexible random coil. Clearly, if the above interpretation is correct and if the motion of the nitroxide radical in the present study reflects closely the rotational mobility of the chain ends, similar behavior should be found in the temperature dependence of τ_c as was observed for k_t .

Figures 7-9 show the Arrhenius plots for τ_c in PMMA-1E, -2E, and -3E, respectively. In each case it was possible to determine both the B and C coefficients in eq 3 and hence two independent correlation times. From the three figures it is clear that the rotational behavior of the spin label is strongly dependent upon molecular weight. For the high molecular weight sample (Figure 7) the Arrhenius plots derived separately from the B and C coefficients are closely parallel and, if due allowance for experimental errors is made, are almost coincident. We take this to indicate that the motion is essentially isotropic and, from previous work,^{2,3} associate it with segmental motion of the polymer chain. A close examination of Figure 7 shows the plots to be slightly nonlinear with a change in slope occurring at -41 ± 4 °C. This effect is more strongly marked in PMMA-2E (Figure 8) for which the "knee" in the Arrhenius plots is found at -45 ± 1 °C. Both these values are in excellent agreement with the "phase transition" temperature obtained by Hughes and North from kinetic and intrinsic viscosity measurements for this polymer. Insofar as the rotational mobility of the chain end is intimately linked with the translational diffusion of the reactive centers of the propagating radicals our results provide direct supporting evidence of the termination mechanism described above.

It is apparent that as the molecular weight decreases there

TABLE II: Spin Hamiltonian Parameters

Polymer	B_0/G	$a_N(\text{iso})/\text{MHz}$	$g(\text{iso})$	T_{zz}/MHz	g_{zz}	$b^a/M \text{ radians s}^{-1}$	$\Delta\gamma/\text{radians}^{-1} \text{ s}^{-1} \text{ G}^{-1}$
PMMA ^b	3301.96	43.52 ± 0.14	$2.006\,08 \pm 0.000\,02$	95.86 ± 0.34	$2.001\,98 \pm 0.000$	10 330.03	5.41×10^4
PMA ^b	3301.60	43.43 ± 0.08	$2.006\,25 \pm 0.000\,02$	98.24 ± 0.37	$2.002\,16 \pm 0.000$	13 344.39	5.40×10^4
PBMA ^b	3301.60	43.18 ± 0.08	$2.006\,06 \pm 0.000\,02$	95.21 ± 0.45	$2.002\,25 \pm 0.000$	15 326.85	5.02×10^4
PMMA-1E ^c							
PMMA-2E ^c	3301.89 ± 0.02	41.80 ± 0.06	$2.005\,99 \pm 0.000\,04$	96.13 ± 0.25	$2.001\,91 \pm 0.000$	$14\,341.30 \pm 1.71$	$(5.38 \pm 0.23) \times 10^4$
PMMA-3E ^c							

^a Previously, we have given b the units MHz; the above units are, however, strictly correct. ^b Side-chain labeled. Isotropic parameters in toluene solution. ^c Enc-labeled. Isotropic parameters in ethyl acetate solution.

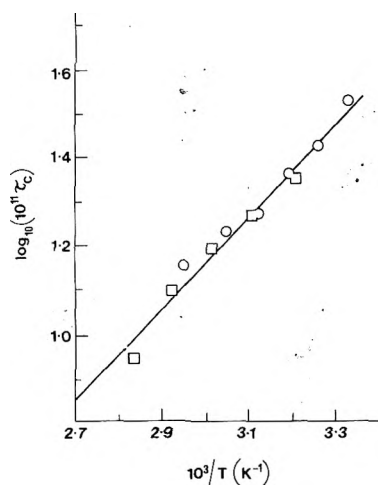


Figure 6. Common Arrhenius plot for two samples of side-chain labeled PMMA: (O) $M_v = 550\,000$; (\square) $M_v = 33\,000$.

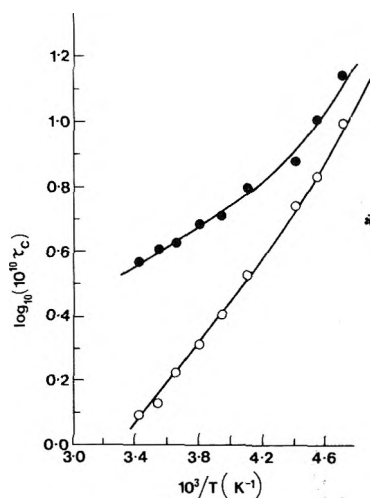


Figure 8. Same as caption to Figure 7 but for PMMA-2E.

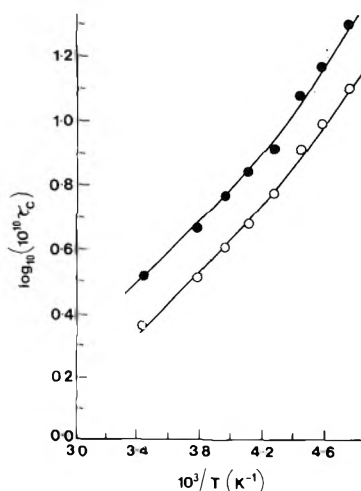


Figure 7. Arrhenius plots for end-labeled PMMA-1E in ethyl acetate: (●) τ_c from coefficient C; (O) τ_c from coefficient B.

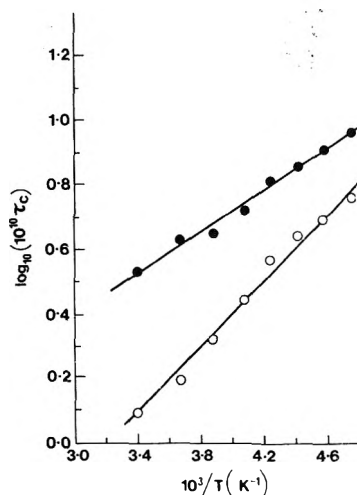


Figure 9. Same as captions to Figures 7 and 8 but for PMMA-3E.

is a concomitant increase in the anisotropy of the rotational motion of the probe. The evidence for this is the increasing divergence of τ_c values separately calculated from the B and C coefficients as the molecular weight decreases. Freed and co-workers have analyzed this situation in some detail with especial reference to the rotational diffusion of the peroxylamine disulfonate ion.²¹ Unfortunately, it is impossible to apply their analysis quantitatively to the present situation.

The reasons are as follows. First the system must be defined by two diffusion tensors \mathbf{R} , one describing the rotation of the whole macromolecule in the laboratory frame of reference and the other describing the local mode or segmental rotation of that part of the chain to which the spin label is bonded. Secondly, it is not possible, as it was in the system studied by Freed et al.,²¹ to make a sensible estimate of the direction cosines between the principal axes of the diffusion tensors and

those of the hyperfine and g tensors. We can, however, assert that the principal source of the observed effect is anisotropy in the rotational motion of the whole macromolecule since the effect becomes more marked at shorter chain lengths. The conclusion is that, at low molecular weights, poly(methyl methacrylate) assumes a nonspherical or rodlike shape.

An alternative interpretation of the results for PMMA-1E, -2E, and -3E could be that the rotational mobility of the chain ends with respect to the rest of the chain increases with decreasing molecular weight. This would imply that, since the anisotropy is evident in PMMA-2E (mol wt 25 000), groups 250 monomer units distant from the nitroxide moiety have a significant effect. This seems rather implausible and is at variance with our previous study of labeled polystyrene.² Further, it might be argued that evidence of anisotropic rotation should be found in the side-chain labeled polymer of mol wt 33 000. However, we have shown previously² that for labeled polystyrene, the contribution to relaxation from the overall rotation of the macromolecule drops off sharply when the molecular weight is such that $\tau(\text{segmental})$ is of the same order as $\tau(\text{eoe})$. [$\tau(\text{eoe})$ is the correlation time for whole-molecule rotation.] It would seem that for PMMA, this situation is reached at a molecular weight of about 30 000. Above this, we expect the observed correlation time to be dominated by segmental relaxation while below it, both segmental and whole molecule rotation will contribute. Certainly Figure 6 clearly shows that the segmental process is dominant for PMMA having a molecular weight greater than, or equal to, 33 000.

In view of some recent fluorescence depolarization measurements of segmental and end group mobilities²² it is of interest to compare the correlation times for these two processes as measured by the spin-labeling technique. At 298 K these are $\tau_c(\text{segmental}) = 3.6 \times 10^{-10}$ s and $\tau_c(\text{chain end}) = (2.8 \pm 0.5) \times 10^{-10}$ s. The latter value is the mean of the values derived from the B and C coefficients for PMMA-1E. A meaningful comparison of these values must take into account the relative viscosities of the two solvents. It was noted in part 7³ that Helfand's treatment²³ of the rate of conformational transitions in polymers in the limit of high viscous damping is given by

$$k = (A/\xi) \exp(-E^*/RT) \quad (4)$$

where A is a constant, ξ the frictional coefficient (proportional to the solvent viscosity η), and E^* is the energy barrier for local conformational changes. If it is assumed that, as in the case of polystyrene, E^* is the same for segmental² and end group

rotation,²⁴ then the two correlation times may be expressed as reduced correlation times τ_c/η . The relevant values of η at 298 K are 0.552 and 0.441 cP for toluene and ethyl acetate, respectively. The reduced correlation times are found to be in excellent agreement thus $6.5 \times 10^{-8} \text{ P}^{-1} \text{ s}^{-1}$ (toluene) and $6.35 \times 10^{-8} \text{ P}^{-1} \text{ s}^{-1}$ (ethyl acetate).

Finally, it is worth noting that a linear dependence of k_t upon $1/\eta$ is to be expected whether termination is controlled by a simple translational diffusion of reacting macroradicals, when the Stokes-Einstein-Debye equation applies, or by the mechanism proposed by Hughes and North when eq 4 is relevant. The dependence of k_t upon $1/\eta$ has been demonstrated by several groups.²⁵ However, the nonlinear Arrhenius plots of the chain end rotational mobility are most readily accommodated by the mechanism involving segmental reorientation.

References and Notes

- (1) A. T. Bullock, J. H. Butterworth, and G. G. Cameron, *Eur. Polym. J.*, **7**, 445 (1971).
- (2) A. T. Bullock, G. G. Cameron, and P. M. Smith, *J. Phys. Chem.*, **77**, 1635 (1973).
- (3) A. T. Bullock, G. G. Cameron, and P. M. Smith, *J. Chem. Soc., Faraday Trans. 2*, **70**, 1202 (1974).
- (4) A. T. Bullock, G. G. Cameron, and P. M. Smith, *J. Polym. Sci., Polym. Phys. Ed.*, **11**, 1263 (1973).
- (5) (a) G. Smets, A. Poot, and G. L. Duncan, *J. Polym. Sci.*, **54**, 65 (1961); (b) T. Otsu and T. Yapima, *Chem. Abstr.*, **81**, 78307x (1974).
- (6) R. Brière, H. Lemaire, and A. Rassat, *Bull. Soc. Chim. Fr.*, 3273 (1965).
- (7) A. T. Bullock, G. G. Cameron, and J. M. Elsom, *Polymer*, **15**, 74 (1974).
- (8) A. Hudson and G. R. Luckhurst, *Chem. Rev.*, **69**, 191 (1969).
- (9) G. Poggi and C. S. Johnson, Jr., *J. Magn. Reson.*, **3**, 436 (1970).
- (10) J. F. Hower, R. W. Henkens, and D. B. Chestnut, *J. Am. Chem. Soc.*, **93**, 6665 (1971).
- (11) D. B. Chestnut and J. F. Hower, *J. Phys. Chem.*, **75**, 907 (1971).
- (12) R. W. Kreilick, *J. Chem. Phys.*, **46**, 4260 (1967).
- (13) R. Brière, H. Lemaire, and A. Rassat, *Bull. Soc. Chim. Fr.*, **12**, 4479 (1967).
- (14) A. T. Bullock and G. G. Cameron, "Structural Studies of Macromolecules by Spectroscopic Methods", K. J. Ivin, Ed., Wiley, New York, N.Y., 1976, Chapter 15.
- (15) C. C. Whishnant, S. Ferguson, and D. B. Chestnut, *J. Phys. Chem.*, **78**, 1410 (1974).
- (16) N. Edelstein, A. Kwok, and A. H. Maki, *J. Chem. Phys.*, **41**, 179 (1964).
- (17) A. M. North, *Chem. Soc. Rev.*, **1**, 49 (1972).
- (18) T. Kurosaki, K. W. Lee, and M. Okawara, *J. Polym. Sci., Polym. Chem. Ed.*, **A-1**, **10**, 3295 (1972).
- (19) J. Hughes and A. M. North, *Trans. Faraday Soc.*, **60**, 960 (1964).
- (20) J. Hughes and A. M. North, *Trans. Faraday Soc.*, **62**, 1866 (1966).
- (21) S. A. Goldman, G. V. Bruno, C. Polnaszek, and J. H. Freed, *J. Chem. Phys.*, **56**, 716 (1972).
- (22) A. M. North and I. Soutar, *J. Chem. Soc., Faraday Trans. 1*, **68**, 1101 (1972).
- (23) E. Helfand, *J. Chem. Phys.*, **54**, 4651 (1971).
- (24) A. T. Bullock, G. G. Cameron, and N. K. Reddy, to be submitted for publication.
- (25) See, for example, A. M. North and G. A. Reed, *Trans. Faraday Soc.*, **57**, 859 (1961); C. H. Bamford and S. Brumby, *Makromol. Chem.*, **105**, 122 (1967); G. M. Burnett, G. G. Cameron, and S. N. Joiner, *J. Chem. Soc., Faraday Trans. 1*, **69**, 322 (1972).

Optical Activity of d-d Transitions in Copper(II) Complexes of Dipeptides and Dipeptide Amides. Molecular Orbital Model

Gary Hilmes, Chin-yah Yeh, and F. S. Richardson*

Department of Chemistry, University of Virginia, Charlottesville, Virginia 22901 (Received January 21, 1976)

Publication costs assisted by the Petroleum Research Fund

The chiroptical properties associated with the d-d and low-lying charge-transfer transitions in a series of four-coordinate and six-coordinate Cu(II)-dipeptide and Cu(II)-dipeptide amide complexes are calculated on a semiempirical molecular orbital model. Electronic rotatory strengths are calculated directly using wave functions of the entire complex generated from the molecular orbital model. Excited states are constructed in the virtual orbital approximation and electric and magnetic dipole transition integrals are computed including all one-, two-, and three-center contributions. The results are compared to those obtained using other theoretical models of molecular optical activity, to semiempirically derived spectra-structure relationships and rules formulated for pseudotetragonal metal complexes, and to empirical data.

I. Introduction

Copper(II) complexes of di-, tri-, and tetrapeptides have been studied extensively because of their importance as models for metalloproteins. Copper(II) promotes the ionization of amide hydrogens in neutral solutions of simple peptides, yielding chelates containing planar, trans amide bonds with trigonal amide nitrogens as donor atoms. These pseudotetragonal copper(II)-peptide complexes provide a nearly planar system of chelate rings to which side chains are attached in known dispositions. Because of the relative structural rigidity of these systems they serve as excellent models for examining the origins of optical activity in chiral transition metal complexes. Furthermore, spectra-structure relationships found applicable to these systems are also expected to be at least qualitatively applicable to spectra-structure correlations in metalloenzymes and metal-protein complexes.

A considerable number of studies on the chiroptical properties of complexes formed between copper(II) and amino acid, dipeptide, and tripeptide ligands have been reported in the literature.^{1,2} Several of these studies have led to the formulation of empirically based spectra-structure relationships which are remarkably successful in correlating the data obtained on various series of similar systems. Additionally, in a few instances these relationships have been interpreted directly in terms of extant theoretical models of molecular optical activity. Of special note is the "hexadecant" sector rule proposed and applied by Martin and co-workers¹ in interpreting the circular dichroism (CD) spectra of a large number of metal ion-amino acid and -peptide complexes. This sector rule derives directly from the one-electron static-coupling model of molecular optical activity as described by Schellman³ and as elaborated upon by Mason^{4,5} and by Richardson.^{6,7} Although the CD associated with the pure ligand-ligand transitions as well as the ligand-metal charge-transfer (CT) transitions have been studied for many metal complexes, it is generally the CD spectra associated with the metal ion d-d or ligand-field transitions which are used as diagnostic probes of structure or structural changes. These transitions generally fall within an easily accessible region of the spectrum, generally exhibit relatively large dissymmetry factors ($\Delta\epsilon/\epsilon$), and are more readily amenable to theoretical analysis than are the less well characterized metal-ligand charge-transfer and ligand-ligand transitions.

Theoretical treatments of optical activity in chiral transition metal complexes have generally developed along three different lines. In one approach an independent systems representation of the complex is adopted wherein the complex is partitioned into an achiral chromophoric group (which includes the metal ion) and a set of extra-chromophoric groups distributed throughout the ligand environment.⁴⁻⁷ Interactions between the chromophoric group and extrachromophoric groups are treated by perturbation techniques and optical activity in the chromophoric transitions is assumed to arise from dissymmetric terms in these interactions. The theoretical bases for most of the sector or regional rules proposed and applied in making spectra-structure correlations in amino and peptide complexes of transition metal ions are found in various forms of the independent systems model.

A second approach to examining the origins of optical activity in transition metal complexes focuses on chiral distortions of donor atom orbitals. These distortions reflect the chiral nature of the ligand environment beyond the donor atom set and communicate chirality to the chromophoric electrons of the metal ion via direct bonding (or antibonding) interactions. This approach has been used with varying degrees of success by Liehr,⁸ Karipedes and Piper,⁹ Strickland and Richardson,¹⁰ and Schäffer.¹¹

The third approach to studying the chiroptical properties of metal complexes involves direct molecular orbital calculations on the entire complex. That is, the entire metal complex is treated as a single entity and the wave functions obtained from molecular orbital calculations on the complex will have dissymmetry built into them directly (reflecting the symmetry properties of the total molecular Hamiltonian operator). This latter approach has been employed by Schreiner and co-workers,¹² by Strickland and Richardson,¹⁰ and by Yeh and Richardson.¹³

In the present study we calculate the electronic rotatory strengths associated with the d-d and low-lying charge-transfer transitions in a series of copper(II)-dipeptide complexes using the molecular orbital model and the direct calculational method. This method is particularly suitable for the Cu(II)-dipeptide complexes since in these systems one may expect strong d- π interactions between the metal ion and the peptide and carboxylate (or amide) groups of the ligands, as well as significant electron delocalization over large parts

of the complex (metal ion + ligands). In these cases it is unlikely that an independent systems model can provide a complete or accurate representation since the basic chromophoric unit for certain of the transitions of interest must be assumed to extend somewhat beyond the metal ion and the donor atoms of the ligands. That is, partitioning the complex into weakly interacting chromophoric and extrachromophoric groups is not easily (or validly) accomplished, and it becomes more appropriate to treat the entire complex as an extended chromophore. The molecular orbital/direct calculational method allows us to do this.

II. Structures

Nineteen Cu(II)-dipeptide complexes were studied. These are: [Cu(GG)(OH)]⁻, [Cu(GG)(H₂O)], [Cu(AG)(OH)]⁻, [Cu(GA)(OH)]⁻, [Cu(AG)(H₂O)], [Cu(GA)(H₂O)], [Cu(AA)(OH)]⁻, [Cu(AA)(H₂O)], [Cu(A'A)(OH)]⁻, [Cu(AA')(OH)]⁻, *trans*-[Cu(GG)(OH)](OH)₂³⁻, *trans*-[Cu(GA)(OH)](OH)₂³⁻, *trans*-[Cu(AG)(OH)](OH)₂³⁻, *trans*-[Cu(AG)(OH)](OH)₂³⁻, *trans*-[Cu(GG-NH)(OH)](OH)₂³⁻, *trans*-[Cu(GA-NH)(OH)](OH)₂³⁻, *trans*-[Cu(AG-NH)(OH)](OH)₂³⁻, *trans*-[Cu(GG)(H₂O)](H₂O)₂, *trans*-[Cu(GA)(H₂O)](H₂O)₂, *trans*-[Cu(AG)(H₂O)](H₂O)₂, where GA = glycyl-*S*-alaninato ligand, AG = *S*-alanyl-glycinato ligand, GG = glycylglycinato ligand, AA = *S*-alanyl-*S*-alaninato ligand, A'A = *R*-alanyl-*S*-alaninato ligand, AA' = *S*-alanyl-*R*-alaninato ligand, GA-NH = glycyl-*S*-alaninamido ligand, AG-NH = *S*-alanyl-glycinamido ligand, and GG-NH = glycylglycinanido ligand. The structure parameters for the chelate rings in these systems were adapted from those reported for crystalline glycylglycinatocopper(II) trihydrate and for crystalline glycylglycinatocopper(II) dihydrate (obtained from x-ray diffraction data).^{14,15} The GG, GA, AG, and AA ligands each function as a tridentate chelate system via an amino group donor, a deprotonated peptide nitrogen donor, and a carboxyl group donor. The CuN₂O₂ (one oxygen atom from either a water molecule or a hydroxyl anion) cluster forms a slightly distorted square. The chelate ring formed by the carboxyl and peptide groups is assumed to be exactly planar in our model structures, whereas the chelate ring formed by the peptide nitrogen and the terminal amino group is very slightly puckered.

The GG-NH, GA-NH, AG-NH, and AA-NH ligands each function as a tridentate chelate system via an amino group donor, a deprotonated peptide nitrogen donor, and an amido group donor. The CuN₃O cluster forms a slightly distorted square and the chelate rings are each nearly planar.

The "in-plane" Cu-OH and Cu-OH₂ bond distances were taken to be 1.95 Å. The axial Cu-OH and Cu-OH₂ bond distances were set at 2.40 Å. The GG and GG-NH complexes were constructed to have exact C₂ symmetry, whereas all the other complexes are entirely lacking in symmetry.

III. Calculations

The direct calculational approach was used to compute the electronic rotatory strengths associated with the d-d and lowest-lying charge-transfer transitions of the Cu(II) systems examined in this study. That is, the rotatory strengths

$$R_{ij} = \text{Im} \langle \psi_i | \hat{\mu} | \psi_j \rangle \cdot \langle \psi_j | \hat{m} | \psi_i \rangle \quad (1)$$

where $\hat{\mu}$ is the electric dipole operator and \hat{m} is the magnetic dipole operator, are calculated using wave functions obtained directly as approximate eigenfunctions of the complete electronic Schrödinger equation for each complex. The shortcomings of this approach reside in the rather serious approximations one must make in solving the electronic

Schrödinger equation for such large systems as are being studied here, and especially in constructing wave functions for the spectroscopic excited states. Despite these obvious shortcomings, this approach is to be preferred over an independent systems or perturbative model for systems in which electron delocalization beyond the metal ion-donor atom cluster is expected to be significant and in which the chromophoric unit is not localized at a center of high symmetry.

In our calculations, ground state electronic wave functions were obtained using a modified Wolfsberg-Helmholz or extended Hückel molecular orbital model. The general procedures employed in carrying out calculations on this model have been described elsewhere^{10,13} and will not be discussed further here. The atomic orbital basis set employed in the present calculations included: (1) 3d, 4s, and 4p orbitals on Cu(II); (2) 2s and 2p orbitals on each carbon, oxygen, and nitrogen atom; and, (3) a 1s orbital on each hydrogen atom. The single- ζ Slater-type-orbitals (STO) of Clementi and Raimondi¹⁶ were chosen for the C, N, and O atoms. For the H atoms, we used a Slater type 1s orbital with $\zeta = 1.2$. The metal ion basis set consisted of single- ζ 4s and 4p orbitals and double- ζ 3d orbitals.¹⁷

Excited state wave functions were constructed in the virtual orbital approximation by promoting an electron from an occupied molecular orbital to an unoccupied (or virtual) orbital.

To calculate electronic rotatory strengths (eq 1) both electric and magnetic dipole transition integrals are required. The electric dipole transition integrals were calculated in the dipole velocity representation and then transformed to the dipole length form according to

$$\langle \psi_i | \partial/\partial q | \psi_j \rangle = m(E_j - E_i) \langle \psi_i | \hat{q} | \psi_j \rangle / \hbar^2 \quad (2)$$

where $q = x, y, \text{ or } z$ (electron positional coordinate) and $m =$ electron mass. All one-, two-, and three-center terms were included in evaluating the electric dipole velocity and angular momentum integrals required for computing the $\langle \psi_i | \hat{\mu} | \psi_j \rangle$ and $\langle \psi_i | \hat{m} | \psi_j \rangle$ matrix elements.

The electric and magnetic dipole transition integrals, dipole strengths (eq 3), rotatory strengths (eq 1), oscillator strengths, and dissymmetry factors (eq 4) were calculated using a program (ROTSTR) previously employed in computing chiroptical properties of nonmetal systems¹⁸ and extended, recently, to handle 4s, 4p, and 3d metal orbitals.¹³

$$D_{ij} = |\langle \psi_i | \hat{\mu} | \psi_j \rangle|^2 \quad \text{dipole strength} \quad (3)$$

$$G_{ij} = 4R_{ij}/D_{ij} \quad \text{dissymmetry factor} \quad (4)$$

IV. Results

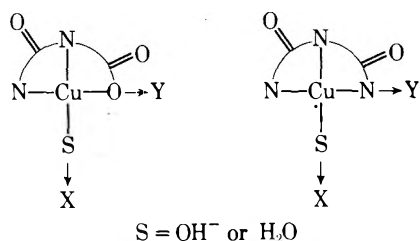
The optical properties computed for the d-d transitions in 15 of the Cu(II)-dipeptide and Cu(II)-dipeptide amide complexes are listed in Tables I-III. The optical properties computed for the three lowest energy charge-transfer transitions in six of these complexes are listed in Table IV.

In each of the four-coordinate systems studied the energy ordering of the 3d metal orbitals was calculated to be: $d_{x^2-y^2}(\epsilon) > d_{xy}(\zeta) > d_{z^2}(\theta) > d_{xz}(\eta) > d_{yz}(\xi)$. In each of the six-coordinate systems the energy ordering of the 3d orbitals was calculated to be: $d_{x^2-y^2}(\epsilon) > d_{z^2}(\theta) > d_{xy}(\zeta) > d_{xz}(\eta) > d_{yz}(\xi)$. The coordinate systems employed in our calculations are depicted in Scheme I. The $d_{xz}(\eta)$ orbital is directed toward the peptide nitrogen atom and the $d_{yz}(\xi)$ orbital points toward the amino nitrogen and carboxyl oxygen (or amide nitrogen) atoms.

TABLE I: Computed Optical Properties of Four Lowest Energy Transitions in Four-Coordinate Cu(II)-Dipeptide Complexes

Complex	λ , nm	D, D^2	$R, 10^{-40}$ esu ² cm ²	$ G $	Transition
[Cu(GG)(OH)] ⁻	643	0.43	0	0	$\zeta \rightarrow \epsilon$
	610	0.26	0	0	$\theta \rightarrow \epsilon$
	604	0.27	0	0	$\eta \rightarrow \epsilon$
	539	0.02	0	0	$\xi \rightarrow \epsilon$
[Cu(AG)(OH)] ⁻	652	0.24	-1.44	0.0023	$\zeta \rightarrow \epsilon$
	610	0.23	2.45	0.0043	$\theta \rightarrow \epsilon$
	601	0.27	-8.41	0.0116	$\eta \rightarrow \epsilon$
	536	0.03	0.06	0.0008	$\xi \rightarrow \epsilon$
[Cu(GA)(OH)] ⁻	651	0.49	-2.66	0.0022	$\zeta \rightarrow \epsilon$
	615	0.11	4.70	0.0171	$\theta \rightarrow \epsilon$
	604	0.23	-18.66	0.0325	$\eta \rightarrow \epsilon$
	537	0.02	-0.26	0.0048	$\xi \rightarrow \epsilon$
[Cu(AA)(OH)] ⁻	661	0.25	-3.22	0.0047	$\zeta \rightarrow \epsilon$
	618	0.43	6.55	0.0057	$\theta \rightarrow \epsilon$
	601	0.25	-22.88	0.0366	$\eta \rightarrow \epsilon$
	534	0.03	-0.03	0.0004	$\xi \rightarrow \epsilon$
[Cu(AA)(OH)] ⁻	654	0.28	0.96	0.0013	$\zeta \rightarrow \epsilon$
	621	0.40	1.46	0.0015	$\theta \rightarrow \epsilon$
	603	0.31	-7.42	0.0095	$\eta \rightarrow \epsilon$
	538	0.04	-0.14	0.0014	$\xi \rightarrow \epsilon$
[Cu(A'A)(OH)] ⁻	654	0.28	-0.96	0.0013	$\zeta \rightarrow \epsilon$
	621	0.40	-1.46	0.0015	$\theta \rightarrow \epsilon$
	603	0.31	7.42	0.0095	$\eta \rightarrow \epsilon$
	538	0.04	0.14	0.0014	$\xi \rightarrow \epsilon$

Scheme I



The four lowest energy transitions calculated for each complex are essentially d-d excitations localized on the metal ion. For all the complexes studied, the three lowest energy charge-transfer transitions involve excitation of an electron out of a predominantly ligand-localized orbital into the half-filled $d_{x^2-y^2}(\epsilon)$ metal orbital. The highest occupied ligand-localized orbital is calculated in each case to be slightly bonding with respect to the $d_{xy}(\zeta)$ metal orbital and it has maximum amplitude in the xy plane. This orbital is designated π' . The second highest occupied ligand-localized orbital is designated π'' and it is found to be entirely nonbonding with respect to the metal orbitals. This orbital has maximum amplitude in the xy plane and is somewhat localized on the carbonyl oxygen atom of the terminal carboxylate or amido moiety. The third highest occupied ligand-localized orbital is an out-of-plane π orbital with maximum amplitude on the nitrogen and oxygen atoms of the central peptide group. We designate this orbital as π . The π'' orbital in our calculations closely resembles a carbonyl oxygen nonbonding or "n" orbital, and the π orbital in our calculations closely resembles the π_0 "nonbonding" orbital found in isolated amide chromophores. (The π_0 orbital in amide groups is often called "nonbonding" because it has a near nodal plane at the carbonyl carbon atom of the OCN group.)

The orbital occupation numbers calculated for the 4s and

4p metal orbitals in the ground state of the various complexes were found to lie in the range 0.45–0.62. The occupation numbers calculated for the $d_{x^2-y^2}(\epsilon)$ orbital in the ground state of the various complexes fall in the range 0.70–0.74. With the several parameter sets we examined in constructing our semiempirical molecular orbital model, very little mixing between the 4s, 4p, and 3d metal orbitals was found among the occupied and low-lying virtual molecular orbitals. The orbital occupation numbers listed above suggest significant participation of the metal 4s and 4p atomic orbitals in metal–ligand bonding in the ground states of the Cu(II)-dipeptide complexes. However, our calculations give little evidence for significant sp^2d hybridization in the ground states of these systems (although this point cannot be settled by the very approximate types of calculations performed in this study).

Axial perturbations by ligands located in the fifth and sixth positions determine the relative ordering of the $d_{z^2}(\theta)$ and $d_{xy}(\zeta)$ orbitals as seen by comparing the calculated results for the four-coordinate and six-coordinate complexes. The dipole strengths and rotatory strengths of the $\theta \rightarrow \epsilon$ and $\zeta \rightarrow \epsilon$ transitions are also quite sensitive to the presence or absence of axial ligands (see Tables I and II).

V. Discussion

As was pointed out in the Introduction, metal ion–peptide complexes provide excellent model systems for testing and investigating theoretical methods for calculating and interpreting molecular chiroptical properties. They have relatively rigid structures and well-defined chromophoric units, and their chiroptical properties have been studied extensively by experimental methods. Previously we have investigated the origins of d-d optical activity in these and similar systems using both the static coupling (one-electron)⁷ and dynamical coupling¹⁹ variants of the independent systems model. The spectra–structure relationships and sector rules most commonly applied to these systems have their basis in the static coupling or one-electron theory as formulated by Schellman³ (and elaborated upon in ref 6 and 7). The "hexadecant" sector rule proposed and applied by Martin^{1,20} has proved to be especially useful in making spectra–structure correlations. Our previous studies have shown, however, that neither the static coupling model nor the dynamical coupling model (carried to first and second order in perturbation theory) provides a complete or adequate representation for chiroptical properties of the metal ion–peptide systems. This does not diminish the importance or utility of the semiempirically derived spectra–structure relationships and sector rules applied to these systems, for these relationships retain their validity independent of theoretical justification. However, it is of some interest to understand better the electronic structural and stereochemical factors responsible for the chiroptical observables in these important model systems. The direct calculational approach based on a molecular orbital description of the molecular electronic states (as used in the present study) provides yet another representation for examining the chiroptical properties of these systems. Given the approximations in the molecular orbital model employed in the present study, this approach is not expected to yield inherently more accurate results or a superior representation of the optical activity mechanisms; rather, it provides an alternative and supplementary view.

In neutral solution, Cu(II)-(AG), Cu(II)-(GA), and Cu(II)-(AA) complexes exhibit a single broad CD band in the region 500–700 nm.^{20,21} This broad band is centered near 650 nm and is generally presumed to span all four d-d transitions.

TABLE II: Computed Optical Properties of Four Lowest Energy Transitions in Six-Coordinate Cu(II)-Dipeptide Complexes

Complex	λ , nm	D , D ²	R , 10 ⁻⁴⁰ esu ² cm ²	$ G $	Transition
<i>trans</i> -[Cu(GG)(OH)](OH) ₂ ³⁻	721	0.09	0	0	$\theta \rightarrow \epsilon$
	641	0.52	0	0	$\zeta \rightarrow \epsilon$
	600	0.30	0	0	$\eta \rightarrow \epsilon$
	532	0.02	0	0	$\xi \rightarrow \epsilon$
<i>trans</i> -[Cu(GG)(H ₂ O)](H ₂ O) ₂	662	0.10	0	0	$\theta \rightarrow \epsilon$
	569	0.71	0	0	$\zeta \rightarrow \epsilon$
	548	0.44	0	0	$\eta \rightarrow \epsilon$
	492	0.12	0	0	$\xi \rightarrow \epsilon$
<i>trans</i> -[Cu(AG)(OH)](OH) ₂ ³⁻	727	0.13	0.88	0.0025	$\theta \rightarrow \epsilon$
	640	0.47	-0.84	0.0007	$\zeta \rightarrow \epsilon$
	604	0.32	-5.15	0.0059	$\eta \rightarrow \epsilon$
	536	0.09	-0.72	0.0032	$\xi \rightarrow \epsilon$
<i>trans</i> -[Cu(AG)(H ₂ O)](H ₂ O) ₂	641	0.18	0.12	0.0003	$\theta \rightarrow \epsilon$
	556	0.54	-1.21	0.0009	$\zeta \rightarrow \epsilon$
	552	0.38	-4.24	0.0045	$\eta \rightarrow \epsilon$
	478	0.08	-0.71	0.0004	$\xi \rightarrow \epsilon$
<i>trans</i> -[Cu(GA)(OH)](OH) ₂ ³⁻	725	0.13	0.66	0.0018	$\theta \rightarrow \epsilon$
	645	0.48	-2.18	0.0017	$\zeta \rightarrow \epsilon$
	609	0.33	-8.44	0.0102	$\eta \rightarrow \epsilon$
	536	0.06	-0.21	0.0014	$\xi \rightarrow \epsilon$
<i>trans</i> -[Cu(GA)(H ₂ O)](H ₂ O) ₂	643	0.18	0.41	0.0009	$\theta \rightarrow \epsilon$
	561	0.51	-2.12	0.0017	$\zeta \rightarrow \epsilon$
	556	0.36	-7.92	0.0088	$\eta \rightarrow \epsilon$
	486	0.09	-0.40	0.0018	$\xi \rightarrow \epsilon$

TABLE III: Computed Optical Properties of Four Lowest Energy Transitions in Six-Coordinate Cu(II)-Dipeptide Amide Complexes

Complex	λ , nm	D , D ²	R , 10 ⁻⁴⁰ esu ² cm ²	$ G $	Transition
<i>trans</i> -[Cu(GG-NH)(OH)](OH) ₂ ³⁻	648	0.06	0	0	$\theta \rightarrow \epsilon$
	564	0.15	0	0	$\zeta \rightarrow \epsilon$
	560	0.24	0	0	$\eta \rightarrow \epsilon$
	526	0.03	0	0	$\xi \rightarrow \epsilon$
<i>trans</i> -[Cu(GA-NH)(OH)](OH) ₂ ³⁻	656	0.01	0.17	0.0044	$\theta \rightarrow \epsilon$
	566	0.21	23.71	0.0421	$\zeta \rightarrow \epsilon$
	563	0.23	-31.81	0.0553	$\eta \rightarrow \epsilon$
	525	0.07	-4.42	0.0249	$\xi \rightarrow \epsilon$
<i>trans</i> -[Cu(AG-NH)(OH)](OH) ₂ ³⁻	661	0.01	0.21	0.0057	$\theta \rightarrow \epsilon$
	565	0.19	24.65	0.0474	$\zeta \rightarrow \epsilon$
	562	0.28	-28.57	0.0384	$\eta \rightarrow \epsilon$
	624	0.04	-1.67	0.0167	$\xi \rightarrow \epsilon$

A single, broad absorption band ($\epsilon \sim 80$) is also observed for these complexes in this spectral region, but the absorption band is centered near 636 nm.²⁰ The $\Delta\epsilon(\lambda \sim 650 \text{ nm})$ values reported for these complexes in neutral solution are as follows:²⁰ Cu(II)-(AG), $\Delta\epsilon = -0.11$; Cu(II)-(GA), $\Delta\epsilon = -0.35$; Cu(II)-(AA), $\Delta\epsilon = -0.47$.

In neutral solution, the Cu(II)-(AG-NH), Cu(II)-(GA-NH), and Cu(II)-(AA-NH) complexes also exhibit a single broad CD band in the visible region of the spectrum.^{20,21} However, in these systems the CD band is centered around 560 nm and spans the region 450-700 nm. A single broad absorption band is observed with a maximum near 600 nm. The reported $\Delta\epsilon(\lambda \sim 560 \text{ nm})$ values are: Cu(II)-(AG-NH), $\Delta\epsilon = -0.11$; Cu(II)-(GA-NH), $\Delta\epsilon = -0.32$; Cu(II)-(AA-NH), $\Delta\epsilon = -0.43$.

In basic solution, the visible CD spectra of Cu(II)-(GA) and Cu(II)-(AA) exhibit two negative extrema, one centered near 680 nm and one centered near 510 nm.^{20,21} The 680-nm band is about twice as intense as the 510-nm band in each case, and Cu(II)-(AA) produces a more intense CD than does

Cu(II)-(GA). The visible CD spectrum of Cu(II)-(AG) in basic solution shows only a single weak CD band centered at ~ 590 nm. As was the case in neutral solution, addition of the visible CD spectra of Cu(II)-(AG) and Cu(II)-(GA) produces almost exactly the visible CD spectrum of Cu(II)-(AA).

In basic solution, the visible CD spectra of Cu(II)-(GA-NH) and Cu(II)-(AA-NH) also exhibit two negative extrema, one centered near 600 nm and the other centered at ~ 490 nm.^{20,21} A single absorption maximum is observed at 570 nm ($\epsilon \sim 75$). The 600-nm CD band is about twice as intense as the 490-nm CD band for each complex, and the Cu(II)-(AA-NH) complex yields a more intense CD than does Cu(II)-(GA-NH). In basic solution, Cu(II)-(AG-NH) gives a single, weak CD band in the visible region which is centered at ~ 530 nm. Again, addition of the Cu(II)-(AG-NH) and Cu(II)-(GA-NH) CD spectra produces almost exactly the CD spectrum of Cu(II)-(AA-NH).

The most remarkable features in the visible CD spectra of the dipeptide and dipeptide amide complexes discussed above are: (1) the additivity of the (AG) and (GA) spectra to produce

TABLE IV: Computed Optical Properties of Three Lowest Energy Charge-Transfer Transitions in Selected Six-Coordinate Cu(II)-Dipeptide and Cu(II)-Dipeptide Amide Complexes

Complex	λ , nm	D , D ²	R , 10 ⁻⁴⁰ esu ² cm ²	$ G $	Transition ^a
<i>trans</i> -[Cu(GG-NH)(OH)](OH) ₂ ³⁻	406	1.18	0	0	$\pi' \rightarrow \epsilon$
	352	2.19	0	0	$\pi'' \rightarrow \epsilon$
	341	0.06	0	0	$\pi \rightarrow \epsilon$
<i>trans</i> -[Cu(GA-NH)(OH)](OH) ₂ ³⁻	409	1.13	6.25	0.0022	$\pi' \rightarrow \epsilon$
	358	2.13	-5.15	0.0010	$\pi'' \rightarrow \epsilon$
	332	0.04	6.70	0.0676	$\pi \rightarrow \epsilon$
<i>trans</i> -[Cu(AG-NH)(OH)](OH) ₂ ³⁻	419	1.08	5.10	0.0018	$\pi' \rightarrow \epsilon$
	350	2.72	-4.68	0.0007	$\pi'' \rightarrow \epsilon$
	326	0.13	3.28	0.0092	$\pi \rightarrow \epsilon$
<i>trans</i> -[Cu(GG)(OH)](OH) ₂ ³⁻	430	0.78	0	0	$\pi' \rightarrow \epsilon$
	372	0.72	0	0	$\pi'' \rightarrow \epsilon$
	348	0.06	0	0	$\pi \rightarrow \epsilon$
<i>trans</i> -[Cu(GA)(OH)](OH) ₂ ³⁻	434	0.71	10.75	0.0056	$\pi' \rightarrow \epsilon$
	376	0.66	-2.68	0.0015	$\pi'' \rightarrow \epsilon$
	350	0.02	7.88	0.1213	$\pi \rightarrow \epsilon$
<i>trans</i> -[Cu(AG)(OH)](OH) ₂ ³⁻	438	0.75	8.89	0.0044	$\pi' \rightarrow \epsilon$
	368	0.79	-2.55	0.0012	$\pi'' \rightarrow \epsilon$
	337	0.03	1.29	0.0169	$\pi \rightarrow \epsilon$

^a π = out-of-plane π orbital which interacts with the $d_{xz}(\eta)$ metal orbital; π' = in-plane ligand orbital which interacts with the $d_{xy}(\zeta)$ metal orbital; π'' = in-plane ligand orbital highly localized on the carbonyl oxygen of the terminal amide or carboxylate moiety.

the (AA) spectrum, and the additivity of the (AG-NH) and (GA-NH) spectra to produce the (AA-NH) spectrum, in both neutral and basic solution; (b) the relatively weak CD observed for (AG) and (AG-NH) vs. that observed for (GA), and (GA-NH); (c) the splittings observed in the CD spectra of (AA), (AA-NH), (GA), and (GA-NH) in basic solution; and, (d) the large blue shift observed in going from dipeptide to dipeptide amide ligands. The additivity phenomenon was first observed and commented upon by Martin^{1,20} and this observation is quite compatible with the basic assumptions of the first-order static coupling (or one-electron) theory of optical activity in metal complexes.^{3,6,7} The differences in CD intensities for (AG) vs. (GA) and for (AG-NH) vs. (GA-NH) complexes are not so easily understood in terms of the simple static coupling model. Qualitatively, one may rationalize this observation by assuming that asymmetry in the (GA) and (GA-NH) complexes is more easily communicated to the metal d electrons through metal-ligand π interactions involving the central peptide nitrogen atom. The asymmetric sites in (GA) and (GA-NH) lie closer to the peptide nitrogen than do the asymmetric sites in (AG) and (AG-NH). This qualitative reasoning is supported to some extent by theoretical results obtained with a dynamical coupling model of d-d optical activity in metal ion-peptide systems.¹⁹ Neither the static coupling model nor the dynamical coupling model provides for comment on the splittings observed in the visible CD spectra (in basic solution) or on the blue shift observed in going from dipeptide to dipeptide amide ligands.

The *net* d-d rotatory strength (i.e., the algebraic sum of the four individual d-d rotatory strengths) calculated for each of the complexes examined in this study is negative, in agreement with experimental observation. Furthermore, the *net* d-d rotatory strengths calculated for the (GA) and (GA-NH) complexes are about twice as large as those calculated for the corresponding (AG) and (AG-NH) complexes, which is also in agreement with experimental observation. In the four-coordinate complexes of (GA), (AG), and (AA), the *net* d-d rotatory strength calculated for the (AA) system is approximately equal to the sum of the *net* d-d rotatory strengths calculated for the (GA) and (AG) complexes. The *net* d-d rotatory strength calculated for the four-coordinate (A'A)

complex has the same sign as that calculated for the (AA) complex and is approximately equal to the difference, $R_{\text{net}}(\text{GA}) - R_{\text{net}}(\text{AG})$. (Recall that the asymmetric carbon atom in A' has the R(D) configuration, whereas in A the asymmetric carbon atom has the S(L) configuration.)

Using *net* d-d rotatory strengths, our calculations are in accord with the additivity phenomenon observed experimentally. Furthermore, the calculated results show that asymmetric substitution at the α carbon of the carboxyl (or amido) terminal chelate ring produces significantly greater optical activity in the d-d transitions than does asymmetric substitution at the α carbon of the amino terminal chelate ring.

Replacing the carboxyl oxygen donor atom of (AG), (GA), and (AA) with the amido nitrogen donor atom of (AG-NH), (GA-NH), and (AA-NH) results in a large blue shift of the d-d transition energies. However, *net* d-d rotatory strengths calculated for analogous dipeptide and dipeptide amide complexes do not differ significantly (although the calculated values for the rotatory strengths of individual d-d transitions do differ significantly).

We note that the relative ordering of the $d_{z^2}(\theta)$ and $d_{xy}(\zeta)$ orbitals is strongly dependent upon the presence or absence of ligands in the fifth and sixth positions of the complexes. In the four-coordinate structures $d_{z^2}(\theta)$ lies below $d_{xy}(\zeta)$ in energy, whereas in the pseudotetragonal six-coordinate structures $d_{xy}(\zeta)$ lies below $d_{z^2}(\theta)$. The presence or absence of axial ligand perturbations also appears to have a strong influence on the magnitude of the $\theta \rightarrow \epsilon$ rotatory strengths. In the six-coordinate structures, the rotatory strengths calculated for this transition are very small and essentially insignificant. However, in the four-coordinate structures the $\theta \rightarrow \epsilon$ rotatory strengths are calculated to be rather large.

Up to this point we have focused our discussion on the *net* d-d rotatory strengths rather than on the rotatory strengths of individual d-d transitions. Given the rather close proximity (in energy) of the individual d-d transitions in most of the structures studied and the rather broad bands generally observed in the CD spectra obtained for solution samples, this seems to be a valid and useful approach. Furthermore, we calculate only the electronic rotatory strengths and completely

ignore any effects which might be introduced by vibronic interactions or couplings between the various d-d states. The d-d excited states in the metal complexes examined here are relatively close in energy and are subject to vibronic interactions of the Jahn-Teller (JT) and pseudo-Jahn-Teller (PJT) type.²² Such interactions can effectively scramble and distort the electronic states involved in the transitions, and lead to sign and intensity patterns in the CD spectra which cannot be interpreted in terms of specific d-d electronic excitations. The *net* rotatory strength associated with the manifold of interacting electronic states remains invariant to PJT interactions, but assignment of specific features in the CD spectra to transitions of specific electronic parentage may no longer be valid.²²

In addition to vibronic effects from JT or PJT type interactions *within* the manifold of d-d excited states, it is likely that coupling between the d-d excited states and opposite parity charge-transfer or d-p excited states via a Herzberg-Teller mechanism will play a significant role in determining d-d absorption intensities and intensity distributions. However, there is little experimental evidence or theoretical basis for ascribing significant *net* d-d CD intensity to vibronic effects arising from Herzberg-Teller type mechanisms. The purely electronic rotatory strengths calculated in the present study can be related directly to the *net* d-d CD intensity. Vibronic interactions will determine how this intensity is distributed among the vibronic sublevels of the d-d states, but should have only very small or negligible effects upon the overall (or *net*) CD intensity.

Although the computed transition energies for the d-d excitations fall generally in the same range as is experimentally observed for the Cu(II)-dipeptide and Cu(II)-dipeptide amide complexes, the calculated values tend to be slightly high. This is especially true when H₂O rather than OH⁻ ligands are placed at the fourth, fifth, and sixth coordination sites. One may expect a slight blue shift when H₂O ligands are replaced by OH⁻ ligands, but not blue shifts of the magnitude we calculate.

The transition energies computed for the three lowest lying charge-transfer excitations are somewhat lower than are observed experimentally. For the Cu(II)-(GA) complex in neutral solution, Martin^{20a} has reported a positive CD band at ~315 nm ($\Delta\epsilon = 0.2$) followed by a more intense negative CD band at ~270 nm. The Cu(II)-(AG) complex in neutral solution exhibits a positive CD band at ~310 nm ($\Delta\epsilon = 0.3$) followed by a more intense negative CD band at ~235 nm.^{20a} The Cu(II)-(AA) complex shows a positive CD band centered near 315 nm ($\Delta\epsilon = 0.3$) and a negative CD band at ~265 nm ($\Delta\epsilon = -1.0$).^{20a} The absorption spectra of these complexes show no peaks or shoulders in the 310-315-nm region and the ϵ values in this region are of the order 100-300.^{20a} The absorption spectra do show a shoulder in the 260-280-nm region where

ϵ values are of the order of 1000. Although the dipole strengths calculated for the two lowest lying charge-transfer transitions are about an order of magnitude greater than those calculated for the most intense d-d transitions, they are still somewhat low. The oscillator strengths calculated for the lowest energy charge-transfer transitions were in the range 0.005-0.010, and for the second charge-transfer transition the computed oscillator strengths were in the range 0.009-0.040. The oscillator strength of the third charge-transfer transition was computed to be very low for each complex.

The parameterizations and inherent approximations of the semiempirical molecular orbital model adopted in this study preclude any detailed comment or conclusions about the optical properties calculated for the charge-transfer transitions.

Acknowledgments. This work was supported in part by grants from the National Science Foundation, the Petroleum Research Fund administered by the American Chemical Society, and the Camille and Henry Dreyfus Foundation (through a Teacher-Scholar Award to F.R.).

References and Notes

- (1) See R. Bruce Martin in "Metal Ions in Biological Systems", Vol. 1, H. Sigel, Ed., Marcel-Dekker, New York, N.Y., Chapter 4 and references therein.
- (2) C. J. Hawkins, "Absolute Configuration of Metal Complexes", Wiley-Interscience, New York, N.Y., 1971, Chapter 5.
- (3) J. A. Schellman, *J. Chem. Phys.*, **44**, 55 (1966).
- (4) S. F. Mason in "Fundamental Aspects and Recent Developments in Optical Rotatory Dispersion and Circular Dichroism", F. Ciardelli and P. Salvadori, Ed., Heyden and Son Ltd., New York, N.Y., 1973, Chapter 3.6.
- (5) S. F. Mason, *J. Chem. Soc. A*, 667 (1971).
- (6) F. S. Richardson, *J. Chem. Phys.*, **54**, 2453 (1971).
- (7) F. S. Richardson, *Inorg. Chem.*, **10**, 2121 (1971).
- (8) (a) A. D. Liehr, *J. Phys. Chem.*, **68**, 665 (1964); (b) *ibid.*, **68**, 3629 (1964).
- (9) A. Karipedes and T. S. Piper, *J. Chem. Phys.*, **40**, 674 (1964).
- (10) R. W. Strickland and F. S. Richardson, *Inorg. Chem.*, **12**, 1025 (1973).
- (11) C. E. Schaffer, *Proc. R. Soc. London, Ser. A*, **297**, 96 (1968).
- (12) R. J. Evans, A. F. Schreiner, and P. J. Hauser, *Inorg. Chem.*, **13**, 2185 (1974).
- (13) C. Yeh and F. S. Richardson, *Inorg. Chem.*, **15**, 682 (1976).
- (14) H. C. Freeman, *Adv. Protein Chem.*, **22**, 257 (1967).
- (15) T. J. Kistenmacher and D. J. Szalda, *Acta Crystallogr., Sect. B*, **31**, 1659 (1975).
- (16) E. Clementi and D. L. Raimondi, *J. Chem. Phys.*, **38**, 3686 (1963).
- (17) (a) J. W. Richardson, N. C. Nieuwpoort, R. R. Powell, and W. F. Edgell, *J. Chem. Phys.*, **36**, 1057 (1962); (b) J. W. Richardson, R. R. Powell, and W. C. Nieuwpoort, *ibid.*, **38**, 796 (1963).
- (18) (a) J. Webb, R. Strickland, and F. S. Richardson, *J. Am. Chem. Soc.*, **95**, 4775 (1973); (b) F. S. Richardson and W. Pitts, *Biopolymers*, **13**, 703 (1974); (c) F. S. Richardson and D. Caliga, *Theor. Chim. Acta*, **36**, 49 (1974).
- (19) R. W. Strickland and F. S. Richardson, *J. Phys. Chem.*, **80**, 164 (1976).
- (20) (a) J. M. Tsangaris, J. W. Chang, and R. B. Martin, *J. Am. Chem. Soc.*, **91**, 726 (1969); (b) J. M. Tsangaris and R. B. Martin, *ibid.*, **92**, 4255 (1970); (c) E. W. Wilson, Jr., and R. B. Martin, *Inorg. Chem.*, **10**, 1197 (1971).
- (21) R. S. Treptow, *J. Inorg. Nucl. Chem.*, **31**, 2983 (1969).
- (22) (a) D. Caliga and F. S. Richardson, *Mol. Phys.*, **28**, 1145 (1974); (b) F. S. Richardson, D. Caliga, G. Hilmes, and J. J. Jenkins, *Mol. Phys.*, **30**, 257 (1975); (c) F. S. Richardson, G. Hilmes, and J. J. Jenkins, *Theor. Chim. Acta*, **39**, 75 (1975); (d) G. Hilmes, D. Caliga, and F. S. Richardson, *Chem. Phys.*, **13**, 203 (1976).

Electronic Properties of *N*-Formylkynurenine and Related Compounds

Marie-Paule Pileni, Paul Warrant, and René Santus*

Laboratoire de Biophysique, Muséum National d'Histoire Naturelle, 61, rue Buffon 75005 Paris, France (Received December 22, 1975)

Publication costs assisted by Muséum National d'Histoire Naturelle

N-Formylkynurenine, a tryptophan photooxidation product and a remarkable photosensitizer, displays unusual luminescence behaviors. At room temperature, in addition to a low quantum yield fluorescence emission ($\lambda_{\max} \approx 430$ nm) an abnormally red-shifted fluorescence ($\lambda_{\max} \approx 510$ nm) is seen whose quantum yield depends upon the hydrogen bonding ability and polarity of the solvent. This abnormal fluorescence is tentatively ascribed to an excited state proton transfer from the formamido group of the benzene ring to the *o*-carbonyl of the side chain. This proton transfer would be favored by intramolecular hydrogen bonding in the molecule as shown by NMR spectroscopy. In low temperature glasses, as already reported for many carbonyl compounds a solvent sensitive dual phosphorescence emission ($\lambda_{\max} \approx 430$ nm) is observed in addition to the 510-nm fluorescence. Surprisingly, no fluorescence emission could be detected in the short wavelength region at 77 K.

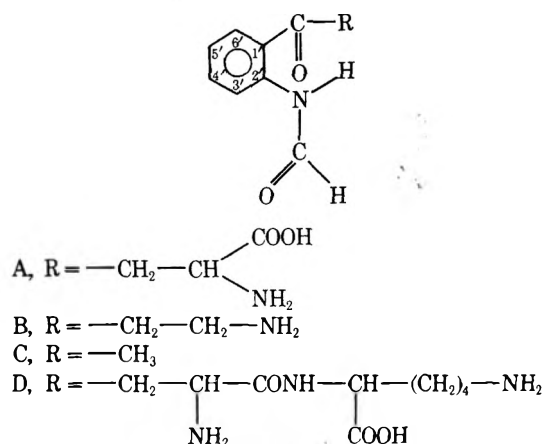
Introduction

N-Formylkynurenine (FK), a tryptophan photooxidation product, has been shown to be a remarkable photosensitizer with respect to amino acids, proteins, DNA constituents, or vitamins.¹⁻³ Its photosensitizing properties involve either a photodynamic action via the formation of singlet oxygen¹ or the substrate oxidation by reacting with the FK triplet state.³ The latter process leads to a semireduced oxidized substrate.³ As FK photosensitization can occur in proteins (the so-called "internal photodynamic effect"²) this internal photodynamic action may involve FK molecules in various environmental conditions when incorporated into the protein core. It is thus of primary importance to determine the FK electronic properties in various solvents such as nonpolar or polar solvents and/or hydrogen bonding solvents which may help to understand the FK photosensitizing behaviors in the various microenvironmental conditions actually found in biological macromolecules.

The purpose of this paper is to show that FK or FK derivatives display absorption spectra and quite unusual luminescence properties which strongly depend upon solvent polarity and hydrogen bonding ability at low or room temperature. As already reported for many other carbonyl compounds⁴⁻⁶ a solvent sensitive dual phosphorescence is observed which probably reflects FK molecules in various interactions with solvent molecules at low temperature. Intramolecular hydrogen bond formation is also shown to play an important role leading to a red-shifted fluorescence emission which may be ascribed to an excited state intramolecular proton transfer from the formamido to the *o*-carbonyl in the FK molecule.

Experimental Section

N-Formylkynurenine and derivatives (A-D) have been prepared by uv irradiation ($\lambda \geq 280$ nm) of the parent indole derivatives¹ (i.e., tryptophan for compound A, tryptamine for B, and skatole for C) in oxygen-saturated aqueous solutions at room temperature. Compound D has been prepared by proflavin-sensitized photooxidation of the TRP-Lys peptide.⁷ Purification was achieved by two or three successive chromatographies on Sephadex G 10 using water or a 5×10^{-3} M phosphate buffer (pH 7.5) as eluent. Polycrystalline sam-



ples were obtained by lyophilizing aqueous solutions of the FK derivatives. However such a procedure could not be used for the C derivative which sublimated under such conditions. Solid C samples were prepared by evaporating a hexane solution obtained by extracting C from water by hexane. Their purity was checked by gas chromatography. Repurified commercial FK supplied by Calbiochem was also used in some experiments. In the case of the anilide derivative (compound C) the structural formula was checked by NMR spectroscopy.

The solvents used for spectrophotometry or luminescence measurements (i.e., carbon tetrachloride, heptane, methanol, 2-propanol, and isopentane) were of the purest available grade (Merck spectroquality reagents). Ethylene glycol was a Fluka product and methylcyclohexane was rechromatographed on activated alumina. Absorption spectroscopy was performed using a Beckman DK-U spectrophotometer. Luminescence emissions have been recorded using a modified Aminco-Bowman spectrofluorophosphorimeter.⁸ Some fluorescence spectra have been recorded at room temperature using a Fica 55 spectrofluorimeter which makes it possible to obtain corrected spectra using Rhodamine B as a quantum counter. Fluorescence lifetimes have been measured using single photon counting equipment which has been described elsewhere⁹ while phosphorescence lifetimes have been obtained using a Tektronix 5103 N oscilloscope.

Results and Discussion

I. Room Temperature Results. A. Absorption Spectroscopy. FK derivative absorption spectra consist of three absorption bands whose maxima are located at about 320, 260, and 230 nm (see Table I and Figure 1). Solvent effects on the absorption spectrum can be conveniently studied using the acetophenone 2'-formylamino derivative which is soluble in polar or nonpolar solvents (compound C).

Decreasing the solvent polarity results in a red shift of the 320-nm band while the 260- and 230-nm bands undergo practically no shift by solvent changes. The effect of the solvent polarity has been considered by McRae,¹⁰ Mataga et al.,¹¹ and Ooshika.¹² These authors showed that spectral shifts could be theoretically predicted taking into account electrostatic interactions between solute and solvent molecules provided the transitions are accompanied by a change in dipole moment. Using McRae formulation¹⁰ we have

$$\Delta\bar{\nu}_{\text{abs}} = \text{dispersive term} + B \left[\frac{n^2 - 1}{2n^2 + 1} \right] + C \left[\frac{D - 1}{D + 2} - \frac{n^2 - 1}{n^2 + 2} \right] \quad (1)$$

where D is the static dielectric constant and n the solvent refractive index. B and C are constants related to the dipolar moment of the solute molecule in the excited and ground states.¹⁰ The second term on the right-hand side of eq 1 are practically constant for all solvents under study, and in Figure 2 are reported the variations of $\bar{\nu}_{\text{abs}}$ as a function of $\left\{ \left[\frac{D - 1}{D + 2} \right] - \left[\frac{n^2 - 1}{n^2 + 2} \right] \right\}$ for the anilide derivative. From this plot it may be deduced that a correlation does exist between $\bar{\nu}_{\text{abs}}$ and $f(D, n)$ which in the light of other studies¹³ suggests that the following.

(i) The 320-nm absorption probably has a strong $n\pi^*$ character. However the molar extinction coefficient, the oscillator strength, and transition moment calculated from the absorption spectrum are too high for a pure $n\pi^*$ character (see Table I).

(ii) The 260-nm absorption band is probably of $\pi\pi^*$ character since we obtain almost constant values for $\bar{\nu}_{\text{abs}}$ whatever the solvent.

(iii) As already noted for other carbonyl compounds¹⁴ eq 1 does not apply to water and dioxane. This is not surprising since dioxane should be practically considered as a polar solvent¹⁰ and water favors hydrogen bond formation. A rough estimate of the hydrogen bond energy for the anilide derivative in water can be obtained using the same considerations as those developed by Ito et al.¹⁵ who consider the hydrogen bond formation between benzophenone and ethanol. Then, according to these authors, the hydrogen bond energy for the anilide derivative can be calculated from the difference between the experimental and calculated $\bar{\nu}_{\text{abs}}$ (from eq 1). In the present case it is found to be 230 cm^{-1} ($0.65 \text{ kcal mol}^{-1}$). In aqueous solutions, FK derivatives are stable in the pH range 4–10.5 which precludes any experiments at low or high pH. No reversible absorption changes are detected indicating that in this pH range no acid–base equilibrium is involved.

B. Fluorescence Studies. The fluorescence spectrum of all FK derivatives in water is rather broad, pH independent, and shows a maximum at λ 430 nm (corrected or uncorrected spectrum). A shoulder is apparent at about 510 nm on a corrected spectrum obtained with the Fica fluorimeter (see Experimental Section and Figure 3). The large fluorescence Stokes' shift (8200 cm^{-1}) suggests a strong interaction between water and solute molecules in the first excited state.

TABLE I: Solvent Effect on the Characteristics of the First Absorption Band of Compounds C^a

Solvent	λ_{max} , nm	ϵ	f (oscillator strength)	M_D (transition moment)
W	315	3200	7.3×10^{-2}	2.2
EGW				
EtOH, MeOH	320	4000	8.3×10^{-2}	2.4
2-PrOH				
Hpt, CH	327	4100	8.5×10^{-2}	2.4
MCH	329	4800	9×10^{-2}	2.5

^a Solvents: water (W); ethanol (EtOH); methanol (MeOH); 2-propanol (2-PrOH); heptane (Hpt); cyclohexane (CH); methylcyclohexane (MCH); ethylene glycol–water (EGW).

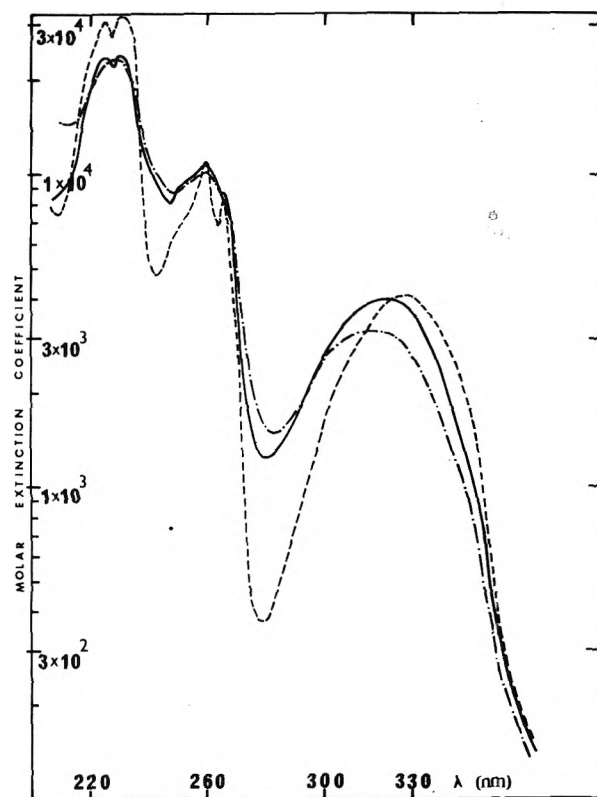


Figure 1. Absorption spectra of the FK derivative from skatole (compound C) in various solvents: (---) H₂O; (- · - ·) *n*-heptane; (—) ethanol, methanol, or 2-propanol.

Using quinine bisulfate as a standard, the fluorescence quantum yield ϕ_F is found to be $(1.0 \pm 0.1) \times 10^{-3}$. Such a low ϕ_F is consistent with the strong $n\pi^*$ character of the 320-nm absorption band and the short lifetime of the fluorescence emission: $(1.0 \pm 0.2) \text{ ns}$ at both 430 and 510 nm.

Decreasing the solvent polarity leads to an increase in the 510-nm fluorescence emission which parallels a fluorescence quenching at 430 nm (see Figure 3). In hexane, a nonpolar solvent, the 430-nm fluorescence band is almost totally quenched and the fluorescence emission maximum lies at 510 nm, $\phi_F = (1.0 \pm 0.1) \times 10^{-3}$. The presence of two distinct fluorescence emissions having the same excitation spectrum (i.e., the absorption spectrum) is further assessed by the temperature dependence of the fluorescence intensity. In a polar solvent such as ethanol the quenching of the 430- and 510-nm fluorescence as a function of temperature corresponds

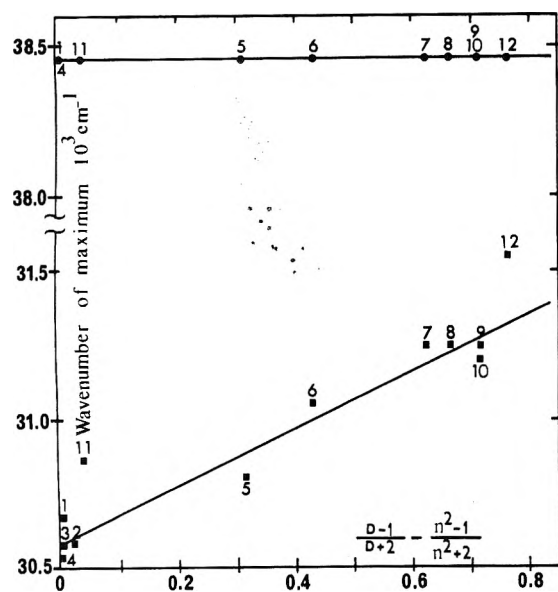


Figure 2. Solvent shifts of the 320-nm (■) and of the 260-nm (●) absorption bands of the FK derivative from skatole (compound C) for the solvents: (1) *n*-heptane; (2) benzene; (3) methylcyclohexane; (4) cyclohexane; (5) diethyl ether; (6) EPA; (7) 2-propanol; (8) ethanol; (9) methanol; (10) acetonitrile; (11) dioxane; (12) H₂O.

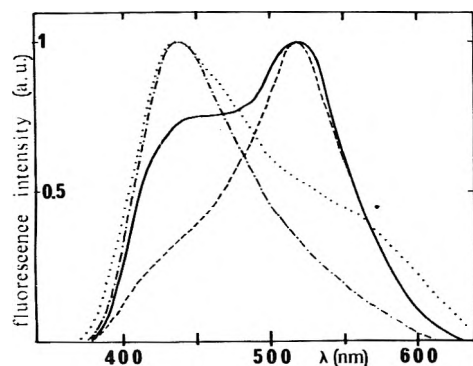


Figure 3. Uncorrected fluorescence emission spectra of the FK derivative from skatole (compound C) at 25 °C in various solvents under excitation at λ 320 or 260 nm: (---) H₂O; (—) ethanol, methanol, or 2-propanol; (- - -) *n*-heptane. (···) represents the corrected fluorescence emission obtained with the Fica 55 fluorimeter (see Experimental Section). All spectra have been normalized to unity at the maximum.

to Arrhenius activation energies of 1.8 and 4 kcal mol⁻¹, respectively. In hexane, this activation energy for the fluorescence quenching is 4 kcal mol⁻¹ at 510 nm as obtained from the Arrhenius plots reported in Figure 4.

The quenching of the 430-nm fluorescence emission in going from polar to nonpolar solvents is in keeping with the strong $n\pi^*$ character of the first absorption band, however, the presence of the 510-nm emission and its enhancement by nonpolar solvents has to be explained.

NMR spectroscopy performed on many anilide derivatives including compound C (see Experimental Section) shows the following:¹⁶

(i) Two different intramolecular hydrogen bondings rather insensitive to temperature effects occur in these molecules. There must be an equilibrium between three different species.

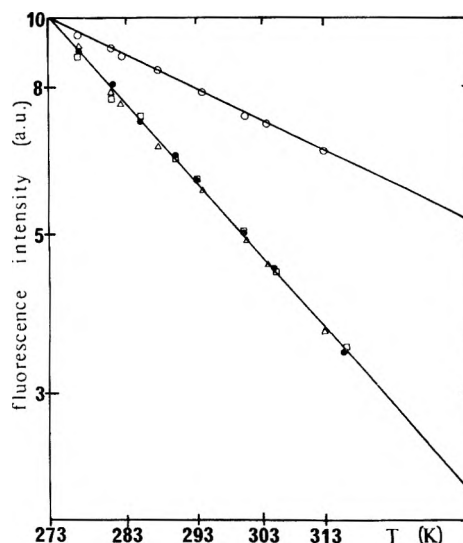
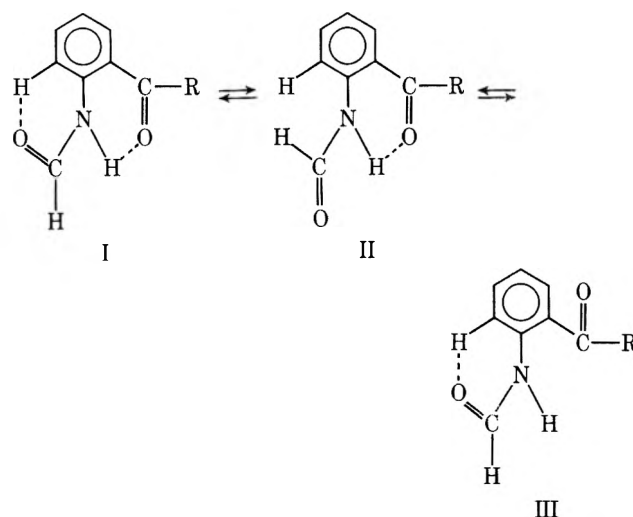


Figure 4. Arrhenius plots of compound C fluorescence intensity: (●), (□) in heptane ($\lambda_{\text{emission}}$ 430 or 510 nm); (○), (Δ) in ethanol ($\lambda_{\text{emission}}$ 430 and 510 nm, respectively).



where - - - represents intramolecular hydrogen bonding.

(ii) In compounds having very good hydrogen bond acceptors (i.e., a carbonyl group in our case) it seems likely that equilibrium II \rightleftharpoons III lies far in favor of the former.

(iii) The greater the hydrogen bonding ability of the solvent the less the deshielding effect for the 3' and the N-H protons.

From the above NMR results we may deduce that in nonpolar solvents intramolecular hydrogen bondings are greatly favored. In particular hydrogen bonding between the N-H and the carbonyl group of the side chain can occur. This intramolecular hydrogen bonding could favor for instance excited state proton transfer between these two groups situated ortho to one another, one of which becoming strongly acidic in the excited state and the other strongly basic as already reported by Weller¹⁷ for salicylic derivatives. Such a proton transfer leads to an abnormally large Stokes' shift.¹⁷ In our case we tentatively suggest the same origin of the 510-nm fluorescence. Addition of minute amounts of hydrogen bonding solvent (i.e., 2-propanol) to hexane weakens the intramolecular hydrogen bonding (as shown by the NMR results¹⁶) and leads to the appearance of the 430-nm fluorescence (see Figure 5). An isoemissive point is obtained at λ 465 nm suggesting that only

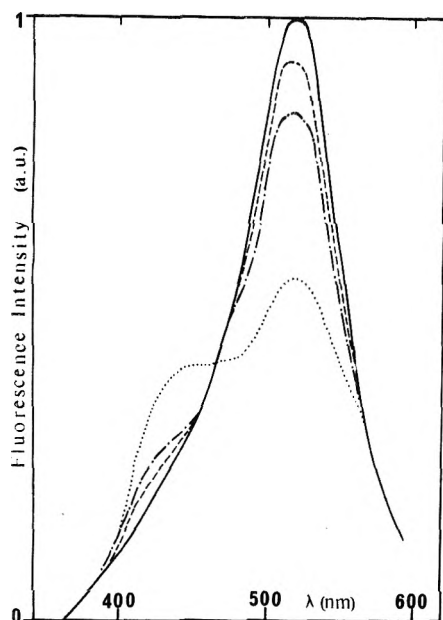


Figure 5. Uncorrected fluorescence emission spectra of the FK derivative from skatole (compound C) at 25 °C for the solvents: (—) *n*-heptane, (---) *n*-heptane-2-propanol 99:1 (v:v); (- · - ·) *n*-heptane-2-propanol 96:4 (v:v); (· · · ·) 2-propanol. Excitation wavelength 320 or 260 nm.

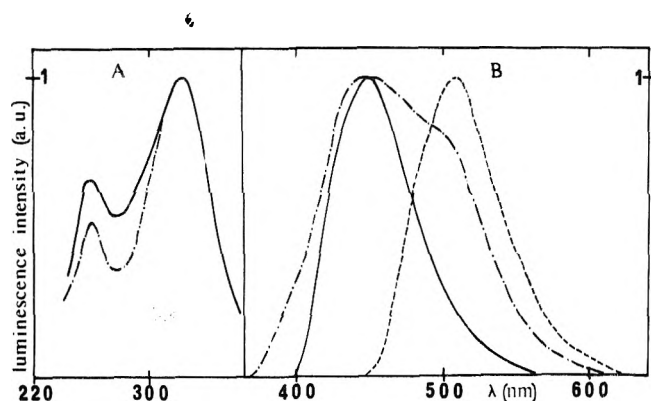


Figure 6 (A) Uncorrected phosphorescence excitation spectra of the FK derivative from skatole (compound C) in a water-ethylene glycol (1:1) (v:v) glass (—) or in a 2-propanol glass (---) at 77 K. The observation wavelength was 450 nm. The spectra have been normalized to unity at the maximum. (B) Uncorrected luminescence emission spectra of compound C in a water-ethylene glycol (1:1) (v:v) glass at 77 K under excitation at 320 nm: (---) total luminescence, (—) phosphorescence, (- · - ·) fluorescence, calculated by subtracting phosphorescence from total luminescence emission. All spectra have been normalized to unity at the maximum. The excitation wavelength was 320 or 260 nm. Most of the scattered excitation light has been suppressed by setting a cut-off filter (λ 380 nm) in front of the photomultiplier (the distortion of the luminescence spectrum at $\lambda \geq 410$ nm is due to remaining scattered light).

two emissive species are in equilibrium under these conditions. Conversely addition of various amounts of ethanol to a water solution of the C derivative leads to an increase of the 510-nm fluorescence intensity at the expense of the 430-nm emission.

It is worth noting that in the case of the indole ring, excited state deprotonation of the —NH group occurs at $\text{pH} \geq 11$ ¹⁸ indicating that, in some cases, the —NH group can be considered as acidic in the first excited singlet state.

Furthermore, it is well-known that carbonyl compounds undergo photochemical dissociation or reactions when they

TABLE II: Solvent Effects on the Phosphorescence λ_{max}

Solvent	EGW	EtOH, MeOH, 2-PrOH	MCH
λ , nm	440	450	470

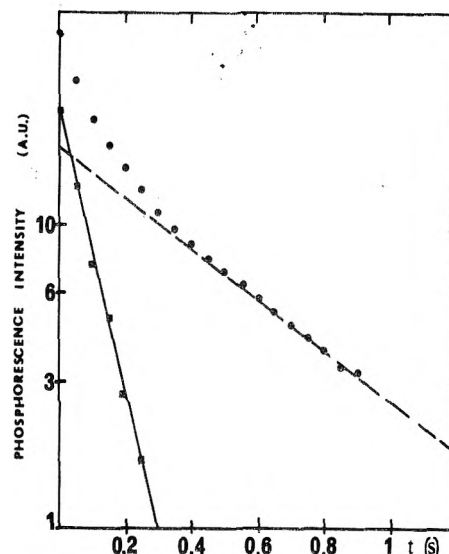


Figure 7. Phosphorescence decay of compound A in ethanol at 77 K plotted from CRO traces. The excitation wavelength was 320 nm. The emission wavelength was 450 nm. The full line corresponding to $\tau_1 = 0.1$ s is obtained from the experimental decay curve by subtracting the long-lived component intensity extrapolated back to the time origin.

are uv irradiated. However, in the present case, the relative intensities of the 430- and 510-nm fluorescences in a given solvent do not depend on the time of uv irradiation or the FK derivative concentration and/or the presence or the absence of oxygen. Thus the involvement of photoproducts or radicals in these two fluorescence emissions seems unlikely.

II. Low Temperature Results. Low temperature emission spectroscopy has been performed in various nonpolar or polar glasses: ethylene glycol-water mixture (1-1 in volume), ethanol, methanol, 2-propanol, methylcyclohexane, and 4 M CaCl_2 in water. The main results are as follows:

(i) No fluorescence emission can be detected in the short wavelength region (380-450 nm). However the 510-nm fluorescence ascribed to an intramolecular proton transfer can be recorded in the absence of a phosphoroscope (see Figure 6B) except in the 4 M CaCl_2 -water glass. It is very surprising that no fluorescence emission corresponding to the 430-nm room temperature fluorescence can be detected at low temperature and this seems to be a rather unique situation in the fluorescence of aromatic compounds. It might be argued that the 430-nm fluorescence emission cannot be detected because of the overlapping phosphorescence emission. However, at 77 K, the 430-nm intensity obtained in the presence of the phosphoroscope is about $\frac{1}{3}$ of the intensity recorded without the phosphoroscope. This undoubtedly corresponds to the reduction factor arising from the presence of the phosphoroscope acting as a neutral density filter on the emission and excitation beams.

Furthermore, the large Stokes' shift of the 430-nm room temperature fluorescence (with respect to the first absorption maximum) suggests, as noted above, a strong interaction between solvent and solute molecules in the first excited singlet state. One may expect a blue shift of the 430-nm fluorescence

TABLE III: Effect of Solvent and Side Chain on the I_2/I_1 and ϵ_2/ϵ_1 Ratios (See Text)^a

Compd	EGW		EtOH		MeOH		2-PrOH		CaCl ₂		MCH
	I_2/I_1	ϵ_2/ϵ_1	I_2/I_1	ϵ_2/ϵ_1	I_2/I_1	ϵ_2/ϵ_1	I_2/I_1	ϵ_2/ϵ_1	I_2/I_1	ϵ_2/ϵ_1	I_2/I_1
A	1.5	3.1	1.7	2.6	2	2.6	2.2	2.6	1.4	3.1	
B	1.5	3.1	1.5	2.6	1.5	2.6	1.6	2.6	1.3	3.1	
C	1.5	3.1	1.8	2.6	1.5	2.6	1.9	2.6	1.4	3.1	1
D	1.5	3.1	1.7	2.6	1.8	2.6	1.8	2.6			

^a I_2 and I_1 represent the phosphorescence intensities obtained under excitation at λ_2 and λ_1 , λ_2 and λ_1 being the two maximums of the phosphorescence excitation spectrum. Accordingly ϵ_2/ϵ_1 represents the ratio of the molar extinction coefficients at the maximum of the absorption bands (λ_2 260 nm, $\lambda_1 \approx 320$ nm). Note that I_2/I_1 refers to uncorrected phosphorescence excitation spectra and that ϵ_2/ϵ_1 cannot be determined in MCH because of the strong absorbance of MCH at 260 nm.

TABLE IV: Solvent Effect on the I_P/I_F Ratio (See Text) at 77 K ($\lambda_{\text{excitation}}$ 320 nm)

Compd	EGW	MeOH	EtOH	2-PrOH	CaCl ₂	MCH
A	1.9	1.08	2	7.5	7	
B	1.9	1.3	1.3	1.3	13	
C	1.9	0.7	0.4	0.66	10	1.2
D	1.9	3.9	3	3		

emission when varying the temperature from 25 °C downward. Such a temperature dependence of the fluorescence maximum in polar solvents has already been shown for indole derivatives in water-ethylene glycol mixtures¹⁹ and has been attributed to exciplex formation between solute and solvent molecules in fluid media. Thus, in the FK case, one might expect the 430-nm room temperature fluorescence to be shifted to shorter wavelengths at 77 K at least in polar glasses.

(ii) A rather intense phosphorescence emission is obtained whose λ_{max} depends upon the solvent (see Table II). In isopentane the phosphorescence λ_{max} is 490 nm. Addition of 3% 2-propanol (in volume), a good hydrogen bonding solvent, induces a blue shift in the phosphorescence spectrum (λ_{max} 465 nm). Further 2-propanol addition (up to 16%) shifted the phosphorescence λ_{max} to 450 nm. This is quite similar to the phosphorescence behavior of the Michler's ketone and has been explained by the hydrogen bonded species emission in hydrocarbon, Michler's ketone emission being a sensitive probe of the solute microenvironment.⁵

Another interesting feature of the FK phosphorescence emission is that a composite phosphorescence decay is always obtained which can be characterized by two distinct lifetimes $\tau_1 \approx 0.1$ s and $\tau_2 \approx 0.5$ s whatever the excitation wavelength (Figure 7). These rather long lifetimes indicate that emissive triplet states are $\pi\pi^*$ in nature despite a strong $n\pi^*$ character of the first singlet excited state. Under our experimental conditions and in view of the phosphorescence spectrum shape which shows no apparent structure, it is not possible to resolve the phosphorescence spectrum into two separate components corresponding to τ_1 and τ_2 lifetimes.

The phosphorescence excitation spectrum resembles the absorption spectrum and then possesses two distinct excitation maxima ($\lambda_{\text{max}} \approx 260$ and 320 nm) (Figure 6A). However there is a slight (although definite) effect of the solvent and/or the side chain on the phosphorescence excitation spectrum, which leads to some variations in the value of the I_2/I_1 ratio obtained from the phosphorescence excitation spectrum (see Table III). This means that the wavelength dependence of the phosphorescence quantum yield observed in most cases (see Table III) is greatly influenced by the solvent and/or the side chain. This is in contrast with the absorption spectrum which

is temperature independent and where the ratio ϵ_2/ϵ_1 does not depend upon the side chain.

It is also worth noting that the ratio I_P/I_F (I_F being the fluorescence intensity measured at 510 nm and I_P the phosphorescence intensity measured at λ_{max}) also depends upon the solvent or the side chain (see Table IV).

The low temperature results, i.e., the existence of the 510-nm fluorescence, the occurrence of a dual phosphorescence emission, and the solvent and side chain effects on the phosphorescence spectrum or the ratio I_P/I_F , can be understood using the NMR results which indicate that whatever the solvent, three isomeric forms of the FK derivatives are to be expected in solutions. If the 510-nm fluorescence emission probably involves forms I and II, the dual phosphorescence emission may imply that forms I, II, and III are present at low temperature. The lack of the "normal" 430-nm fluorescence at low temperature and the $\pi\pi^*$ character of the phosphorescence emissions suggest that a $n\pi^*$ triplet state is strongly coupled to a $\pi\pi^*$ triplet state which is the phosphorescent state. The solvent and the side chain effects on the low temperature luminescence and excitation spectra can be rationalized in light of the strong dependence of the intramolecular hydrogen bonding upon the hydrogen bonding ability of the solvent or the side chains. Electrostatic interactions between the side chain and the substituted benzene ring may also be taken into account. While the room temperature results deal with a weighted time average for the rapid exchange between the intramolecular hydrogen bond, the low temperature ones correspond to "frozen" equilibrium in which discrete changes in molecular structures can be detected by emission spectroscopy.

Conclusion

N-Formylkynurenine derivatives show quite unusual luminescence properties. An abnormally red-shifted fluorescence emission is recorded at both low and room temperature. This fluorescence seems to be due to an excited state proton transfer from the formamido group of the benzene ring to the *o*-carbonyl of the side chain. This proton transfer would be favored by intramolecular hydrogen bonding as evidenced by NMR spectroscopy. At low temperature, a solvent sensitive dual phosphorescence is observed whose quantum yield depends upon solvent polarity and/or the side chain. Excitation spectra indicate that FK is a sensitive probe of its own microenvironment as previously found for other carbonyl compounds. Surprisingly enough, no fluorescence emission corresponding to the phosphorescence emission is detected in the short wavelength region. However the present experiments do not make it possible to draw any definite conclusion regarding the mechanism of the fluorescence quenching at low

temperature. Synthesis of various substituted anilide derivatives are underway in order to help clarifying this unusual behavior.

The spectroscopic study of FK derivatives may be of the greatest importance for the understanding of the sensitizing potentialities of FK derivatives with respect to many biological substrates.

Acknowledgments. We wish to thank Professor J. P. Grivet of the Centre de Biophysique Moléculaire (Orléans) for NMR measurements and very helpful discussions and Professor G. Laustriat and collaborators (Université Louis Pasteur, Strasbourg) for fluorescence lifetime measurements.

References and Notes

- (1) P. Walrant and R. Santus, *Photochem. Photobiol.*, **19**, 101 (1974).
- (2) P. Walrant and R. Santus, *Photochem. Photobiol.*, **20**, 455 (1974).
- (3) P. Walrant, R. Santus, and L. I. Grossweiner, *Photochem. Photobiol.*, **22**, 63 (1975).
- (4) A. A. Lamola, *J. Chem. Phys.*, **47**, 4810 (1967).
- (5) P. R. Callis and R. W. Wilson, *Chem. Phys. Lett.*, **13**, 417 (1972).
- (6) R. D. Rauh and P. A. Leermakers, *J. Am. Chem. Soc.*, **90**, 2246 (1968).
- (7) P. Walrant, M. Charlier, and R. Santus, *Photochem. Photobiol.*, **24**, 13 (1976).
- (8) M. Aubailly, M. Bazin, and R. Santus, *Chem. Phys.*, **2**, 203 (1973).
- (9) C. Pfeffer, H. Lami, G. Laustriat, and A. Coche *C.R. Acad. Sci.*, **23**, 74 (1963).
- (10) E. G. McRae, *J. Phys. Chem.*, **61**, 562 (1957).
- (11) N. Mataga, Y. Kaitu, and M. Koizumi, *Bull. Chem. Soc. Jpn.*, **29**, 465 (1956).
- (12) W. Ooshika, *J. Phys. Soc. Jpn.*, **9**, 594 (1954).
- (13) M. B. Ledger and P. Suppan, *Spectrochim. Acta, Sect. A*, **23**, 641 (1967).
- (14) M. B. Ledger and G. Porter, *J. Chem. Soc., Faraday Trans. 1*, **68**, 539 (1972).
- (15) M. Ito, K. Inuzuka, and S. Imanishi, *J. Am. Chem. Soc.*, **82**, 1317 (1960).
- (16) G. W. Gribble and F. P. Bousquet, *Tetrahedron*, **27**, 3785 (1971).
- (17) A. Weller, *Z. Elektrochem.*, **60**, 1144 (1956).
- (18) E. vander Dohckt, *Prog. React. Kinet.*, **5**, 5 (1970).
- (19) J. Eisinger and G. Navon, *J. Chem. Phys.*, **50**, 2069 (1969).

Spectroscopic Studies of Charge-Transfer Complexes of Diazabenzenes with Iodine¹

P. A. Clark,* T. J. Lerner, S. Hayes, and S. G. Fischer

Department of Chemistry, Vassar College, Poughkeepsie, New York 12601 (Received September 26, 1975; Revised Manuscript Received April 22, 1976)

Publication costs assisted by Vassar College

We have used shifted-iodine bands (visible spectrum) to obtain equilibrium constants and heats of formation for charge-transfer complexes of iodine and pyridine, pyrimidine, and pyrazine. We find that oscillator strengths of the shifted iodine bands vary linearly with the heats of formation, as predicted by Mulliken, but find no linear relationship between charge-transfer energies (near ultraviolet spectrum) and ionization potentials, contrary to McConnell's prediction.

Introduction

The formation of charge-transfer (CT) complexes of nitrogen heterocycles with iodine is known to involve the non-bonding electrons on the nitrogen atoms.²⁻¹³ It has been established that the shift in the iodine band in the visible region of the spectrum toward higher energy, which occurs upon complexation, parallels the equilibrium constant for the formation of the complex⁵⁻⁸ and the pK_a of the donor.⁵⁻⁹ Some studies have been made to investigate Mulliken's proposal¹⁴ of a linear relationship between the heats of formation of complexes and the intensities of the absorption bands, notably by Krishna and Bhowmik,¹¹ who found the relationship to hold reasonably well for complexes with nitrogen heterocycles as donors. Other studies have been made to investigate the relationship proposed by McConnell et al.¹⁵ between the CT energies and the ionization potentials of the donors.^{5,8}

In the present work we report results of investigations of the spectroscopic and thermodynamic properties of complexes of pyrimidine and pyrazine with iodine. Previous studies of these complexes have been limited to the determination of the formation constants at a single temperature.⁵ In order to test Mulliken's relationship and to provide additional data for the

theoretical interpretation of the electronic structure of these complexes, we have measured the temperature dependence of the equilibrium constants and have evaluated the heats of formation and the oscillator strengths. Our results for the much-studied pyridine-iodine complex have been included for comparison with published values as a criterion for the reliability of our data. The diazabenzene donors studied here are of interest because of the effects of interaction between the two nitrogen atoms in the ring and because each is the first member of a series of substituted donors in which the effects of geometrical isomerism may be studied.

Experimental Section

Donor compounds were purchased from Aldrich Chemical Co. Pyrimidine was used without further purification. Pyridine, dried over NaOH, and pyrazine were distilled over CaH₂ in a nitrogen atmosphere. The compounds were checked for purity by comparing infrared spectra with the Stadler spectra series, where possible; compounds were stored in glass-stoppered flasks in desiccators. Iodine obtained from Baker Chemical Co., USP grade, was sublimed before use and stored in a desiccator. As reported by other workers,⁵ pyridazine has

TABLE I: Spectroscopic and Thermodynamic Results from Analysis of the Shifted Iodine Band

Donor	K_c , M ⁻¹ (298 K)		λ_{\max} , nm	ϵ_{\max}	$-\Delta H$, kcal/mol		
	This work	Others ^a			This work	Others ^a	f
Pyridine	175 ± 28	185 (2) 160 (11) 137 (10) 96 (5)	420.0	1380 ± 50	7.69 ± 0.15	7.8 (2) 7.47 (11) 7.8 (21)	0.024 ± 0.001
Pyrimidine	19.3 ± 2.4	17 (5)	432.5	1180 ± 100	6.45 ± 0.30		0.019 ± 0.002
Pyrazine	15.7 ± 0.2	12 (5)	435.0	1300 ± 16	5.53 ± 0.29		0.015 ± 0.001

^a Numbers in parentheses indicate references.

only limited solubility in a nonpolar solvent and could not be included in the present study. Spectrochemical grade *n*-heptane from Fisher Scientific was used in all work.

Stock solutions of the donors and of iodine were prepared fresh each day by weighing the solute and diluting to volume in standard volumetric glassware at the desired constant temperature. In preparing the donor solutions, the heterocyclic compound was transferred to a volumetric flask almost filled with solvent in order to prevent contamination by oxygen or water vapor. Mixed donor-acceptor solutions were prepared immediately before measuring the spectra, allowing sufficient time for thermal equilibration. Measurements were made on a series of solutions in which the concentrations of donor and acceptor were varied by combining different pipetted volumes of the stock solutions. For example, for the pyridine-iodine complex at 25 °C, the concentration ranges were 0.1–0.7 M donor, 2.5–7.0 × 10⁻⁴ M acceptor.

Spectra were run on a Cary 14 spectrophotometer using 0.500- and 1.000-cm cells obtained from Varian Inc. Temperature control was achieved using a Haake Model FS2 circulating water bath with a temperature constancy of ±0.01 °C, and a thermostated cell jacket from Varian.

Results and Discussion

Spectroscopic and thermodynamic results obtained from analysis of the shifted iodine band in the visible region are summarized in Table I, with some previously reported values included for comparison. In the present work, equilibrium constants and molar absorptivities have been calculated by means of the Liptay method.¹⁶ This includes a weighted least-squares solution of the Scott equation,^{17,18} with modifications similar to those used by Julien et al.¹⁹ to correct for absorption due to uncomplexed iodine. The standard deviations in the slope and intercept give the errors in K_c and ϵ listed in Table I. Heats of formation, ΔH , are obtained from the slopes of the van't Hoff plots shown in Figure 1; oscillator strengths, f , are evaluated in the manner of Krishna and Bhowmik.¹¹ The linear relationship between ΔH and f , predicted by Mulliken,¹⁴ is illustrated in Figure 2. We have observed a slight temperature dependence of the oscillator strengths, with f decreasing as temperature increases, but the variations are within experimental error and thus may have no significance.

The linear relationship proposed by McConnell et al.¹⁵ between the observed CT energies and the ionization potentials (IP) of the donors is not observed for these complexes, as shown by the data in Table II. In fact, the CT energy decreases as both the n and the π ionization potentials increase. However, the range of energies represented by these data is very small and cannot provide any conclusive evidence for or against the proposed relationship. Krishna and Chowdhury⁵

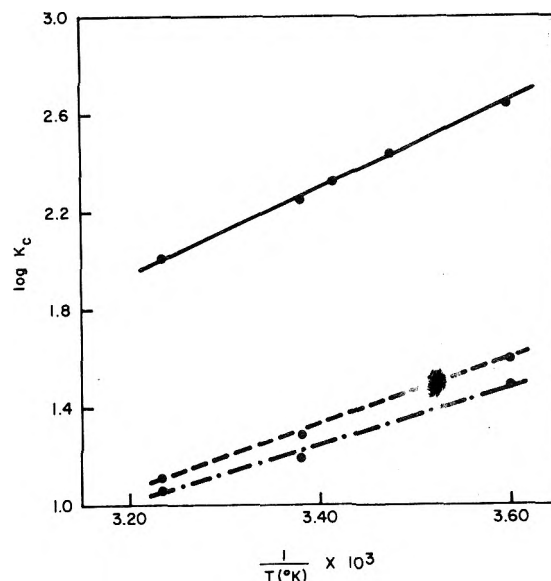


Figure 1. Temperature dependence of the equilibrium constants for the formation of complexes between pyridine (—), pyrimidine (---), and pyrazine (- · -) with iodine, using the van't Hoff equation.

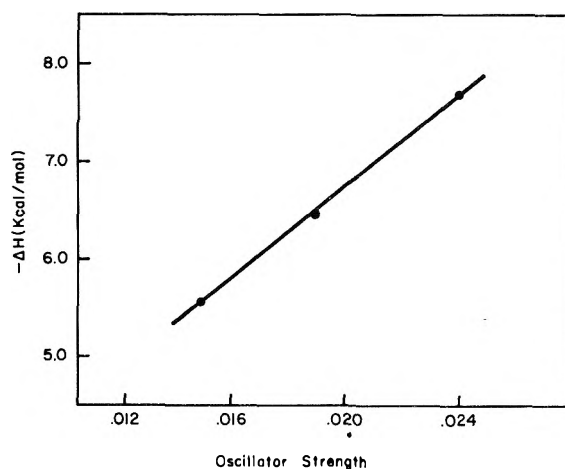


Figure 2. Correlation between heats of formation of complexes of pyridine, pyrimidine, and pyrazine with iodine and the intensity of the shifted iodine absorption band.

attempted to distinguish between the n - and π -electron IP's in the diazabenzenes on the basis of the observed CT energies; more recent results²⁰ from photoelectron spectroscopy give more reliable assignments of the observed IP's. While the ionization spectrum shows the two n orbital energy levels to be split by about the same amount (ca. 1.5 eV) in the two

TABLE II: Energies of Charge-Transfer Bands in the Ultraviolet and Donor Ionization Potentials

Donor	λ_{\max} , nm	$h\nu_{CT}$, eV	IP, eV ^a	
Pyridine	235	5.27	9.60 n	
			9.73 π	
Pyrazine	240	5.16	9.63 n	
			10.18 π	
Pyrimidine	244	5.08	11.35 n	
			239	9.73 n
				10.41 π
			11.23 n	

^a See ref 20.

diazabenzene as a result of lone pair interactions, only pyrimidine has a splitting in the CT spectrum.

Equilibrium constants for the diazabenzene-iodine complexes could not be evaluated from the CT absorption band because of overlapping donor absorption; Krishna and Chowdhury reported similar difficulties.⁵ This is a problem frequently encountered, although often one can compensate for donor absorption, as in the case of the pyridine-iodine complex.^{2,7} In the present studies on much weaker complexes, attempts to use similar techniques were not successful.

In summary, earlier work¹¹ and the results presented here demonstrate that complexes of nitrogen heterocycles with iodine have heat of formation and absorption intensities that

follow Mulliken's linear relationship reasonably well. On the other hand, available data on charge transfer energies and ionization potentials do not as clearly support McConnell's relationship. Further studies on substituted azabenzene and azanaphthalenes will provide a better basis for evaluation.

References and Notes

- (1) (a) Based in part on a thesis submitted by T. J. Lerner in partial fulfillment of the requirements for the degree of Master of Arts in Chemistry, Vassar College, 1974. (b) Supported by a Dreyfus Foundation Teacher-Scholar Grant to P. A. Clark.
- (2) C. Reid and R. S. Mulliken, *J. Am. Chem. Soc.*, **76**, 3869 (1954).
- (3) A. I. Popov and R. H. Rygg, *J. Am. Chem. Soc.*, **79**, 4622 (1957).
- (4) J. N. Chaudhuri and S. Basu, *Trans. Faraday Soc.*, **55**, 898 (1959).
- (5) V. G. Krishna and M. Chowdhury, *J. Phys. Chem.*, **67**, 1067 (1963).
- (6) I. Ilmet and M. Krasij, *J. Phys. Chem.*, **70**, 3755 (1966).
- (7) G. Aloisi, G. Cauzzo, and U. Mazzucato, *Trans. Faraday Soc.*, **63**, 1858 (1967).
- (8) K. R. Bhaskar and S. Singh, *Spectrochim. Acta, Part A*, **23**, 1155 (1967).
- (9) W. J. McKinney, M. K. Wong, and A. I. Popov, *Inorg. Chem.*, **7**, 1001 (1968).
- (10) H. D. Bist and W. B. Person, *J. Phys. Chem.*, **71**, 2750 (1967).
- (11) V. G. Krishna and B. B. Bhowmik, *J. Am. Chem. Soc.*, **90**, 1700 (1968).
- (12) W. J. McKinney and A. I. Popov, *J. Am. Chem. Soc.*, **91**, 5215 (1969).
- (13) R. S. Mulliken and W. B. Person, "Molecular Complexes", Interscience, New York, N.Y., 1969.
- (14) R. S. Mulliken, *J. Am. Chem. Soc.*, **74**, 811 (1952).
- (15) H. M. McConnell, J. S. Ham, and J. R. Platt, *J. Chem. Phys.*, **21**, 66 (1953).
- (16) W. Liptay, *Z. Elektrochem.*, **65**, 375 (1961).
- (17) R. L. Scott, *Recl. Trav. Chim. Pays-Bas*, **75**, 787 (1956).
- (18) S. D. Christian, E. H. Lane, and F. Garland, *J. Phys. Chem.*, **78**, 557 (1974).
- (19) L. M. Julien, W. E. Bennett, and W. B. Person, *J. Am. Chem. Soc.*, **91**, 6915 (1969).
- (20) R. Gleiter, E. Heilbronner, and V. Hornung, *Helv. Chim. Acta*, **55**, 255 (1972).
- (21) C. D. Schmulbach and D. M. Hart, *Helv. Chim. Acta*, **86**, 2347 (1964).

Raman Spectra of Cystine-Related Disulfides. Effect of Rotational Isomerism about Carbon-Sulfur Bonds on Sulfur-Sulfur Stretching Frequencies¹

H. E. Van Wart² and H. A. Scheraga*

Department of Chemistry, Cornell University, Ithaca, New York 14853 (Received December 1, 1975)

The Raman spectra of a series of disulfides structurally related to cystine have been studied in the 250–650-cm⁻¹ region. These compounds all contain the unstrained CCSSCC structural unit and have very similar conformations about their S–S bonds (i.e., CS–SC dihedral angles near ±90°), but a wide variety of conformations about their C–S bonds. The effects of varying conformation about their C–S bonds on their S–S stretching frequencies, $\nu(\text{S–S})$, have been examined. From the spectra of those crystalline disulfides whose structures are known from x-ray studies, it has been found that *primary* disulfides with *trans* and either of two nonequivalent *gauche* conformations about their C–S bonds (SS–CC dihedral angles of roughly 180 and ±60°, respectively) all have values of $\nu(\text{S–S})$ of about 510 cm⁻¹. This is in disagreement with the frequency-conformation correlation proposed previously by other workers, whereby it was thought that CCSSCC moieties with *trans* conformations about their C–S bonds have values of $\nu(\text{S–S})$ of about 540 cm⁻¹. Instead, it is suggested that a value of $\nu(\text{S–S})$ of 540 cm⁻¹ in primary disulfides arises from the presence of conformations (referred to as A conformations) with small (~30°) SS–CC dihedral angles. The existence of these A conformations has been suggested by recent CNDO/2 calculations carried out on several alkyl disulfides. These A conformations are shown to comprise ~20% of all occurrences of the values of $\chi(\text{SS–CC})$ found for cystine residues in eight proteins, as determined by x-ray crystallography. The use of the values of $\nu(\text{S–S})$ for the determination of conformation about the C–S bonds of cystine residues in proteins is discussed.

I. Introduction

The results of several recent investigations^{3–9} on model organic disulfides have shown that Raman spectroscopy is a useful tool for the study of disulfide stretching vibrations. These investigations have been concerned with the correlation of S–S stretching frequencies, $\nu(\text{S–S})$, with the conformational properties of the CCSSCC fragment. Such correlations could be used to determine the conformations of the side chains of cystine residues in proteins from their Raman spectra. However, the correlations that have been proposed are not mutually consistent, and a unified interpretation of all of the available vibrational data does not yet exist.

On the basis of the Raman spectra of a series of alkyl disulfides [all with CS–SC dihedral angles, $\chi(\text{CS–SC})$, near ±90°], Sugeta et al.^{4,5} have proposed a correlation between $\nu(\text{S–S})$ and the conformation about the C–S bonds of the CCSSCC moiety. These authors *assumed* that internal rotation about the C–S bonds of primary¹⁰ alkyl disulfides resulted in significant amounts of only two rotamers—a *trans* and one of two possible *gauche* conformations¹¹ [with SS–CC dihedral angles, $\chi(\text{SS–CC})$, of 180 and +60°, respectively, for $\chi(\text{CS–SC}) = +90^\circ$]. Recently we reexamined⁹ the temperature dependence of the low-frequency Raman spectrum of methyl ethyl disulfide in conjunction with an electron diffraction study¹² of this compound. The Raman data indicated the existence of significant amounts of at least *three* rotamers at room temperature. Furthermore, two of these rotamers were thought to have the same value of $\nu(\text{S–S})$. In light of these results, we have reexamined here the Raman spectra of other alkyl disulfides, since a reinterpretation of their Raman spectra in terms of conformation may be required.

In a previous study⁷ of cyclic disulfides with *strained* S–S bonds [disulfides with values of $\chi(\text{CS–SC})$ in the range of 0 to about ±65°], we reported a correlation between the values of $\nu(\text{S–S})$ and $\nu(\text{CS–SC})$. These results are not in agreement with those of another group,^{6,8} who found no correlation be-

tween these quantities. To resolve these conflicting reports concerning the dependence of $\nu(\text{S–S})$ on the conformation about the C–S^{4,5,9} and S–S bonds^{6–8} [i.e., on the values of $\chi(\text{SS–CC})$ and $\chi(\text{CS–SC})$, respectively], we have reinvestigated this problem using both theoretical^{13–15} and experimental¹⁶ techniques. In this paper, we report the Raman spectra of aliphatic disulfides that are structurally related to cystine, with values of $\chi(\text{CS–SC})$ of about ±90°, but with a wide variation in the values of $\chi(\text{SS–CC})$. These additional experimental data provide a better understanding of how differences in conformation about C–S bonds affect the values of $\nu(\text{S–S})$ of the CCSSCC unit. In the accompanying paper,¹⁶ we report the Raman spectra of a series of disulfides with widely different values of $\chi(\text{CS–SC})$, and consider there the effects of varying conformation about the S–S bond on $\nu(\text{S–S})$. These studies enable us to formulate a unified interpretation for the conformational dependence of $\nu(\text{S–S})$ that is consistent with all of the available theoretical and experimental evidence.

II. Experimental Section

A. Materials. Of the compounds listed in Tables I–III, 20, 25, 27, 29–30, and 32–34 were provided by Dr. A. Fredga, 14 and 31 by Dr. R. Parthasarathy, 23 by Dr. K. Seff, 18 by Dr. V. duVigneaud, 16 by Dr. B. Kamber, and 19 by Dr. L. Field. These were all obtained pure and used as received. All of the other compounds studied were obtained from commercial sources. The alkyl disulfides listed in Table I were distilled under vacuum until there was no change in their Raman spectra. The solids were recrystallized at least once by standard procedures.

B. Raman Measurements. The system used to collect the Raman data has been described previously.⁹ All measurements were made with an instrumental resolution of 2 cm⁻¹. Whenever possible, Raman spectra of the solids shown in Tables II and III were also obtained in solution. In all cases,

TABLE I: Raman Spectra of Neat Liquid Alkyl Disulfides between 250 and 650 cm^{-1}

Compd	$\Delta\nu$, cm^{-1}	Intensity ^b	Compd	$\Delta\nu$, cm^{-1}	Intensity ^b
(1) 2-Hydroxyethyl disulfide ^a	283	m	(6) Diisopentyl disulfide	308	s
	327	m		386	m
	400	ms		419	s
	463	m		450	w
	~494	sh		~493	sh
	510	vs		511	vs
	~523	sh		524	s
	640	s		~535	sh
	663	ms		637	s
	268	w		655	m
	(2) Di- <i>n</i> -propyl disulfide	284		w	(7) Diisopropyl disulfide
323		w	302	m	
346		w	329	m	
379		ms	354	m	
412		w	413	sh	
435		w	417	m	
510		vs	464	w	
524		s	511	w	
~533		sh	527	s	
582		vw	543	s	
~610		sh	595	s	
(3) Di- <i>n</i> -butyl disulfide	630	s	(8) Di- <i>sec</i> -butyl disulfide	625	vs
	655	ms		256	m
	274	w		286	w
	305	w		309	m
	326	w		335	m
	351	s		355	sh
	404	w		379	s
	436	m		424	m
	469	m		460	m
	478	m		475	w
	510	vs		~504	sh
524	s	~509	sh		
~533	sh	526	vs		
634	s	543	s		
659	s	587	s		
(4) Diisobutyl disulfide	243	w	(9) Di- <i>tert</i> -butyl disulfide	618	vs
	273	w		634	s
	343	m		650	s
	377	vw		257	m
	401	m		291	w
	429	ms		303	w
	485	w		322	w
	~498	sh		363	m
	512	vs		398	w
	525	s		411	m
	~530	sh		507	w
(5) Di- <i>n</i> -pentyl disulfide	665	w	(10) Di- <i>tert</i> -pentyl disulfide	540	s
	306	s		569	vs
	345	m		283	w, bd
	368	w		313	w
	399	m		337	w
	453	w		373	m
	489	w		399	w
	510	vs		422	w
	525	s		438	w
	~538	sh		480	w
	634	s		541	s
659	m	560	vs		
			616	s	

^a The spectrum of compound 1 is included in this table with the other liquids, even though it is not an alkyl disulfide.

^b The letters in this column have the following meanings; s, strong; m, medium; w, weak; v, very; sh, shoulder, and bd, broad.

water was the solvent of first choice. Compounds that were not water soluble were dissolved in either methanol, tetrahydrofuran, benzene, dimethylformamide, or dimethyl sulfide. Many of these solvents have Raman bands of their own in the 250–650- cm^{-1} region. However, the $\nu(\text{S-S})$ region, from 450 to 550 cm^{-1} , is free from Raman bands in all of these solvents.

III. Results

A. *Raman Spectra.* The bands observed in the Raman spectra of a series of neat liquid alkyl disulfides between 250 and 650 cm^{-1} are listed in Table I. Portions of the spectra of some of the compounds listed in this table have been reported previously;^{4,5} we list several new bands in these previously

TABLE II: Solid and Solution-Phase Raman Spectra of Primary Disulfides^a Related to Cystine between 250 and 650 cm⁻¹

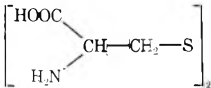
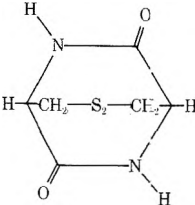
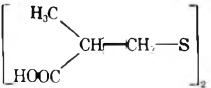
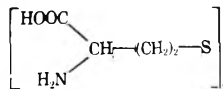
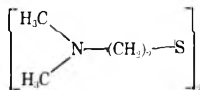
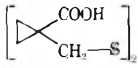
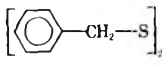
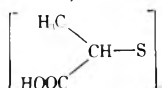
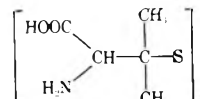
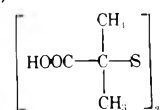
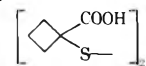
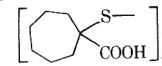
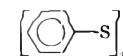
Compound	Solid ^b		Solution		Solvent ^d	
	$\Delta\nu$, cm ⁻¹	Intensity ^c	$\Delta\nu$, cm ⁻¹	Intensity ^c		
(11) L-Cystine (hexagonal)	269	w	507	s	1 N HCl and dilute NaOH (same spectra in both solvents)	
	317	m	~525	sh		
	327	sh				
	377	vw				
	387	w				
	450	m				
	458	sh				
	499	vs				
	542	m				
	(12) L-Cystine·2HCl	247	s	Same as 11		
		256	sh			
		303	m			
		352	m			
	368	m				
	479	s				
	509	sh				
	519	s				
	587	m				
(13) L-Cystine·2HBr ^e	466	m	Same as 11			
	499	w				
	519	m				
	589	w				
	663	s				
(14) L-Cystine·2HBr·2H ₂ O	263	w	Same as 11			
	294	w				
	305	w				
	338	w				
	394	w				
	413	vw				
	502	s				
	518	w				
	535	w				
(15) <i>meso</i> -Cystine	451	w	Same as 11			
	478	m				
	507	s				
	551	w				
	591	w				
(16) <i>cyclo</i> -L-Cystine	251	s	431	w	Dimethyl sulfoxide	
	295	s	454	w		
	336	s	507	s		
	437	w	~513	sh		
	448	m				
	505	s				
	516	m				
	(17) <i>N,N'</i> -Diglycyl-L-cystine	513	m	509	w	1 N HCl
(18) Mixed disulfide of cysteine and β -mercaptopropionic acid cys-SCH ₂ CH ₂ COOH	301	m	507	s		
	334	s	~522	sh		
	363	m				
	446	sh				
	464	s				
	477	sh				
	529	s				
	536	sh				
	563	w				
(19) Mixed disulfide of cysteine and β -mercaptoethylamine cys-SCH ₂ CH ₂ NH ₂	397	w				
	452	w				
	500	s				
	543	w				
(20) β -Dithiodiisotutyric acid	258	w	503	s	Dimethyl sulfoxide	
	266	w	~520	sh		
	278	w				
	289	w				
	391	m				
	396	sh				
	497	s				
	514	w				

TABLE II (Continued)

Compound	Solid ^b		Solution		Solvent ^d
	$\Delta\nu$, cm ⁻¹	Intensity ^c	$\Delta\nu$, cm ⁻¹	Intensity ^c	
(21) L-Homocystine 	527	w			
	549	w			
	601	w			
	270	m	509	s	1 N HCl
	357	w	~520	sh	
	408	m			
	466	w			
	509	s			
	542	m			
(22) Cystamine·2HCl [H ₂ N(CH ₂) ₂ S] ₂ ·HCl	248	m	398	w	1 N HCl
	294	w	509	s	
	331	w	~525	sh	
	400	m			
	471	w			
	510	s			
(23) Bis[2-(N,N'-dimethylamino)-ethyl] disulfide 	271	w	320	m	1 N HCl
	318	m	405	m	
	327	m	445	m	
	403	w	469	m	
	416	w	506	s	
	450	m	~528	sh	
	466	w			
	503	vs			
	532	m			
(24) Dithioglycolic acid (HOOCCH ₂ S) ₂	270	m	270	m	1 N HCl
	293	w	429	m, bd	
	419	w	506	s	
	431	w	~517	sh	
	481	w	542	w	
	508	vs	576	m	
	549	w			
	569	w			
	581	m			
(25) β-Dithiodipropionic acid [HOOC(CH ₂) ₂ S] ₂	296	m	468	m	Dimethyl sulfoxide
	305	sh	507	s	
	343	m	~518	sh	
	500	s	586	w	
	532	m			
	560	m			
(26) 3-Carboxypropyl disulfide [HOOC(CH ₂) ₃ S] ₂	300	m	508	s	1 N NaOH and methanol (same spectra in both solvents)
	317	w	~524	sh	
	334	w			
	449	w			
	459	w			
	469	w			
	~500	sh			
	509	s			
	578	w			
(27) Dicyclopropyl methyl disulfide-1,1'-dicarboxylic acid 	290	m	501	s	Dimethylformamide
	314	w	572	m	
	339	w			
	349	m			
	372	s			
	401	m			
	488	w			
	518	vs			
	533	m			
	573	w			
(28) Dibenzyl disulfide 	595	w			
	289	w	403	w	Benzene
	307	m	468	m	
	340	w	490	w	
	407	w	512	m	
	469	s	563	w	
	505	vs			
	569	w			

^a Primary disulfides are ones in which the carbons adjacent to the disulfide bond are primary carbon atoms. ^b Finely divided crystals. ^c The letters in this column have the same meanings as in Table I. ^d In some solutions there are strong Raman bands between 250 and 750 cm⁻¹ due to the solvent which obscure the solute scattering. ^e The 250–400-cm⁻¹ region of the spectrum of this compound was not recorded.

TABLE III: Solid and Solution-Phase Raman Spectra of Secondary and Tertiary Disulfides^a Related to Cystine between 450 and 650 cm⁻¹

Compound	Solid ^b		Solution		Solvent ^d	
	$\Delta\nu$, cm ⁻¹	Intensity ^c	$\Delta\nu$, cm ⁻¹	Intensity ^c		
(29) α -Dithiodipropionic acid (racemic) 	457	s	480	m	Methanol	
	480	m	507	m		
	535	s	526	m	Dimethylformamide	
	632	m	543	sh		
			577	m		
			503	m		
			526	m		
			536	sh		
	(30) same as 29, but meso	450	s	~502	m, bd	Dimethyl sulfoxide
		480	m	522	sh	
507		vs	535	sh		
522		vs				
576		s				
636		w				
(31) D-Penicillamine disulfide 	472	w	534	m	1 N HCl	
	532	m	546	m		
	543	m	~570	sh		
	572	m				
	580	m				
	629	m				
(32) α -Dithiodiisobutyric acid 	510	s	482	m	Methanol	
	525	s	540	m		
	549	m	649	m		
					Dimethylformamide	
			487	s		
			539	s		
			481	m		
			535	m	Dimethyl sulfoxide	
			585	m		
	(33) Dicyclobutyl disulfide 1,1'-dicarboxylic acid 	436	s	422	s	Methanol
509		m	513	m		
529		m	538	m		
628		m	622	ms		
640		sh				
(34) Dicycloheptyl disulfide 1,1'-dicarboxylic acid 	270	w	518	w	Dimethylformamide	
	313	w	539	m		
	356	w	581	m		
	392	m				
	441	sh				
	457	m				
	527	s				
	558	m				
	585	m				
	642	s				
(35) Diphenyl disulfide 	462	w	471	s	Benzene	
	471	m	512	vs		
	496	w	525	vs		
	542	vs	~537	sh		
	554	w	614	s		
	613	s				

^a Secondary and tertiary disulfides are ones in which the carbons adjacent to the disulfide bond are secondary and tertiary carbon atoms, respectively. ^b Finely divided crystals. ^c The letters in this column have the same meanings as in Table I. ^d In some solutions, there are strong Raman bands between 250 and 650 cm⁻¹ due to the solvent which obscure the solute scattering.

reported regions, and report for the first time data for the 250–450-cm⁻¹ region. Included in the 250–650-cm⁻¹ region are bands due to the S–S stretching motion, ν (S–S), and the CCS and CCC skeletal deformations, γ (CCS) and γ (CCC), respectively. This region has been studied because it has been proposed^{4,5} that trans and gauche rotamers about the C–S bonds in these molecules have different values of ν (S–S) because of different degrees of vibrational coupling between their ν (S–S) and γ (CCS) modes; the variations in the frequencies of these modes from compound to compound may help decide if this hypothesis is valid. Compounds 1–6 are primary, 7 and 8 secondary, and 9 and 10 tertiary disulfides.¹⁰

The bands in the solid and solution-phase Raman spectra of a series of primary disulfides related to cystine are listed in Table II, and those of secondary and tertiary disulfides in Table III. These compounds differ structurally from cystine in that various additions, deletions, and substitutions of groups have been made around the central CSSC nucleus. These compounds can be considered to be “intermediate” in structure between cystine and the alkyl disulfides of Table I because they contain charged and polar groups. Since it has been suggested^{4,5} that variations in ν (S–S) can reflect conformational changes about the C–S bonds in such noncyclic disulfides, the observed variations in ν (S–S) between the

TABLE IV: Structural Parameters of the CCSSCC Fragment of Some Disulfides Obtained from X-Ray Data^a

Compound ^b	$R(S-S)$, Å	$R(S-C)$, Å	$\tau(SSC)$, deg	$\tau(SCC)$, deg	$\chi(SS-CC)$, deg	$\chi(CS-SC)$, deg	Ref
(11) L-Cystine (hexagonal)	2.032	1.820	104.5	116.2	82	74	17
(12) L-Cystine·2HCl	2.041	1.810	104.0	114.7	-89	-82	18
(13) L-Cystine·2HBr	2.024	1.862	103.9	111.9	-89	-81	19
(14) L-Cystine·2HBr·2H ₂ O	2.044	1.80	102.3	114.6	-82	-80	20
(16) <i>cyclo</i> -L-Cystineacetic acid	2.00	1.83	105	116	63	-91	21
			1.79	105	115	67	
			1.87	103	105	97	
(17) <i>N,N'</i> -Diglycyl-L-cystine·2H ₂ O	2.04	1.87	103	105	97	79	22
(23) Bis[2-(<i>N,N'</i> -dimethylamino)ethyl] disulfide	2.037	1.807	103.6	115.4	55	82	23
			1.814	102.8	111.4	67	
(24) Dithioglycolic acid	2.025	1.806	102.0	110.5	-167	-86	24
(28) Dibenzyl disulfide	2.02	1.84	103.3	114.3	73	92	25
			1.85	102.9	112.3	72	
(31) D-Penicillamine disulfide	2.049	1.866	105.5	106.8	70	115	26
			103.3	-173			
			113.8	-53			
			109.9	67			
			103.1	-175			
(35) Diphenyl disulfide	2.03	1.81	105.8	123.7	18	84	27
			1.79	106.5	124.3	0	
L-Cystine diamide·2HCl ^c	2.05	1.76	104.5	116.2	82	74	28
L-Cystine dimethyl ester·2HCl·H ₂ O ^c	2.045	1.808	103.1	113.6	-79	-84	29
			1.805	100.0	112.8	-77	

^a For molecules in which only one value of $R(S-C)$, $\tau(SSC)$, $\tau(SCC)$, and $\chi(SS-CC)$ is listed, these values are the same for both sides of the molecule because of C_2 symmetry about an axis perpendicular to the S-S bond. Otherwise, the two halves of the molecule differ slightly. ^b The compounds have the same numbers as in Tables II and III. ^c Raman spectra of these compounds were reported in ref 6.

compounds listed in Tables II and III might imply that the various additions, deletions, etc., of groups influence the conformation about the C-S bonds in the CCSSCC moiety. As in Table I, data are included in Tables II and III for the 250–450-cm⁻¹ region of these compounds.

B. Related X-Ray Structural Data. To aid in correlating the Raman data for the compounds in Tables II and III with the conformational properties of the CCSSCC moiety, the structural data in Table IV have been compiled from x-ray data in the literature.^{17–29} Only data for molecules whose spectra are presented here, or elsewhere,⁶ are given. The Raman data for compounds 12, 14, and 31 were obtained from the same batch of crystals that was used in the structural determination.

The histogram shown in Figure 1 depicts the frequency of occurrence of various ranges of values of $|\chi(SS-CC)|$ ³⁰ found for cystine residues in proteins as determined by x-ray crystallography. These dihedral angles have been calculated from the Cartesian coordinates of papain,³¹ carboxypeptidase A,³² ribonuclease S,³³ bovine pancreatic trypsin inhibitor,³⁴ lysozyme,³⁵ α -chymotrypsin,³⁶ trypsin,³⁷ and elastase^{38,39} in which there are a total of 30 cystine residues [60 values of $\chi(SS-CC)$].

C. Prominent Bands in the Raman Spectra of Liquid Alkyl Disulfides. Referring to Table I, there is a remarkable similarity in the frequencies and relative intensities of the two major bands in the $\nu(S-S)$ region between the Raman spectra of the primary disulfides listed (and also of methyl ethyl and diethyl disulfides, studied earlier⁹). For all these molecules, there are very strong bands near 510 cm⁻¹ and strong bands near 525 cm⁻¹, even though the alkyl group bonded to the sulfur atoms varies in size from an ethyl to an *n*-pentyl group. In the $\nu(S-S)$ region of the spectra of the two secondary disulfides 7 and 8, the prominent bands are at about 526 and 543 cm⁻¹, while in the tertiary disulfides 9 and 10, the only intense $\nu(S-S)$ band in this region lies at 540 cm⁻¹. These observations have been made earlier by Sugeta et al.;^{4,5} these authors at-

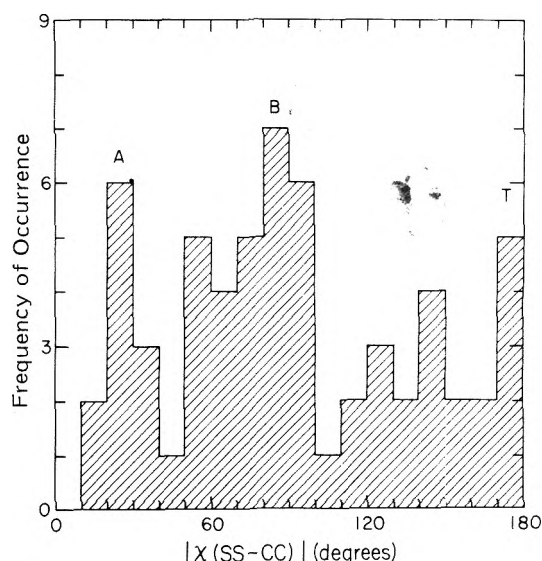


Figure 1. Frequency of occurrence of various ranges of SS-CC dihedral angles, $|\chi(SS-CC)|$, of cystine residues in eight proteins whose structures have been determined by x-ray crystallography, irrespective of the CS-SC dihedral angle.

tributed the presence of more than one $\nu(S-S)$ band in the spectra of primary and secondary alkyl disulfides to the coexistence of rotational isomers.

In addition to the prominent bands mentioned above, there are shoulders and other weak bands in the $\nu(S-S)$ region of these molecules that have not been reported earlier. There are no apparent similarities between the spectra of these disulfides in the region below 500 cm⁻¹ in which the $\gamma(CCS)$ and $\gamma(CCC)$ skeletal deformations are expected to lie. In fact, for the primary disulfides, this low-frequency region of the spectra becomes increasingly more complex as the length of the alkyl

substituent increases, with little or no effect on the bands in the $\nu(\text{S-S})$ region.

D. Prominent Bands in the Solution-Phase Spectra of Primary Cystine-Like Disulfides. Although the solid-phase spectra of the primary cystine-like disulfides of Table II have many bands in the $\nu(\text{S-S})$ region, their solution-phase spectra, almost without exception, have their strongest bands in the 505–510- cm^{-1} region. In addition, the solution-phase spectra of almost all these compounds have a characteristic shoulder near $\sim 525 \text{ cm}^{-1}$. For compounds 17 and 27, the solution-phase spectra were not of sufficient quality (because of a fluorescent background) to be able to ascertain whether or not there was a shoulder on the bands near 510 cm^{-1} . A suitable solution-phase spectrum of compound 19 could not be obtained, also because of a fluorescent background. The only primary disulfide studied that definitely did not show this $\sim 525\text{-cm}^{-1}$ shoulder was compound 28.

The intense band near 510 cm^{-1} with the shoulder near 525 cm^{-1} in these spectra are similar to the bands at roughly 510 and 525 cm^{-1} in the spectra of the primary alkyl disulfides of Table I. The bands in the solution-phase spectra listed in Table II are broader than the corresponding bands of Table I; as a result, the bands at $\sim 525 \text{ cm}^{-1}$ are not resolved and appear as shoulders on the stronger bands near 510 cm^{-1} . The shoulder in the solution-phase spectrum of compound 16 at about 513 cm^{-1} is probably of a different origin than those near $\sim 525 \text{ cm}^{-1}$ in the other compounds (in which these shoulders are thought to be due to rotational isomers). Compound 16 is rigid and cannot undergo rotational isomerism about its C-S bonds in the solution phase. Furthermore, the shoulder at 513 cm^{-1} in its solution-phase spectrum probably corresponds to the medium intense band at 516 cm^{-1} in the solid. As was the case for the alkyl disulfides in Table I, the spectra listed in Table II do not seem to have any bands in common outside of the $\nu(\text{S-S})$ region.

The similarities in the number, frequencies, and relative intensities of the major bands in the $\nu(\text{S-S})$ region of the spectra of the primary alkyl disulfides of Table I and the solution-phase spectra of the compounds in Table II and also of L-cystine dimethyl ester, L-cystinediamide, oxidized glutathione, N,N'-dimethyl-L-cystine, N,N,N',N',N'-hexamethyl-L-cystine, and L-homocystine diethyl ester, reported elsewhere,⁶ do not indicate that the solution-phase conformations about the C-S bonds of these primary disulfides are very different. While the compounds of Table II generally tend to have relatively less intense 525-cm^{-1} bands compared to those of Table I, there is no basis on which to conclude that the conformation of the CCSSCC moiety is influenced greatly by the presence of charged and polar groups. In fact, in going from a low to a high pH, which changes the state of charge of both the carboxyl and amino groups of compounds 11–15, no changes in the $\nu(\text{S-S})$ region of their spectra are observed. Finally, the use of different solvents for obtaining the solution-phase spectra in Tables II and III probably has little effect on the observed $\nu(\text{S-S})$ bands since the addition of 50% v/v of methanol, dimethyl sulfoxide, dimethylformamide, or benzene does not change the $\nu(\text{S-S})$ region of diethyl disulfide at all (not shown here).

E. Division of Primary Cystine-Like Disulfides into Classes. From a comparison of the solid- and solution-phase spectra of the primary disulfides of Table II, two types of behavior can be discerned. For some compounds (11–14, 18, 25, and 27), there are marked differences in both the intensities and frequencies of the major bands between the solid and solution-phase spectra, while in the other compounds (15–17,

20–24, 26, and 28), the major spectral features of the solid-phase spectra are retained in going to the solution phase.⁴⁰ For reasons to be brought out in section IVB, it is felt that the solid-phase spectra of compounds in the first class (to be referred to as class I) cannot be used in conjunction with x-ray data for frequency-conformation correlations, while those in the latter class (to be referred to as class II) can.

Our claim that the solid-phase Raman spectra of class I compounds cannot provide unambiguous information about the conformations of their CCSSCC fragments is illustrated by the properties of compounds 11–14. In spite of the fact that all of these molecules have nearly identical conformations about their C-S and S-S bonds (see Table IV), their solid-phase Raman spectra, especially in the $\nu(\text{S-S})$ region, are quite different. This indicates that factors other than conformational changes are responsible for the observed variations in the spectra of these crystalline substances.

Among the compounds in class II, there are five (16, 17, 23, 24, and 28) whose crystal structures have been determined and whose CCSSCC structural parameters are listed in Table IV. Of these five compounds, 17, 23, and 28 have gauche,¹¹ 16 has gauche,¹¹ and 24 trans conformations about their C-S bonds. In spite of these differences in conformation, all five compounds exhibit a single $\nu(\text{S-S})$ band with a frequency of $508 \pm 5 \text{ cm}^{-1}$ in the solid state. It is especially noteworthy that compound 24, which is known from x-ray studies²⁴ to have trans conformations about its C-S bonds, does not have its strong $\nu(\text{S-S})$ band at 540 cm^{-1} , as would have been predicted from the frequency-conformation correlation of Sugeta et al.^{4,5} When this compound is dissolved in 1 N HCl, it too exhibits the familiar shoulder at $\sim 525 \text{ cm}^{-1}$ which is due to an as yet unspecified conformation. Except for this shoulder at about 525 cm^{-1} and for slight shifts in frequencies normally associated with such a phase change, there are no other discernible changes in the solution compared to the solid phase spectrum of this compound.

F. Secondary and Tertiary Disulfides. The solution-phase spectra of secondary disulfides 29 and 30 of Table III have major bands in the $\nu(\text{S-S})$ region at about 525 and 540 cm^{-1} , as was the case for the secondary alkyl disulfides 7 and 8 of Table I. All of the tertiary disulfides in Table III have a major $\nu(\text{S-S})$ band near 540 cm^{-1} , as do the tertiary alkyl disulfides 9 and 10. It is of interest that tertiary disulfide 31, which is known from x-ray studies²⁶ to have trans conformations about its C-S bonds, exhibits its $\nu(\text{S-S})$ band at about 540 cm^{-1} in both the solid and solution phases, in agreement with the correlation of Sugeta et al.^{4,5} Compound 35 is included in Table III, even though it differs structurally from the other compounds listed. In the solid state, in which this compound is known to have conformations with low values ($0\text{--}20^\circ$) of $\chi(\text{SS-CC})$ across its C-S bonds (Table IV),²⁷ the lone $\nu(\text{S-S})$ band falls at 542 cm^{-1} . In solution, however, strong $\nu(\text{S-S})$ bands are evident at 512 and 525 cm^{-1} , with only a shoulder near 540 cm^{-1} .

IV. Discussion

The primary aim of this work is to provide an understanding of the factors responsible for the variations in the frequencies of $\nu(\text{S-S})$ bands of these alkyl and cystine-related disulfides and, if possible, to correlate these bands with specific conformations of the CCSSCC moiety. Previously, Sugeta et al.^{4,5} have advanced an hypothesis which attributes the variations in the $\nu(\text{S-S})$ frequencies of these disulfides to changes in the conformations about their C-S bonds. Before discussing the variations in the $\nu(\text{S-S})$ bands found here in terms of confor-

mation, it is appropriate to review, briefly, this hypothesis and the evidence which supports it.

A. *Frequency-Conformation Correlation of Sugeta et al.*^{4,5} In the Raman spectra of dimethyl, methyl ethyl, and diethyl disulfides and the alkyl disulfides shown in Table I (and in all previously published spectra^{4,5,9}), those compounds with primary and secondary alkyl groups larger than methyl groups have more than one major band in the $\nu(\text{S-S})$ region (at ~ 510 and ~ 525 cm^{-1} for primary disulfides, and ~ 525 and ~ 540 cm^{-1} for secondary disulfides), while dimethyl, methyl *tert*-butyl, and di-*tert*-butyl disulfides have only one (at about 510, 525, and 540 cm^{-1} , respectively⁴). The multiplicity of bands in the spectra of the primary and secondary disulfides has been attributed^{4,5} to the coexistence of *gauche* and *trans* rotational isomers about their C-S bonds. This interpretation is consistent with the observation that, in diethyl disulfide, only one $\nu(\text{S-S})$ band is present when the compound is crystallized.⁵ The single bands in dimethyl, methyl *tert*-butyl, and di-*tert*-butyl disulfides were attributed⁴ to the presence of only one rotamer in each case. On the basis of this evidence, it has been suggested^{4,5} that the frequency of the $\nu(\text{S-S})$ bands in aliphatic disulfides are roughly 510, 525, and 540 cm^{-1} , depending upon whether there are two hydrogen atoms, one carbon and one hydrogen atom, or two carbon atoms, *trans* to the distal sulfurs across the C-S bonds. These three conformations have been designated as $\nu(\text{H,H})$, $\nu(\text{H,C})$, and $\nu(\text{C,C})$, respectively. Hence, the effect of a C atom *trans* to a distal S atom about either C-S bond would be to raise $\nu(\text{S-S})$ by about 15 cm^{-1} ; i.e., the increase from 510 to 525 cm^{-1} would be due to the presence of one such *trans* C atom, and the further increase from 525 to 540 cm^{-1} would be due to the presence of a second such *trans* C atom. This increase in $\nu(\text{S-S})$ for the *trans* rotamers has been attributed^{4,5} to the greater degree of vibrational coupling between $\gamma(\text{CCS})$ and $\nu(\text{S-S})$ modes in *trans* relative to *gauche* conformations. By carrying out a normal mode calculation on several disulfides in which coupling between $\gamma(\text{CCS})$ and $\nu(\text{S-S})$ modes was introduced explicitly, Sugeta⁴¹ reported that he confirmed the above correlation.

B. *Correlation of X-Ray Structural Information with Solid-Phase Raman Spectra.* One attractive feature of Raman spectroscopy is that it is applicable to the study of both solids and solutions. In principle, then, by obtaining Raman spectra of solids whose crystal structures have been determined, one should be able to correlate Raman peak positions, intensities, etc., with known structural or conformational properties of molecules. These correlations could then be used to study the conformations of molecules in solution or in solids where their structures are not known. Since we have available here both Raman spectral (Tables II and III) and x-ray structural (Table IV) information on several disulfides with different conformations about their C-S bonds, we can use this approach to check the validity of the frequency-conformation correlation of Sugeta et al.,^{4,5} which was formulated from the spectra of *liquid* alkyl disulfides, whose structures were not known, but only *assumed*. However, this approach is valid only if it can be shown that the values of $\nu(\text{S-S})$ obtained from the spectra of crystalline compounds are really indicative of identical conformations of these same compounds in solution. That is, one must be cautious not to attribute observed variations in the values of $\nu(\text{S-S})$ that are obtained from solid samples, and caused by factors operative only in molecular crystals, to changes in conformation. Therefore, it is worthwhile to consider, briefly, the nature and origin of some of these factors.

Because of the unique arrangement of the atoms in any

molecular crystal, there are static fields present that are not encountered in the corresponding fluids. These static crystal fields can cause shifts in frequencies and changes in intensities in the vibrational spectra of crystals compared to similar spectra in, e.g., the solution phase.^{42,43} Hence, the internal vibrational frequencies observed for compounds in molecular crystals can be influenced (to an extent determined by the strength of the intermolecular forces present) by the presence of neighboring molecules and cannot always be taken to be indicative of those of the "free" molecule (as in the gas or solution phase).

In addition to the effects of static fields, there can be resonance interactions between identical vibrational modes of different molecules in the unit cell that lead to band splitting (Davydov splitting),^{42,44} even for nondegenerate modes. It may well be that the solid-phase spectra of the class I compounds are influenced by such interactions, since they generally exhibit either more than one band or shoulders on the main band in their $\nu(\text{S-S})$ region, while those of class II compounds do not. Since the $\nu(\text{S-S})$ mode is nondegenerate, these splittings are not explainable on the basis of site symmetry. Splittings in several of the bands, including the $\nu(\text{S-S})$ band, of the predominant rotational isomer of methyl ethyl disulfide have also been observed upon crystallization.⁵ If the class I compounds are influenced by Davydov splitting, this would account for the fact that the solid-phase spectra of compounds 11-14 are so dissimilar in the $\nu(\text{S-S})$ region, in spite of the fact that the conformations of their CCSSCC groups, known from x-ray studies, are nearly identical. This would also help explain why the solid and solution phase spectra of class I compounds differ, since the interactions between molecules in the unit cell, responsible for such splittings in the crystal, are absent in solution.

Although the frequencies of the $\nu(\text{S-S})$ bands observed in the spectra of these crystalline disulfides are not *necessarily* indicative of the stretching frequencies of the free molecules, in many cases they are; e.g., in diethyl disulfide, the frequencies of the bands due to the predominant rotational isomer do *not* change or show splitting when they are crystallized.⁵ Hence, the criterion that we will use here for interpreting the frequencies of the bands in the solid-phase spectra is that these frequencies remain the same (to a good approximation) for the solution-phase (in which the effects of crystal fields, etc., are removed). The fact that the vibrational frequencies do not change very much on going from solid to solution suggests not only that they are but minimally influenced by crystal effects, but further that no major conformational changes about the C-S bonds have accompanied dissolution. This follows from the results of an earlier study⁹ in which it was found that many of the Raman bands in the 250-650- cm^{-1} region, arising from the rotational isomers of methyl ethyl and diethyl disulfides, have different frequencies. In cases in which the vibrational frequencies *do* change upon going from the solid to the solution phase (as for the class I compounds), one would not know whether to attribute this to a conformational change or to the lifting of crystal field effects. Hence, of the two classes of compounds delineated in section III E, only the frequencies of the compounds in the solid-state spectra of class II (which do not change on going from the solid to the solution phase) will be correlated with the conformations of their CCSSCC fragments obtained from x-ray data.

C. *Variation of S-S Stretching Frequencies with Conformation about C-S Bonds.* From a comparison of the solid-phase Raman spectra of class II compounds 16, 17, 23, 24, and

28 (Table II) with the conformations of their CCSSCC fragments (Table IV), several important conclusions can be drawn. First, the observation that compound 24, which has trans conformations about both of its C-S bonds, exhibits its $\nu(\text{S-S})$ at about 510 cm^{-1} contradicts the hypothesis of Sugeta et al.^{4,5} that such trans conformations lead to values of $\nu(\text{S-S})$ of about 540 cm^{-1} in primary disulfides. Second, since all five of the above class II compounds have nearly the same value of $\nu(\text{S-S})$, in spite of the fact that the conformations about their C-S bonds differ considerably (being either gauche, gauche', or trans), it is clear that simple rotation about the C-S bond does not cause $\nu(\text{S-S})$ to vary in a uniform manner, as would have been expected if vibrational coupling between $\gamma(\text{CCS})$ and $\nu(\text{S-S})$ motions affected $\nu(\text{S-S})$. Moreover, these experimental results would seem to invalidate any conclusions about the values of $\nu(\text{S-S})$ that were drawn from a normal mode calculation⁴¹ which utilized coupling between $\gamma(\text{CCS})$ and $\nu(\text{S-S})$ modes as the mechanism for the variations in $\nu(\text{S-S})$.

The very similar values of $\nu(\text{S-S})$ found here for compounds known to have different conformations about their C-S bonds is consistent with the results of an earlier study⁹ on methyl ethyl and diethyl disulfides in which it was found that there exist at least two rotational isomers about the C-S bond with $\nu(\text{S-S})$ values of about 508 cm^{-1} . In the spectra of primary alkyl disulfides 1, 4, and 6, there are shoulders at about 495 cm^{-1} on the major $\nu(\text{S-S})$ band at about 508 cm^{-1} . It is possible that the two different rotamers about the C-S bonds of methyl ethyl and diethyl disulfides, that had the same value of $\nu(\text{S-S})$, are not degenerate in compounds 1, 4, and 6 because of some difference in the molecular motions of their alkyl groups, and that the band near 495 cm^{-1} is due to one of these conformations.

From the increases in $\nu(\text{S-S})$, observed in going from dimethyl ($\sim 510\text{ cm}^{-1}$) to methyl *tert*-butyl ($\sim 525\text{ cm}^{-1}$) to di-*tert*-butyl disulfides ($\sim 540\text{ cm}^{-1}$), Sugeta et al.^{4,5} concluded that the presence of a C atom in a trans position across a C-S bond would increase $\nu(\text{S-S})$ by about 15 cm^{-1} . These authors then proposed that the values of $\nu(\text{S-S})$ for primary, secondary, and tertiary disulfides were determined solely on the basis of whether or not there were carbon atoms in the trans positions. The implicit assumption that they made is that the substitution of two methyl groups for two hydrogens on the β carbons¹⁰ of dimethyl disulfide would have the same effect on the value of $\nu(\text{S-S})$ of primary and secondary disulfides as rotation of a carbon atom about the C-S bond from a gauche into a trans position previously occupied by a hydrogen atom. Since it has been shown above that their correlation does not hold for primary disulfides, it appears that this assumption is incorrect, and that the observed increases in $\nu(\text{S-S})$ in compounds with secondary and tertiary β carbons must arise from the presence of *additional* groups bonded to the β carbons. In fact, the correlation proposed by Sugeta and co-workers may describe accurately the effects of *substitution* (of additional groups for β -hydrogen atoms) on $\nu(\text{S-S})$. The spectrum of tertiary disulfide 31, known from x-ray data to have a $\nu(\text{C,C})$ conformation, does have a value of $\nu(\text{S-S})$ of about 540 cm^{-1} . Hence, this correlation holds for tertiary disulfides. Furthermore, there is no evidence to suggest that the correlation does not hold for secondary disulfides, as well. Thus, it may be true that the replacement of a gauche β hydrogen by a C atom does not affect $\nu(\text{S-S})$ appreciably, while the replacement of a trans β hydrogen by a C atom increases $\nu(\text{S-S})$ by about 15 cm^{-1} . In the accompanying paper,¹⁶ there is evidence to suggest that this, in fact, is the case.

The explanation^{4,5} proposed for the increase in $\nu(\text{S-S})$ from 510 to 525 or 540 cm^{-1} due to the alleged^{4,5} presence of $\nu(\text{C,H})$ and $\nu(\text{C,C})$ conformations, respectively, is that there is a greater degree of vibrational coupling between $\gamma(\text{CCS})$ and $\nu(\text{S-S})$ modes in the trans (compared to the gauche) rotamer. It seems unlikely that such coupling, if it exists, would be similar for primary, secondary, and tertiary disulfides, or even for primary disulfides with alkyl groups of different lengths. As the length of the alkyl substituent increases, in the *n*-alkyl disulfide series, one would expect the $\gamma(\text{CCS})$ and $\nu(\text{C,C})$ modes, which are of similar frequency, to interact mechanically, changing the character and frequency of the modes involving movements of the CCS fragment. If these movements of this fragment were coupled, even weakly, to those of the $\nu(\text{S-S})$ mode, then one would expect the values of $\nu(\text{S-S})$ to show *some* variation as the length of the alkyl substituent increased. Instead, the values of $\nu(\text{S-S})$ for di-*n*-pentyl through methyl ethyl disulfide remain *remarkably constant*. This observation leads one to conclude that it is some other local interaction within the CCSSCC fragment that is responsible for the 525-cm^{-1} band in these primary disulfides.

On the basis of the preceding considerations, we conclude that the frequency-conformation correlation proposed by Sugeta et al.^{4,5} is not applicable to *primary* aliphatic disulfides.

D. Conformation Responsible for the $\sim 525\text{-cm}^{-1}$ Band in the Spectra of Primary Disulfides. It seems clear that there is a rotational isomer about the C-S bond of primary disulfides that has a value of $\nu(\text{S-S})$ of $\sim 525\text{ cm}^{-1}$. Unfortunately, the structures of the rotational isomers of methyl ethyl disulfide (the smallest primary disulfide that exhibits this $\sim 525\text{-cm}^{-1}$ band) have not been determined uniquely. Only the presence of trans rotamers (in a mixture with other undefined conformers) has been established.¹² Furthermore, we have not been able to observe such a band in the solid-phase spectra of any of the class II disulfides of Table IV whose structures are known from x-ray studies. Hence, the conformation of the CCSSCC group responsible for this $\sim 525\text{-cm}^{-1}$ band is, at this stage of the discussion, unknown.

A possible clue to the identity of the $\sim 525\text{-cm}^{-1}$ band may come from the results of recent CNDO/2 calculations on the potential functions for internal rotation about the C-S bonds of several alkyl disulfides.^{14,15} These calculations suggest that there are rotamers with low values of $\chi(\text{SS-CC})$ (less than those of gauche rotamers). These conformations are thought to exist^{14,15} because of a weak attractive interaction between sulfur atoms and CH groups across the C-S bonds, referred to as a 1,4 carbon-sulfur interaction, which brings these groups into close contact. The existence of such an attractive interaction has been supported by a relatively large number of short nonbonded carbon-sulfur contact distances found in the crystal structures of organosulfur molecules.¹⁵ From previous work, it has not been possible to establish whether such conformations about the C-S bonds of alkyl disulfides actually exist or if their presence (deduced from the CNDO/2 calculations) arises from some defect in the CNDO/2 method, since such conformations have not been found in crystals of small aliphatic cystine-related disulfides. If such conformations of the CCSSCC moiety do exist, they may be responsible for the value of $\nu(\text{S-S})$ of $\sim 525\text{ cm}^{-1}$ observed for primary disulfides.

The first direct observation of the conformation discussed above is illustrated in the histogram of Figure 1, in which the frequency of occurrence of various ranges of values of

$\chi(\text{SS-CC})$ for cystine residues in proteins is plotted. One would expect those values of $\chi(\text{SS-CC})$ that correspond to minima in the potential function for rotation about the C-S bond to be those most highly populated. In accordance with this expectation, most of the cystine residues (~45%) have values of $\chi(\text{SS-CC})$ that lie under the peak centered at about 80–90°. This is consistent with the observation that almost all of the cystine-related disulfides of Table IV have values of $\chi(\text{SS-CC})$ in this same region (which we have thus far referred to as gauche rotamers). About 35% of all occurrences in this histogram lie under the broad peak centered near the trans conformation ($\chi = 180^\circ$). Among the disulfides of Table II, only the dithioglycolic acid²⁴ and the *n*-propyl half of thiamine *n*-propyl disulfide⁴⁵ have been reported from x-ray data to adopt such trans conformations. Finally, the peak centered near 20–30°, which accounts for about 20% of all occurrences, indicates the existence of a third conformation which has a low value of $\chi(\text{SS-CC})$ —smaller than that for a gauche conformation—as predicted earlier.¹⁵

We encounter here the problem of designating the three conformations about the C-S bonds of cystine discussed above. Since the commonly used terms *cis*, *gauche*, *skew*, and *trans* [$\chi(\text{SS-CC})$ values of about 0, ± 60 , ± 120 , and 180° , respectively] do not cover all of the conformations encountered in the above histogram and leave ranges of $\chi(\text{SS-CC})$ unaccounted for, they are inadequate and their use is abandoned here. Unfortunately, the terminology suggested by Klyne and Prelog⁴⁶ provides no solution to this problem since the conformations of interest here fall at the borders which separate their *sp* from their *sc* and their *sc* from their *ac* conformations. To solve this problem, we will arbitrarily refer to conformations with $\chi(\text{SS-CC})$ values of about 20–30° (which are neither *cis* nor *gauche*) as A conformations, those with $\chi(\text{SS-CC})$ values near 90° (which are neither *gauche* nor *skew*) as B conformations, and those with $\chi(\text{SS-CC})$ values near 180° as T (for *trans*) conformations.

The occurrence of three conformations (A, B, and T) about the C-S bonds of cystine is consistent with our earlier studies⁹ on methyl ethyl disulfide in which the existence of *three* distinct rotational isomers were indicated. Since the A rotamer occurs least frequently in cystine residues in proteins (smallest peak area in Figure 1), it should be the one of highest energy, in which case it should be associated with the $\nu(\text{S-S})$ band at $\sim 525 \text{ cm}^{-1}$ in methyl ethyl and diethyl disulfides which decreases in intensity as the temperature is lowered⁹ and which disappears upon crystallization.⁵ Presumably, the reason that the A conformation has not been observed in x-ray studies on crystals of model disulfides is that it is of higher energy than the B and T conformations.

It is interesting to note that the x-ray data that have been accumulated on aromatic disulfides (those in which the sulfur atoms are bonded directly to aromatic rings) *do* confirm the existence of A conformations with $\chi(\text{SS-CC})$ values of roughly 10–20° [and also B conformations with $\chi(\text{SS-CC})$ values of roughly 80°] in these molecules.¹⁵ The reason for this could be that the 1,4 carbon-sulfur interaction thought to be responsible for the A conformation is stronger for aromatic CH groups than for aliphatic ones. Compound 35, which is known from x-ray data to have A conformations about *both* of its C-S bonds, has its solid phase $\nu(\text{S-S})$ at 542 cm^{-1} . However, in solution, it has $\nu(\text{S-S})$ bands at roughly 510, 525, and 540 cm^{-1} . This is consistent with the coexistence, in solution, of two different conformations (the A and the B rotamers) about *each* C-S bond. The $\sim 540\text{-cm}^{-1}$ band in solution would then be due to conformations similar to the one found in the crystal

[i.e., A conformations about *both* C-S bonds which we shall designate $\nu(\text{A,A})$], the $\sim 510\text{-cm}^{-1}$ band due to one with B conformations about *both* C-S bonds, $\nu(\text{B,B})$, and the $\sim 525\text{-cm}^{-1}$ band due to molecules with one of each of these conformations, $\nu(\text{A,B})$ or $\nu(\text{B,A})$. Hence, we suggest that the $\sim 525\text{-cm}^{-1}$ band in primary disulfides is due to a $\nu(\text{A}, [\text{B or T}])$ conformation.

Another related observation is that those compounds whose spectra have shoulders at $\sim 525 \text{ cm}^{-1}$ have CH groups (or in the case of compound 24 a carbonyl carbon, which has also been found in many short contacts with sulfur atoms¹⁵) capable of participating in 1,4 carbon-sulfur interaction across the C-S bonds. Such 1,4 interactions would be expected to lead to the A conformation. The only compound in Table II that definitely does not have a $\sim 525\text{-cm}^{-1}$ band is 28, which also does *not* have CH groups capable of interacting with sulfur atoms across the C-S bonds. One would expect that the presence of the bulky phenyl rings on the β carbons of this compound would result in an increase in the population of the *trans* rotamer compared to its homologue, dimethyl disulfide. In spite of this expected increase in the *trans* population, compound 28 has no band at $\sim 525 \text{ cm}^{-1}$. This is additional evidence that the $\sim 525\text{-cm}^{-1}$ band is not due to $\nu(\text{C,H})$ conformations. Hence, the weight of evidence that has accumulated so far suggests that the presence of an A, not a T, conformation about either C-S bond results in an increase of about 15 cm^{-1} in $\nu(\text{S-S})$.

It seems worthwhile to consider briefly why A conformations might be expected to have values of $\nu(\text{S-S})$ different from those of the B or T forms. One possible reason is that the A rotamer has some different structural feature in its CCSSCC moiety. For example, the A conformations about the C-S bonds of aromatic disulfides have larger values of $\tau(\text{SSC})$ and $\text{R}(\text{C-S})$ than the B rotamer;¹⁵ i.e., as $\chi(\text{CC-SS})$ approaches zero (or approaches the *cis* conformation), the SSC bond angle could increase to relieve otherwise-close contacts in the close-to-*cis* conformation. Such differences between the CCSSCC structural features of two rotamers might be expected to lead to small changes in the values of $\nu(\text{S-S})$. Alternatively, the short nonbonded carbon-sulfur contacts associated with the A conformation could be the perturbation responsible for the different values of $\nu(\text{S-S})$. It should be emphasized that the 525-cm^{-1} band in primary aliphatic disulfides is only about 3% higher in frequency than the 510-cm^{-1} band for the other rotamers; hence, only subtle changes in the molecular motions or forces would be required to cause such a small frequency shift.

E. *The Use of S-S Stretching Frequencies for Conformational Analysis of CCSSCC Fragments in Proteins and Other Disulfide-Containing Compounds.* One of the original goals of this work was to formulate a correlation between the frequencies of the $\nu(\text{S-S})$ bands of aliphatic disulfides [whose $\chi(\text{CS-SC}) \approx \pm 90^\circ$] and the conformations about their C-S bonds. We now consider what conformational information can be abstracted from the values of $\nu(\text{S-S})$ obtained from the Raman spectra of proteins and other disulfides of unknown conformation.

For primary disulfides (e.g., cystine residues in proteins), there is strong evidence from this work to suggest that both B and T conformers about the C-S bonds result in a value of $\nu(\text{S-S})$ of $\sim 510 \text{ cm}^{-1}$. This is unfortunate and limits the use of values of $\nu(\text{S-S})$ for conformational analysis in proteins. If, in the Raman spectrum of a protein which contains four cystine residues, for example, a single $\nu(\text{S-S})$ band near 510 cm^{-1} is observed, it is not possible to conclude that the conforma-

tion about their C-S bonds is the same, since B and T (and possibly intermediate) conformations exhibit the same frequency. Furthermore, changes in the conformation about the C-S bonds (for example, in going from solid to solution) may occur with no apparent effect on observed values of $\nu(\text{S-S})$ alone.

On the other hand, the presence of A conformations about the C-S bonds of primary disulfides can be distinguished from the B and T conformations, since A conformations lead to values of $\nu(\text{S-S})$ greater than $\sim 510 \text{ cm}^{-1}$. In the Raman spectra of proteins in which $\nu(\text{S-S})$ bands near ~ 525 and $\sim 540 \text{ cm}^{-1}$ occur, the presence of $\nu(\text{A}, [\text{B or T}])$ and $\nu(\text{A,A})$ conformations, respectively, can be inferred. If the spectrum exhibits only the 510-cm^{-1} band, then the absence of the A conformation can be concluded. In disulfide-containing molecules in which there is the possibility of strain in the S-S bond [molecules with $\chi(\text{CS-SC})$ values in the range of 0 to about $\pm 65^\circ$], the effects of this strain, which are the subject of the following paper,¹⁶ must be taken into account, and the above interpretation of the 510- , 525- , and 540-cm^{-1} bands does not apply. The frequency-conformation correlation of Sugeta et al.,^{4,5} although inapplicable for primary disulfides, may still be applicable to secondary disulfides.

In addition to the limitations mentioned above, there are other problems associated with the estimation of the values of $\chi(\text{SS-CC})$ of cystine residues in proteins from the $\nu(\text{S-S})$ region of their Raman spectra. For one, there is the possibility that vibrational modes other than the $\nu(\text{S-S})$ mode may have frequencies in the $500\text{-}550\text{-cm}^{-1}$ region. For example, tryptophan has been reported³ to be responsible for a Raman band near 540 cm^{-1} . This may lead to ambiguity in band assignment. Another complicating feature is the possibility that the different rotamers about the C-S bonds may have $\nu(\text{S-S})$ bands of unequal molar intensity. For example, there is evidence to suggest that A rotamers have somewhat weaker $\nu(\text{S-S})$ bands than B rotamers.⁹ This factor complicates the precise interpretation of band areas of rotamer populations.

As an application of the results of this study, we consider the $\nu(\text{S-S})$ region of the Raman spectrum of lysozyme (which contains four disulfide bonds). Referring to the spectrum of Nakanishi et al.,⁴⁷ a neutral aqueous solution of this protein is observed to have bands in the $\nu(\text{S-S})$ region at 507 , 528 , and 544 cm^{-1} in about a 6.3:2.9:2.4 proportion (as estimated by us from the peak heights of their Figure 1). Such a combination of bands could arise from the presence of two $\nu(\text{B or T}, \text{B or T})$, one $\nu(\text{A}, \text{B or T})$, and one $\nu(\text{A,A})$ cystines. The slightly lower intensities for the $\nu(\text{S-S})$ bands of cystines with A conformations are consistent with previous observations.⁹ It is of interest to compare this prediction with the conformation of the cystines derived from the x-ray crystallographic study of this enzyme (making the assumption that the conformation of the cystine side chains is the same in the crystal and solution phases). The pairs of values of $\chi(\text{SS-CC})$ for the four cystine residues are $(-36, -51)$, $(142, 42)$, $(-87, -80)$, and $(83, -55)$.³⁵ While it is somewhat difficult to decide what value of $\chi(\text{SS-CC})$ distinguishes A rotamers from B, a value of about 50° is reasonable (see Figure 1). Keeping in mind that the error in the dihedral angles obtained from the x-ray data is of the order of $20\text{-}30^\circ$, the above four sets of dihedral angles are consistent with the designations $\nu(\text{A,A})$, $\nu(\text{T,A})$, $\nu(\text{B,B})$, and $\nu(\text{B,B})$, respectively. Hence, within experimental error, the predictions made on the basis of our correlations are consistent with the x-ray results.

Acknowledgment. The authors thank Dr. A. Fredga, Dr. R.

Parthasarathy, Dr. K. Seff, Dr. V. duVigneaud, Dr. B. Kamber, and Dr. L. Field for sending us the disulfides studied here. We also thank Shirley Rumsey for calculating the SS-CC dihedral angles used to construct Figure 1.

References and Notes

- (1) This work was supported by research grants from the National Institute of General Medical Sciences of the National Institutes of Health, U.S. Public Health Service (GM-14312), and from the National Science Foundation (BMS75-08691).
- (2) NIH Predoctoral Trainee, 1970-1974.
- (3) R. C. Lord and N. T. Yu, *J. Mol. Biol.*, **50**, 509 (1970).
- (4) H. Sugeta, A. Go, and T. Miyazawa, *Chem. Lett.*, **83** (1972).
- (5) H. Sugeta, A. Go, and T. Miyazawa, *Bull. Chem. Soc. Jpn.*, **46**, 3407 (1973).
- (6) E. J. Bastian, Jr., and R. B. Martin, *J. Phys. Chem.*, **77**, 1129 (1973).
- (7) H. E. Van Wart, A. Lewis, H. A. Scheraga, and F. D. Saeva, *Proc. Natl. Acad. Sci. U.S.A.*, **70**, 2619 (1973).
- (8) R. B. Martin, *J. Phys. Chem.*, **78**, 855 (1974).
- (9) H. E. Van Wart, F. Cardinaux, and H. A. Scheraga, *J. Phys. Chem.*, **80**, 625 (1976).
- (10) As used in this paper, the terms primary, secondary, and tertiary disulfide refer to disulfides in which the carbon atoms adjacent to the disulfide bond (to be referred to, by analogy with cystine, as the β carbons) are primary ($-\text{CH}_2-\text{S}-$), secondary ($>\text{CH}-\text{S}-$), or tertiary ($>\text{C}-\text{S}-$) carbon atoms, respectively.
- (11) Two gauche conformations can be defined for specifying the rotation about either C-S bond of the CCSSCC unit, viz., those with $\chi(\text{SS-CC}) = \pm 60^\circ$. Since the S-S bond is a chiral center and the CSSC unit has C_2 symmetry, two results arise. First, for a given screw sense of the disulfide bond, these two gauche conformations are nonequivalent and, hence, not necessarily isoenergetic. When $\chi(\text{CS-SC})$ is about $+90^\circ$, the gauche rotamer with $\chi(\text{SS-CC}) = -60^\circ$ is thought⁴ to be of higher energy than the other because of nonbonded repulsions between CH groups across the S-S bond. We will refer to the higher-energy rotamer as the gauche' conformation, and reserve the term gauche for the lower-energy rotamer. Second, for the gauche rotamer, $\chi(\text{SS-CC}) = +60^\circ$ when $\chi(\text{CS-SC}) = +90^\circ$, but $\chi(\text{SS-CC}) = -60^\circ$ when $\chi(\text{CS-SC}) = -90^\circ$.
- (12) A. Yokozeki and S. H. Bauer, *J. Phys. Chem.*, **80**, 618 (1976).
- (13) H. E. Van Wart, L. L. Shipman, and H. A. Scheraga, *J. Phys. Chem.*, **78**, 1848 (1974).
- (14) H. E. Van Wart, L. L. Shipman, and H. A. Scheraga, *J. Phys. Chem.*, **79**, 1428 (1975).
- (15) H. E. Van Wart, L. L. Shipman, and H. A. Scheraga, *J. Phys. Chem.*, **79**, 1436 (1975).
- (16) H. E. Van Wart and H. A. Scheraga, *J. Phys. Chem.*, **80**, 1823 (1976).
- (17) "Structure Reports for 1959", Vol. 23, W. B. Pearson, L. D. Calvert, J. M. Bijvoet, and J. D. Dunitz, Ed., 1959, p 593.
- (18) D. D. Jones, I. Bernal, M. N. Frey, and T. F. Koetzle, *Acta Crystallogr., Sect. B*, **30**, 1220 (1974).
- (19) J. Peterson, L. K. Steinrauf, and L. H. Jensen, *Acta Crystallogr.*, **13**, 104 (1960).
- (20) R. E. Rosenfield, Jr., and R. Parthasarathy, *Acta Crystallogr., Sect. B*, **31**, 816 (1975).
- (21) H. C. Mez, *Cryst. Struct. Commun.*, **3**, 657 (1974).
- (22) H. L. Yakel, Jr., and E. W. Hughes, *Acta Crystallogr.*, **7**, 291 (1954).
- (23) T. Ottersen, L. G. Warner, and K. Seff, *Acta Crystallogr., Sect. B*, **29**, 2954 (1973).
- (24) R. Parthasarathy, private communication; structure to be published.
- (25) J. D. Lee and M. W. R. Bryant, *Acta Crystallogr., Sect. B*, **25**, 2497 (1969).
- (26) R. E. Rosenfield, Jr., and R. Parthasarathy, *Acta Crystallogr., Sect. B*, **31**, 462 (1975).
- (27) J. D. Lee and M. W. R. Bryant, *Acta Crystallogr., Sect. B*, **25**, 2094 (1969).
- (28) M. O. Chaney and L. K. Steinrauf, *Acta Crystallogr., Sect. B*, **24**, 1564 (1968).
- (29) B. K. Vijayalakshmi and R. Srinivasan, *Acta Crystallogr., Sect. B*, **31**, 993 (1975).
- (30) There is a roughly equal distribution of disulfide screw senses in proteins. In order to plot the frequency of occurrence of the values of $\chi(\text{SS-CC})$ conveniently on one graph, we have plotted $|\chi(\text{SS-CC})|$ and, hence, have not distinguished between, for example, gauche and gauche' conformations. However, as expected, the majority of occurrences lie in the unprimed domain¹¹ of the values of $\chi(\text{SS-CC})$.
- (31) J. Drenth, J. N. Jansonius, R. Koekoek, and B. G. Wolthers, *Adv. Protein Chem.*, **25**, 79 (1971).
- (32) F. A. Quiocho and W. N. Lipscomb, *Adv. Protein Chem.*, **25**, 1 (1971).
- (33) H. W. Wyckoff, D. Tsernoglou, A. W. Hanson, J. R. Knox, B. Lee, and F. M. Richards, *J. Biol. Chem.*, **245**, 305 (1970).
- (34) J. Deisenhofer and W. Steigemann, *Acta Crystallogr., Sect. B*, **31**, 238 (1975).
- (35) D. C. Phillips, personal communication.
- (36) J. J. Birktoft and D. M. Blow, *J. Mol. Biol.*, **68**, 187 (1972).
- (37) R. M. Stroud, L. M. Kay, and R. E. Dickerson, *J. Mol. Biol.*, **83**, 185 (1974).
- (38) D. M. Shotton and H. C. Watson, *Nature (London)*, **225**, 811 (1970).
- (39) D. M. Shotton and B. S. Hartley, *Biochem. J.*, **131**, 643 (1973).
- (40) There actually is a systematic change in the spectra of some of these class II molecules in going to solution as mentioned in section IIID—the appearance of the shoulder near $\sim 525 \text{ cm}^{-1}$. This is attributable to a con-

formational change in a small percentage (probably <20%) of the molecules upon dissolution.

- (41) H. Sugeta, *Spectrochim. Acta, Part A*, **31**, 1729 (1975).
 (42) M. M. Sushchinskii, "Raman Spectra of Molecules and Crystals", Israel Program for Scientific Translations, New York, N.Y., 1972, p 330.
 (43) R. Savoie in "The Raman Effect", Vol. 2, A. Andersen, Ed., Marcel Dekker,

New York, N.Y., 1973, Chapter 10, p 765.

- (44) O. V. Fialkovskaya, *Opt. Spektrosk.*, **17**, 397 (1964).
 (45) M. Nishikawa, K. Kamiya, Y. Asahi, and H. Matsumaru, *Chem. Pharm. Bull. (Tokyo)*, **17**, 932 (1969).
 (46) W. Klyne and V. Prelog, *Experientia*, **16**, 521 (1960).
 (47) M. Nakanishi, H. Takesada, and M. Tsuboi, *J. Mol. Bio.*, **89**, 241 (1974).

Raman Spectra of Strained Disulfides. Effect of Rotation about Sulfur-Sulfur Bonds on Sulfur-Sulfur Stretching Frequencies¹

H. E. Van Wart² and H. A. Scheraga*

Department of Chemistry, Cornell University, Ithaca, New York 14853 (Received December 1, 1975)

The Raman spectra of a series of disulfides with CS-SC dihedral angles, $\chi(\text{CS-SC})$, in the 0 to about $\pm 65^\circ$ range (strained disulfides) have been studied in the S-S stretching region. The observed variations in the S-S stretching frequencies, $\nu(\text{S-S})$, of these compounds, all of which contain the $\text{C}^\alpha\text{C}^\beta\text{SSCC}^\alpha$ unit, are attributed to differences in the degree of substitution at their β carbons and to differences in conformation about their S-S bonds. When the effects of substitution at the β carbons were taken into account, the effects leading to reduced values of $\chi(\text{CS-SC})$ were isolated. As $\chi(\text{CS-SC})$ is lowered from near 90° to near 0° , an approximately linear reduction in $\nu(\text{S-S})$ is observed. These experimental findings are in good qualitative agreement with the trend in $\nu(\text{S-S})$ reported previously, and also calculated previously for the model compound dimethyl disulfide using the CNDO/2 molecular orbital method. The use of values of $\nu(\text{S-S})$ for the estimation of $\chi(\text{CS-SC})$ for cystine residues in proteins and other primary disulfides is discussed.

I. Introduction

In the preceding accompanying paper,³ the Raman spectra of aliphatic disulfides with a wide range of SS-CC dihedral angles, $\chi(\text{SS-CC})$, but with CS-SC dihedral angles, $\chi(\text{CS-SC})$, close to their minimum-energy values of $\pm 90^\circ$ (unstrained disulfides) were studied. The purpose of the earlier paper³ was to assess the effects of different conformations about the C-S bonds of the CCSSCC moiety on its S-S stretching frequency, $\nu(\text{S-S})$. In the present paper, the Raman spectra of a series of disulfides with values of $\chi(\text{CS-SC})$ in the 0 to about $\pm 65^\circ$ range (strained disulfides) are considered, in order to study the effects of rotation about S-S bonds on the values of $\nu(\text{S-S})$.

The results of an earlier study⁴ on several strained disulfides indicated an approximately linear relationship between $\nu(\text{S-S})$ and $\chi(\text{CS-SC})$. Since that time, however, several compounds have been encountered which do not obey this relationship. This prompted our reinvestigation^{3,5-8} of the conformational dependence of the values of $\nu(\text{S-S})$ of the CCSSCC fragment, and has led to new ideas concerning the effects of conformation about C-S bonds on these values. These new results, together with additional data on other strained disulfides, are considered here, and the effects of variations in $\chi(\text{CS-SC})$ on the values of $\nu(\text{S-S})$ are re-formulated. We find that, when proper account is taken of the effects of substitution at the β carbon (where, by analogy with cystine, the β carbons are those adjacent to the disulfide bond), the conclusions of our earlier study,⁴ while modified slightly, are essentially upheld.

II. Experimental Section

A. *Materials.* Of the compounds listed in Tables I-III, 1 was

kindly provided by Dr. A. Schöberl, 2 by both Drs. R. B. Martin and M. Carmack, 3, 4, 10, and 11 by Dr. A. Fredga, 5 by Dr. D. Harpp, 8 and 9 by Dr. D. McCormick, 12 by Dr. F. Saeva, 13 and 22 by Dr. I. Bernal, 14, 16, and 17 by Dr. R. Nagarajan, 15 by Dr. D. Hauser, 18 by both Drs. R. B. Martin and M. Bodanszky, 19-21 by Dr. A. Alberti, and 23-25 by Dr. L. Field. These were all obtained pure and used as received. Compounds 6 and 7 were obtained commercially and recrystallized twice before use.

B. *Raman Measurements.* The system used to collect the Raman data has been described previously.⁸ All measurements were made with an instrumental resolution of 2 cm^{-1} . The positions of the bands were calibrated with the emission lines of the laser; for sharp bands, the reported values are accurate to $\pm 1\text{ cm}^{-1}$. Many of these strained disulfides have absorptions in or near the visible region, and the tails of their absorption bands can extend as far out as 514.5 nm. Since some of these substances have been known to polymerize rapidly⁹ when exposed to light with wavelengths near their absorption bands, the Raman spectra of all compounds were obtained using the 647.1-nm exciting line of a Coherent Radiation 52G-K krypton ion laser. Whenever possible, Raman spectra of the solids of Tables I-III were also obtained in solution phase. Since many of these compounds are only sparingly soluble in any solvents, solution-phase spectra sometimes could not be obtained.

III. Results

A. *Raman Spectra.* The Raman spectra in the $400\text{--}650\text{ cm}^{-1}$ region of a series of aliphatic strained disulfides (in the solid and solution phases) are listed in Table I. Similar data

TABLE I: Solid and Solution-Phase Raman Spectra of Aliphatic^a Strained Disulfides between 400 and 650 cm⁻¹

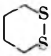
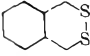
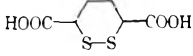
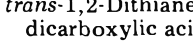
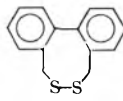
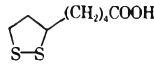
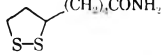
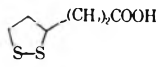
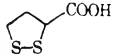
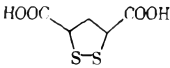
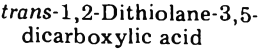
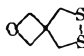
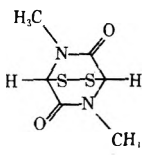
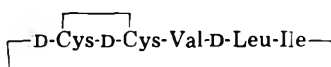
Compound	Solid		Solution		Solvent
	$\Delta\nu$, cm ⁻¹	Intensity ^b	$\Delta\nu$, cm ⁻¹	Intensity ^b	
(1) 1,2-Dithiane 	460 508 521 631 ~638 658	w s sh m sh m	488 509	w m	Dimethyl sulfoxide
(2) <i>trans</i> -2,3-Dithiadecalin 	438 472 513 533 556	w m vs vw m	475 512	m s	Dimethyl sulfoxide
(3) <i>cis</i> -1,2-Dithiane-3,6-dicarboxylic acid (meso) 	425 443 457 517 527 571 584 616	s m sh vs sh w w m	518	s	Dimethylformamide
(4) <i>trans</i> -1,2-Dithiane-3,6-dicarboxylic acid (racemic) 	413 434 473 531 652	s m w s w	532	m	Dimethylformamide
(5) 5 <i>H</i> ,8 <i>H</i> -dibenzo[<i>d,f</i>][1,2]-dithiocin 	470 484 509 534 561 571 592 620 646 659	m w mw vw vw vw w w sh s			
(6) D,L-6,8-thioctic acid 	416 456 ~501 511 559 634	m m sh s m m	508 ~530 582 632	s sh w, bd w	Methanol
(7) D,L-6,8-Thioctic acid amide 	403 437 496 ~504 533 585 623 650	w w vs sh w m vw vw	506 ~530	s sh	Dimethyl sulfoxide
(8) Bisnorthoctic acid 	435 476 503 573 597 637	w m vs w m w	504 523 593 630	s sh m m	Methanol
(9) Tetranorthoctic acid 	434 506 548 658	w vs m w	508 ~524	s sh	Methanol
(10) <i>cis</i> -1,2-Dithiolane-3,5-dicarboxylic acid 	435 508 544 610 628	w vs m w vw	512 542	ms m	Dimethylformamide
(11) <i>trans</i> -1,2-Dithiolane-3,5-dicarboxylic acid 	507 556	vs vs	518 545 508 518 546	s m s s m	Tetrahydrofuran Methanol

TABLE I (Continued)

Compound	Solid		Solution		Solvent
	$\Delta\nu$, cm^{-1}	Intensity ^b	$\Delta\nu$, cm^{-1}	Intensity ^b	
(12) 2-Oxa-6,7-dithiaspiro[3,4]- octane 	412	m			
	437	m			
	492	vs			
	588	vw			
(13) Epidithiosarcosine anhydride 	416	m			
	466	m			
	486	vs			
	607	m			
(14) Chaetocin ^c	422	m	~512	w	Dimethyl sulfoxide
	493	w			
	511	ms			
	573	w			
	590	m			
	609	w			
(15) Di-O-acetylchaetocin	417	m	~509	w	Dimethyl sulfoxide
	474	w			
	496	w			
	506	m			
	513	m			
	588	m			
(16) Acetylaranotin ^c	439	s			
	493	m			
	505	m			
	511	ms			
	523	w			
	549	m			
	566	m			
	598	m			
	636	m			
	(17) Gliotoxin ^c	510	w		
(18) Malformin A 	483	s	492	m	Dimethyl sulfoxide
	515	vw			
	583	w			
	595	w			
	632	m			

^a Aliphatic disulfides are those in which the sulfur atoms are bonded to aliphatic carbons. ^b The letters in this column have the following meanings: s, strong; m, medium, w, weak; v, very; sh, shoulder; and bd, broad. ^c The structures of these molecules are shown in Figure 1.

for aromatic disulfides (those in which the sulfur atoms are bonded directly to aromatic rings) and for compounds containing the $-(C=S)SS-$ group are listed in Tables II and III, respectively. All of the compounds in Tables I and II and compound 25 of Table III are thought to have strained S-S bonds. The structures of compounds 14, 16, and 17 are shown in Figure 1. Solution-phase spectra of compounds 5, 12, 13, 16, and 17 could not be obtained.

B. *X-Ray Structural Data.* In Table IV are listed the structural parameters for the CCSSCC groups of compounds 4-6, 13, 14, 16, 17, 19, and several other strained disulfides; these have been compiled from x-ray data in the literature.¹⁰⁻²⁰ These data will help in correlating the conformations of the CCSSCC groups in the compounds studied with their Raman spectra. To illustrate the effects of torsion about the S-S bond on the strengths of the S-S and S-C bonds in strained disulfides, the variations in $R(S-S)$, the S-S bond length, and in $R(S-C)$, the S-C bond length, with $|\chi(CS-SC)|$ are plotted in Figure 2. Finally, the frequency of occurrence of strained disulfide bonds in cystine residues in eight proteins whose structures are known from x-ray crystallography is illustrated in Figure 3. The plotted values of $|\chi(CS-SC)|$ were

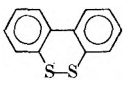
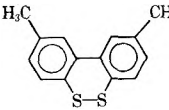
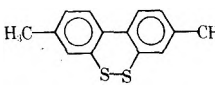
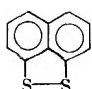
calculated from the Cartesian coordinates of papain,²¹ carboxypeptidase A,²² ribonuclease S,²³ bovine pancreatic trypsin inhibitor,²⁴ lysozyme,²⁵ α -chymotrypsin,²⁶ trypsin,²⁷ and elastase.^{28,29}

IV. Discussion

A. *Band Assignment.* The solid-phase Raman spectra of the disulfides of Tables I-III often have more than one band in the $\nu(S-S)$ region (450-550 cm^{-1}). Similar behavior was observed in the preceding paper³ for crystalline unstrained disulfides. To assign $\nu(S-S)$ bands unambiguously in these compounds, we rely on the solution-phase spectra (which are not complicated by the possible effects of crystal fields,³ etc.) to reveal their inherent intensity. Hence, we assign the strongest band in the 450-550- cm^{-1} region of the solution-phase spectrum to the $\nu(S-S)$ mode. Since these cyclic compounds are not very flexible, it is unlikely that conformational changes, which can alter $\nu(S-S)$, occur upon dissolution.

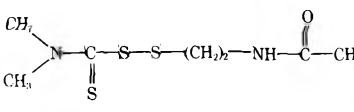
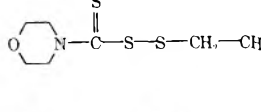
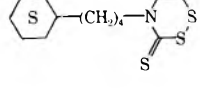
For compounds 5, 12, 13, 16, and 17, solution-phase spectra could not be obtained, and other procedures were used for assigning their $\nu(S-S)$ bands. Compounds 12 and 13 each exhibit only one strong band between 450 and 550 cm^{-1} in the

TABLE II: Solid and Solution-Phase Raman Spectra of Aromatic^a Strained Disulfides between 400 and 650 cm⁻¹

Compound	Solid		Solution		Solvent
	$\Delta\nu$, cm ⁻¹	Intensity ^b	$\Delta\nu$, cm ⁻¹	Intensity ^b	
(19) 2,2'-Biphenyl disulfide 	415 435 468 ~515 522 540 562 612	<i>m</i> <i>s</i> <i>m</i> <i>sh</i> <i>vs</i> <i>vw</i> <i>w</i> <i>w</i>	526	<i>s</i>	Benzene
(20) 5,5'-Dimethyl-2,2'-biphenyl disulfide 	394 411 461 484 ~513 520 542 599 634 656	<i>s</i> <i>mw</i> <i>w</i> <i>vw</i> <i>sh</i> <i>vs</i> <i>w</i> <i>w</i> <i>w</i> <i>m</i>	523	<i>s</i>	Benzene
(21) 4,4'-Dimethyl-2,2'-biphenyl disulfide 	400 432 473 493 ~516 523 541 578 624	<i>s</i> <i>m</i> <i>m</i> <i>m</i> <i>sh</i> <i>vs</i> <i>m</i> <i>w</i> <i>w</i>	525	<i>s</i>	Benzene
(22) 1,8-Naphthalene disulfide 	448 462 475 514 534 572 610	<i>w</i> <i>vw</i> <i>m</i> <i>ms</i> <i>m</i> <i>s</i> <i>w</i>	~513	<i>w</i>	1,2,4-Trichlorobenzene

^a Aromatic disulfides are those in which the sulfur atoms are bonded directly to aromatic rings. ^b The letters in this column have the same meaning as in Table I.

TABLE III: Solid and Solution-Phase Raman Spectra of Compounds Containing the C(=S)-S-S- Group between 400 and 650 cm⁻¹

Compound	Solid		Solution		Solvent
	ν , cm ⁻¹	Intensity ^a	ν , cm ⁻¹	Intensity ^a	
(23) 	444 543 563 637 655	<i>m</i> <i>ms</i> <i>ms</i> <i>m</i> <i>w</i>	541 562	<i>m</i> <i>m</i>	Methanol
(24) 	411 537 549 641 645	<i>s</i> <i>vs</i> <i>m</i> <i>m</i> <i>sh</i>	533	<i>vs</i>	Carbon disulfide
(25) 	427 441 476 487 536 559 572 600	<i>w</i> <i>w</i> <i>s</i> <i>s</i> <i>m</i> <i>m</i> <i>w</i> <i>m</i>	480	<i>m</i>	Carbon disulfide

^a The letters in this column have the same meanings as in Table I.

solid phase; hence we assign these as $\nu(\text{S-S})$ modes. The solid-phase spectrum of compound 5, on the other hand, does not have any one strong band in the 450–550-cm⁻¹ region and, hence, we are unable to assign the $\nu(\text{S-S})$ mode for this sub-

stance unambiguously. The $\nu(\text{S-S})$ band for compound 16 is taken to be the strongest one in its solid-phase spectrum, viz., 511 cm⁻¹. Finally, the only band in the spectrum of compound 17 is assigned as $\nu(\text{S-S})$. The assignments for compounds 16

TABLE IV: Structural Parameters of the CCSSCC Moiety Obtained from X-Ray Studies on Strained Disulfides

Compound ^a	<i>R</i> (S-S), Å	<i>R</i> (S-C), Å	τ (SSC), ^b deg	χ (CS-SC), ^b deg	χ (CS-SC), deg	Ref
(19) 2,2'-Biphenyl disulfide	2.050	1.757	98.2		69	10
(4) <i>trans</i> -1,2-Dithiane-3,6-dicarboxylic acid	2.069	1.85	98.9	63	60	11
(5) 5 <i>H</i> ,8 <i>H</i> -dibenzo[<i>d</i> , <i>f</i>]-[1,2]dithiocin	2.035	1.835	103.8	-92	56	12
(6) D,L-6,8-Thioctic acid	2.053	1.79	95.5	20	35	13
		1.83	92.8	43		
1,2-dithiolane-4-carboxylic acid ^c	2.096	1.83	92.6	59	27	14
		1.85	96.6	4		
(16) Acetylaranotin	2.082	1.882	97	<i>d</i>	17	15
(17) Gliotoxin	2.08	1.88	98.5	<i>d</i>	-12	16
		1.89	97.2			
(14) Chaetocin	2.077	1.879	98.5	65	+11	17
		1.886	97.5	64		
Sporidesmin ^c	2.08	1.91	97.3	70	-10	18
		1.90	98.7	66		
(13) Epidithiosarcosine anhydride	2.07	1.85	99	<i>d</i>	10	19
Tetrathiotetracene ^c	2.11			~0	~0	20

^aThe structures of all these compounds except those in footnote *c* are given in Table I, Table II, or Figure 1. ^bValues of τ (SSC) and χ (SS-CC) are listed only for those atoms in the ring that contains the S-S bond. ^cThe Raman spectra of these compounds were not obtained. ^aThe values of χ (SS-CC) for these compounds are very similar to those of chaetocin and sporidesmin.

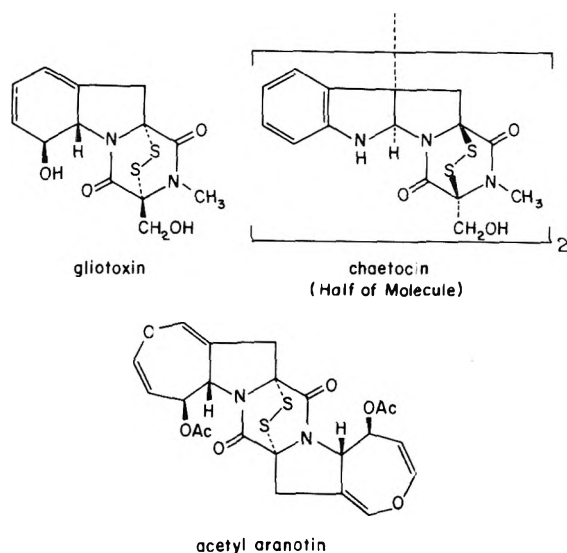


Figure 1. Chemical structures of several disulfides listed in Table I.

and 17 are consistent with the observation that compounds 14 and 15, which have nearly identical CCSSCC conformations,¹⁵⁻¹⁸ have solid and solution-phase ν (S-S) bands at ~ 510 cm^{-1} . These assignments are summarized in column 4 of Table V.

B. Variations in ν (S-S) Due to Substitution at the β Carbons of Strained Disulfides. Since the compounds whose Raman spectra are listed in Tables I-III have a wide variation of values of χ (CS-SC), the data in these tables can be used to determine the effects of such variations on ν (S-S). However, these compounds also have different degrees of substitution at their β carbons. Since it has been observed³ that higher degrees of substitution at the β carbons can lead to higher values of ν (S-S), the observed variations in ν (S-S) of the compounds of Tables I-III must be due to variations in both the degree of substitution at their β carbons and the strain in their S-S bonds. Hence, in order to assess the manner in which these values of ν (S-S) vary with χ (CS-SC) alone, the varia-

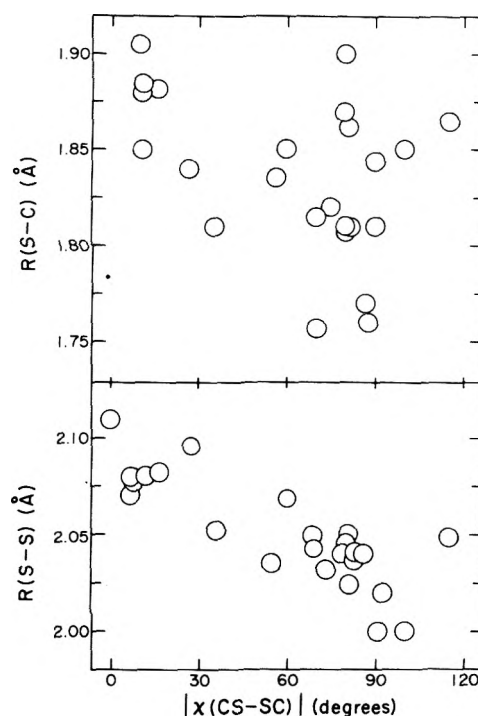


Figure 2. Variation in the S-S and S-C bond lengths, *R*(S-S) and *R*(S-C), respectively, with CS-SC dihedral angle, $|\chi$ (CS-SC)|, in strained disulfides, as determined from x-ray studies. The values for $|\chi$ (CS-SC)| $\geq 69^\circ$ are for the "unstrained" compounds of ref 3.

tions in ν (S-S) due to the effects of substitution of groups at their β carbons must be "subtracted out".

In the preceding paper,³ it was suggested that a modification of a correlation proposed by Sugeta et al.^{30,31} might account for the effects of substitution at the β carbons on the values of ν (S-S) of the CCSSCC group. According to this correlation, the replacement of a *trans* β -hydrogen atom (i.e., a hydrogen atom *trans* to a distal sulfur of the CCSSCC unit across either C-S bond) by a carbon atom increases ν (S-S) by about 15 cm^{-1} , while the replacement of a *gauche* β -hydrogen

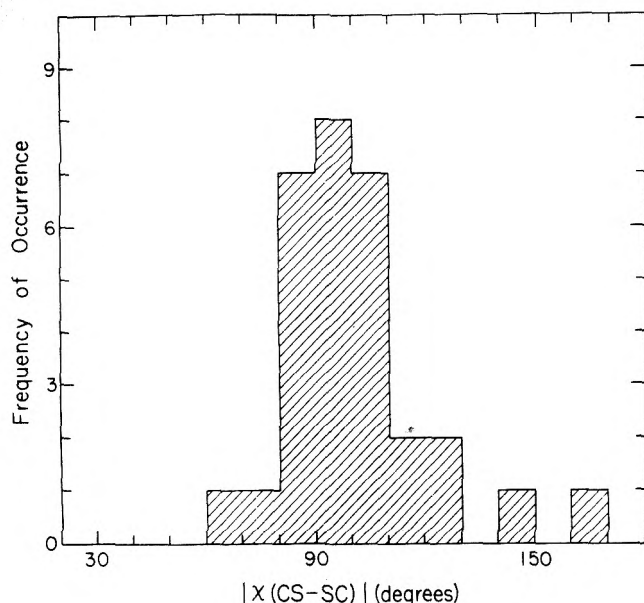


Figure 3. Frequency of occurrence of various ranges of CS-SC dihedral angles, $|\chi(\text{CS-SC})|$, of cystine residues in eight proteins whose structures have been determined by x-ray crystallography (a total of 30 S-S bonds).

atom does not affect $\nu(\text{S-S})$ appreciably. Conformations of the CCSSCC unit in which there are two hydrogens, one hydrogen and one carbon, and two carbon atoms in the trans positions will be designated by the symbols $\nu(\text{H,H})$, $\nu(\text{C,H})$, and $\nu(\text{C,C})$, respectively. If it could be established that this modified correlation is applicable to the compounds studied here, it could be used to "subtract out" the effects of substitution at the β carbons on $\nu(\text{S-S})$, and permit the direct comparison of the values of $\nu(\text{S-S})$ for primary, secondary, and tertiary disulfides.³² It is demonstrated below from the data of Table I that this correlation is, indeed, valid for the aliphatic disulfides studied here.

From the structures of the compounds in Table I, it can be seen that there are three classes of cyclic disulfides with very similar ring structures and, hence, very similar values of $\chi(\text{CS-SC})$. These are the 1,2-dithianes (compounds 1-4), the 1,2-dithiolanes (compounds 6-12), and the S-S bridged piperazinediones (compounds 13-17). Within these three classes, the compounds differ from each other structurally in the degree of substitution at their β carbons. Hence, to establish that the above correlation accounts for the effects of substitution at the β carbons, the values of $\nu(\text{S-S})$ of the compounds within each of the three classes mentioned above will be compared with each other (since the CS-SC dihedral angle can be assumed to be about the same within each class), and it will be shown that the observed differences in $\nu(\text{S-S})$ can be attributed, quantitatively, to differences in the number of trans carbon atoms.

Compounds 1 and 2 have the $\nu(\text{H,H})$ conformations, since neither can have carbon atoms in the trans positions. The structure of compound 4 has been determined from x-ray studies.¹¹ Both of the carboxyl carbons are in equatorial positions in the ring (which place them in trans positions relative to their distal sulfurs across their C-S bonds), with values of $\chi(\text{SS-CC}) = 169^\circ$. Hence, this compound has a $\nu(\text{C,C})$ conformation. The value of $\chi(\text{CS-SC})$ of compound 3, in which the carboxyl groups are cis, is expected to be close to that of compound 4 and the pucker of the 1,2-dithiane ring should

be similar for these two molecules. Their absorption spectra, which reflect changes in $\chi(\text{CS-SC})$,³³ are very similar,³⁴ supporting the above conclusion. Thus, since the two carboxyl carbons in compound 3 are cis to one another, one will be equatorial and the other axial. Hence, this compound has the $\nu(\text{C,H})$ conformation. The effects of changing from the $\nu(\text{H,H})$ conformation in compounds 1 and 2 to the $\nu(\text{C,H})$ in compound 3 is to raise $\nu(\text{S-S})$ from about 510 to 518 cm^{-1} , and of changing from the $\nu(\text{C,H})$ conformation of compound 3 to the $\nu(\text{C,C})$ conformation of compound 4 is to raise $\nu(\text{S-S})$ from 518 to 532 cm^{-1} .

Of those compounds which contain the 1,2-dithiolane ring, only compound 12 has a $\nu(\text{H,H})$ conformation, as can be seen from its structure. Compound 6 is known from x-ray studies¹³ to have its side chain in a very nearly equatorial position in the ring with a value of $\chi(\text{SS-CC}) = 167^\circ$. Hence, it has a $\nu(\text{C,H})$ conformation. Since compounds 7-9 are structurally very similar to compound 6, and have almost the same value of $\nu(\text{S-S})$, it seems safe to assume that they also have a $\nu(\text{C,H})$ conformation. It is difficult to specify the conformations of compounds 10 and 11 exactly. However, it seems likely from the structural preference shown for compound 6 that at least one of the carboxyl carbons will be very nearly equatorial. Proceeding on this assumption, the most likely conformation for compound 11, in which the carboxyl carbons are trans to one another across the ring, is $\nu(\text{C,C})$, similar to the case for compound 4. For compound 10, in which the carboxyl carbons are cis to each other, one would expect one carbon to be axial, making this a $\nu(\text{C,H})$ conformation. The values of $\nu(\text{S-S})$ in this series increase from 492 cm^{-1} for the $\nu(\text{H,H})$ conformation of compound 12 to about 507 cm^{-1} for the $\nu(\text{C,H})$ of compounds 6-10, to 518 cm^{-1} for the $\nu(\text{C,C})$ of compound 11. It should be noted that there seems to be two values of $\nu(\text{S-S})$ for compound 11 in methanol solution, possibly suggesting two different ring puckerings. We assign the 518- cm^{-1} band to the $\nu(\text{C,C})$ conformation by analogy with the increase observed in going from the $\nu(\text{C,H})$ to the $\nu(\text{C,C})$ conformations in compounds 3 and 4.

Referring now to the compounds with the S-S bridged piperazinedione structure, the structure¹⁹ of compound 13 indicates that it has hydrogen atoms in the trans positions and, hence, has the $\nu(\text{H,H})$ conformation. Compounds 14-17 are all known from their x-ray structures¹⁵⁻¹⁸ to have the $\nu(\text{C,C})$ conformation. The values of $\nu(\text{S-S})$ increase from 486 cm^{-1} for compound 13 to about 510 cm^{-1} for compounds 14-17.

The increases in the values of $\nu(\text{S-S})$, for the three classes of structures discussed above, average to 13 cm^{-1} in going from $\nu(\text{H,H})$ to $\nu(\text{C,H})$ conformations, to 11 cm^{-1} in going from $\nu(\text{C,H})$ to $\nu(\text{C,C})$ conformations, and to 24 cm^{-1} in going from $\nu(\text{H,H})$ to $\nu(\text{C,C})$ conformations. These results are internally consistent, and show that the effect of substitution by each additional trans carbon atom at the β carbon of the strained primary aliphatic disulfides of Table I is to increase $\nu(\text{S-S})$ by about 12 cm^{-1} . This value differs slightly from the value of 15 cm^{-1} suggested by Sugeta et al.^{30,31} for unstrained disulfides. Hence, on the basis of the above results, one can "subtract out" the increases in the values of $\nu(\text{S-S})$ due to the presence of trans carbon atoms in secondary and tertiary disulfides. This allows one to compare the values of $\nu(\text{S-S})$ of the primary, secondary, and tertiary strained disulfides of Table I directly (see section IVC).

C. Variation of S-S Stretching Frequencies with CS-SC Dihedral Angles in Strained Disulfides. In this section, we isolate, in an approximate way, the effect of variation in $\chi(\text{CS-SC})$ alone on the values of $\nu(\text{S-S})$ of the strained di-

TABLE V: Variation of S-S Stretching Frequencies with CS-SC Dihedral Angle in Strained Aliphatic Disulfides

Compd	Nature of substitution at β carbons	$\nu(\text{S-S})$ obsd, cm^{-1}	$\nu(\text{S-S})^a$ corr, cm^{-1}	Average $\nu(\text{S-S})$, cm^{-1}	CS-SC dihedral angle
1	$\nu(\text{H,H})$	509	509	508.8	~60°
2	$\nu(\text{H,H})$	512	512		
3	$\nu(\text{C,H})$	518	506		
4	$\nu(\text{C,C})$	532	508		
6	$\nu(\text{C,H})$	508	496	494.9	~30°
7	$\nu(\text{C,H})$	506	494		
8	$\nu(\text{C,H})$	504	492		
9	$\nu(\text{C,H})$	508	496		
10	$\nu(\text{C,H})$	512	500		
11	$\nu(\text{C,C})$	518	494	486.4	~10°
12	$\nu(\text{H,H})$	492	492		
13	$\nu(\text{H,H})$	486	486		
14	$\nu(\text{C,C})$	512	488		
15	$\nu(\text{C,C})$	509	485		
16	$\nu(\text{C,C})$	511	487		
17	$\nu(\text{C,C})$	510	486		

^a $\nu(\text{S-S})$ [corrected] is obtained by subtracting 12 and 24 cm^{-1} from $\nu(\text{S-S})$ [observed] for $\nu(\text{C,H})$ and $\nu(\text{C,C})$ conformations, respectively.

sulfides of Table I. For this purpose, the values of $\nu(\text{S-S})$ observed for the secondary and tertiary disulfides will be corrected, where necessary, for the presence of trans carbon atoms. Accordingly, the values of $\nu(\text{S-S})$ of those compounds with $\nu(\text{C,H})$ and $\nu(\text{C,C})$ conformations will be reduced by 12 and 24 cm^{-1} , respectively. The variations in the values of $\nu(\text{S-S})$ that remain after this correction is made will then be attributed to the effects of strain in the S-S bond, and the resulting values of $\nu(\text{S-S})$ will pertain to a primary disulfide (e.g., cystine).

In accordance with the procedure adopted above, the nature of the substitution at the β carbons of the aliphatic disulfides of Table I is listed in Table V along with the observed and corrected values of $\nu(\text{S-S})$. These compounds have been grouped into three categories—those that are known to have values of $\chi(\text{CS-SC})$ of roughly 60, 30, and 10° (see Table IV). Because of the approximate nature of this scheme for isolating the effects of strain in the S-S bond from those of varied C-S substitution, it was not felt justified to specify these dihedral angles more accurately. The average values of $\nu(\text{S-S})$ obtained for the above three classes of compounds are 508.8, 494.9, and 486.4 cm^{-1} , respectively. In Figure 4, these average values of $\nu(\text{S-S})$ are plotted against $|\chi(\text{CS-SC})|$ as circles whose diameters vary in proportion to the average deviation of the values of $\nu(\text{S-S})$ within each group. The dashed line is the relationship proposed earlier.⁴ It can be seen from this plot that the reduction in $\nu(\text{S-S})$ in the strained rings varies monotonically with their values of $|\chi(\text{CS-SC})|$, as found earlier theoretically⁵ (and the same as that found experimentally,⁴ except above about 60°). The major difference between the results shown in Figure 4 and our earlier relationship⁴ is that this new curve is rather flat near values of $|\chi(\text{CS-SC})|$ of 70–90°, and levels off at a value of $\nu(\text{S-S})$ corresponding to about 510 cm^{-1} for a primary disulfide. This curve was previously thought⁴ to increase past 510 cm^{-1} to 519 cm^{-1} for unstrained primary disulfides, since the solid-phase Raman spectra⁴ of cystine hydrochloride and cystine hydrobromide have values of $\nu(\text{S-S})$ of about 519 cm^{-1} . However, the high values of $\nu(\text{S-S})$ in these compounds are now thought to arise from the perturbations of their Raman spectra by crystal fields, and are not thought to be indicative of their conformation.³

In Table II, the Raman spectra of four strained aromatic disulfides are listed. The modified correlation of Sugeta et

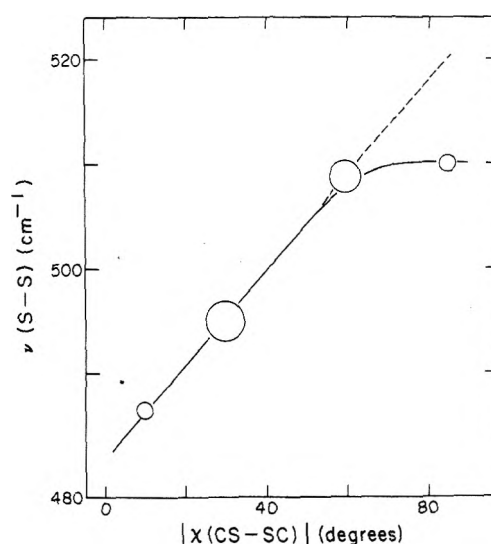


Figure 4. Variation of $\nu(\text{S-S})$ with $|\chi(\text{CS-SC})|$ in primary disulfides (data of Table V). The dashed line is the relationship reported previously.⁴

al.^{30,31} is not applicable to these compounds, which have sp^2 -hybridized β carbons. Moreover, a direct comparison of the values of $\nu(\text{S-S})$ of these aromatic disulfides with those of the aliphatic disulfides of Table I would not be meaningful, since the strain in the S-S bond may induce redistributions of the π electrons in the aromatic compounds. However, it can be seen from the data in Table II that the reduction of $|\chi(\text{CS-SC})|$ from a value of ~60° in compounds 19–21 to a lower value (probably ~20–30°) in compound 22 reduces $\nu(\text{S-S})$ from about 525 to 513 cm^{-1} . This result is in qualitative agreement with the trend observed in Figure 4 for the aliphatic disulfides.

Finally, the data shown in Table III serve to illustrate the effects of greatly reduced values of $\chi(\text{CS-SC})$ on the value of $\nu(\text{S-S})$ of the $-\text{C}(=\text{S})-\text{S}-\text{S}-$ group. When this group is not under strain, as in compounds 23 and 24, the $\nu(\text{S-S})$ band lies at 530–540 cm^{-1} . However, in compound 26, in which $\chi(\text{CS-SC})$ is very low due to the presence of the $-\text{N}-\text{C}(=\text{S})-\text{S}-\text{S}-$ group (which is planar in compounds 23 and 24) in the ring, the value of $\nu(\text{S-S})$ is reduced to 480 cm^{-1} . This again

illustrates the effect of strain in the S-S bond upon its value of $\nu(\text{S-S})$.

D. Factors Responsible for the Reduction in S-S Stretching Frequencies in Strained Disulfides. From the analysis of the data on the various strained disulfides discussed in the previous sections, it has been found that the lower the values of $|\chi(\text{CS-SC})|$, the greater the reduction in $\nu(\text{S-S})$. It is of interest to consider the cause for this reduction. There are certain structural changes in the CSSC unit that correlate with the lowering of $|\chi(\text{CS-SC})|$ in these compounds. While the values of $\tau(\text{SSC})$ of these cyclic disulfides do not vary monotonically with $|\chi(\text{CS-SC})|$, the values of $R(\text{S-S})$ and possibly the values of $R(\text{S-C})$ do (Figure 2). The length of the disulfide bond increases by almost 0.1 Å as $|\chi(\text{CS-SC})|$ is reduced from near 90 to near 0°. This trend has been pointed out by Hordvik.³⁵ The trend in $R(\text{S-C})$ is not as pronounced—probably because of the many different types of carbon atoms found bonded to the sulfurs in the compounds whose structures have been determined. The increases in the values of $R(\text{S-S})$ and $R(\text{S-C})$ in compounds with lowered values of $|\chi(\text{CS-SC})|$ is consistent with a weakening of these bonds; such bond weakening would also result in a lowering of the force constant for the S-S stretching motion⁵ and account for the observed reductions in $\nu(\text{S-S})$.

Recently, we have used the CNDO/2 semiempirical molecular orbital method to calculate the variations in the energy, and in the values of $R(\text{S-S})$ and $\nu(\text{S-S})$ of the model compound dimethyl disulfide as a function of $\chi(\text{CS-SC})$.⁵ These calculations indicated a substantial weakening of the S-S bond as $\chi(\text{CS-SC})$ was varied away from its equilibrium value of $\pm 85^\circ$. This weakening was accompanied by both an increase in $R(\text{S-S})$ and a reduction in $\nu(\text{S-S})$ for a pure S-S stretching motion, in good qualitative agreement with the results shown in Figures 2 and 4, respectively. While the $\nu(\text{S-S})$ bands observed for the compounds studied here are almost certainly not due to a pure S-S stretching motion, we attribute their net reduction in frequency at least in part to the weakening of the S-S bond. Sugeta has recently carried out a normal mode analysis for several disulfides, including dimethyl disulfide, in which the dependence of $\nu(\text{S-S})$ upon $\chi(\text{CS-SC})$ "... was calculated on the assumption that the force field and the structural parameters except $\chi(\text{CS-SC})$ are independent of conformation."³⁶ It was concluded that $\nu(\text{S-S})$ was nearly independent of $\chi(\text{CS-SC})$. Since the results of Figure 4 clearly show that $\nu(\text{S-S})$ does vary as a function of $\chi(\text{CS-SC})$, we conclude that the assumption³⁶ of a constant force field with structural parameters [except, of course, $\chi(\text{CS-SC})$] insensitive to conformation is a poor one. The results of the CNDO/2 calculations mentioned above,⁵ together with the data shown in Figure 2, support this conclusion.

There are circumstances other than ring closure that can cause a weakening of the S-S bond and which also cause a reduction in $\nu(\text{S-S})$. For example, bis[2-(*N,N'*-dimethylamino)ethyl] disulfide (compound 23 in ref 3) is known to form a complex with copper ions in which the disulfide bonding electrons are delocalized away from the region between the sulfur nuclei. This reduces the strength of the S-S bond and causes it to lengthen. The uncomplexed CSSC moiety³⁷ has an equilibrium S-S bond length of 2.037 Å and a CS-SC dihedral angle of 82° while its copper complex³⁸ has a bond length of 2.075 Å and a dihedral angle of 106°. This bond lengthening is much larger than one would expect on the basis of the small change in $\chi(\text{CS-SC})$ (see Figure 2). The values of $\nu(\text{S-S})$ of this molecule and of its copper complex are 506 and 463 cm^{-1} , respectively,³⁸ reflecting the smaller value of the

S-S stretching force constant in the complex. This example illustrates the effects of S-S bond weakening on the values of $\nu(\text{S-S})$ in a system in which the reduction in the S-S stretching force constant is made without constraining the S-S bond to be in a covalently bonded ring.

E. The Use of S-S Stretching Frequencies for the Detection of Strain in the S-S Bonds of Cystine Residues in Proteins and Other Primary Aliphatic Disulfides. It has been well established from a variety of molecular orbital calculations³⁹ that rotation about the S-S bond is very hindered. This is consistent with the observation that all acyclic disulfides (not including disulfide loops of proteins) whose structures are known from x-ray studies have values of $|\chi(\text{CS-SC})|$ within 30° of the equilibrium value of roughly 90°. Occasionally, however, circumstances such as ring closure or intermolecular packing forces may result in values of $|\chi(\text{CS-SC})|$ outside of the 60–120° range. For example, in Figure 3, 4 out of 30 of the values of $\chi(\text{CS-SC})$ found for cystine residues in eight proteins lie outside this range and would be expected to have reduced values of $\nu(\text{S-S})$. Since unstrained aliphatic primary disulfides have not been observed to have values of $\nu(\text{S-S})$ lower³ than about 505 cm^{-1} , the observation of values of $\nu(\text{S-S})$ lower than this would imply the presence of strained S-S bonds.

It should be emphasized that the reductions in $\nu(\text{S-S})$ associated with low values of $\chi(\text{CS-SC})$, although thought to be due predominantly to the weakening of the S-S bond, are still *net* effects. That is, these reductions reflect all of the changes in conformation of the CCSSCC unit associated with strained S-S bonds [such as abnormal values of $\tau(\text{SSC})$, etc.]. It is expected that CCSSCC units with strained S-S bonds will have abnormal structural parameters. Hence, the plot shown in Figure 4 can be used to estimate the values of $\chi(\text{CS-SC})$ of aliphatic disulfides directly from their low values of $\nu(\text{S-S})$. It is not anticipated that the values of $\chi(\text{SS-CC})$ in CCSSCC moieties with strained S-S bonds will affect the values of $\nu(\text{S-S})$ appreciably; it was found in the previous paper³ that simple rotation about the C-S bonds of unstrained disulfides does not, in itself, affect $\nu(\text{S-S})$. Only A conformations, thought to involve weak 1,4 carbon-sulfur interactions, were found to have different values of $\nu(\text{S-S})$, and such *weak* interactions would not be expected to exist in strained CCSSCC units. Hence, the estimate of $\chi(\text{CS-SC})$ from values of $\nu(\text{S-S})$ can be made *without* prior knowledge of the conformation about the C-S bonds of the CCSSCC moiety. On the other hand, no conclusions regarding the conformations about the C-S bonds of strained CCSSCC groups can be deduced from their values of $\nu(\text{S-S})$.

One inherent problem with the estimation of $\chi(\text{CS-SC})$ from low values of $\nu(\text{S-S})$ is that the strain in the S-S bond can potentially be caused by values of $\chi(\text{CS-SC})$ greater or less than 90° (e.g., from either 0–60° or 120–180°), since the S-S bond weakens in both regions.⁵ Hence, use of the plot shown in Figure 4 for the estimation of $\chi(\text{CS-SC})$ from values of $\nu(\text{S-S})$ lower than about 505 cm^{-1} is limited to cases in which it can be established from prior knowledge that the strain is due to low, not high, values of $\chi(\text{CS-SC})$. The estimation of values of $\chi(\text{CS-SC})$ for disulfides with strained S-S bonds in the range greater than 90° is not yet possible because of the lack of suitable model compounds for study.

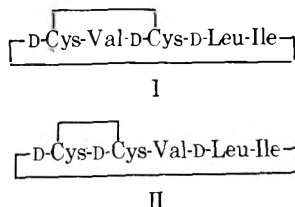
As an application of the relationship shown in Figure 4, consider malformin A (compound 18). Martin⁴⁰ has pointed out that our previous prediction⁴ of the value of $\chi(\text{CS-SC})$ for malformin A from its uv-vis spectrum was based upon an absorption band that was due to an impurity⁴¹ and not to

TABLE VI: Summary of the Conclusions That Can Be Drawn about the Values of $\chi(\text{SS-CC})$ and $\chi(\text{CS-SC})$ of Primary Disulfides from the Observed Values of $\nu(\text{S-S})$

Obsd value of $\nu(\text{S-S}), \text{cm}^{-1}$	$ \chi(\text{SS-CC}) , ^\circ$ deg	$ \chi(\text{CS-SC}) , \text{deg}$
480–505	<i>b</i>	$\begin{cases} 0-65 \\ \text{(use Figure 4)} \\ 115-180 \end{cases}$
510 ± 5	50–180 50–180	85 ± 20
525 ± 5	0–50 50–180	85 ± 20
540 ± 5	0–50 0–50	85 ± 20

^a One range of dihedral angles is specified for each C–S bond of the CCSSCC moiety. ^b No information is obtainable.

malformin A itself. The Raman spectrum of pure malformin A in dimethyl sulfoxide is shown in Table I; hence we can now estimate its $\chi(\text{CS-SC})$ from this spectrum using Figure 4. The low value of the $\nu(\text{S-S})$ band of 492 cm^{-1} clearly indicates the presence of strain in its S–S bond. This strain may be due to values of $\chi(\text{CS-SC})$ either much lower than ($<60^\circ$) or much larger than ($>120^\circ$) the normal value of about 90° . If the strain were due to values on the low side, our relationship would predict a value of $\chi(\text{CS-SC})$ of about 35° —a perturbation of about 50° from the normal value of 85° . It is difficult to estimate the effects of strain on the high side quantitatively, since suitable model compounds are not available for study. However, if the effects of strain on the high and low sides are similar, a perturbation of 50° on the high side would result in a value of $\chi(\text{CS-SC})$ of about 135° . Ptak⁴² has analyzed the CD and NMR spectra of malformin A and has proposed a value of $\chi(\text{CS-SC})$ of $130-140^\circ$. Unfortunately, his analysis of the data was based on structure I for malformin A, which has now been shown to be incorrect.⁴³ The revised structure II is also shown. The effect of this revision of structure on Ptak's prediction of $\chi(\text{CS-SC})$ from these data is difficult to assess. From an examination of space-filling models, however, it seems unlikely that $\chi(\text{CS-SC})$ is as large as 130° . Hence, we favor a value of $\chi(\text{CS-SC})$ of about 35° .



As an example of the application of the relationship shown in Figure 4 to a protein, we consider the Raman spectrum of insulin crystals obtained by Yu et al.⁴⁴ Their spectrum shows a band at 492 cm^{-1} which we now assign as a $\nu(\text{S-S})$ mode. Since it is known that insulin has a rather small loop in the A chain due to the disulfide bond between cysteine residues 6 and 11, it seems reasonable to assume that the 492-cm^{-1} band arises from this bond and that the low value of $\nu(\text{S-S})$ is due to a low value of $\chi(\text{CS-SC})$. By using the relationship shown in Figure 4, the value of $\chi(\text{CS-SC})$ can be estimated to be about 35° . Unfortunately, at the time of this writing, the dihedral angles for the cystine side chains of insulin obtained by x-ray crystallography are not available for comparison.

V. Summary

The conclusions that can be drawn about the values of $\chi(\text{SS-CC})$ and $\chi(\text{CS-SC})$ of primary disulfides from the observed values of $\nu(\text{S-S})$ are summarized in Table VI. In general, values below 505 cm^{-1} can be interpreted in terms of strained S–S bonds while values above 510 cm^{-1} indicate the presence of A conformations about C–S bonds. While these results clearly do not allow one to specify the conformations of cystine side chains uniquely, they do permit certain conclusions to be drawn and represent one of the very few means by which one can obtain information about side-chain conformations of proteins both in the crystal and solution phases.

Acknowledgment. The authors thank Dr. A. Fredga, Dr. A. Schöberl, Dr. R. B. Martin, Dr. M. Carmack, Dr. D. Harpp, Dr. D. McCormick, Dr. F. Saeva, Dr. I. Bernal, Dr. R. Nagarajan, Dr. D. Hauser, Dr. A. Alberti, Dr. L. Field, and Dr. M. Bodanszky for sending us the disulfides studies here. We also thank Shirley Rumsey for calculating the CS–SC dihedral angles used to construct Figure 3.

Addendum

The reader is referred to ref 45, which appears in this issue, in which the present authors and R. B. Martin have resolved earlier differences of interpretation.

References and Notes

- (1) This work was supported by research grants from the National Institute of General Medical Sciences of the National Institutes of Health, U.S. Public Health Service (GM-14312), and from the National Science Foundation (BMS75-08691).
- (2) NIH Predoctoral Trainee, 1970–1974.
- (3) H. E. Van Wart and H. A. Scheraga, *J. Phys. Chem.*, **80**, 1812 (1976).
- (4) H. E. Van Wart, A. Lewis, H. A. Scheraga, and F. D. Saeva, *Proc. Natl. Acad. Sci. U.S.A.*, **70**, 2619 (1973).
- (5) H. E. Van Wart, L. L. Shipman, and H. A. Scheraga, *J. Phys. Chem.*, **78**, 1848 (1974).
- (6) H. E. Van Wart, L. L. Shipman, and H. A. Scheraga, *J. Phys. Chem.*, **79**, 1428 (1975).
- (7) H. E. Van Wart, L. L. Shipman, and H. A. Scheraga, *J. Phys. Chem.*, **79**, 1436 (1975).
- (8) H. E. Van Wart, F. Cardinaux, and H. A. Scheraga, *J. Phys. Chem.*, **80**, 625 (1976).
- (9) J. A. Barltrop, P. M. Hayes, and M. Calvin, *J. Am. Chem. Soc.*, **76**, 4348 (1954).
- (10) I. Bernal and J. Ricci, 7th International Congress on Crystallography, Moscow, 1966, supplement to *Acta Crystallogr., Sect. A*, **21**, 104 (1966).
- (11) O. Foss, K. Johnsen, and T. Reistad, *Acta Chem. Scand.*, **18**, 2345 (1964).
- (12) G. H. Wahl, Jr., J. Bordner, D. N. Harpp, and J. G. Gleason, *J. Chem. Soc., Chem. Commun.*, 985 (1972).
- (13) R. M. Stroud and C. H. Carlisle, *Acta Crystallogr., Sect. B*, **28**, 304 (1972).
- (14) O. Foss and O. Tjomsland, *Acta Chem. Scand.*, **12**, 1810 (1958).
- (15) D. B. Cosulich, N. R. Nelson, and J. H. van den Hende, *J. Am. Chem. Soc.*, **90**, 6518 (1968).
- (16) J. Fridrichsons and A. McL. Mathieson, *Acta Crystallogr.*, **23**, 439 (1967).
- (17) H. P. Weber, *Acta Crystallogr., Sect. B*, **28**, 2945 (1972).
- (18) F. Fridrichsons and A. McL. Mathieson, *Acta Crystallogr.*, **18**, 1043 (1965).
- (19) I. Bernal, personal communication.
- (20) J. Toussaint and O. Dideberg, *Bull. Soc. R. Sci. Liege*, **36**, 666 (1967).
- (21) J. Drenth, J. N. Jansonius, R. Koekoek, and B. G. Wolthers, *Adv. Protein Chem.*, **25**, 79 (1971).
- (22) F. A. Quiocho and W. N. Lipscomb, *Adv. Protein Chem.*, **25**, 1 (1971).
- (23) H. W. Wyckoff, D. Tsernoglou, A. W. Hanson, J. R. Knox, B. Lee, and F. M. Richards, *J. Biol. Chem.*, **245**, 305 (1970).
- (24) J. Deisenhofer and W. Steigemann, *Acta Crystallogr., Sect. B*, **31**, 238 (1975).
- (25) D. C. Phillips, personal communication.
- (26) J. J. Birktoff and D. M. Blow, *J. Mol. Biol.*, **68**, 187 (1972).
- (27) R. M. Stroud, L. M. Kay, and R. E. Dickerson, *J. Mol. Biol.*, **83**, 185 (1974).
- (28) D. M. Shotton and H. C. Watson, *Nature (London)*, **225**, 811 (1970).
- (29) D. M. Shotton and B. S. Hartley, *Biochem. J.*, **131**, 643 (1973).
- (30) H. Sugeta, A. Go, and T. Miyazawa, *Chem. Lett.*, 83 (1972).
- (31) H. Sugeta, A. Go, and T. Miyazawa, *Bull. Chem. Soc. Jpn.*, **46**, 3407 (1973).
- (32) As used in this paper, the terms primary, secondary, and tertiary disulfide refer to disulfides in which the carbon atoms adjacent to the disulfide bond (to be referred to, by analogy with cystine, as the β carbons) are primary ($-\text{CH}_2-\text{S}-$), secondary ($>\text{CH}-\text{S}-$), or tertiary ($>\text{C}-\text{S}-$) carbon atoms, re-

- spectively.
- (33) D. B. Boyd, *J. Am. Chem. Soc.*, **94**, 8799 (1972).
 (34) L. Schotte, *Ark. Kem.*, **8**, 579 (1956).
 (35) A. Hordvik, *Q. Rep. Sulfur Chem.*, **5**, 21 (1970).
 (36) H. Sugeta, *Spectrochim. Acta, Part A*, **31**, 1729 (1975).
 (37) T. Ottersen, L. G. Warner and K. Seff, *Acta Crystallogr., Sect. B*, **29**, 2954 (1973).
 (38) T. Ottersen, L. G. Warner, and K. Seff, *Inorg. Chem.*, **13**, 1904 (1974).
 (39) See ref 5 for a summary of these.
- (40) R. B. Martin, *J. Phys. Chem.*, **78**, 855 (1974).
 (41) S. Marumo and R. W. Curtis, *Phytochemistry*, **1**, 245 (1961).
 (42) M. Ptak, *Biopolymers*, **12**, 1575 (1973).
 (43) M. Bodanszky and G. L. Stahl, *Proc. Natl. Acad. Sci. U.S.A.*, **71**, 2791 (1974).
 (44) N. T. Yu, B. H. Jo, R. C. C. Chang, and J. D. Huber, *Arch. Biochem. Biophys.*, **160**, 614 (1974).
 (45) H. E. Van Wart, H. A. Scheraga, and R. B. Martin, *J. Phys. Chem.*, **80**, 1832 (1976).

COMMUNICATIONS TO THE EDITOR

Agreement Concerning the Nature of the Variation of Disulfide Stretching Frequencies with Disulfide Dihedral Angles

Sir: From the analysis of Raman and infrared data in the S-S stretching region of a series of disulfides, Bastian and Martin found, previously, that "... a strong Raman band, identifiable as a S-S stretching frequency, occurs uncorrelated with (disulfide) dihedral angle in the range of 496-511 cm^{-1} in almost all cases. ..."¹ Subsequent to this work, and from the analysis of similar Raman data, Van Wart et al.² reported an approximately linear decrease in the S-S stretching frequency, $\nu(\text{S-S})$, as the CS-SC dihedral angle, $\chi(\text{CS-SC})$, was reduced from near 90° to near 0°. Shortly thereafter, Martin³ re-evaluated the available experimental data and reaffirmed his original view that the values of $\nu(\text{S-S})$ are nearly invariant to $\chi(\text{CS-SC})$.

Since Martin's report³ appeared, a reinvestigation of the dependence of the values of $\nu(\text{S-S})$ on the conformation about the C-S and S-S bonds of disulfides containing the $\text{C}^\alpha\text{C}^\beta\text{SSC}^\beta\text{C}^\alpha$ moiety, using both theoretical^{4,5} and experimental⁶⁻⁸ techniques has been carried out by Van Wart et al.⁴⁻⁸ From a study of the Raman spectra of more than two dozen strained and three dozen unstrained disulfides, previously unconsidered effects of (1) substitution at the β carbon of the $\text{C}^\alpha\text{C}^\beta\text{SSC}^\beta\text{C}^\alpha$ moiety and of (2) crystal field perturbations on the values of $\nu(\text{S-S})$ obtained from crystalline compounds have been identified, and the effects of strain in the S-S bond on $\nu(\text{S-S})$ have been reevaluated⁸ in the light of these new ideas. As a result, the differences in interpretation

between the earlier studies of Bastian and Martin^{1,3} and Van Wart et al.² have been resolved. The revised⁸ and originally proposed² relationships between $\nu(\text{S-S})$ and $\chi(\text{CS-SC})$ are shown in Figure 4 of ref 8. The reader is referred to ref 8 for the details of the revision. The major feature of the newer correlation is the reduction in the values of $\nu(\text{S-S})$ from about 520 to 510 cm^{-1} for $|\chi(\text{CS-SC})|$ values in the 65-85° range. This means that, for values of $|\chi(\text{CS-SC})|$ in the 65-85° range, $\nu(\text{S-S})$ is almost invariant to $\chi(\text{CS-SC})$, in agreement with the findings of Martin,³ however, between 0 and 65°, $\nu(\text{S-S})$ does vary with $\chi(\text{CS-SC})$, as originally proposed by Van Wart et al.²

References and Notes

- (1) E. J. Bastian, Jr., and R. B. Martin, *J. Phys. Chem.*, **77**, 1129 (1973).
- (2) H. E. Van Wart, A. Lewis, H. A. Scheraga, and F. D. Saeva, *Proc. Natl. Acad. Sci. U.S.A.*, **70**, 2619 (1973).
- (3) R. B. Martin, *J. Phys. Chem.*, **78**, 855 (1974).
- (4) H. E. Van Wart, L. L. Shipman, and H. A. Scheraga, *J. Phys. Chem.*, **78**, 1848 (1974).
- (5) H. E. Van Wart, L. L. Shipman, and H. A. Scheraga, *J. Phys. Chem.*, **79**, 1428 (1975).
- (6) H. E. Van Wart, F. Cardinaux, and H. A. Scheraga, *J. Phys. Chem.*, **80**, 625 (1976).
- (7) H. E. Van Wart and H. A. Scheraga, *J. Phys. Chem.*, **80**, 1812 (1976).
- (8) H. E. Van Wart and H. A. Scheraga, *J. Phys. Chem.*, **80**, 1823 (1976).

Department of Chemistry
Cornell University
Ithaca, New York 14853

Chemistry Department
University of Virginia
Charlottesville, Virginia 22901

H. E. Van Wart
H. A. Scheraga*

R. Bruce Martin

Received December 1, 1975



Research Reviewed

**Authoritative
critical discussions
by internationally
recognized
chemists in**



CHEMICAL REVIEWS

Reactions, mechanisms, syntheses, spectroscopy and more—the many facets of theoretical chemistry explored in comprehensive, authoritative and critical articles in CHEMICAL REVIEWS. A timesaver for the serious scientist, bimonthly CHEMICAL REVIEWS covers in single articles the material that might otherwise require reading many papers from many sources. To keep current on new chemical insights and new correlations, mail the coupon below.

CHEMICAL REVIEWS

1976

American Chemical Society

1155 Sixteenth Street, N.W.

Washington, D.C. 20036

Yes, I would like to receive CHEMICAL REVIEWS at the one-year rate checked below:

	U.S.	Canada**	Latin America**	Other Nations**
ACS Member One-Year Rate*	<input type="checkbox"/> \$15.00	<input type="checkbox"/> \$18.50	<input type="checkbox"/> \$18.25	<input type="checkbox"/> \$18.50
Nonmember	<input type="checkbox"/> \$60.00	<input type="checkbox"/> \$63.50	<input type="checkbox"/> \$63.25	<input type="checkbox"/> \$63.50

Bill me Bill company Payment enclosed

Air freight rates available on request.

Name _____

Street _____

Home
Business

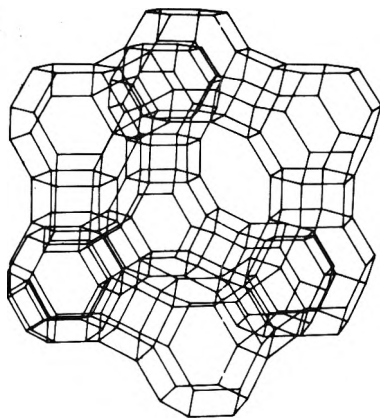
City _____

State _____

Zip _____

Journal subscriptions start January '76

*NOTE: Subscriptions at ACS member rates are for personal use only. **Payment must be made in U.S. currency, by international money order, UNESCO coupons, U.S. bank draft, or order through your book dealer.



Zeolite Chemistry and Catalysis

ACS MONOGRAPH 171

Jule A. Rabo, *Editor*

A comprehensive overview of all important aspects of zeolite catalysis according to structure, chemistry and mechanism, and technology.

Chemists, material scientists, and chemical engineers working in the areas of catalysis and material science related to the petroleum and chemical industry will find this volume a useful and valuable addition to their reference library.

Specific topics include:

- origin and structure; IR studies of surfaces and surface reactions; stability and ultrastable zeolites
- salt occlusion in zeolite crystals; ESR studies; diffusion hydrocarbon transformations; molecules containing hetero atoms; metal-containing zeolites
- shape selective catalysis; preparation and performance of cracking catalysts; hydrocracking, isomerization, and other industrial processes

796 pages (1976) clothbound \$65.00
LC 76-17864 ISBN 0-8412-0276-1

SIS/American Chemical Society
1155 16th St., N.W./Wash., D.C. 20036

Please send _____ copies of *Zeolite Chemistry and Catalysis* at \$65.00 per book.

Check enclosed for \$ _____ Bill me.
Postpaid in U.S. and Canada, plus 40 cents elsewhere.

Name _____
Address _____
City _____ State _____ Zip _____



Successful chemists keep up with chemistry

ACS AUDIO COURSES keep up with successful chemists

The best way to keep pace with chemistry's rapid progress is to learn from the chemists who help make it happen.

More than 25 ACS Audio Courses are now available — all prepared and recorded by leading chemists teaching their own specialties. All courses include audiotape cassettes and comprehensive manuals with information, diagrams and other visual material, many with exercises so you can combine the ease of listening with the challenge of doing as you learn.

The courses cover all levels and interests, introductory and refresher topics, specialized subjects and techniques, non-technical courses to aid your personal development.

Best of all, all ACS Audio Courses are offered on a money-back guarantee basis . . . so you can't lose.

Send coupon below for more information.



Department of Educational Activities
American Chemical Society
1155 Sixteenth Street, N.W.
Washington, D. C. 20036

Please send information on ACS Audio Courses

Name _____

Organization _____

Address _____

City _____

State _____ Zip _____

8-0700-2019 ✓